

SMIP04

SMIP04 SEMINAR ON UTILIZATION OF STRONG-MOTION DATA

Sacramento, California
May 17, 2004

PROCEEDINGS

Sponsored by

California Strong Motion Instrumentation Program
California Geological Survey
California Department of Conservation

Co-Sponsors

California Seismic Safety Commission
California Office of Emergency Services
California Department of Transportation
Office of Statewide Health Planning and Development



The California Strong Motion Instrumentation Program (CSMIP) is a program within the California Geological Survey (previously known as the Division of Mines and Geology) of the California Department of Conservation. It is advised by the Strong Motion Instrumentation Advisory Committee (SMIAC), a committee of the California Seismic Safety Commission. Major program funding is provided by an assessment on construction costs for building permits issued by cities and counties in California, with additional funding from the California Office of Emergency Services, the California Department of Transportation, the Office of Statewide Health Planning and Development and the California Department of Water Resources.

In 1997, a joint project, TriNet, between CSMIP, Caltech and USGS at Pasadena was funded by the Federal Emergency Management Agency (FEMA) through the California Office of Emergency Services (OES). The goals of the project were to record and rapidly communicate ground shaking information in southern California, and to analyze the data for the improvement of seismic codes and standards. TriNet produced ShakeMaps of ground shaking, based on shaking recorded by stations in the network, within minutes following an earthquake. The ShakeMap identifies areas of greatest ground shaking for use by OES and other emergency response personnel in the event of a damaging earthquake.

In July 2001, the California Office of Emergency Services began funding for the California Integrated Seismic Network (CISN), a newly formed consortium of institutions engaged in statewide earthquake monitoring that grew out of TriNet, and includes CGS, USGS, Caltech and UC Berkeley. The CISN will improve seismic instrumentation and provide statewide ground shaking intensity maps. It will also distribute and archive strong-motion records of engineering interest and seismological data for all recorded earthquakes, and provide training for users.

DISCLAIMER

Neither the sponsoring nor supporting agencies assume responsibility for the accuracy of the information presented in this report or for the opinions expressed herein. The material presented in this publication should not be used or relied upon for any specific application without competent examination and verification of its accuracy, suitability, and applicability by qualified professionals. Users of information from this publication assume all liability arising from such use.

SMIP04

SMIP04 SEMINAR ON UTILIZATION OF STRONG-MOTION DATA

Sacramento, California
May 17, 2004

PROCEEDINGS

Edited by

Moh Huang

Sponsored by

California Strong Motion Instrumentation Program
California Geological Survey
California Department of Conservation

Co-Sponsors

California Seismic Safety Commission
California Office of Emergency Services
California Department of Transportation
Office of Statewide Health Planning and Development

PREFACE

The California Strong Motion Instrumentation Program (CSMIP) in the California Geological Survey (previously known as the Division of Mines and Geology) of the California Department of Conservation established a Data Interpretation Project in 1989. Each year the CSMIP funds several data interpretation contracts for the analysis and utilization of strong-motion data. The primary objectives of the Data Interpretation Project are to further the understanding of strong ground shaking and the response of structures, and to increase the utilization of strong-motion data in improving post-earthquake response, seismic code provisions and design practices.

As part of the Data Interpretation Project, CSMIP holds annual seminars to transfer recent research findings on strong-motion data to practicing seismic design professionals, earth scientists and post-earthquake response personnel. The purpose of the annual seminar is to provide information that will be useful immediately in seismic design practice and post-earthquake response, and in the longer term, in the improvement of seismic design codes and practices. The SMIP04 Seminar is the fifteenth in this series of annual seminars.

The SMIP04 Seminar is divided into four sessions. Session I includes two presentations on ground motion topics. Session II will focus on improvement of analysis procedures using strong-motion data from bridges and buildings. Session III will include two presentations on visualization of recorded building and bridge motions. Session IV will include two presentations on the new San Francisco-Oakland Bay Bridge East Span and the 1-story hospital in Templeton. The Seminar will end with a field trip to the State Capitol. Before the field trip, we have invited Joe Nicoletti to discuss the rehabilitation of the California State Capitol. Director Darryl Young of the Department of Conservation will present a luncheon address.

The seminar will include presentations by investigators of five CMIP-funded projects. The project by Rakesh Goel has been completed and his final reports will be available this year. The other four projects are scheduled to be completed by the end of 2004, so the investigators can only present preliminary or interim results. The final results will be presented at the next year's seminar (SMIP05).

Moh J. Huang
Data Interpretation Project Manager

**Members of the
Strong Motion Instrumentation Advisory Committee**

Main Committee

Chris Poland, Chair, Degenkolb Engineers
Bruce Bolt, UC Berkeley
Anil Chopra, UC Berkeley
Bruce Clark, Seismic Safety Commission, Leighton & Associates
C. Allin Cornell, Stanford University
Wilfred Iwan, California Institute of Technology
Jerve Jones, Peck/Jones Construction Corp.
Michael Keever, Caltrans
Vern Persson, DWR Div. of Safety of Dams (retired)
Daniel Shapiro, Seismic Safety Commission, SOHA Engineers
Edward Bortugno (ex-officio), Office of Emergency Services
Richard McCarthy (ex-officio), Seismic Safety Commission

Ground Response Subcommittee

Bruce Bolt, Chair, UC Berkeley
Brian Chiou, Caltrans
Marshall Lew, Law/Crandall
Geoffrey Martin, Univ. of Southern California
Maurice Power, Geomatrix Consultants

Buildings Subcommittee

Chris Poland, Chair, Degenkolb Engineers
Kenneth Honda, URS Corporation
Donald Jephcott, Structural Engineer
Jerve Jones, Peck/Jones Consttuction Corp.
Jack Meehan, Structural Engineer
Farzad Naeim, John A. Martin & Associates
John Robb, Structural Engineer
Zan Turner, City and County of San Francisco
Chia-Ming Uang, UC San Diego

Lifelines Subcommittee

Vern Persson, Chair, DWR Div. of Safety of Dams (retired)
Martin Eskijian, California State Lands Commission
David Gutierrez, DWR Div. of Safety of Dams
Michael Keever, Caltrans
LeVal Lund, Civil Engineer
Edward Matsuda, BART
Ron Tognazzini, Los Angeles Dept. of Water and Power

Data Utilization Subcommittee

Wilfred Iwan, Chair, California Institute of Technology
Representatives from each Subcommittee

TABLE OF CONTENTS

Seminar Program

Design Ground Motion Library1
Maurice Power, Robert Youngs, and Chih-Cheng Chin

Seismological Implications of the Ground Motion Data from the 2003 San Simeon Earthquake25
Vladimir Graizer and Douglas Dreger

Seismic Analysis of the Sylmar Interstate 5 and Highway 14 Connector Bridge41
Robert Dowell

Evaluation of Nonlinear Static Procedures Using Strong-Motion Building Records61
Rakesh Goel

CSMIP Instrumented Building Response Analysis and 3-D Visualization System (CSMIP-3DV)83
Farzad Naeim, Hung Lee, Hussain Bhatia, Scott Hagie and Konstantinos Skliros

Visualization of Seismic Bridge Motions103
Robert Dowell

Design and Instrumentation of the New San Francisco-Oakland Bay Bridge East Span113
Brian Maroney, Pat Hipley and Moh Huang

Recorded Response and Observed Performance of a Wood-Frame Hospital Building During the 2003 San Simeon Earthquake125
Moh Huang and Chris Tokas

Rehabilitation of the California State Capitol137
Joseph Nicolletti

**SMIP04 SEMINAR ON
UTILIZATION OF STRONG-MOTION DATA**

Sacramento Convention Center, Sacramento, California
May 17, 2004

FINAL PROGRAM

8:00 am **REGISTRATION**

9:00 am **WELCOMING REMARKS**

Chris Poland, Chair, Strong Motion Instrumentation Advisory Committee (SMIAC)
Michael Reichle, Acting State Geologist, California Geological Survey
Anthony Shakal, Program Manager, Strong Motion Instrumentation Program

INTRODUCTION

Moh Huang, Strong Motion Instrumentation Program

SESSION I

Moderator: *Bruce Bolt*, UC Berkeley, SMIAC

9:15 am **Design Ground Motion Library**

Maurice Power, Robert Youngs and Chih-Cheng Chin, Geomatrix Consultants

9:40 am **Seismological Implications of the Ground Motion Data from the 2003 San Simeon Earthquake**

Vladimir Graizer, CSMIP and *Douglas Dreger*, UC Berkeley

10:05 am **Questions and Answers for Session I**

10:15 am Break

SESSION II

Moderator: *Vern Persson*, SMIAC

10:35 am **Seismic Analysis of the Sylmar Interstate 5 and Highway 14 Connector Bridge**

Robert Dowell, Dowell-Holombo Engineering

11:00 am **Evaluation of Nonlinear Static Procedures Using Strong-Motion Building Records**

Rakesh Goel, California Polytechnic State University, San Luis Obispo

11:25 am **Questions and Answers for Session II**

SMIP04 Seminar Proceedings

11:35 am **Luncheon**

Introduction *Michael Reichle*, Acting State Geologist, California Geological Survey
Speaker: *Darryl Young*, Director, Department of Conservation

SESSION III

Moderator: *Chris Poland*, Degenkolb Engineers, SMIAC

12:45 pm **CSMIP Instrumentated Building Response Analysis and 3-D Visualization System (CSMIP-3DV)**

Farzad Naeim, Hung Lee, Hussain Bhatia, Scott Hagie and Konstantinos Skliros, John A. Martin & Associates

1:10 pm **Visualization of Seismic Bridge Motions**

Robert Dowell, Dowell-Holombo Engineering

1:35 pm **Questions and Answers for Session III**

1:45 pm Break

SESSION IV

Moderator: *Wilfred Iwan*, Caltech, SMIAC

2:00 pm **Design and Instrumentation of the New San Francisco-Oakland Bay Bridge East Span**

Brian Maroney, *Pat Hipley*, Caltrans, and Moh Huang, CSMIP

2:25 pm **Recorded Response and Observed Performance of a Wood-Frame Hospital Building during the 2003 San Simeon Earthquake**

Moh Huang, CSMIP and *Chris Tokas*, OSHPD

2:50 am **Questions and Answers for Session IV**

3:00 pm Field Trip Introduction

Rehabilitation of the California State Capitol

Joseph Nicoletti, Engineer of Record

3:15 pm Field Trip to **Seismically Strengthened California State Capitol**

DESIGN GROUND MOTION LIBRARY

Maurice S. Power, Robert R. Youngs, and Chih-Cheng Chin
Geomatrix Consultants, Inc., Oakland, California

Abstract

Criteria and guidelines being utilized to form a Design Ground Motion Library (DGML) are summarized in this paper. The DGML is being formed as an electronic library of selected recorded acceleration time histories considered to be suitable for use by engineering practitioners for the time history dynamic analysis of various facility types in California and other parts of the Western United States (WUS). The broad criterion governing selection of records is that the records be representative of ranges of design earthquakes and ground motions expected for the WUS seismic environment. Separate sets of records are being developed for different ranges of earthquake magnitude and earthquake source-to-site distance, for soil and rock site conditions, and for different period ranges of significance for different types of structures. Ground motion characteristics that are used in criteria for record selection include measures of response spectral shape characteristics and, for near-source record sets, pulsive characteristics of ground motion caused by rupture directivity effects.

Introduction

This paper summarizes criteria and guidelines currently being utilized in the formation of a Design Ground Motion Library (DGML). The objective of the DGML project is to create an electronic library of selected sets of recorded ground motion acceleration time histories suitable for use by engineering practitioners for time-history dynamic analyses of various facility types in California and other parts of the western United States. The DGML project is jointly sponsored by the California Strong Motion Instrumentation Program (CSMIP) and the Pacific Earthquake Engineering Research Center-Lifelines Program (PEER-LL). The DGML is currently limited to recorded time histories from shallow crustal earthquakes of the types that occur in the western United States. Time histories recorded during subduction zone earthquakes will not be part of the Library during this project. However the project sponsors envision that future development of the DGML will add records from subduction zone earthquakes (appropriate for these types of earthquakes occurring in northwest California, Oregon, Washington, and Alaska) and will also supplement recorded motions with time histories simulated by ground motion modeling methods.

Initial criteria and guidelines for the DGML were developed during late 2002 and 2003. In the spring of 2003, the DGML project was put on hold because of improvements being made to the PEER strong motion data base, which is a data base of strong motion recordings obtained by CSMIP, USGS, and other strong motion network operators. As part of the PEER-LL's Next Generation of Attenuation Relationships (NGA) project, a large number of records have been added to the ground motion data base along with an expansion of the supporting information on the earthquake sources, travel path, and site conditions associated with the records. The PEER-LL's strong motion database has been compiled using a systematic quality assurance review

process. This expanded data base is an improved resource from which to select records for the DGML. The data base will be completed in May 2004, and the Library will therefore be completed in the next few months. The criteria and guidelines for developing the Library have been revised and are described herein.

The principal criteria being developed for the DGML pertain to the selection of the records and the formation of record sets for the Library. This paper focuses mainly on these criteria. However, two other aspects of the Library will also be briefly discussed—the quantification of parameters of the records and supporting information to be included for records placed in the Library; and guidelines for utilization of record sets.

The principal strategy in conducting the project is to utilize a team of experts in the selection and use of time history records to develop the criteria for the DGML, select the records for the DGML using these criteria, and develop utilization guidelines. Accordingly, a multi-disciplinary project team of practitioners and researchers in structural engineering, geotechnical engineering, and seismology is conducting the project. The team comprises expertise in the time history dynamic analysis of buildings, bridges, dams, other heavy civil structures, lifeline structures and systems, and base isolated structures. The project team includes the following organizations and individuals: Geomatrix Consultants, Inc., prime contractor (Maurice Power, Robert Youngs, Faiz Makdisi, and Chih-Cheng Chin); Simpson Gumpertz & Heger, Inc. (Ronald Hamburger and Ronald Mayes); T.-Y. Lin International (Roupen Donikian); Quest Structures (Yusof Ghanaat); Pacific Engineering & Analysis (Walter Silva); URS Corporation (Paul Somerville); Earth Mechanics (Ignatius Po Lam); Professor Allin Cornell, Stanford University; and Professor Stephen Mahin, University of California, Berkeley.

Library Concept

Based on input from the project sponsors, the DGML is to be distinctly different from a ground motion data base. Data bases, such as those of PEER, COSMOS, CSMIP, and USGS, contain large numbers of time history records but do not provide guidance on how to select records for specific application. On the other hand, the DGML will contain small groups of time history records that, based on the criteria and judgment of the project team, are considered to be suitable for use for defined categories of the seismic hazard environment and structure characteristics.

Although record sets for the DGML are selected based on criteria and judgment involving relatively few seismological, ground motion, and site parameters, many more parameters will be quantified or characterized for the records placed in the Library. These parameters include ground motion parameters of the records and characteristics of the earthquake sources, source-to-site travel paths, and site conditions that resulted in the records. This is done to fully describe the records and provide additional information that may be considered when using the records. For example, these additional parameters could be considered in evaluating results from structural analysis for different records in a set.

Having selected a record set from the Library, the user would then scale each record to the level of the design response spectrum for the project site. Scaling of records will be addressed in the utilization guidelines.

Criteria for selecting records and forming record sets for the DGML

Overview of Criteria and Process

The criteria and process for selecting records and forming record sets for the DGML is fundamentally related to the characteristics of the seismic environment and ground motions of the design earthquake. Record sets are formed for ranges of earthquake magnitudes (M) and closest source-to-site distances (R) that encompass magnitudes and distances of design earthquakes that are either selected for a deterministic analysis or found to be the dominant contributors to the site hazard through deaggregation of a probabilistic seismic hazard analysis (PSHA). Furthermore, record sets are separately formed for ground motion records recorded on rock or soil. The different magnitude and distance ranges together with the site classification (S) are termed magnitude-distance-site classification (M-R-S) bins. In application, a user of the Library selects a set or sets of records from the M-R-S bin that includes the M, R, and S for his design earthquake.

Spectral shape over a period range of significance to structural response has been found to be closely correlated to inelastic structural response and behavior in studies by PEER and PEER-LL (e.g. Shome et al. 1998; Cordova et al. 2001; Luco and Cornell 2003; Bazzurro and Luco 2003; Cornell et al. 2003; Jalayer 2003; Baker and Cornell 2004; Luco and Bazzurro 2004). The period range may include periods shorter than the fundamental structure period because of higher mode effects and periods longer than the fundamental structure period because of structure softening to longer periods in the inelastic range. Therefore, period ranges are defined encompassing period ranges of significance (period-range sub-bins), and records are selected for each period-range sub-bin within the M-R-S bins as a function of the spectral shape of the records over the defined period range in comparison to the median and variation of spectral shapes for all the records (from the entire data base) in the M-R-S bins.

In the near-source region, the criteria for selecting records also considers the effects of rupture directivity causing strong time-domain pulsive ground motion characteristics (e.g. pulse velocity, pulse period, and number of pulses). These near-source characteristics of ground motion have been shown to be very damaging to structures in studies by Krawinkler and Alavi (1998). Studies by Bazzurro and Luco (2003) have not shown a significant improvement in damage predictability associated with pulse period or velocity over the correlation with response spectral characteristics alone for a data set of spectrum-matched time histories.

The following paragraphs briefly describe the criteria for definition of the M-R-S bins and the period-range sub-bins and the selection of records and formation for record sets for the DGML. This description is followed by an example indicating how the criteria may be applied.

Definition of Magnitude-Distance-Site Conditions (M-R-S) bins

The general criteria for defining the magnitude and distance ranges of the M-R-S bins are the following:

(1) Magnitudes and distance ranges for the bins should be selected such that they define systematic differences in response spectral shapes between the bins. Figures 1 and 2 indicate the effects of magnitude and distance on response spectral shape using the ground motion attenuation relationship of Abrahamson and Silva (1997). Relationships such as shown on these figures as well as statistical analysis of the records in the data base within selected magnitude and distance ranges will be used to define the M and R limits for each bin. For site conditions, a simple soil or rock criteria has been adopted. Further refinement in site classification could be done, but are not adopted for the Library, because it would reduce the number of records to choose from in each bin and because a refined classification is not confidently determined at many recording station sites.

(2) The differences in M and R for each bin should be large enough to have an adequate record population to choose from but small enough so that “unreasonable” amounts of scaling of records to the design spectrum would not be required.

(3) The farthest distance for near-source M-R-S bins should be large enough to capture records potentially having significant near-source ground motion characteristics.

(4) The farthest M-R-S bins may be selected on the basis of ground motion amplitudes (using ground motion attenuation relationships) and the potential use of the records for time history analysis. Time history analyses are unlikely to be done where design ground motions have very low amplitudes. Similarly, the need for M-R-S bins for M less than 6 should be evaluated on the basis of ground motion amplitudes and the likelihood that time history analysis would be done for design earthquakes having M less than 6.

These criteria will be applied to the new data base in the near future. A preliminary selection of M-R-S bins based on judgment and experience is shown in Table 1. The overlapping magnitude of 6.9 in the two highest magnitude bins is done to increase the number of earthquakes and records in the largest magnitude bins. Having overlapping magnitudes in other bins is also being considered.

Definition of Period-Range Sub-bins

The definition of period ranges appropriate for evaluating response spectral shapes is based on evaluation of typical period ranges of significance for different structure types. Another consideration is that the period bands should be wide enough that differences in spectral shapes between records would be significant. A third consideration is that some designers might prefer a set of time histories selected on the basis of the entire response spectrum band (say, from 0 to 5 seconds) The judgment of the project team resulted in a short-period band, a long-period band, and a broad band encompassing short and long periods. These bands are shown in Table 2. Consideration is also being given to one or two other bands. Furthermore, it is possible that

records selected in an M-R-S bin for one period band might also be appropriate records for one or more other period bands, thus effectively expanding the number of period-range sub-bins.

Definition of Criteria for Evaluating Response Spectral Shape Characteristics Over a Period Band

The spectral shape of the records in an M-R-S bin and for the period ranges of the sub-bins is compared to the median spectral shape for the bin and sub-bin. The median spectral shape is determined by statistical analysis of the response spectra for all the records in the bin. In the near-source bins, spectral shapes are expected to vary for fault-normal and fault-parallel components, and this must be evaluated for the bins. These spectral shapes will be smoothed to remove small-scale irregularities using ground motion attenuation relationships to guide the smoothing.

Before evaluating spectral shape characteristics of the records relative to a target median shape for a bin, the records are first scaled to the level of the smooth median spectra. The scaling criterion is that the spectrum of the record has equal differences above and below the median spectrum over the period range for the defined sub-bin. Two measures are then used to calculate and evaluate response spectral shapes of records in comparison to the median spectral shape. The first measure is the mean squared error (MSE) of the differences between the median spectrum and the spectrum of the record after scaling. This measure determines the overall “fit” of the spectrum of the record to the target median spectral shape over the period band. Records with lower MSE more closely match the target spectrum. The equations for scaling and for determining the MSE of a record are given below.

$$\text{Scale Factor} = \bar{\varepsilon} = \frac{1}{n} \sum_i \varepsilon(t_i), \text{ and}$$

$$\text{MSE} = \frac{1}{n} \sum_i (\varepsilon(t_i) - \bar{\varepsilon})^2,$$

$$\text{where } \varepsilon(t_i) = \ln \left[\frac{SA^{\text{target}}(t_i)}{SA^{\text{recording}}(t_i)} \right] \text{ and } t_i \text{ is period.}$$

The number of periods n is determined by specifying equally spaced values of $\ln(t)$ using fifty points per period decade.

The second measure of the spectral shape of the record relative to the median shape is the “slope” of the record spectrum compared to the slope of the median spectrum across the period band. It is determined by regressing on the spectral differences with period between an actual record spectrum and the median spectrum. Spectra with larger slopes (positive or negative) relative to the median spectrum are more skewed relative to the median shape. The equations for determining the slope of the spectra of the records are given below.

$$\text{Slope} = \frac{\sum_i [\ln(t_i) - \overline{\ln(t)}] \times [\varepsilon(t_i) - \bar{\varepsilon}]}{\sum_i [\ln(t_i) - \overline{\ln(t)}]^2}$$

$$\text{where } \overline{\ln(t)} = \frac{1}{n} \sum_i \ln(t_i)$$

The MSE and the slope of the spectral shape of a record relative to the target spectral shape can be displayed by plotting the slope versus MSE as shown schematically in Figure 3. Indicated on the figure are regions of the MSE-slope space representing various qualitative descriptions of the degree of agreement between the spectral shape of the individual record and the target spectrum.

Development of Record Sets

The following paragraphs summarize different elements of criteria for forming the record sets having established the record binning criteria and the spectral shape characteristics as described above.

Criteria for Record Selection as Related to the Number of Records in the Set. Two record sets will generally be defined for each period-range sub-bin within an M-R-S bin. One set will have three records and the second will have ten records. The choice of these numbers of records partly reflects current building code criteria and partly the judgment of the project team with regard to size of record sets relative to the interpretation of building responses when sets of different sizes are used.

For record set sizes of three, the criterion for record set selection would be the closest fit, with respect to MSE and slope of spectral shapes, of the record spectra to the target median spectra. It is recommended, consistent with building code requirements, that when three records are used in time history dynamic analysis, the largest responses given by the three analyses be used for design.

For record set sizes of ten, the criterion for record set selection is that the record sets selected have spectral shapes that vary from the median shape in a similar way as the variation for all the records in the bin. Thus records can be selected by plotting the MSE and slope of each record in the bin in a plot similar to Figure 3, and then selecting records that reasonably sample each region of the plot, considering both the scatter of data throughout the plot and the density of data in sub regions of the plot. Consistent with minimum building code requirements, the user could remove up to three records from the ten provided. Also consistent with the building code requirements, as a guideline, the average responses from time history analyses using seven to ten records could be used in design.

Note that the criteria for record set selection summarized in this section are appropriate for record sets for M-R-S bins at distances greater than the near-source bins. Additional criteria for record sets for the near-source bins are described in a later section.

Supplemental Criteria as Related to Two-Dimensional (2D) or Three-Dimensional (3D) Time History Analyses. For 2D time history analyses where only one horizontal component is required, a record set consists of a set of three or ten horizontal components. The vertical components (if needed) are those for the records selected on the basis of the horizontal component characteristics. Vertical components are scaled by the same factors as the horizontal components of the records. For 3D analyses where two horizontal components are required, the record set consists of both horizontal components scaled together by the same factor. The MSE for the record is determined based on scaling to obtain the minimum MSE for both horizontal components taken together. The slope is determined as the average slope for the two components. The vertical components (if needed) are scaled by the same factors as the horizontal components.

Additional Criteria for Near-Source Record Sets. In addition to the criteria based on the representativeness of the spectral shape of the selected records, directivity characteristics of the records in the near-source M-R-S bins must also be considered for period ranges that would be expected to exhibit near-source effects on ground motions. Because near-source effects are generally thought to be prominent only for periods greater than 0.5 seconds, directivity considerations would affect only those sub-bins having periods beyond 0.5 seconds. Only record sets consisting of ten records, each containing a fault-normal and a fault-parallel horizontal component (as well as a vertical component), will be formed for near-source sub-bins requiring considerations of directivity; the project team judged that three records would not adequately sample directivity and fault-normal to fault-parallel variations. Separate fault-normal and a fault-parallel target spectra will be defined for the near-source bins based on the statistics of the fault-normal and fault-parallel components, respectively, for the records in the bin.

Two record sets are being considered to be formed for each sub-bin requiring directivity considerations. The records in one set would have directivity considered to be representative of locations subjected to rare design earthquakes in high-seismic areas. Deaggregation on directivity from PSHA's from such locations indicates that moderate to strong forward directivity, as characterized by the seismological directivity parameters defined by Somerville et al. (1997), may be expected. Thus, most records selected will have been recorded under conditions of moderate to strong forward directivity. For designers who favor the incorporation of available recordings exhibiting the strongest directivity effects with regard to strong velocity pulses and pronounced fault-normal to fault-parallel ground motion ratios, a second set will be formed that includes only those records.

Example of Selection of Record Set

To illustrate the application of the criteria discussed above, an example is presented using the existing PEER data base. The development of actual record sets will be accomplished using the updated PEER-LL NGA data base, as discussed previously. The example is for a near-source M-R-S bin of magnitude equal to or greater than 6.9, distance 0 to 20 km, and rock site conditions. (To increase the sample size of records for this example, the distance range was extended to 20 km). The record set is summarized in Table 3 and consists of 12 records (24 horizontal components). It is noted that the final data base for this M-R-S bin will be

substantially larger and will include records from several additional earthquakes, including the 1999 earthquakes in Duzce and Kocaeli, Turkey, 1999 Chi-Chi, Taiwan earthquake, 2002 Denali, Alaska earthquake, and 1980 Irpinia, Italy earthquake.

The median spectral shape determined for the M-R-S bin is shown in Figure 4 for the fault-normal component. For purposes of this example, the shape was smoothed using a non-parametric smoothing operator, as illustrated in Figure 4. Spectral shape characteristics were determined for the records for a period-range sub-bin of 0.5 to 4.0 seconds.

Spectral shapes for two of the records after scaling are compared with the median shape in Figure 5 for the fault-normal component of the Tabbas, Dayhook (day) record and the Kobe University (kbu) record. For the period range of 0.5 to 4.0 seconds, the Dayhook record illustrates a close fit to the target median spectrum based on small values of MSE and slope. The Kobe University record illustrates a moderate MSE and positive slope. Figure 6 compares the spectral shapes of the fault-normal components of the Loma Prieta BRAN (brn) and the Landers Lucerne (lcn) records with the median shape. These spectral comparisons illustrate large MSEs and large slopes for the two records. Figure 7 presents a plot of MSE vs. slope for the fault-normal components. This plot shows the range of fit of the spectra of the records with respect to the target median spectrum in terms of MSE and slope. A “by-eye” selection of five records was made to illustrate how a limited number of records (not the planned full size of ten records because of the limited number of records in the preliminary data base) can be made to approximate the variability of the data base spectral shapes in the M-R-S bin. The “selected” records are denoted by the circled MSE/slope data points in the figure. For the period range 0.5-4.0 second, Figure 8 shows the fit of the spectra of the records with respect to the target median spectrum for all twelve records for the fault-normal component, whereas Figure 9 shows the fit of just the five selected components. It can be seen that the variability of fit is similar for the two plots. This example is limited to illustrating the application of spectral fit criteria in the selection of a data set. Although the seismological directivity parameters of Somerville et al. (1997) are shown in Table 3 as the $X_{\cos}(\theta)$ and $Y_{\cos}(\phi)$ values, these parameters or the time-domain pulsive characteristics of the records were not used in the selection process for the example. For selection of actual record sets for near-source bins, the directivity criteria summarized earlier will be as or more important than the spectral shape criteria in the selection process.

Quantification of parameters for records selected for the DGML

Parameters of the ground motion records selected for the DGML as well as supporting information (metadata) about the earthquake source, path, and site conditions that are of interest to and possible use by users of the Library will be included for records placed in the Library. Ground motion record parameters being considered for quantification include those summarized in Table 4. It is desirable but not essential that there be published ground motion attenuation relationships for parameters to be quantified so that the parameter values for records in the Library could be compared with the statistical variation in parameter values for similar M, R, and S parameters. Parameters for which published attenuation relationships currently exist are indicated in Table 4. In addition, an attenuation relationship for inelastic response spectral values has recently been developed by Tothong and Cornell (2004), and a relationship for cumulative absolute velocity (CAV) has been developed by Mitchell and Kramer (2004).

Parameters which the project team presently proposes to quantify are also indicated in Table 4. Similarly, supporting information about the records presently proposed to be quantified for records in the DGML is summarized in Table 5. All these parameters and others will be available from the expanded PEER data base.

Utilization Guidelines for the DGML

Utilization guidelines will be prepared to provide guidance to the engineering practitioner on the use of the DGML. Topics that will be covered include:

- (1) Explanation of the criteria, judgments, and processes that were used in developing the various record sets for the DGML so that the Library can be used with full knowledge of the bases on which it was developed.
- (2) Guidance on the size of record sets as related to the interpretation of time history analysis results for design applications, e.g. interpretation of results for record sets consisting of 3 records or seven to ten records.
- (3) Any limitations on scaling of records to the design response spectrum. Several studies have been conducted to evaluate whether the amount of scaling of a recorded motion biases the calculated inelastic response of a structure, e.g. Shome et al. (1998), Cornell et al. (2003), and Luco and Bazzurro (2004). Because the records will be selected for the DGML to have certain characteristics considered appropriate for formation of record sets as discussed in this paper, it is not anticipated that limitations on scaling of the records would be recommended. However, this issue will be further examined and results of research on scaling will be discussed as appropriate.
- (4) Guidance on typical period increments for evaluating the aggregate fit of scaled spectra to a design spectrum and discussion of the degree of fit typically specified in practice.

References

- Abrahamson, N.A., and Silva, W.J., 1997, Empirical response spectral attenuation relations for shallow crustal earthquakes: *Seismological Research Letters*, v. 68, no. 1, p. 94-127.
- Baker, J.W. and Cornell, C.A. 2004, Choice of a vector of ground motion intensity measures for seismic demand hazard analysis, *Proceedings 13th World Conference on Earthquake Engineering*, Vancouver, Canada, August (in press).
- Bazzurro, P. and Luco, N. 2003, Parameterization of non-stationary time histories, *Draft Report for Task 1G00 to PEER-Lifelines Program*.
- Cordova, P.P., Mehanny, S.S.F. Deierlein, G.G., Cornell, C.A., 2000, Development of a two-parameter seismic intensity measure and probabilistic assessment procedure, *Proceedings of the 2nd U.S.-Japan Workshop on Performance-Based Seismic Earthquake Engineering Methodology for Reinforced Concrete Building Structures*, Sapporo, Japan, pp. 195-214.

Cornell, A., Jalayer, F., Iervolino, I., and Baker, J., 2003, Record selection for nonlinear time history analysis, Presentation at PEER Annual Meeting, Palm Springs, California.

Jalayer, F., 2003, Direct probabilistic seismic analysis: implementing non-linear dynamic assessments, PhD thesis, Department of Civil and Environmental Engineering, Stanford University.

Krawinkler, H., and Alavi, B., 1998, Development of improved design procedures for near-fault ground motions, Proceedings SMIP98 Seminar on Utilization of Strong-Motion Data, Oakland, California Strong Motion Instrumentation Program, California Geological Survey, p. 21-41.

Luco, N. and Bazzurro, 2004, Effects of ground motion scaling on nonlinear structural response, Presentation at PEER Annual Meeting, Palm Springs, CA, February.

Luco, N. and Cornell, C.A., 2003, Structure-specific scalar intensity measures for near-source and ordinary earthquake ground motions, paper under revision for Earthquake Spectra.

Mitchell, R.A. and Kramer, S., 2004, Ground motion intensity measures for liquefaction hazards evaluation, paper in preparation.

Shome, N. Cornell, C.A., Bazzurro, P., and Carballo, J.E., 1998, Earthquake records and nonlinear response, Earthquake Spectra, v. 14, no. 3, p. 469-500.

Somerville, P.G., Smith, N.F., and Graves, R.W., 1997, Modification of empirical strong ground motion attenuation relations to include the amplitude and duration effects of rupture directivity: Seismological Research Letters, v. 68, no. 1, p. 199-222.

Tothong, P. and Cornell, C.A., 2004, Ground motion prediction of inelastic spectral displacement, Bi-Annual Affiliates Meeting, John A. Blume Earthquake Engineering Center, Stanford University, April 30.

Table 1

Preliminary M-R Bins for DGML

Moment Magnitude, M	Earthquake Closest Source-to-Site Distance, R (km)
5.5 – 5.9	0 – 15, >15 – 30
6.0 – 6.4	0 – 15, >15 – 30, >30 – 50
6.5 – 7.0	0 – 15, >15 – 30, >30 – 50, >50 – 100
6.9 – 7.9	0 – 15, >15 – 30, >30 – 50, >50 – 100

Table 2

**Preliminary Period Range Sub-Bins for DGML
(seconds)**

0.05 – 0.5
 0.5 – 5.0
 0.1 – 5.0

Table 3
Ground Motion Record Parameters for Example Selection of Record Set

Earthquake	M _w	Station	Dist (km)	X	theta (deg)	X*cos(theta)	Y	phi (deg)	Y*cos(phi)	FP/FN	PGA (g)	PGV (cm/s)	PGD (cm)
1978 Tabas, Iran	7.4	Dayhook (day)	17.0	0.01	87.18	0.00	0.36	37.46	0.29	FP FN	0.307 0.328	25.3 31.9	8.53 9.34
1989 Loma Prieta	6.9	BRAN (brn)	10.3	0.19	33.63	0.16	0.83	32.33	0.70	FP FN	0.414 0.630	35.5 52.7	5.90 7.03
		Cornalitos (cls)	5.1	0.13	42.69	0.10	0.83	7.35	0.82	FP FN	0.514 0.484	41.6 45.5	7.18 14.19
		Gilroy - Gavilan Coll. (gil)	11.6	0.50	22.99	0.46	0.83	14.23	0.80	FP FN	0.302 0.382	28.4 32.4	4.74 6.52
		Gilroy Array 1 (g01)	11.2	0.50	22.80	0.46	0.83	13.70	0.81	FP FN	0.444 0.428	28.7 38.6	6.33 7.16
		Gilroy Array 6 (g06)	19.9	0.50	35.36	0.41	0.83	19.38	0.78	FP FN	0.168 0.185	10.7 17.5	2.75 5.73
		LGPC (lgp)	6.1	0.45	14.21	0.44	0.83	7.96	0.82	FP FN	0.440 0.648	57.1 102.3	20.24 37.27
		UCSC (uc2)	18.1	0.24	53.84	0.14	0.68	64.44	0.29	FP FN	0.310 0.384	11.9 11.6	3.20 2.13
		UCSC Lick Observatory (lob)	17.9	0.01	52.75	0.01	0.83	18.99	0.78	FP FN	0.512 0.406	19.5 17.7	4.42 4.63
1992 Landers	7.3	Lucerne (lcn)	1.1	0.61	17.30	0.58	0.47	33.70	0.39	FP FN	0.796 0.723	32.2 143.7	45.79 161.72
1995 Kobe, Japan	6.9	Kobe University (kbu)	0.2	0.42	5.34	0.42	0.89	0.98	0.89	FP FN	0.236 0.323	39.7 42.9	7.27 13.21
		KJMA (kjm)	0.6	0.31	6.03	0.31	0.89	0.33	0.89	FP FN	0.548 0.854	53.5 96.0	10.29 24.57

Table 4

**Ground Motion Record Parameters (Intensity Measures)
Considered for Quantification in DGML**

Parameter	Published Attenuation Relationship Available	Presently Proposed to be Quantified for Records in DGML
• PGA, PGV, PGD	•	•
• Elastic response spectra	•	•
• Inelastic response spectra	*	•
• Duration	•	•
• Cumulative Absolute Velocity (CAV)	*	•
• Energy		
• Damage indices		
• Arias Intensity	•	•
• Housner Spectrum Intensity		•
• Near-source record characteristics		
- pulse velocity	•	•
- pulse period	•	•
- no. of pulses	•	•

* Relationships developed, not yet published.

Table 5

**Supporting Information about Records
Considered for Quantification in DGML**

Parameter or Characteristic	Presently Proposed to be Quantified for Records in DGML
• Earthquake moment magnitude	•
• Faulting mechanism (strike slip, reverse, normal, reverse-oblique, normal-oblique)	•
• Hanging wall vs. foot wall	•
• Source-to-site distance (closest distance to rupture surface, Joyner-Boore distance)	•
• Near-fault directivity parameters: Somerville et al. (1997): s or d, X or Y, $\cos \theta$, $\cos \Phi$, $X \cos \theta$, $Y \cos \Phi$	•
• Site classification(s): Geomatrix; NEHRP	•
• Basin response influence	

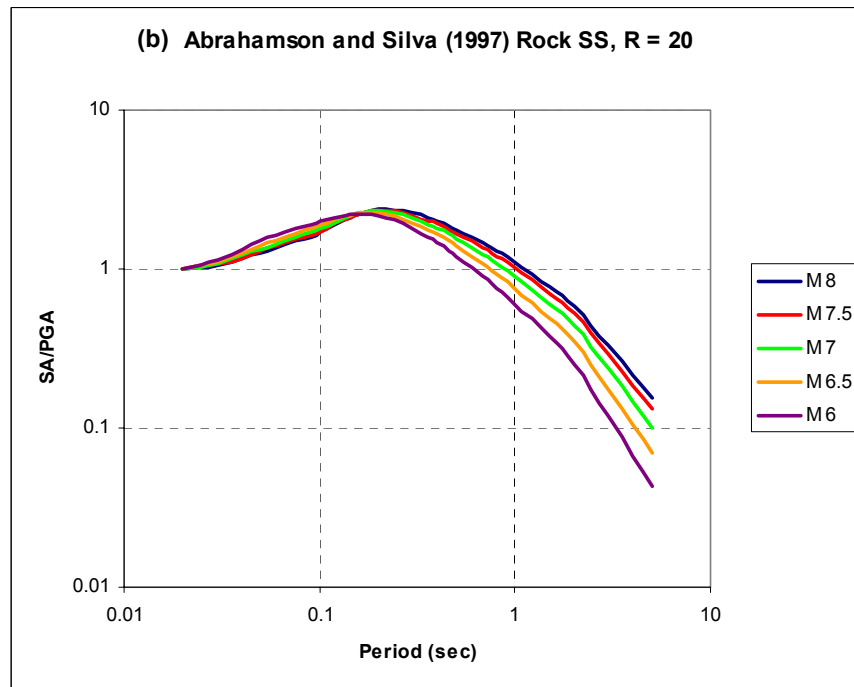
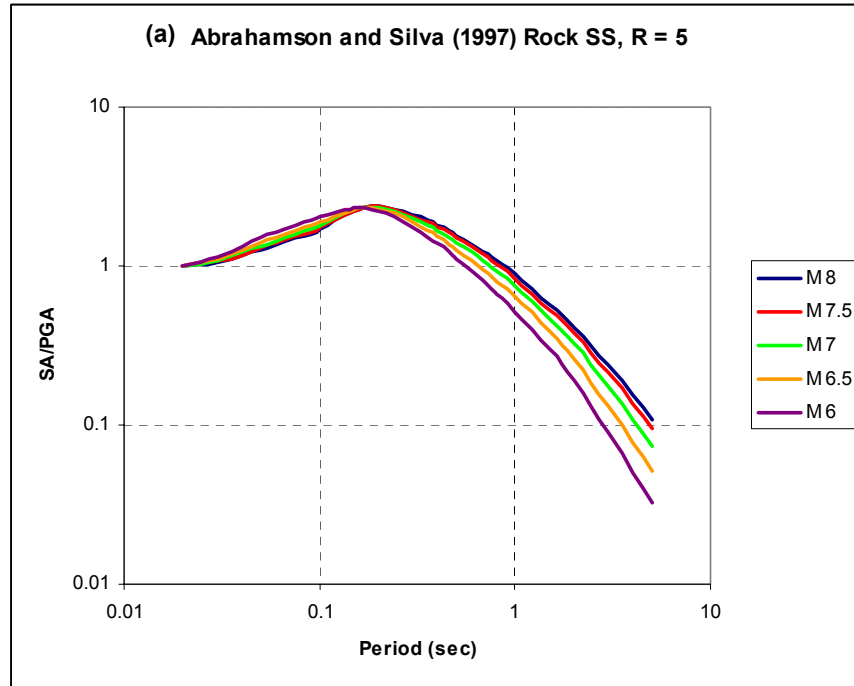


Figure 1 Effects of earthquake magnitude on response spectral shape.

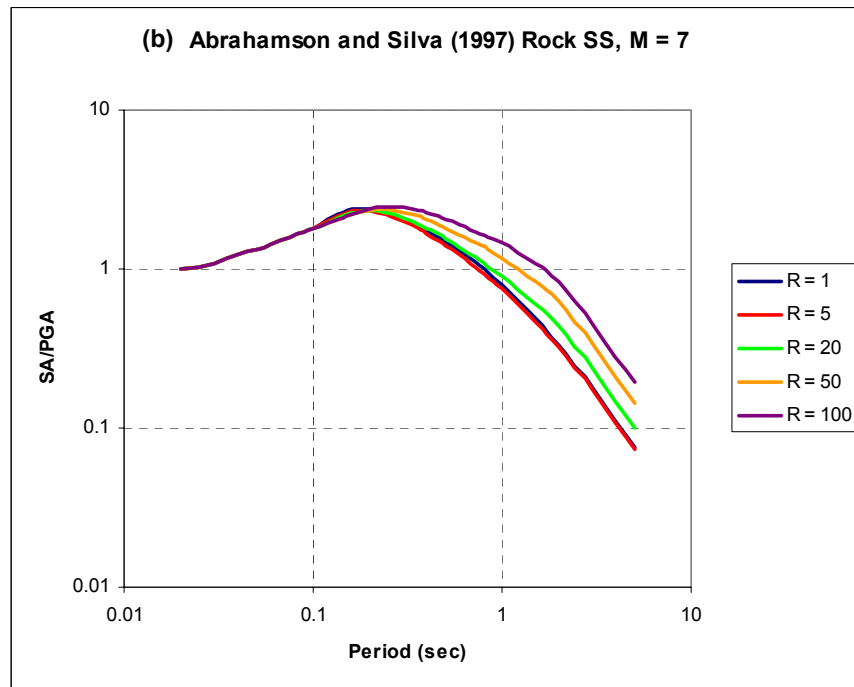
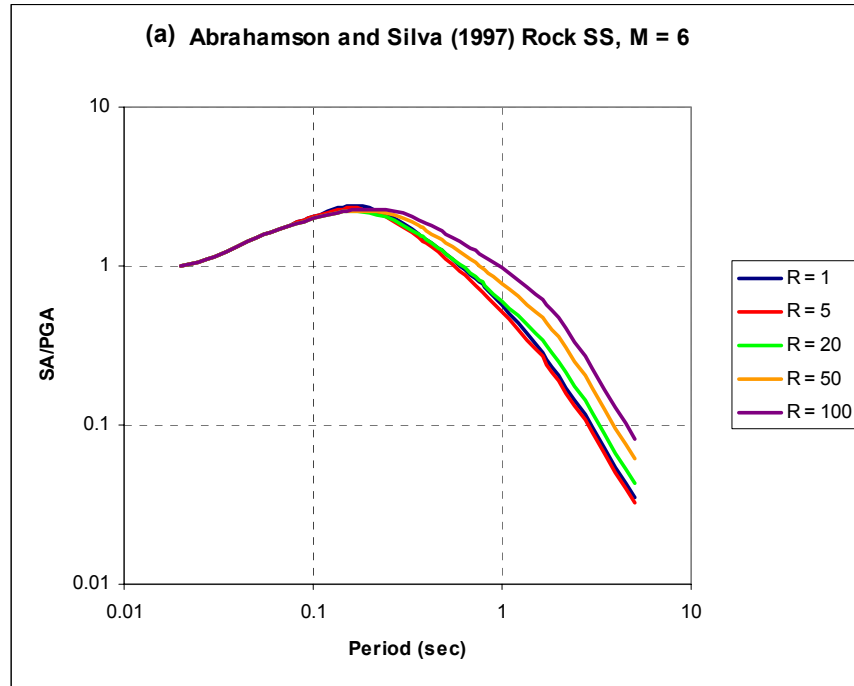


Figure 2 Effects of distance on response spectral shape.

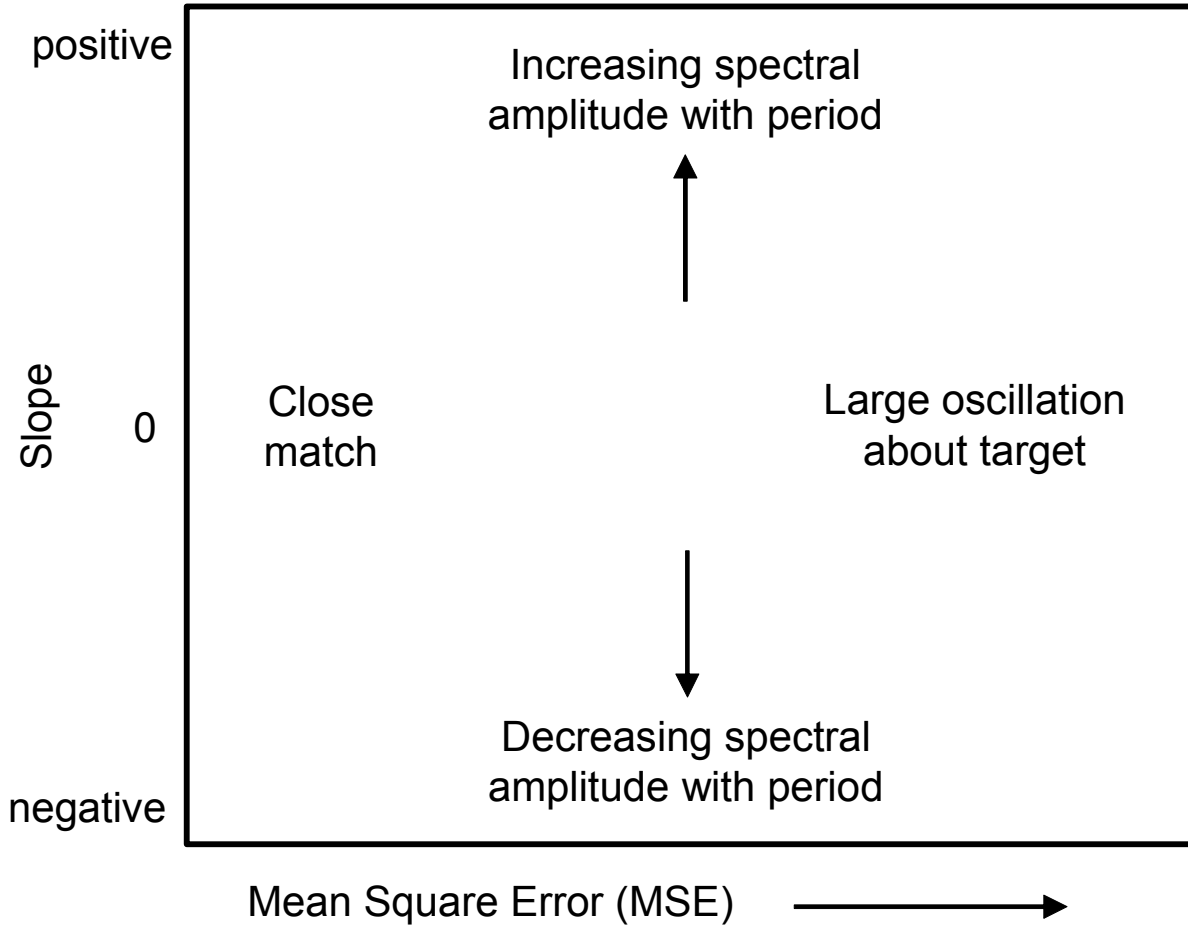


Figure 3 Type of plot illustrating variation of mean square error and slope characteristics of spectral shapes of records with respect to target spectral shape.

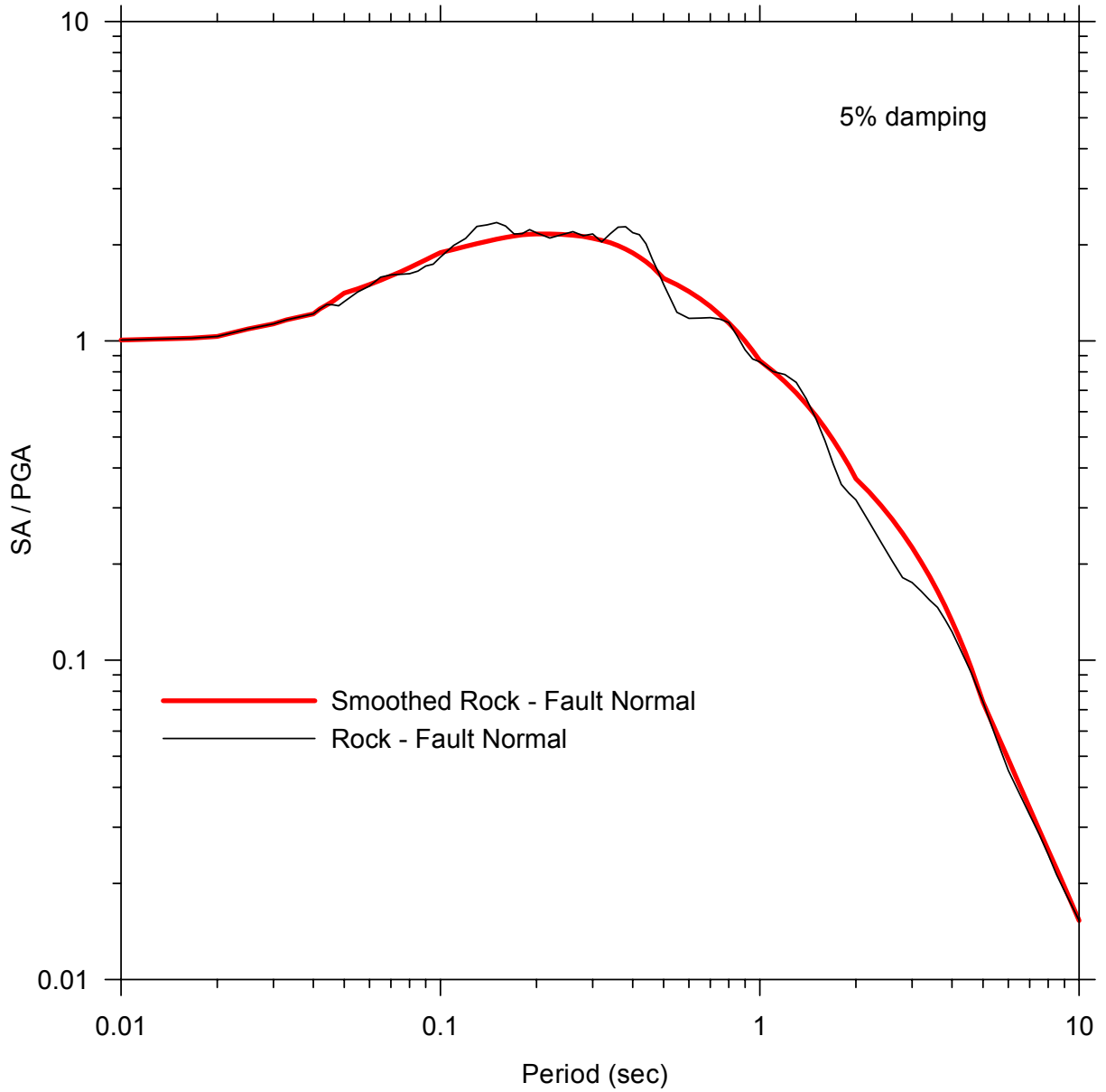


Figure 4 Median fault-normal response spectral shapes for M-R-S bin for $M \geq 6.9$, $R = 0-20$ km, rock.

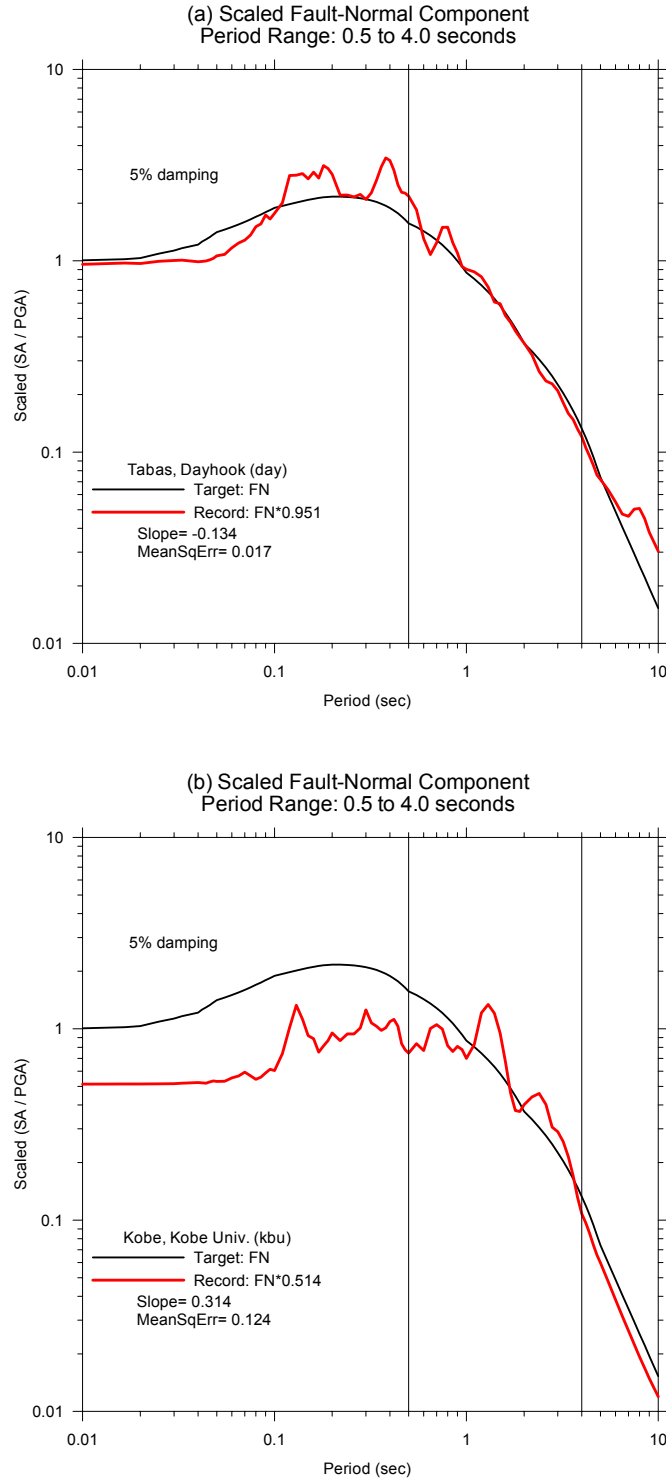


Figure 5 Comparison of response spectral shapes with target median shape for fault-normal components of two records -- period range 0.5 to 4.0 seconds.

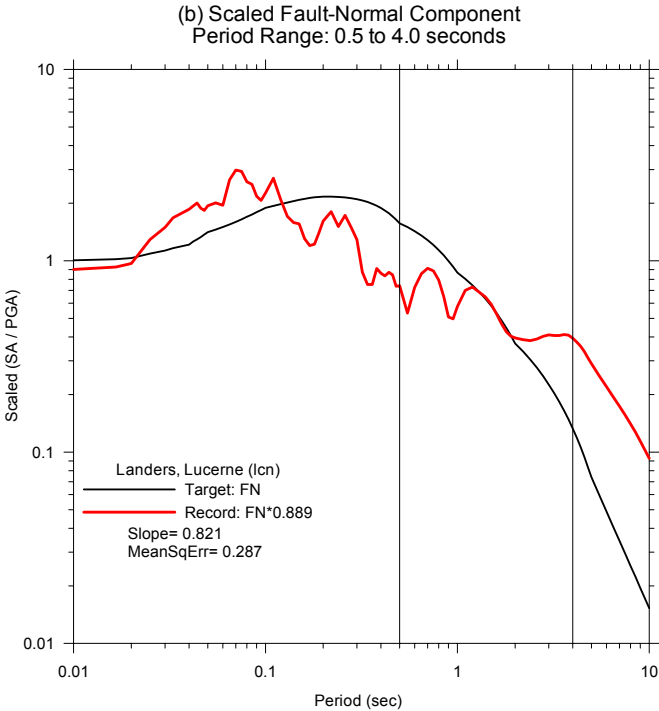
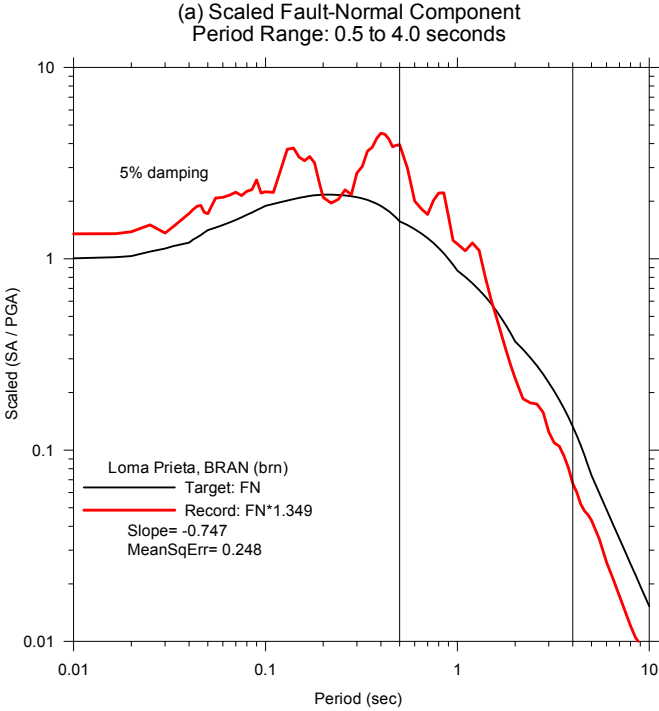


Figure 6 Comparison of response spectral shapes with target median shape for fault-normal components of two records -- period range 0.5 to 4.0 seconds.

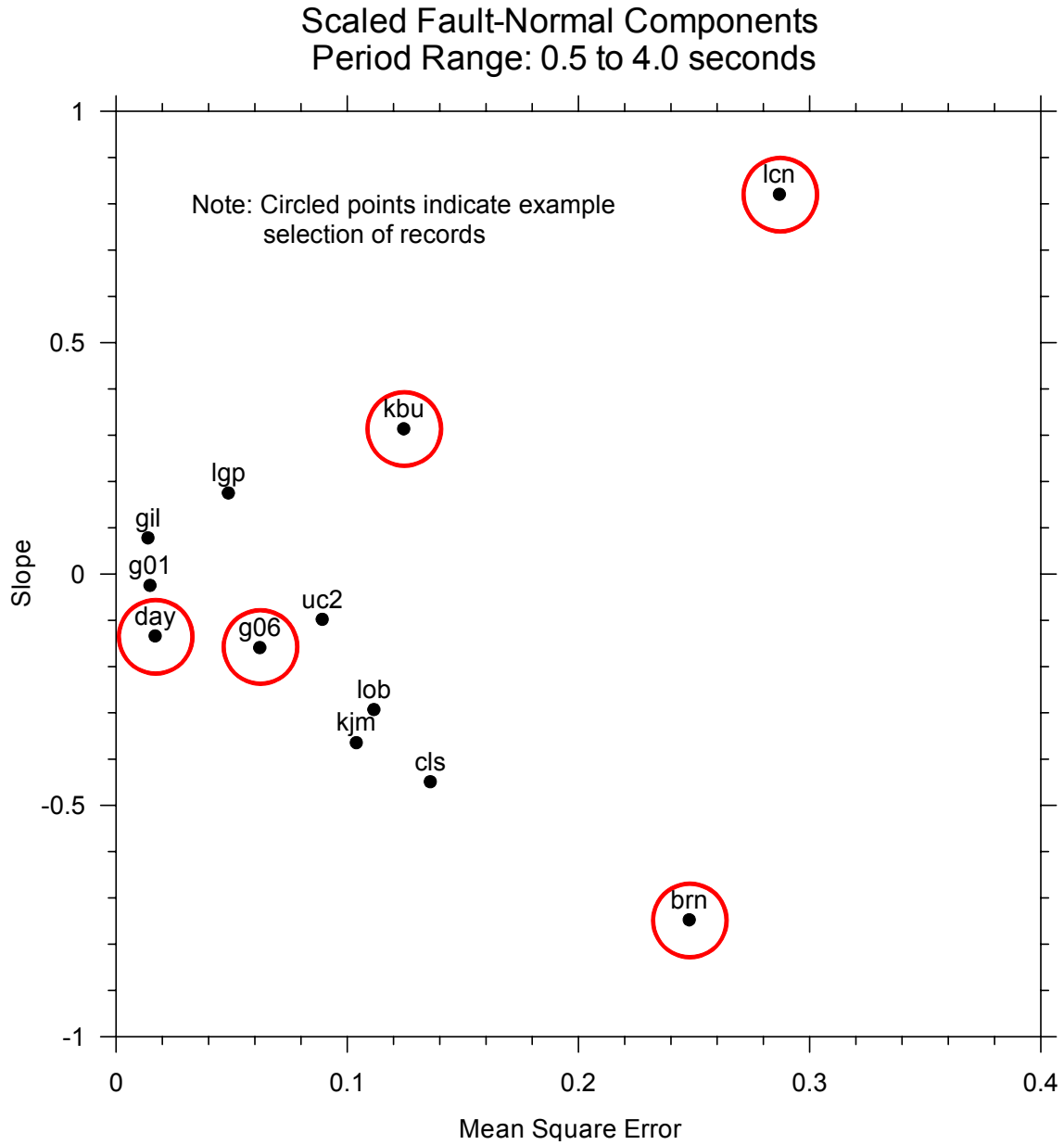


Figure 7 Mean square errors and slopes for fault-normal components of 12 records in M-R-S bin $M \geq 6.9$, $R = 0-20$ km, rock -- period range 0.5 to 4.0 seconds.

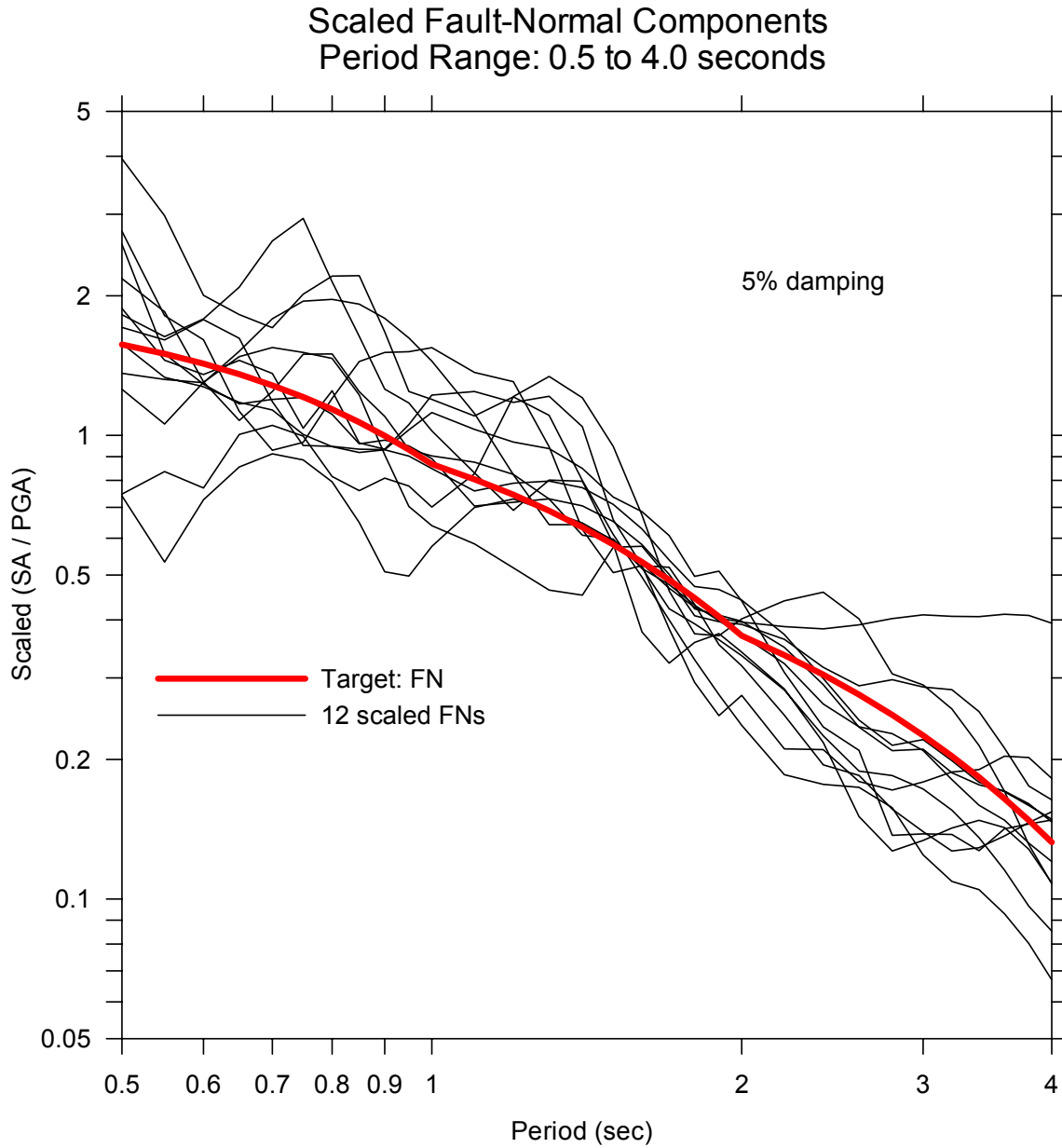


Figure 8 Comparison of response spectral shapes of fault-normal components of 12 records with target median spectral shape for M-R-S bin $M \geq 6.9$, $R = 0-20$ km, rock -- period range 0.5 to 4.0 seconds.

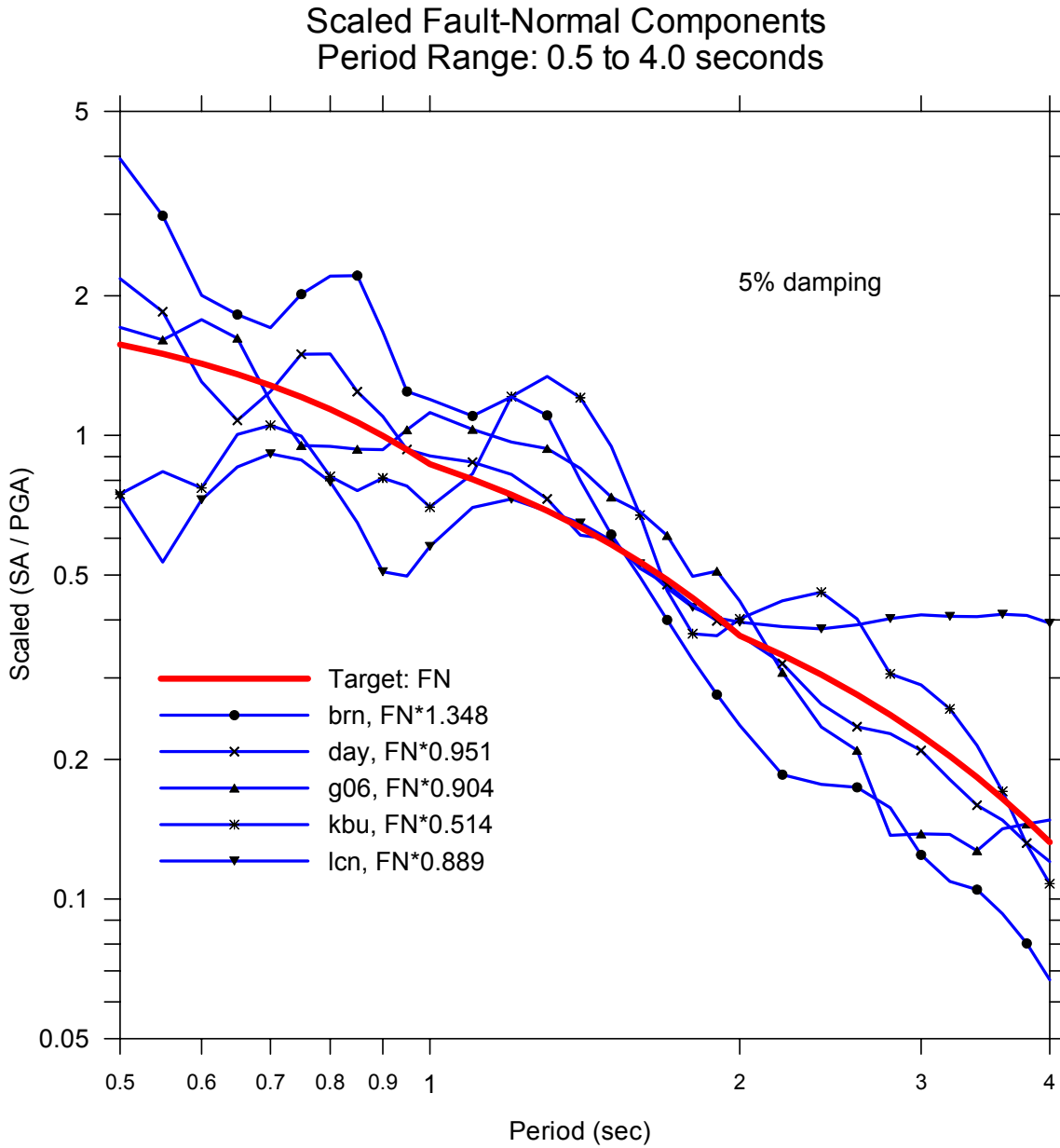


Figure 9 Comparison of response spectral shapes of fault-normal components of 5 selected records with target median spectral shape for M-R-S bin $M \geq 6.9$, $R = 0-20$ km, rock -- period range 0.5 to 4.0 seconds.

SEISMOLOGICAL IMPLICATIONS OF THE GROUND MOTION DATA FROM THE 2003 SAN SIMEON EARTHQUAKE

Vladimir Graizer
California Geological Survey, Strong Motion Instrumentation Program

Douglas Dreger
University of California, Berkeley Seismological Laboratory

Abstract

The San Simeon earthquake occurred on a previously unknown blind thrust fault. No surface rupture associated with the earthquake has been identified. It was recorded at more than 100 strong motion stations out to distances of over 300 km with relatively few stations at less than 50 km distance. The biggest acceleration of 0.48 g was recorded at the Templeton hospital 38 km SE of the epicenter. Data demonstrates strong directivity effect in the direction of rupture propagation. Combined inversion of GPS and seismic waveform data allowed constructing a finite-source model of the earthquake.

Introduction

The M_w 6.5 San Simeon earthquake occurred in central California on December 22 2003 at 11:15:56 a.m. local time. The epicenter was located 7 miles northeast of the town of San Simeon (Hardebeck et al., 2004). The San Simeon earthquake occurred on a reverse fault striking northwest and most likely dipping to the northeast. Earthquake parameters as reported by the California Integrated Seismic Network (CISN) are shown in Table 1.

Table 1. Earthquake Epicenter Information from CISN

Date & Time (Local):	2003/12/22 11:15:56 (PST)
Date & Time (UTC):	2003/12/22 19:15:56 (UTC)
Location:	35.71N 121.10W 7 miles (11 km) NE of San Simeon and 24 miles (39 km) WNW of Paso Robles
Depth (km):	7.5
Magnitude:	6.5 M_w
Mechanism:	Reverse Fault

The earthquake was followed by an active aftershock sequence. Location of the epicenter of the mainshock and aftershocks distribution show that the earthquake most likely ruptured on a

previously unknown blind thrust fault northeast of the Oceanic fault (Jennings, 1994; Hauksson and Oppenheimer, 2004).

The San Simeon area was searched for signs of surface rupture due to earthquake. No features that could be associated with coseismic surface faulting were found. Almost all the earthquake ground effects that were observed are best ascribed to rockfalls, landslides and liquefaction or to the settlement or slumping of man made fills (Hardebeck et al., 2004; Treiman et al., 2004).

Strong Ground Motion

The first automatic CISN ShakeMap was posted on the web 8 minutes after the event based on only 29 stations contributing (Gee et al., 2004). The distribution of CISN strong motion stations in the area is shown in Fig.1. It clearly demonstrates the fact that there are not enough digital stations in the area. The updated versions of the instrumental intensity and peak ground acceleration maps are shown in Fig. 2 and 3.

Strong-motion data for engineering applications after major earthquakes are distributed via the Internet Quick Report (IQR) through the CISN Engineering Data Center. San Simeon earthquake strong-motion data recorded by modern digital instruments were made available through the CISN Engineering Data Center at <http://www.cisn-edc.org> on the day of earthquake (Fig. 4).

The San Simeon earthquake was recorded at more than 100 strong motion stations out to distances of over 300 km, though with relatively few stations at less than 50 km distance. The Internet Quick Report lists the 98 records recovered so far and their peak values and distances. It also provides links to station information, and allows downloading digital data. Many of strong motion stations that recorded this earthquake are the early film recorders, and the films have been developed and scaled. For film records, only peak acceleration is listed. The film records from the three stations (San Antonio Dam, Lopez Lake, and Point Bouchon) have already been digitized and processed, and made available for view and download through the IQR.

The three stations closest to the epicenter recorded peak ground accelerations of:

- 0.18 g at Cambria (Fig. 5)
- 0.12 g at San Antonio Dam
- 0.48 g at Templeton (Fig. 6)

All three stations are operated by the California Geological Survey (CGS) Strong Motion Instrumentation Program. Comparison of the records at Cambria (Fig. 5) and at Templeton (Fig. 6) show significantly higher accelerations and velocities at Templeton due to the directivity in rupture propagation. Data shows apparent strong directivity in the direction of the rupture propagation, from the epicenter toward the ESE (toward Templeton) (Boatwright & Seekins, 2004; Shakal et al., 2004).

The largest recorded shaking was at an instrumented 1-story hospital in Templeton, about 38 km SE of the epicenter (though much closer, about 16 km to the projected southern end of the rupture). The record at the 1st floor of the Templeton Hospital and response spectra compared to

UBC are shown in Figure 6 and 7. The response spectra in Figure 7 show that shaking was low energy, with strongest shaking exceeding UBC only at high frequencies. A peak value of 1.3 g was recorded at the roof of the hospital (1-story, wood-frame construction). Reports indicate little structural damage in the hospital, an important outcome. The ground level of the hospital is a good indication of the shaking in the vicinity, because the hospital is small and light.

After the earthquake a free field station (Templeton Hospital Ground) was reinstalled near the Templeton Hospital. Newly obtained records of 8 aftershocks at Templeton Hospital Ground demonstrate in average 1.37 (Standard Deviation $SD = 0.37$) higher peak ground acceleration than at the first floor of the hospital. Peak ground velocity was in average 1.18 higher ($SD = 0.20$). This suggests that most likely peak ground acceleration during the San Simeon earthquake in Templeton area was about 0.66 g with the corresponding peak ground velocity of about 39 cm/sec. Templeton is about 10 km from Paso Robles, where significant damage occurred.

Some of the next closest records are from the Parkfield area, with peak acceleration of 0.23 g at the Cholame 12W station (this station is closest to Paso Robles). The Parkfield Array, operated by CGS, recorded peak accelerations that ranged from 0.04 to 0.23 g, very similar to the range observed for the 1983 M 6.5 Coalinga earthquake.

Ground Motion Attenuation

A comparison of the peak acceleration data (103 data points) vs distance to the fault with that predicted by the Boore-Joyner-Fumal (BJF97, Boore et al., 1997) attenuation relationship is shown in Figure 8. The distances range from 12 km, for the Cambria station, to many stations at distances of over 250 kilometers. The data shows reasonable agreement with BJF97 in its applicable range. Coefficients for a reverse fault and an average shallow V_s of 700 m/sec were used; the thin line indicates distances beyond the suggested limit of the authors, 80 km. Beyond that, higher attenuation with distance than predicted by the extrapolated BJF97 curve is indicated. These new data, and other recent data from digital instruments, allow extending the existing relationships to greater distances.

The point above the BJF97 curve at about 16 km is Templeton, which had 0.48g, the largest value recorded in this earthquake; lying above the curve is consistent with directivity-increased shaking in the rupture direction. The two closest stations, Cambria and San Antonio Dam, both plot below the curve, consistent with directivity-reduced values in the direction away from the rupture.

Finite-Source Modeling

Finite-source modeling provides information about the length, width, average slip and when coverage is sufficient the detailed slip distribution and rupture kinematics (timing). These source parameters are important for better understanding source influences on near-fault strong ground motion. There are many different methods for the determination of this information. The method developed by Hartzell and Heaton (1983) has been used in various forms in numerous papers of the peer-reviewed literature, and today it is common to combine seismic, geodetic and

surface slip data to obtain greater constraint on the rupture process (e.g. Kaverina et al., 2002). Recently a method for the realtime determination of finite-source parameters was developed by Dreger and Kaverina (2000). A similar approach (Kuge et al. 2003) has been developed for Japan. The method outlined by Dreger and Kaverina (2000) was used to analyze strong ground motions recorded for the 22 December 2003 Mw6.5 San Simeon earthquake. The obtained finite-source information was used to update the ShakeMap the day of the earthquake compensating for the lack of near-fault observations of strong ground motions (Dreger et al., 2004).

For the past two years the Berkeley Seismological Laboratory has been operating a realtime finite-source method patterned after the approach outlined in Dreger and Kaverina (2000). Figure 9 illustrates the steps in this method. First a location and magnitude are determined from the dense short-period network operated by the USGS in Northern California. Second, if the local magnitude exceeds 3.4 then moment tensor software at the BSL is triggered to determine the scalar seismic moment, moment magnitude (M_w) and the focal mechanism. Third, if the event is greater than $M_w5.5$ finite-source inversions are performed to determine which of the nodal planes of the focal mechanism is the rupture plane, the dimensions of the rupture, the slip distribution and the rupture velocity. Details about how the fault model and the assumed rise time are scaled can be found in Dreger and Kaverina (2000). Very rapid line-source calculations and also plane-fault inversions are performed. The final step involves using the derived fault slip model to estimate the near-fault strong ground motions. In ShakeMap model estimates of ground motions from empirical relationships are used for interpolation purposes between the observations. Finite-source information can be used to adjust these empirical relations for directivity in a variety of waves, which include: 1) using source finiteness to calculate the distance to the closest point on the fault instead of to the epicenter, 2) using empirical attenuation relationships adjusted for directivity (e.g. Somerville et al., 1997), and 3) integration of the slip model to generate synthetic near-fault time histories which are then used to determine key ground motion parameters such as PGV, and S_a at 0.3, 1 and 3 seconds period.

The San Simeon earthquake provided the first test of this system, and the results are encouraging. Figure 10 shows the location of the earthquake, the surface projection of fault slip, and the locations of seismic stations and GPS deformation sites used to obtain the updated model. The seismic moment tensor and initial finite-source model for the San Simeon earthquake determined on the day of the earthquake has been published in Hardebeck et al. (2004). The finiteness determined from the analysis described above was used to update the published ShakeMap the day of the event. Figure 11 compares several instrumental intensity (e.g. Wald et al., 1999) ShakeMaps for the event. The top left panel shows the ShakeMap produced with the available M_w . This map suffers from a lack of stations and is therefore controlled by estimated ground motions from empirical attenuation relations and site corrections. The top right panel shows the map in which the finite-source information was used to adjust the distance measure so that it was to the closest point to the fault. The finite-source modeling described below indicated that the event extended about 25 km to the SE of the epicenter (shown as the thick line on the ShakeMap). This addition greatly increased the area of large instrumental intensity and also shifted large instrumental intensity to the SE to Paso Robles consistent with where most of the damage was concentrated. Directivity also played an important role in the elevation of ground motions to the SE. The finite-source model used to infer source dimensions for ShakeMap on the day of the earthquake is published in Hardebeck et al. (2004).

The current ShakeMap is shown in the bottom right panel. In this map the finite-source extent and also near-fault strong motion observations were combined. This map compares closely with the initial finite-source map (without near-fault observations, top right) and the final map without the finite-source constraint (bottom left). Thus the addition of finite-source information at a time when near-fault strong motion recordings were not yet available resulted in a ShakeMap much closer to the truth than the initial map without the data. It is notable that even with the near-fault strong motion stations the finite-source extent contributes significantly to the ShakeMap and likely gives a truer estimate of the near-fault shaking given the relatively sparse instrumental coverage.

We have refined the finite-source model for the event by incorporating additional seismic stations, adding GPS deformation data, and testing the rupture velocity and rise time parameter space. The updated model shown in Figure 12 is for a rupture velocity of 2.6 km/s and utilizes 6 time windows following the method of Hartzell and Heaton (1983) to account for rupture velocity and rise time variability during the rupture process. As Figure 12 shows the slip is generally shallower than the hypocenter with the peak slip occurring in the 8 to 4 km range. The lateral extent of slip is much greater with a total length of about 30 km to the SE of the hypocenter inferred from the model. This is an unusual slip aspect ratio for a dip-slip earthquake. Figure 13 shows the fit to the seismic waveform data, which is found to be very good, and as shown on Figure 10 the fit to the GPS data is also very good. Using this slip model the velocity time histories for Templeton, CA site were simulated and are compared to the observations in Figure 14. The rock synthetics were site adjusted for the low surficial velocities at the Templeton station. Although Templeton was not used to derive the slip distribution the predicted motions compare very favorably with the observations in terms of both peak amplitudes and waveform.

The derived slip distribution was also used to compute a synthetic rock motion peak ground velocity (PGV) ShakeMap which is shown in Figure 15a for the actual model, and in Figure 15b for a model assuming that the slip occurred on a vertical strike-slip fault. This simulation shows that while directivity in the San Simeon earthquake was indeed important in elevating the ground motions to the SE of the epicenter and ruptured fault, the directivity was relatively mild. The hypothetical vertical strike-slip earthquake would have produced peak velocities as much as a factor of three larger at some sites, extended the region of high ground velocity (greater than 10 cm/s) tens of kilometers further to the SE, and increased the ground area experiencing greater than 10 cm/s peak velocity 4-fold.

Results

A comparison of the peak ground acceleration vs distance to the fault with that predicted by the BJF97 attenuation relationship shows reasonable agreement in its applicable range. Beyond 80 km from the fault, higher attenuation with distance than that predicted by the extrapolated BJF97 curve is indicated. These new data, and other recent data from digital instruments, allow extending the existing relationships to greater distances.

Significant directivity in ground motion due to rupture propagation to southeast toward Paso Robles & Templeton was observed in strong motion data, and matches concentration of damage SE of the epicenter.

The combined inversion of GPS and seismic waveform data for the kinematic rupture process of the San Simeon earthquake reveals an elongated rupture over a narrow, shallow depth range. While directivity was also a factor in the strength of the ground motions comparative simulations between the deep-slip case and a hypothetical strike-slip case reveals that a $M_w 6.5$ strike-slip event with identical slip distribution would result in about 3-4 times increase in PGV.

Acknowledgements

The authors highly appreciate contribution of A. Shakal, M. Huang, H. Haddadi, K.W. Lin, C. Petersen, A. Cramlet and P. Roffers. Douglas Dreger would like to acknowledge support received from the USGS, PG&E and the CEC through the PEER lifelines program to develop the automated finite-source method.

References

- Boatwright J., Seekins L.C. (2004). Directivity in the near-field and regional recordings of the 22 December 2003 San Simeon earthquake. *Seismological Research Letters*. V. 75, No. 2, 265.
- Boore, D. M., W. B. Joyner and T. E. Fumal (1997). Equations for estimating horizontal response spectra and peak acceleration from western North American earthquakes: A summary of recent work. *Seismological Research Letters*. V. 68, No. 1, 128-153.
- Dreger, D. S. and A. Kaverina (2000). Seismic remote sensing for the earthquake source process and near-source strong shaking: a case study of the October 16, 1999 Hector Mine earthquake, *Geophys. Res. Lett.*, 27, 1941-1944.
- Dreger, D. S., P. Lombard, J. Boatwright, D. J. Wald and L. S. Gee (2004). Finite source models of the 22 December 2003 San Simeon earthquake and applications to ShakeMap, *Seismo. Res. Lett.*, 75, 293.
- Gee L., Oppenheimer D., Shakal T., Given D., Hauksson E. (2004). Performance of the CISN during the 2003 San Simeon earthquake. CISN Report at http://www.cisn.org/docs/CISN_SanSimeon.pdf
- Hardebeck J.L., Boatwright J., Dreger D., Goel R., Graizer V., Hudnut K., Ji C., Jones L., Langbein J., Lin J., Roeloffs E., Simpson R., Stark K., Stein R., and J. Tinsley (2004). Preliminary report on the 22 December 2003, M 6.5 San Simeon, California Earthquake. *Seismological Research Letters*. V. 75, No. 2, 155-172.
- Hartzell, S. H., and T. H. Heaton (1983). Inversion of strong ground motion and teleseismic waveform data for the fault rupture history of the 1979 Imperial Valley, California, earthquake, *Bull. Seism. Soc. Am.*, 73, 1553-1583.

Hauksson E., Oppenheimer D. (2004). Preliminary 3D Vp model for the 2003 M_w 6.5 San Simeon mainshock – aftershock region. *Seismological Research Letters*. V. 75, No. 2, 265.

Jennings C.W. (1994). Fault activity map of California and adjacent areas, with locations and ages of recent volcanic eruptions. *California Division of Mines and Geology, Geologic Data Map No. 6, map scale 1:750,000*.

Kaverina, A., D. Dreger, and E. Price (2002). The combined inversion of seismic and geodetic data for the source process of the 16 October, 1999, Mw7.1 Hector Mine, California, earthquake, *Bull. Seism. Soc. Am.*, 92, 1266-1280.

Kuge, K. (2003). Source modeling using strong-motion waveforms: toward automated determination of earthquake fault planes and moment-release distributions, *Bull. Seism. Soc. Am.*, 93, 639-654.

Shakal A., Graizer V., Savage W., Stephens C. (2004). Preliminary analysis of strong-motion data from the M 6.5 San Simeon earthquake of 22 December 2003. *Seismological Research Letters*. V. 75, No. 2, 265.

Treiman J.A, Tinsley J.C., Rosenberg L.I., Keefer D.K, Knudsen K.I., Loyd R.C., Manson M.W., McCrink T.P., Reid M.E., Schmidt K., Wilson R.I. (2004). Surface effects of the 22 December 2003 Mw 6.5 San Simeon earthquake. *Seismological Research Letters*. V. 75, No. 2, 264.

Wald, David J., Vincent Quitoriano, Thomas H. Heaton, Hiroo Kanamori, Relationships between Peak Ground Acceleration, Peak Ground Velocity and Modified Mercalli Intensity in California, *Earthquake Spectra*, **15**, 557-564

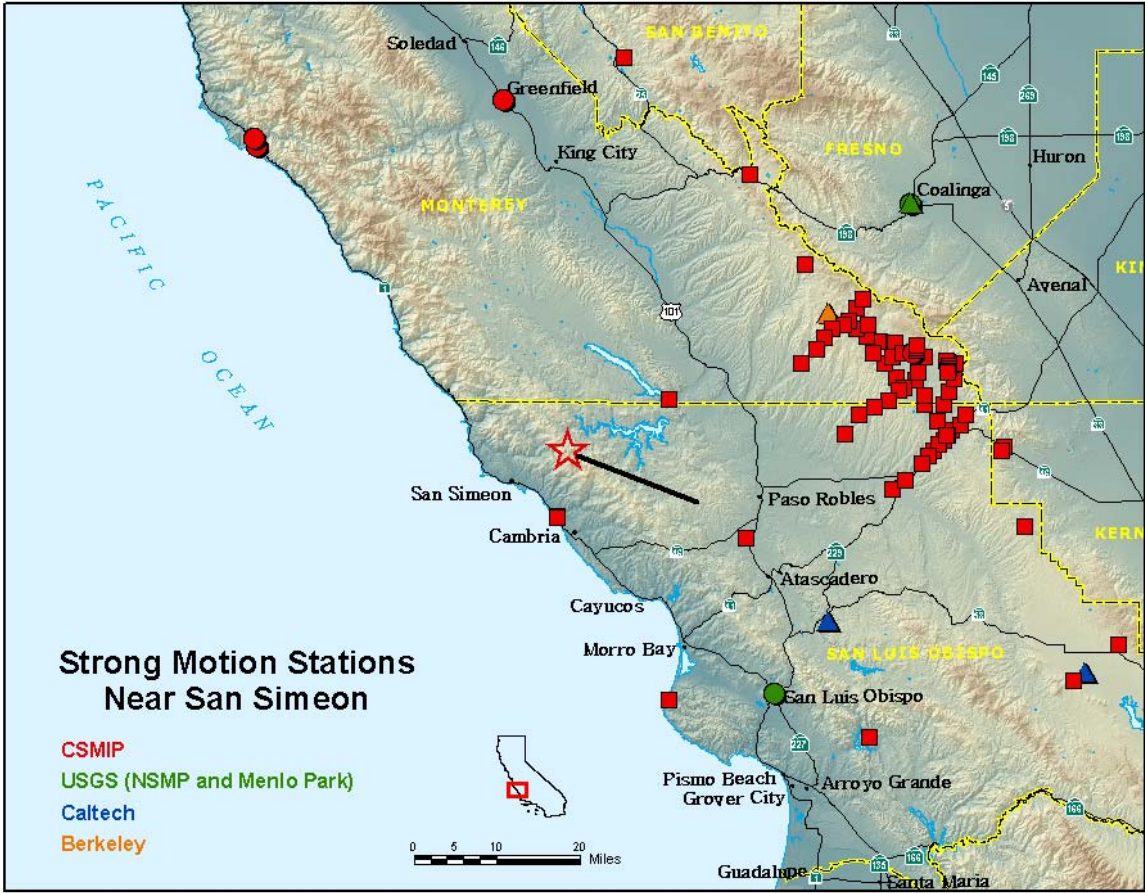


Figure 1. CISN strong-motion stations in San Simeon area.

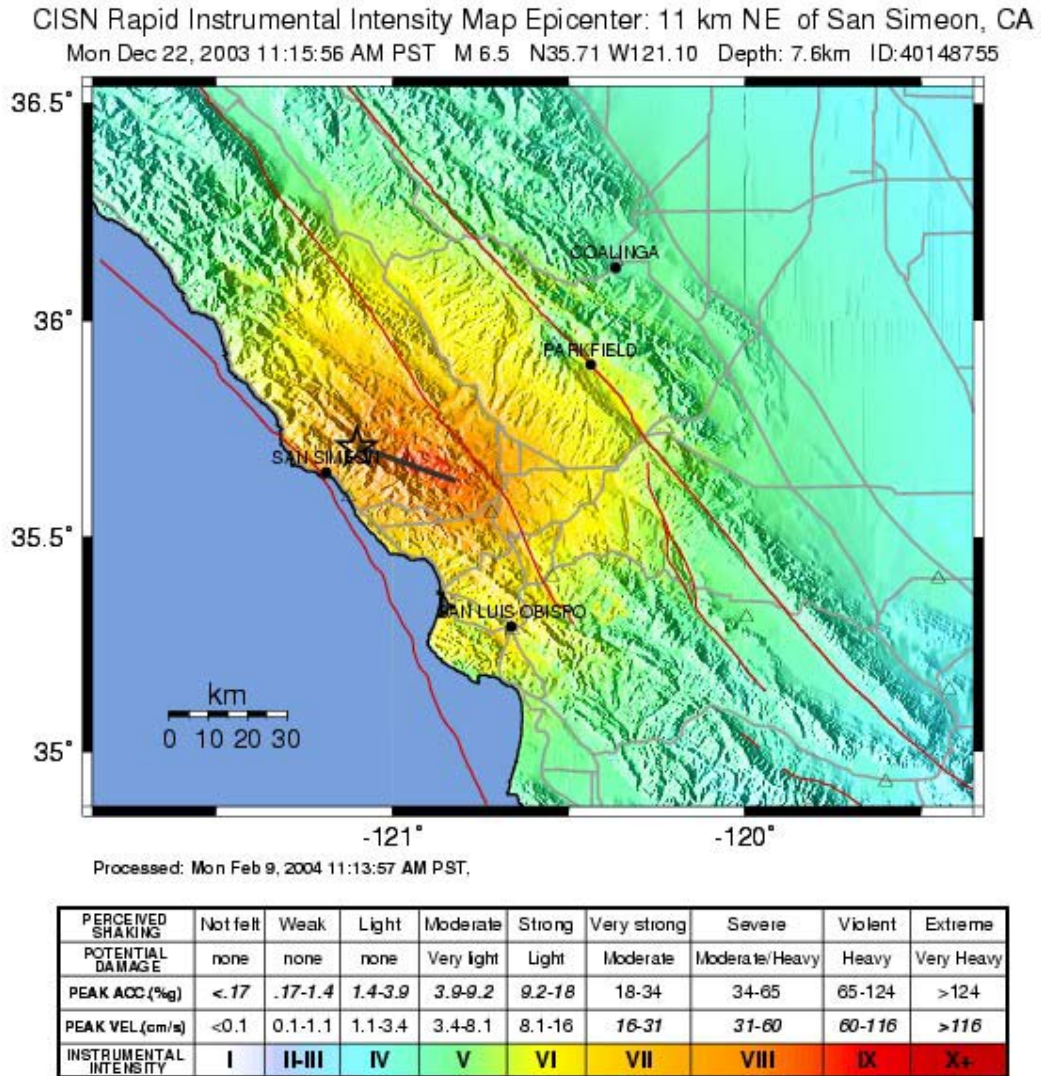


Figure 2. Instrumental Intensity ShakeMap for the M6.5 San Simeon earthquake.

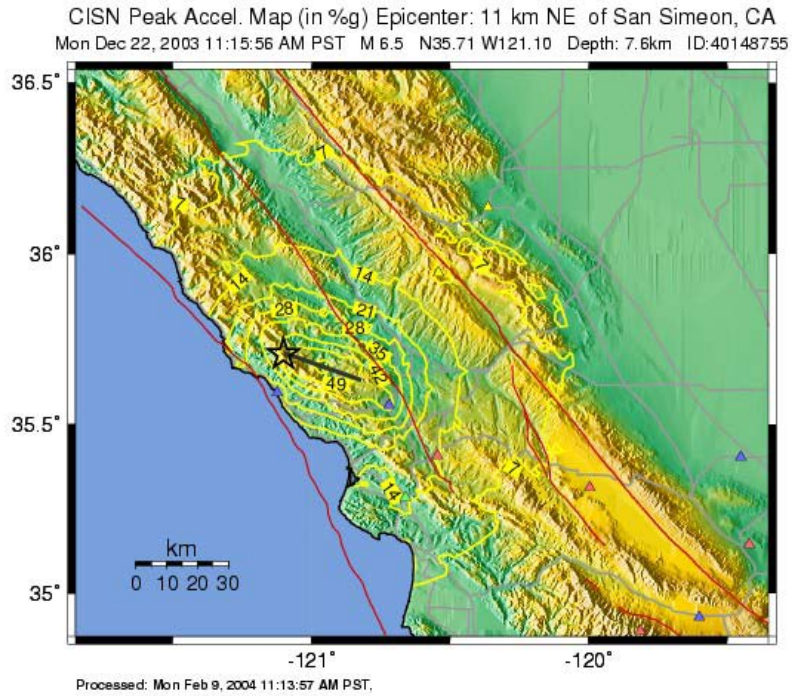


Figure 3. Peak ground acceleration ShakeMap for the San Simeon earthquake.

San Simeon Earthquake of 22 Dec 2003, 11:15:56 AM PST, 6.5Mw - Microsoft Internet Explorer

Address: http://www.quake.ca.gov/cisn-ed/IQR/SanSimeon_22Dec2003/iqr_dist.htm

CISN Internet Quick Report
 Strong-Motion Data Set For

San Simeon Earthquake of 22 Dec 2003
 6.5 ML, 11:15:56 AM PST, 35.706N 121.102W Depth 7.6km.

Earthquake Information: [Update/Data Highlights](#) [Hypocenter](#) [ShakeMap](#)

Stations listed in increasing **Epicentral Distance** (Alternatively, select [alphabetical listing](#))

Table Last Updated: 05 Apr 2004 12:37

Station Name	Station No./ID	Network	Dist. (km)	Horiz Apk (g)		View	Download
				Ground	Struct.		
Cambria - Hwy 1 Caltrans Bridge Grnds	37737	CGS	13	.179	--	<input type="radio"/>	<input type="radio"/>
San Antonio Dam	36258	CGS	22	.12	.22	<input type="radio"/>	<input type="radio"/>
Templeton - 1-story Hospital	36695	CGS	38	.483	1.28	<input type="radio"/>	<input type="radio"/>
Parkfield - Vineyard Canyon 6W	36441	CGS	49	.09	--	<input type="radio"/>	<input type="radio"/>
Point Buchon - Los Osos	36427	CGS	52	.089	--	<input type="radio"/>	<input type="radio"/>
Parkfield - Vineyard Canyon 5W	36440	CGS	52	.06	--	<input type="radio"/>	<input type="radio"/>
Parkfield - Vineyard Canyon 4W	36446	CGS	55	.04	--	<input type="radio"/>	<input type="radio"/>
Parkfield - Vineyard Canyon 3W	36176	CGS	57	.09	--	<input type="radio"/>	<input type="radio"/>
Parkfield - Vineyard Canyon 2W	36447	CGS	59	.07	--	<input type="radio"/>	<input type="radio"/>
Parkfield - Fault Zone 15	36445	CGS	61	.06	--	<input type="radio"/>	<input type="radio"/>
San Luis Obispo - Rec Ctr	01083	USGS	62	.165	--	<input type="radio"/>	<input type="radio"/>
Parkfield - Fault Zone 9	36443	CGS	62	.08	--	<input type="radio"/>	<input type="radio"/>
Parkfield - Fault Zone 14	36456	CGS	62	.09	--	<input type="radio"/>	<input type="radio"/>
Parkfield - Vineyard Canyon 1E	36455	CGS	63	.10	--	<input type="radio"/>	<input type="radio"/>

Figure 4. CISN Internet Quick Report for the San Simeon earthquake.

SMIP04 Seminar Proceedings

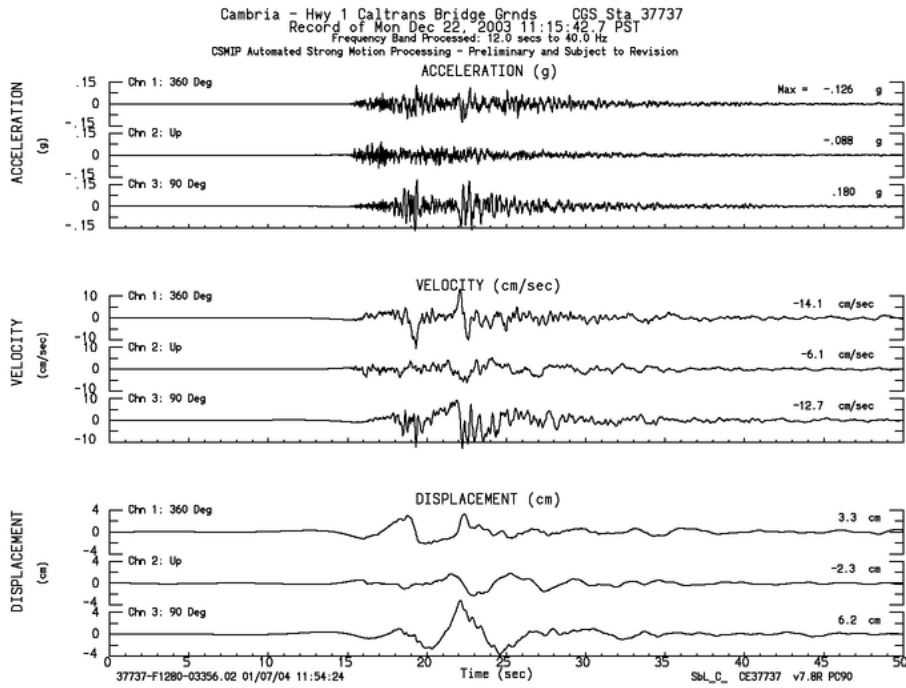


Figure 5. Acceleration, velocity and displacement recorded in Cambria during the San Simeon earthquake.

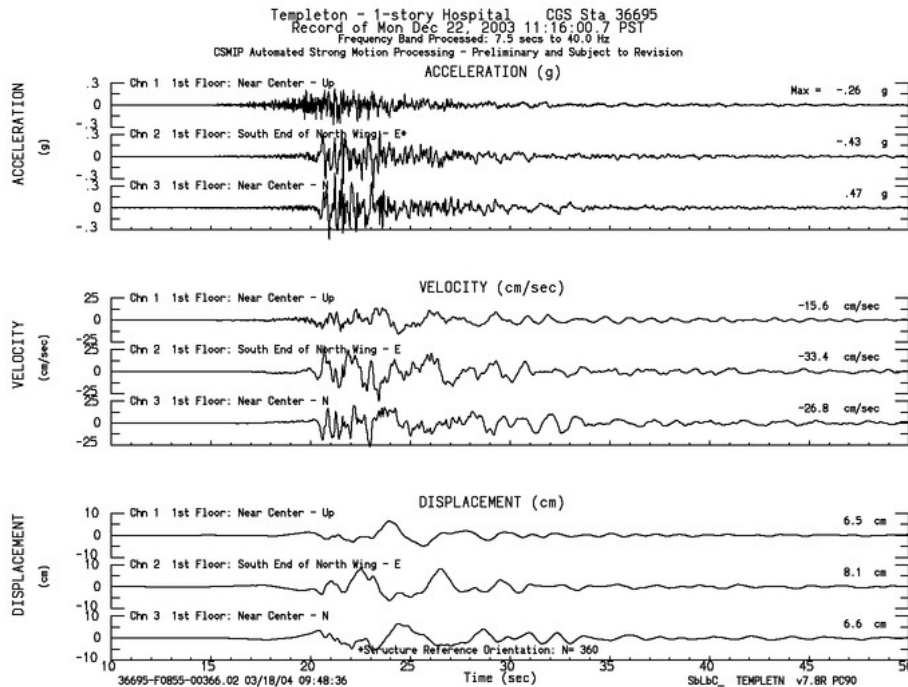


Figure 6. Acceleration, velocity and displacement recorded at the 1st floor of the one-story Templeton Hospital.

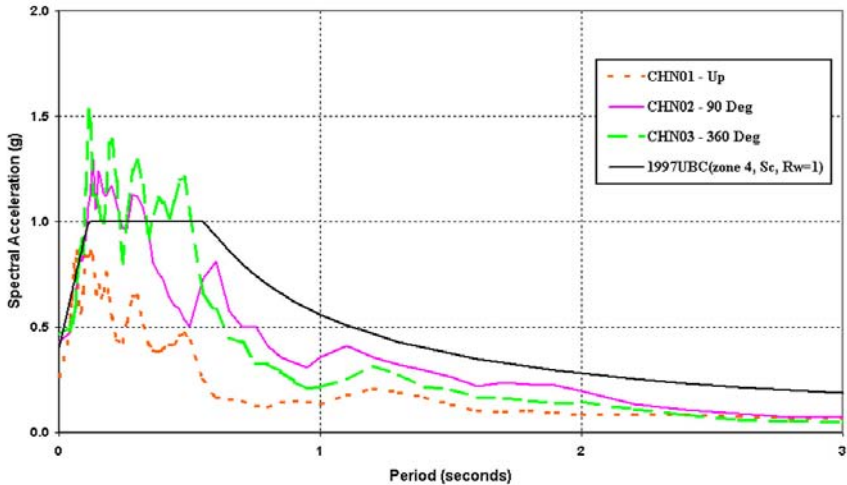


Figure 7. 5% damped response spectra for the 1st floor channels of the Templeton Hospital compared to the Universal Building Code (UBC). Figure courtesy of M. Huang.

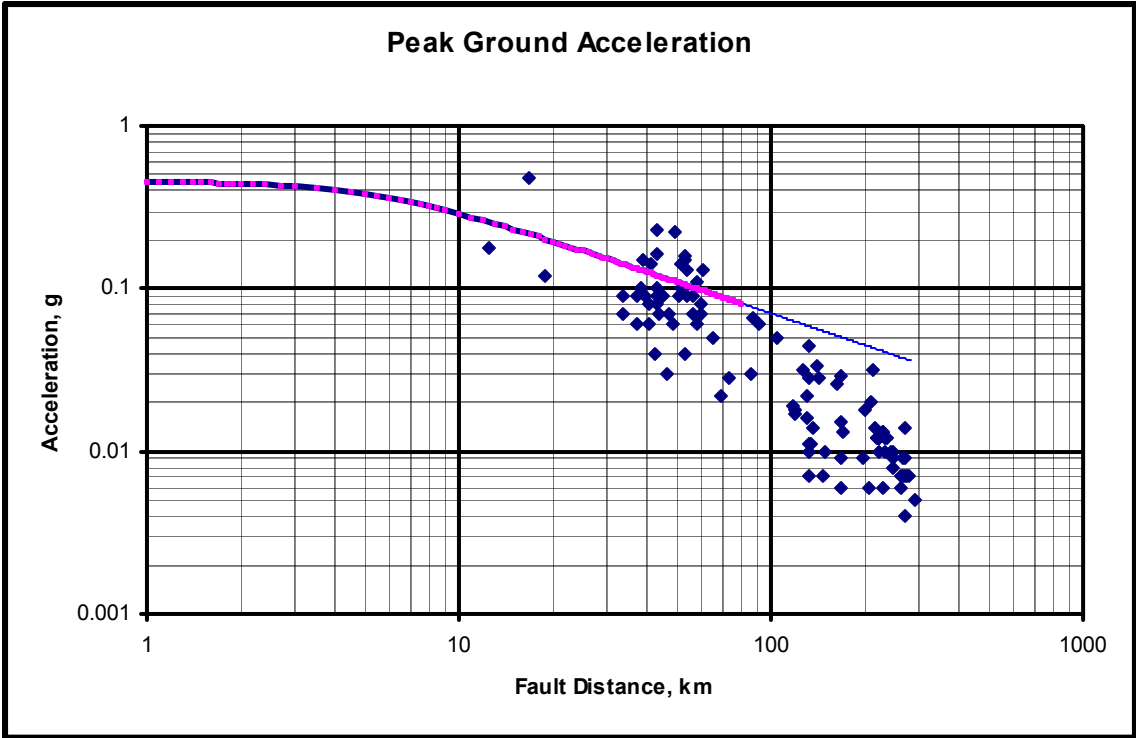


Figure 8. Peak horizontal ground acceleration data plotted against the distance to the fault, and the Boore-Joyner-Fumal (BJF97, Boore et al., 1997) attenuation relationship. The data shows reasonable agreement with BJF97 in its applicable range of 80 km. Beyond that, higher attenuation with distance than predicted by the extrapolated BJF97 curve is indicated (the thin line indicates distances beyond the suggested limit of the authors).

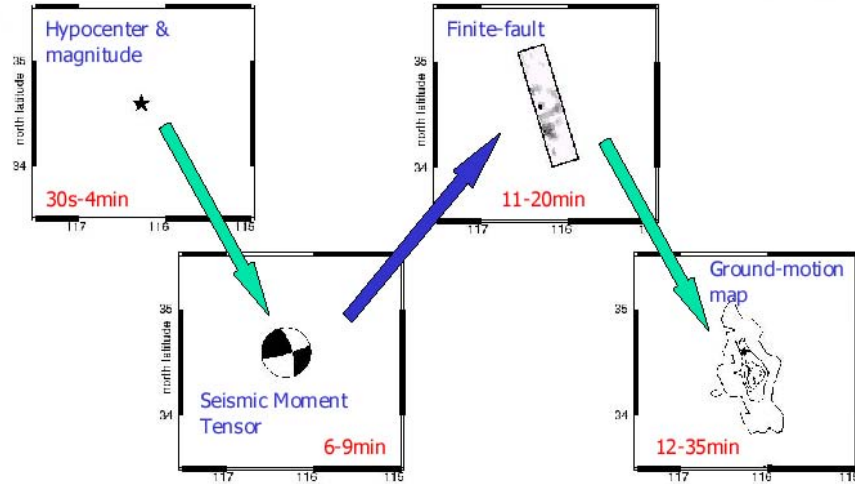


Figure 9. Illustration of automatic processing system at Berkeley. The times shown are elapsed time from the event origin time. In the last panel near-fault ground motions are simulated from the slip distribution.

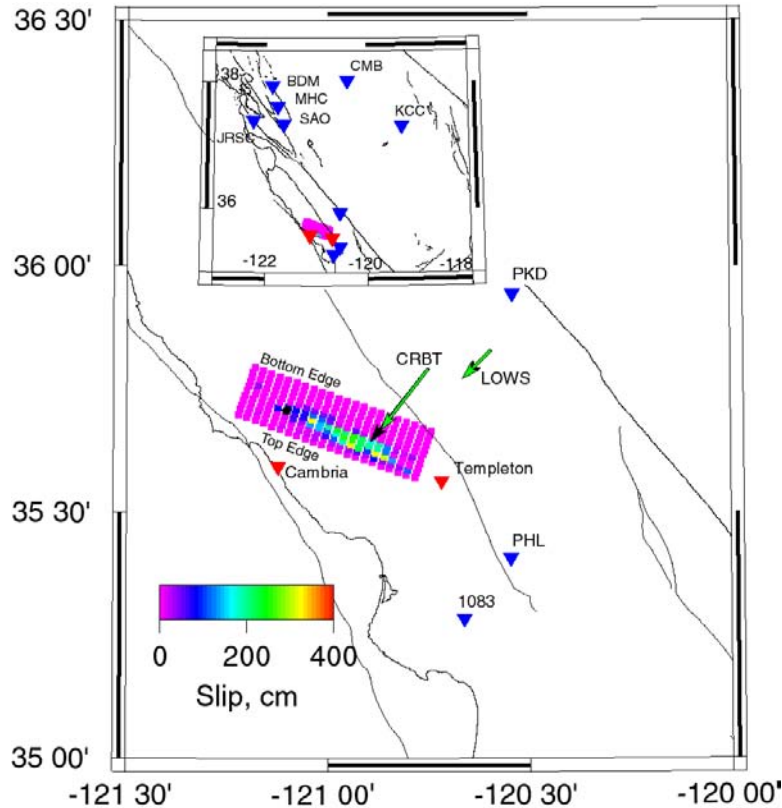


Figure 10. Location map and map-view projection of fault slip. The epicenter is marked by the black circle. Seismic stations used to determine the fault slip are shown as the blue inverted triangles. The red inverted triangles are for sites that have been used to test forward predictions of ground motions from the derived model. Observed GPS deformation (black arrow) at two near-fault sites are compared to predictions (green arrows) from the model. Slip extends about 30 km to the SE toward Templeton and Paso Robles. This source finiteness and a SE directivity contributed to the large motions recorded at Templeton and the damage at Paso Robles.

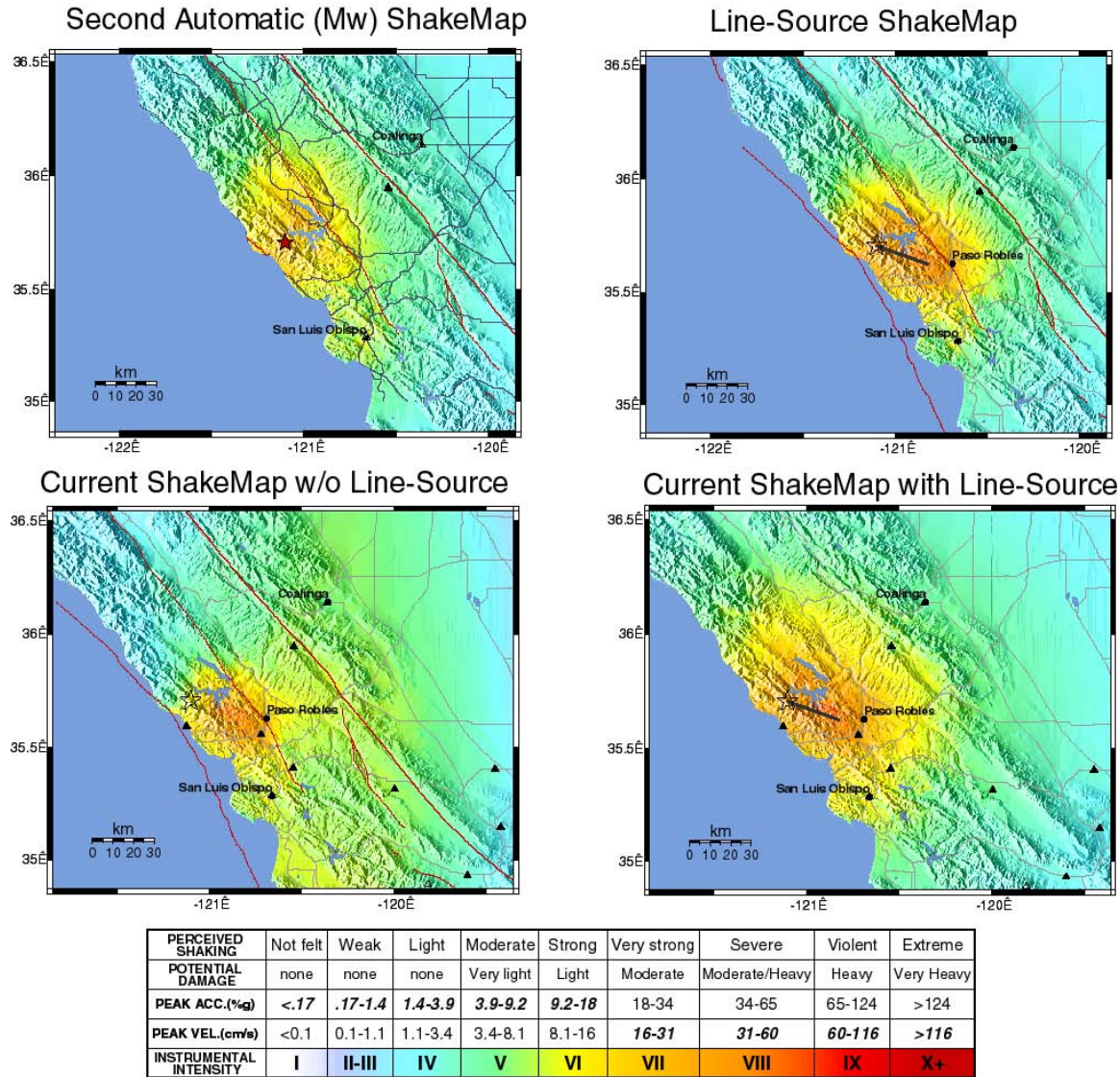


Figure 11. Automatic instrumental intensity ShakeMap (top left). Finite fault adjusted ShakeMap (top right). The line shows the extent of fault rupture used to calculate the distance to the fault in the calculation of the ShakeMap. Note the lack of near-fault, realtime strong motion stations in the affected area. The most up to date ShakeMap (current map), which includes available near-fault ground motion values is shown in the lower right panel. The lower left panel shows the current map without the source finiteness component. A comparison of the top right and lower left panels illustrates that the addition of finite-source information greatly improved the ShakeMap in the near-fault and damage zones in the absence of near-fault ground motion information. Furthermore the finite-source adjusted map is a much truer estimate of ground motion than the automatic map based only on Mw, distant recordings and empirical ground motion estimates.

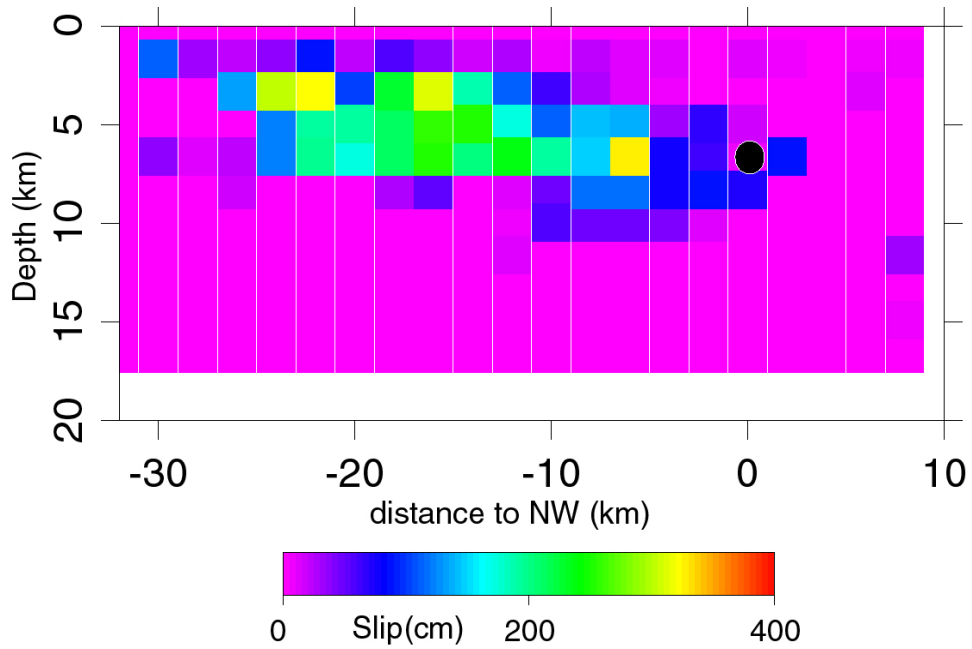


Figure 12. Fault slip. Slip is shallower than the hypocenter (black circle), peaked in the 8 to 3 km depth range, and extends 25 km to the SE of the hypocenter.

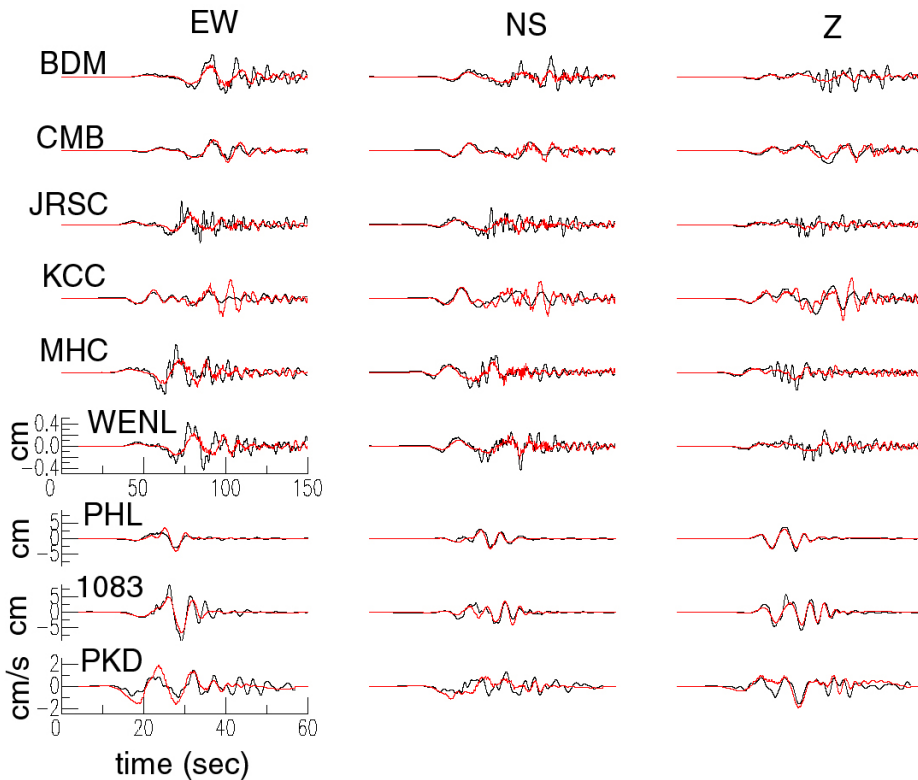


Figure 13. Observed displacement and velocity (black traces) are compared to synthetics (red traces) constructed for the model shown in Figure 4. The data and synthetics are broadband with a high pass filter at 0.01 Hz and a nyquist frequency of 5 Hz.

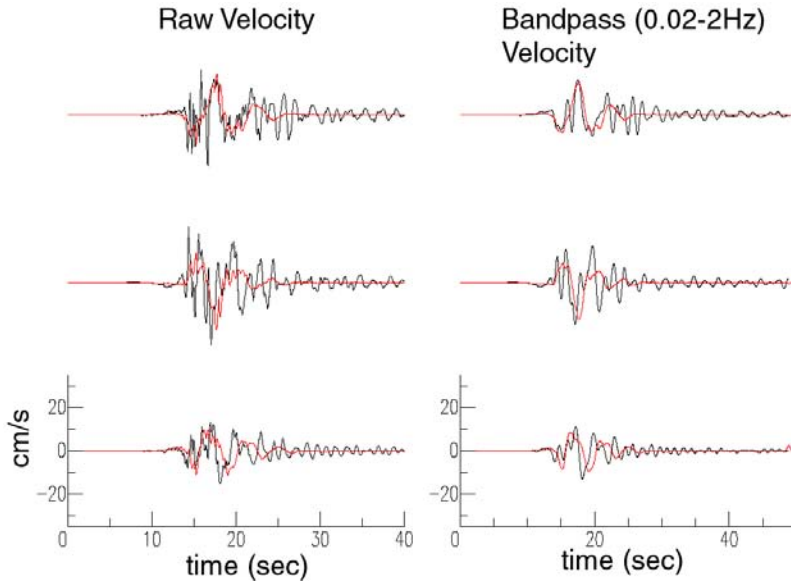


Figure 14. Observed (black) and predicted (red) ground velocity at the Templeton site. The hard rock synthetics were site-corrected.

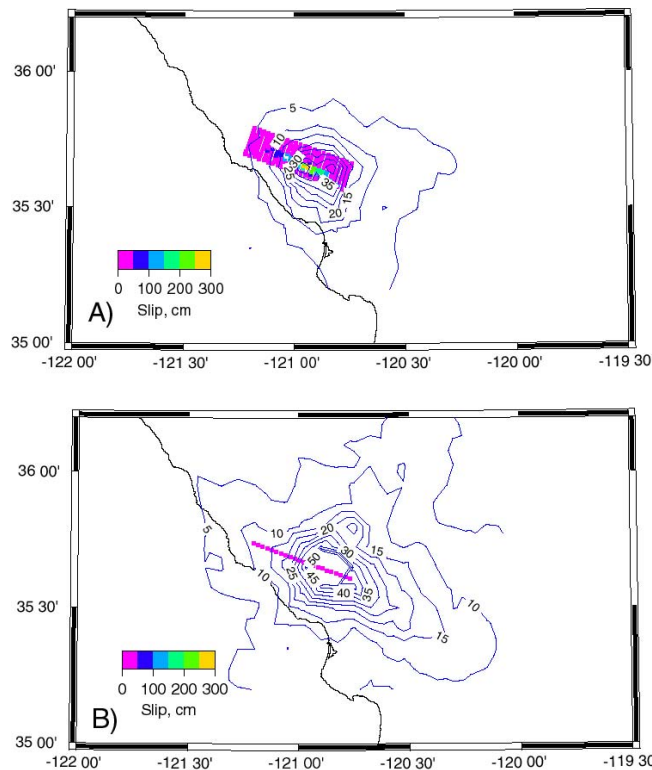


Figure 15. Simulated peak ground velocity in cm/s for the San Simeon earthquake slip model (a), and a hypothetical vertical strike-slip fault (b). In each case an identical slip distribution and slip time history was assumed. The only difference is the orientation of the plane and the direction of the slip (perpendicular to strike in (a), and parallel to strike in (b)). The Green's functions that were used is for a represented hard rock model for the region. This plot illustrates that the laterally extending dip-slip rupture of the San Simeon earthquake produces a relatively mild directivity effect compared to a vertical strike-slip fault in the same place.

**SEISMIC ANALYSIS OF THE SYLMAR INTERSTATE 5 AND HIGHWAY 14
CONNECTOR BRIDGE**

Robert K. Dowell

Dowell-Holombo Engineering, Inc.
Department of Structural Engineering
University of California, San Diego

Abstract

This paper presents measured and analysis time-history results of the heavily instrumented 10-span North Connector Bridge (53-2795F) at the 5/14 Interchange, subjected to the M7.1 Hector Mine earthquake. Relatively simple spine and more detailed shell element models were developed. Measured base motions were used as input for the finite element models, with absolute and relative superstructure displacement time-histories compared to measured responses. Results show that 5% equivalent viscous damping is realistic, as is the concrete strength of 5 ksi. It was found that the rotational mass inertia of the superstructure is an important quantity for spine models of single-column-bent bridges.

Introduction

The California Strong Motion Instrumentation Program (CSMIP) has been measuring the behavior of bridges subjected to earthquakes for several years, allowing researchers and practitioners to better understand the (1) seismic behavior of various types of bridge structures and (2) capabilities of their analysis tools to properly model the seismic response of bridges. The end result is improved seismic bridge design and analysis, with increased safety against structural failure and associated loss of life, as well as significant savings to the State from more efficient designs. The State of California has instrumented over 60 bridges, providing measured accelerations at various locations on the structure and in its vicinity. Displacement and velocity time-histories are determined from integrating and filtering measured accelerations. Herein the term “measured” is applied to recorded accelerations as well as to velocities and displacements that were derived from these accelerations. Strictly speaking, however, only the accelerations were measured. In this project, the focus is on the seismic response of a single prestressed concrete, box-girder connector bridge, discussed in the following.

The 1582 ft long, 10-span, 5/14 North Connector Bridge (Bridge No. 53-2795F) has been heavily instrumented with 42 sensors that measure seismic accelerations at various locations on and below the bridge, including the (1) superstructure, (2) abutments and (3) columns. Sensors were also placed 91 ft below ground in the large-diameter CIDH shaft of Bent 7 and at a free-field location adjacent to Abutment 1. In the time since the bridge was constructed and instrumented in 1994, several small earthquakes produced large enough accelerations to automatically turn on, or trigger, the instrumentation and begin recording data. Once triggered, all of the instrumentation is activated and recorded for the duration of the earthquake.

For the North Connector Bridge, three earthquakes are listed in the CSMIP database. Of these records, only the Magnitude 7.1 Hector Mine Earthquake was considered as it resulted in 50 times larger structure displacements than the other two earthquakes. This earthquake occurred on October 16, 1999 with the epicenter 47 miles ESE of Barstow. Various photographs showing different views of the connector bridge and 5/14 Interchange are given in Figures 1 through 4.

The purpose of this study is to use the measured strong motion data of the 2-frame, 10-span connector bridge to determine how well the seismic behavior of a long connector bridge can be captured by a global bridge analysis model and to determine what level of sophistication is required in the analysis (spine model versus shell model). Several studies have focused on the 2-span Painter Street Bridge [1], but this is the first study to compare measured and analysis results of a much longer, single-column-bent connector bridge. Initially, the complete structure was modeled with beam elements and compared to measured results. A more detailed structural model was then developed that consisted of shell elements for the superstructure and bent caps with beam elements for the columns and large-diameter shafts.

Measured data and analysis model results demonstrate that the two bridge frames are uncoupled from each other due to the unique expansion joint between frames (Figure 4). This allowed the shell model to be developed for only one frame, without any loss in accuracy, in order to compare its behavior to both measured and spine model results. As Frame 1 spine model results compared well to measured behavior, and more sporadic comparisons were found for Frame 2 due to soft soil at three of the bents in this frame, it was decided that little would be gained by modeling Frame 2 with shell elements. Therefore, a more detailed shell model was developed for Frame 1 only, with no loss of accuracy by not including both frames in the model.

Typically, an expansion joint is placed at the approximate dead load point-of-inflection in a span (about 20% of the total span length), with the result that the long span sits on a hinge seat provided by the short span. Since the previous bridge at this site failed by unseating of the long span at the hinge, the new hinge detail has two closely spaced columns at Bents 5 and 6, with short cantilever spans that do not touch at the middle, resulting in a several inch gap between frames and no shear transfer between them (Figure 4). Thus it is not possible for this bridge to have failure from unseating of a span at the hinge, since neither span is supporting the other. As the bridge displacements were relatively small from the Hector Mine Earthquake, the frames never came into contact. Measured time-history results on both sides of the hinge clearly show this, with adjacent frames moving independently of each other at different natural periods. It is important to note, however, that while the frames did not contact each other in the Hector Mine Earthquake, they will bang into each other when subjected to larger and/or closer earthquakes in the future.

Instrumentation

Instrumentation locations for the bridge are given in Figure 5. For the North Connector Bridge, 42 channels of acceleration data were recorded from the Hector Mine Earthquake. This provided valuable measured data of transverse bridge response at each bent, as well as longitudinal and transverse responses at both abutments and the base of some of the columns.

Vertical behavior was recorded at several locations. Measured displacements at the abutments and the base of Bent 5 were used to develop unique input motions for all of the supports in the analysis models.

Computational Models

Spine Model

For seismic bridge design the basic analysis tool is a spine model that represents the bridge superstructure, columns and shafts with beam elements positioned along the centroid of each member (Figure 6). For the North Connector Bridge, a series of beam elements were used to model the prestressed concrete, multi-cell box girder superstructure. Due to the 3-D nature of the curved bridge and applied loading, 3-D beams were required which have 3 translational and 3 rotational displacement degrees-of-freedom at each end, for a total of 12 degrees-of-freedom for each beam element. General beam sections are defined by their area and inertia in both principal directions as well as the torsional constant. For the spine model these section properties were calculated by hand as the SAP computer program [2] could not generate them automatically, as it can for many other shapes. In addition, the section description requires that the concrete material property be given, allowing distributed mass and weight to be automatically included. The general-purpose finite element program SAP2000, Version 8 [2] was used for all analyses presented in this paper.

From comparing time-history analyses and measured results it was determined that the unconfined concrete strength was 5 ksi at the time of the measured earthquake. This is a reasonable increase to the 28-day concrete strength of 4 ksi listed on the bridge plans for the superstructure, columns and shafts, and matches the Caltrans recommended value for seismic analysis and design [3]. As discussed later, however, only after fully developing the shell model, and comparing these results to spine model and measured results, was it realized that the modulus of elasticity must be larger than the ACI value [4] for an unconfined concrete strength of 5 ksi.

The ACI modulus of elasticity [4] is based on a secant stiffness through 50% of the concrete strength. However, for this analysis the initial modulus of elasticity is required rather than the standard ACI value due to the nonlinear stress-strain curves of concrete and the low concrete stresses from the earthquake. The initial modulus is reported in [5] to be about 10% higher than the ACI value [4]. Thus the modulus of elasticity used in all reported analyses is 10% higher than the ACI value based on a 5 ksi concrete. Concrete weight is taken as 150 pcf and unit mass is this weight divided by gravity of 32.2 ft/s².

Initially, modal and time-history results did not match between the spine and shell models. To better understand these initial, and unexpected, differences, separate breakout spine and shell models were developed of a single, straight, box-girder span. This allowed modes shapes, mass distribution and stiffness characteristics to be compared more directly. It was found that mass and stiffness values of the breakout models agreed well, but that there were large differences in the modal behavior; no torsional mode developed for the breakout beam model, whereas this was the primary response of the breakout shell model. This is interesting because

the shell model has only translational mass terms, with no rotational mass included. However, since the mass is distributed across the width and height of the shell model superstructure, rotational mass inertia naturally develops about the centroidal axis of the member, based only on translational mass terms. To verify this, the rotational mass of the box-section was calculated by hand about its centroidal axis and then lumped at each node of the breakout spine model. Results from this analysis showed that the breakout spine model now had the same torsional mode and period of vibration as the breakout shell model.

To more directly compare the behavior of the spine and shell models, a second spine model was developed by eliminating Frame 2 from the original complete spine model (the shell model was developed only for Frame 1). Spine and shell models are shown in Figures 7 and 8. Rotational mass inertia values were computed by hand for each superstructure node and added to the Frame 1 spine model, resulting in similar mode shapes and natural periods as the shell model (see Figure 9 for direct comparisons of Modes 1 through 3). These results demonstrate that the bridge mass, stiffness and boundary conditions have been realistically modeled.

Including rotational mass increases the 1st Mode transverse period of the spine model by 3.4%. Without rotational mass included, the Frame 1 spine model still develops a transverse 1st Mode response. This is because the 1st Mode is a combination of transverse column bending and torsion of the superstructure. Thus the translational mass is also important in this mode. As discussed previously with regard to the breakout spine model, a straight bridge that is constrained to allow a pure torsion mode will not develop this mode and will have no torsion response if rotational mass is not provided. For the Frame 1 spine model this makes some difference, but not nearly as dramatic a difference as with the breakout spine model.

Following initial time-history analyses of Frame 1 it became clear that there were two quantities that still needed to be defined for the connector bridge: The level of equivalent viscous damping and the modulus of elasticity of concrete. Frame 1 was used for these assessments because the shafts are founded in rock and do not have the added unknown soft soil properties at Bents 7, 8 and 9 of Frame 2. Any conclusions about damping and concrete properties found for Frame 1 should be equally valid for Frame 2 and, therefore, are applied to both frames. The multi-support ground input is defined by measured displacements at the abutments and base of Bent 5. Each bent is provided with unique time-history base motions in the global longitudinal and transverse directions. Base motions are applied to the ends of soil springs that are connected to the large-diameter shafts. Damping primarily affects the magnitude of response while the modulus of elasticity primarily affects the natural period.

Absolute measured transverse deck displacements at Bent 5 are compared to analysis results with 4, 5 and 6 ksi concrete strengths (E is increased over the ACI value by 10% for all cases, as discussed elsewhere) and 5% damping in Figure 10. Based on the closest period response, these results suggest that the bridge had a 5 ksi concrete at the time of the earthquake. The most realistic equivalent viscous damping value was determined in a two-part process. Initially, 2%, 5% and 10% damping (constant for all modes) was considered (Figure 11). These results indicate that the best value of damping is somewhere between 2% and 5%, with 10% damping resulting in reduced magnitudes and damped-out vibrations, and 2% causing more oscillations and larger magnitude response than measured. A second set of analyses was

conducted to refine the damping levels further, allowing time-history comparisons at 3%, 4% and 5% damping, with 5% providing slightly better results.

This 5% damping value is consistent with Caltrans recommendations and seismic design practice, and appears to be the best overall value based on the time-history comparisons discussed above. Note that both modal and direct-integration time-history analyses were conducted and it was found that the results were very close to each other, with modal analyses producing a much quicker solution. An added advantage of modal time-history analysis is that it is possible to specify constant damping for all modes, whereas for direct integration a mass and stiffness proportional damping is used. Coefficients for Rayleigh damping were found by setting the damping to 5% at periods of 0.5 and 1.5 seconds. Between these periods the damping reduces to a low of about 4%. However, time-history results were virtually identical between direct integration with Rayleigh damping and modal analysis with 5% damping for all modes. Thus, modal analysis with constant 5% damping was used for all time-history results presented herein. The minimum number of modes specified for the complete spine model and the Frame 1 spine model was 50 and 20, respectively. Close comparisons to direct integration demonstrated that more modes were not required.

Absolute and relative transverse deck displacement time-histories at Bent 5 are compared between the (1) spine model with rotational mass, (2) spine model without rotational mass and (3) more detailed shell model (Figures 12). These results clearly show the importance of including superstructure and bent cap rotational mass in a spine model for seismic analysis of a typical connector bridge that has single-column-bents, resulting in very similar behavior between the spine model and more detailed shell model. With rotational mass not included the spine model transverse displacements are often smaller than measured and shell model results. Adding rotational mass will be even more important for intermediate frames of long, multi-frame, single-column-bent viaducts that do not have the beneficial restraint from abutments. However, this may not be so important for multiple-column-bent structures since the superstructure will tend to stay flat as it moves transversely.

Columns were modeled with beam elements, as were the large-diameter pile shafts. In design, the column lengths were extended at Bents 2, 3, 4 and 10 by providing isolation casings over the top 30 ft of soil to allow these regions to move freely, resulting in similar stiffness to the columns along each frame of the structure. This results in improved seismic response with no single bent or column being overloaded. All of the bent shafts for Frame 1 are embedded in hard rock-like soil, based on the log-of-test-borings shown on the plans. The soil springs are very stiff at these rock sites compared to sand. By running several analyses with the full range of possible soil spring stiffness values, it was determined that these variations have little effect on the response of the structure, in terms of natural periods and time-history displacement traces. Spring constants were based on recommended values provided in the LPILE User's manual [6].

In order to capture the proper natural mode shapes and periods and to have a reasonable distribution of mass, the superstructure spans were modeled with 4 beams, columns with 3 beams and large-diameter shafts were modeled with multiple elements at 10 ft spacing between nodes to allow for interaction with longitudinal and transverse soil springs. Ground motions were applied

to the spring ends at all bents and to the abutments. Lateral spring stiffness' were provided in mutually perpendicular directions at 10 ft spacing

Note that the spring constant represents the initial stiffness given in [6], with nonlinear soil behavior not included in the model as the motions were relatively small: Initial elastic stiffness values provide a good representation of the soil behavior throughout the loading. As presented above, three of the Frame 2 column shafts were founded on soft soil above the rock-like material. Based on the log-of-test borings and Frame 2 analysis results from the spine model, the soft soil was taken to be loose sand (defined in [6]). Below the water table the spring stiffness values were reduced, as suggested in [6]. Spine model behavior was compared to measured time-history results of Frame 2 for various soft soil properties at Bents 7, 8 and 9. It was found that the loose sand assumption provided the best overall spine model results for Frame 2, but still not as good as the excellent analysis results for Frame 1. For the spine model, the added weight and mass of the bent caps and soffit flares were lumped at the top of the columns, including the rotational mass of the bent cap about the axis of the superstructure.

Shell Model

The shell model is similar to the Frame 1 spine model discussed above, with the exception that the beam elements representing the bridge superstructure have been replaced by shell elements (compare Figures 7 and 8). Shell elements combine plate and membrane behavior into one element. Rather than determining the section properties by hand, such as area, inertias and torsional constant, and then assigning these properties to the beam elements, the shell elements are positioned to completely define the section geometry, including the deck, soffit, girders and overhangs. So long as the elements are given the correct thickness and location in 3-D space they automatically develop the correct behavior of the structure (this is why the shell model is a good verification for the spine model). Shell elements were also used to model the bent caps and end diaphragms. The columns and large-diameter pile shafts are modeled identically to the spine model. To reduce local shell deformations at the base of the cap/column joint, the column was extended to the top of the superstructure and connected to top and bottom nodes of the bent cap. Within the bent cap, a material property that has no mass and weight was assigned to the column elements so that the concrete would not be included twice in these joint regions.

Since the Frame 1 spine model results matched measured results better than the more variable Frame 2 spine model results, it was decided to develop the shell model only for Fame 1. This produced Frame 1 shell model results that are identical to having both frames included in the shell model, since there is no interaction between frames from the Hector Mine Earthquake.

Boundary conditions of the shell model are similar to the spine model. At the abutment the width and depth of the shell model presented some difficulty in providing the same restraints and releases: The shell model is constrained directly under the girder lines at the soffit level in the longitudinal, transverse and vertical directions. By not constraining the deck or girders, the superstructure is free to rotate in the principal direction but constrained in the other directions, as is the spine model. Along the large-diameter shafts the boundary conditions and applied time-

history ground motions are identical between the two models. Material properties and damping are the same as previously discussed for the spine model.

Time-History Analysis Results

This section compares measured absolute and relative (between deck and ground) time-history results from the (1) spine model and (2) more detailed shell model. Relative displacements between the superstructure and ground are important as they define the deformations and damage of the bridge columns. Absolute and relative time-history displacements for all columns are given elsewhere [7].

Frame 1 spine model analyses were used to define the damping level, modulus of elasticity and concrete strength for (1) Frames 1 and 2 of the spine model and (2) the more detailed shell model that was developed for Frame 1 only. This is because several large-diameter shafts of Frame 2 were placed in soft soil, rather than the rock-like material found at all other locations. Uncertainty from soft and unknown soil properties resulted in sporadic comparisons to measured time-history results associated with arbitrary modifications to the soil properties. This provided little confidence that the damping level and concrete strength could be defined with reasonable accuracy from these Frame 2 time-history analyses. Thus the Frame 1 analyses served to define the damping and concrete properties for both frames and both types of models, removing some of the uncertainty in the analysis of Frame 2.

Results from the spine and shell models indicate that the transverse deck response at Bent 4 (absolute and relative) closely resembles the measured response in magnitude and form for the 25 seconds of recorded strong earthquake motion (Figures 13 and 14), clearly showing that the chosen level of damping and concrete modulus of elasticity are reasonable. Note that dead load sidesway displacements were removed from all analysis results presented herein, unless otherwise indicated, as they were not in the recorded data. This is because any developed sidesway occurred at the time of construction, following the removal of falsework that supported the structure.

Overall comparisons between measured and shell model Frame 1 relative transverse bridge responses are given from 25 to 50 seconds of strong earthquake shaking in Figure 15. Such plots allow all of the measured transverse bent results (bottom figure) to be compared to analysis results (top figure) on a single page. The similarity between measured and analysis plots is quite remarkable, demonstrating that relatively simple analysis models are very capable of realistically capturing the complete response of a bridge structure of this type. Note that the overall transverse response of Frame 1 from the spine model was very similar to the shell model results presented in Figure 15.

The overall period of vibration, form and magnitude of response is very good for the full 25 seconds of strong earthquake loading. These excellent results give further validation of the damping level and concrete properties derived from the Frame 1 spine model analyses and used in the shell model discussed here.

Developing the shell model for Frame 1 proved to be an excellent exercise, demonstrating the capabilities of both shell and spine models to capture measured dynamic time-history responses of a multi-span, prestressed concrete, box-girder connector bridge. It also resulted in the discovery of a significant shortcoming of typical spine modeling procedures for single-column-bent bridges, relating to the inherent lack of rotational mass of the superstructure and bent caps. Results demonstrated that this difficulty is resolved by adding rotational mass of the superstructure to the nodes of the spine model, with excellent comparisons to shell model and measured behaviors.

Measured results indicate that, overall, the shell model is slightly better at capturing the response of the bridge, especially in the axially stiff longitudinal direction. Transversely, there is very little difference between shell and spine model results, so long as rotational mass is included in the spine model.

Conclusions and Recommendations

Acceleration time-history measurements taken on and around the North Connector Bridge of the 5/14 Interchange, from the 1999 Hector Mine Earthquake, have provided immensely valuable information for verifying seismic analysis and design tools that are required for California bridge projects. This structure, in particular, is of interest because it is a heavily instrumented, 10-span, 2-frame connector bridge, with single-column-bents and variable ground motion, requiring multiple support excitations to be provided as displacement time-history input functions. While ground motions were not recorded at all bents, they were measured at the abutments and at the base of Bent 5, in the vicinity of the expansion joint between frames. Thus the measured local ground displacements were rotated into global coordinates of the analysis model and interpolated between abutments and the base of Bent 5, in order to develop unique longitudinal and transverse input motions for the remaining bents.

A relatively simple spine model was developed for the entire connector bridge, consisting of beam elements for the superstructure, columns and large-diameter shafts. A more detailed shell model was also developed for Frame 1, which was identical to Frame 1 of the spine model, with the exception that the superstructure, bent caps and diaphragms were modeled with shell rather than beam elements. Initial comparisons between the shell and spine models revealed that something was wrong with one of the models, but it was not clear what was causing a difference of about 4% in the 1st mode response period (transverse bending of columns and torsion of superstructure) of the two models. Mass and stiffness values for the two models were within 1% of each other, and a 4% error in period indicates that one of these terms must be in error by the square of 1.04, or 8%.

After developing breakout spine and shell models of a single straight span with the cross-section of the connector bridge it was realized that the difference between the models was that the spine model had no rotational mass while the shell model naturally develops it due to the distribution of translational mass away from its centroidal axis. When this rotational mass was added to the breakout spine model, the torsional mode shape and period agreed with the breakout shell model. Based on these results, the rotational mass was calculated by hand and added to each of the superstructure nodes in the spine model. It was shown that by adding the rotational

mass of the superstructure, about its axis, to a spine model, time-history responses are improved and are very similar to the more detailed shell model and measured responses. With no rotational mass included, the overall time-history behavior drifted away from the more accurate shell model and measured bridge responses.

It was also found that in order to match the period of the structure and the measured time-history response, a 10% increase to the ACI modulus of elasticity [4] was required for a concrete strength of 5 ksi. The increase to the ACI modulus of elasticity recognizes that for the small stresses from the Hector Mine Earthquake, the concrete is near the beginning of its nonlinear stress-strain curve and that the initial tangent modulus of elasticity should be used rather than the softer secant ACI value. The initial tangent modulus is reported to be about 10% greater than the ACI value [5], which defines its secant value at 50% of the concrete strength. Analyses with concrete strengths of 4 ksi and 6 ksi were also performed, but comparisons to measured results indicate that the most realistic stiffness was based on the 5 ksi model. Comparisons between Frame 1 spine model results and measured results show that the most realistic overall damping level is 5%. Other damping levels investigated include 2% and 10%, followed by more refined damping levels of 3% and 4%.

Thus the results of this study have shown that (1) spine models can accurately capture time-history behavior of a connector bridge subjected to an earthquake, as demonstrated by direct comparisons to measured responses and the more detailed shell model, (2) damping levels of 5% used by Caltrans and others appears to be a reasonable value and (3) a concrete strength of 5 ksi is realistic for seismic design and analysis of concrete bridge structures, with a 10% increase to the modulus of elasticity for small load levels. The 10% increase to the ACI modulus of elasticity was used in the analyses presented here because the seismic loading was much smaller than the seismic levels expected in design. Therefore, for seismic bridge design, it is recommended that the modulus of elasticity still be based on the ACI expression without the 10% increase, as the concrete will be subjected to much larger stresses under the design level earthquake than the concrete of the North Connector was from the Hector Mine Earthquake.

An important discovery about the spine model was found by comparing spine model results to results from the more detailed shell model, which lead to the realization that the rotational mass of the superstructure and bent caps, about the axis of the superstructure, needed to be included in the model. This is because all of the mass of the superstructure runs along its spine, which has no thickness or height and, therefore, develops no rotational mass inertia. The shell model develops this rotational mass inertia quite naturally as the translational mass is distributed over the width and height of the section. It is recommended that in future analyses, Caltrans include the rotational mass of the bridge superstructure by lumping it at each node of the spine model. Bent cap rotational mass should also be added to the rotational mass of the superstructure, at the nodes where the columns and superstructure meet.

For single-column-bent structures, the rotational mass is significant to its dynamic response due to the rotation of the superstructure as it moves back and forth transversely. This will be amplified for long, multi-frame viaducts, with interior frames that do not have an abutment at either end to provide some restraint. This should not be a concern for multi-column-bent structures, as the superstructure will remain relatively flat as it moves transversely.

However, both multi-column-bent structures and long, multi-frame, single-column-bent viaducts should be investigated in the near future to provide insight into their seismic behavior and to give recommendations regarding these important structures.

In concluding, it is important to note that the bridge exhibited linear-elastic behavior when subjected to the relatively small ground shaking from the distant Hector Mine Earthquake. Thus the developed structural models were also linear-elastic, with excellent comparisons between time-history analysis results and the measured bridge response. From a larger earthquake, nonlinear behavior of the bridge is expected, including plastic hinging of the columns, banging of frames at the hinge and crushing of soil. It would be of great value to the engineering community if the present study, which showed that good linear-elastic dynamic results for a connector bridge can be achieved with relatively simple spine models and the more detailed shell models, was extended to model a bridge structure that was subjected to much larger ground motions so that nonlinear behavior of the bridge resulted.

The contents of this report were developed under Contract No. 1001-763 from the California Department of Conservation, California Geological Survey, Strong Motion Instrumentation Program. However, these contents do not necessarily represent the policy of that agency nor endorsement by the State Government.

References

1. McCallen, D. B., Romstad, K. M., “*Seismic Response Computations for a Simple Overcrossing*”, *Proceedings, The Third Annual Seismic Research Workshop*, Sacramento, California, 1994.
2. SAP2000, Version 8, User’s Manuals, Computers and Structures, Inc., Berkeley, California, 2002.
3. Caltrans Seismic Design Criteria, Version 1.2, Caltrans, Sacramento, California, 2001.
4. *ACI Building Code Requirements for Structural Concrete (ACI 318-95)*, American Concrete Institute, Farmington Hills, Mich., 1995.
5. MacGregor, J. G., *Reinforced Concrete Mechanics and Design*, Prentice Hall, Upper Saddle River, N. J., 1997.
6. LPILE Plus for Windows, Version 4.0, User’s Manuals, ENSOFT, Inc., Austin, Texas, 2000
7. Dowell, R. K., *Time-History Analyses versus Measured Seismic Responses of the 5/14 Connector Bridge*, Report No. DH-04-02, Dowell-Holombo Engineering, Inc., San Diego, California, 2004.



Figure 1. North Connector, looking north



Figure 2. North Connector, looking northeast at Abutment 11



Figure 3. North Connector, looking east.



Figure 4. North Connector, looking east at hinge detail.

Sylmar - I5/14 Interchange Bridge
 Caltrans Bridge No. 53-2795F (07-LA-5-24.5)
 CSMIP Station No. 24694

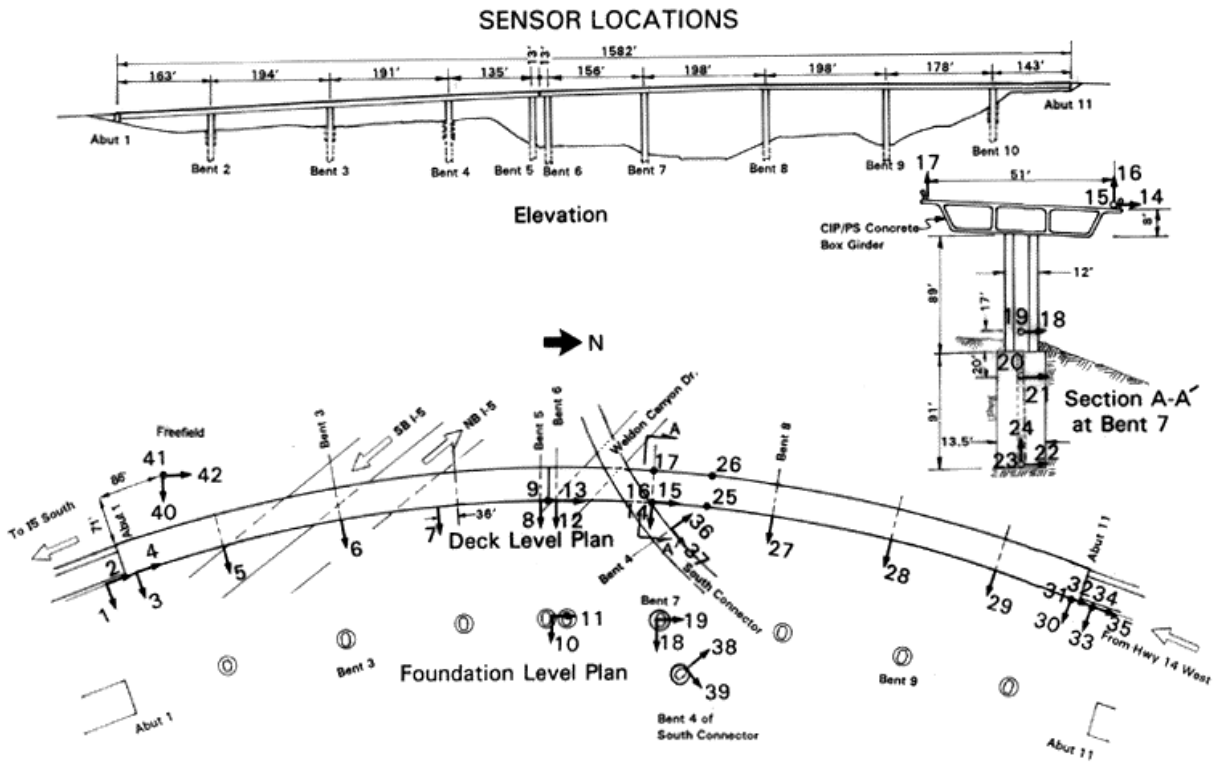


Figure 5. Bridge details and instrumentation layout

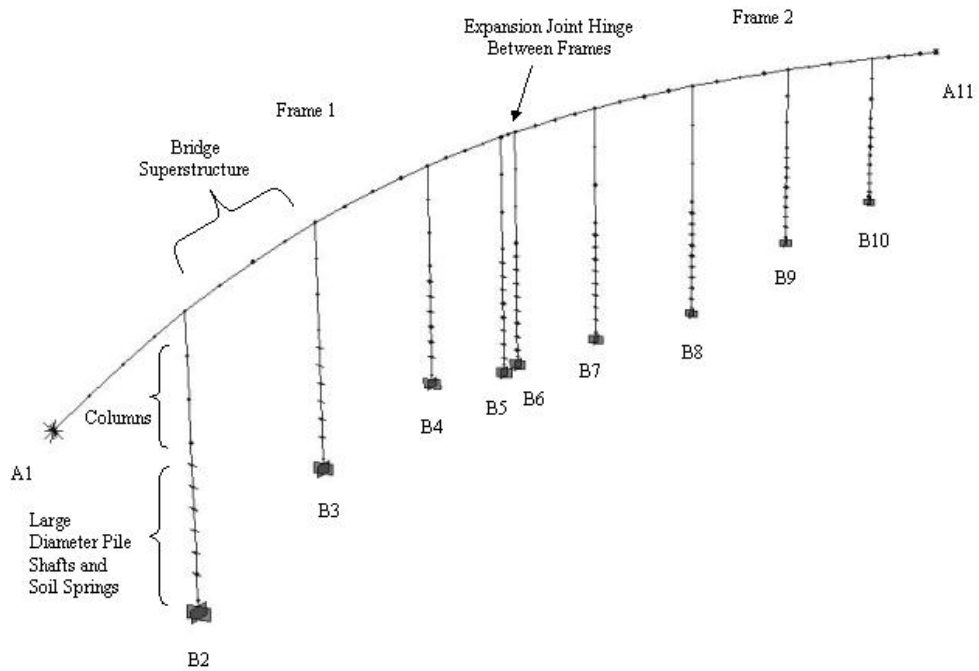


Figure 6. Isometric view of complete spine model of North Connector Bridge

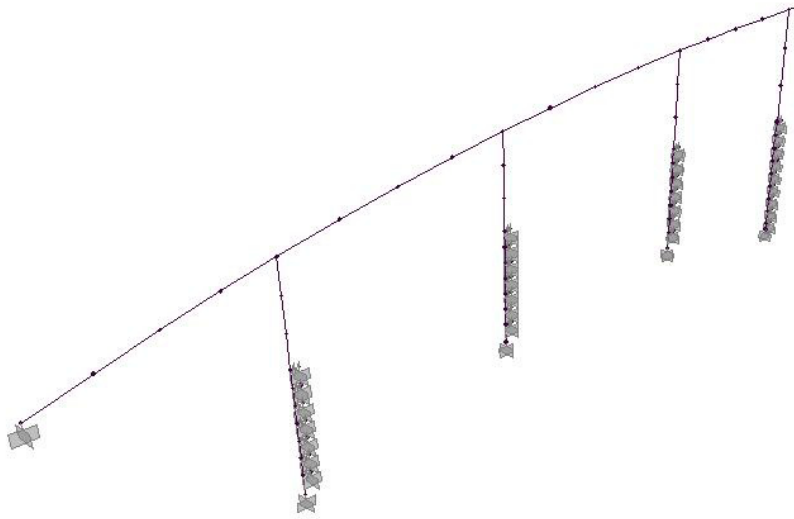


Figure 7. View of Frame 1 spine model from above looking northwest

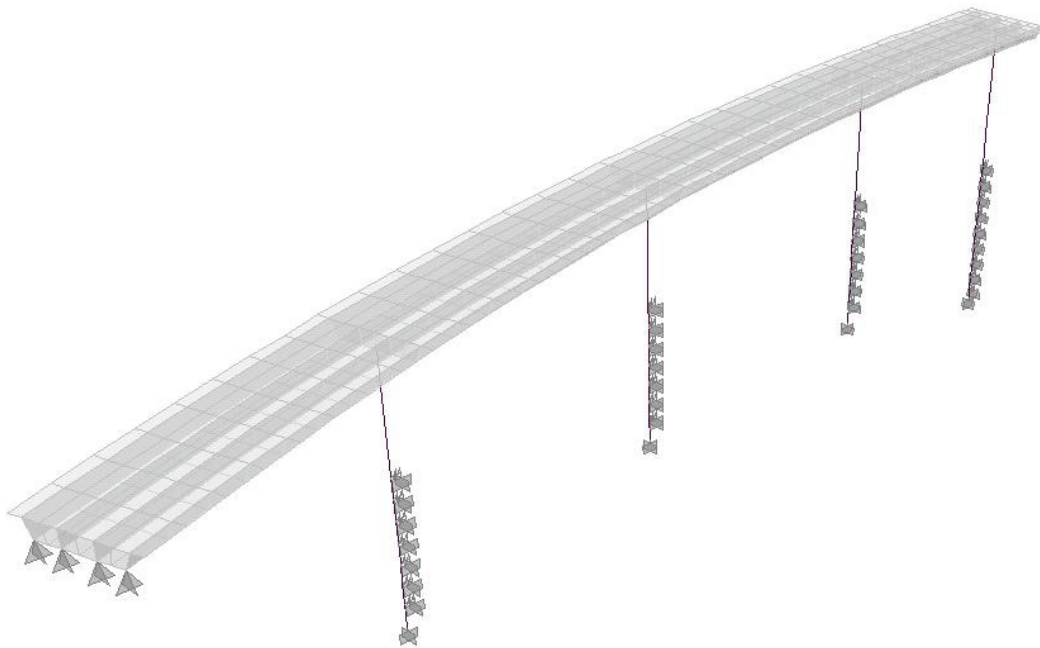
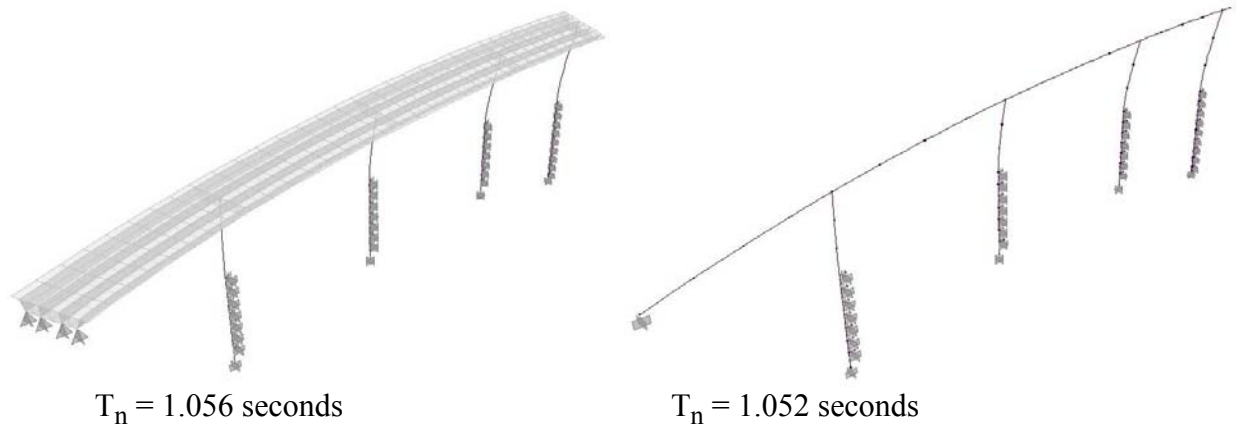
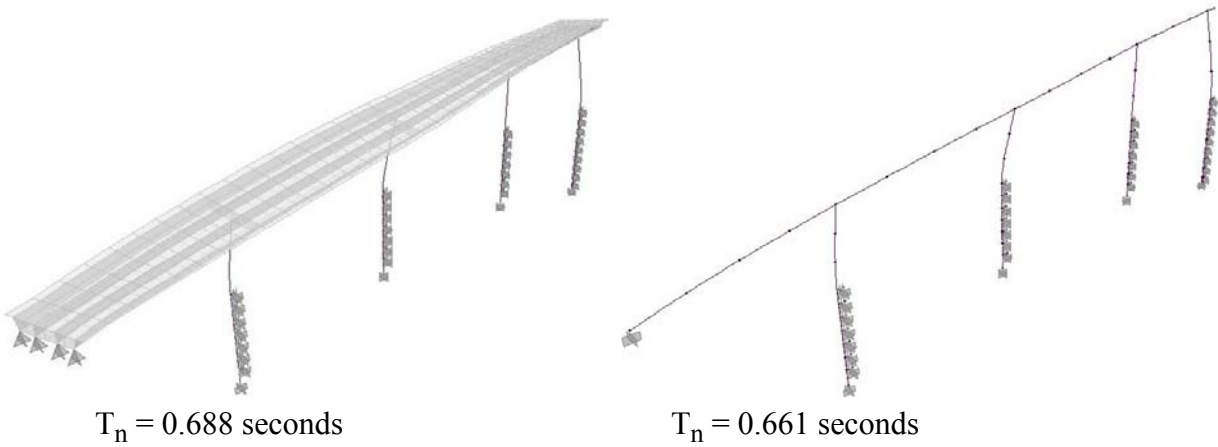


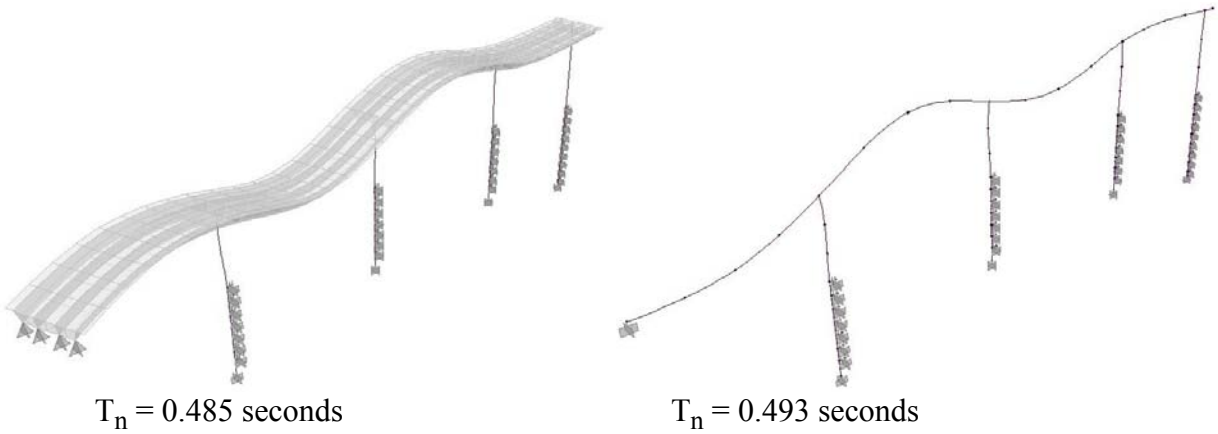
Figure 8. View of Frame 1 shell model from above looking northwest



(a) Mode 1 (transverse/torsion)



(b) Mode 2 (double transverse)



(c) Mode 3 (vertical)

Figure 9. Modes 1 through 3, Frame 1 shell and spine models

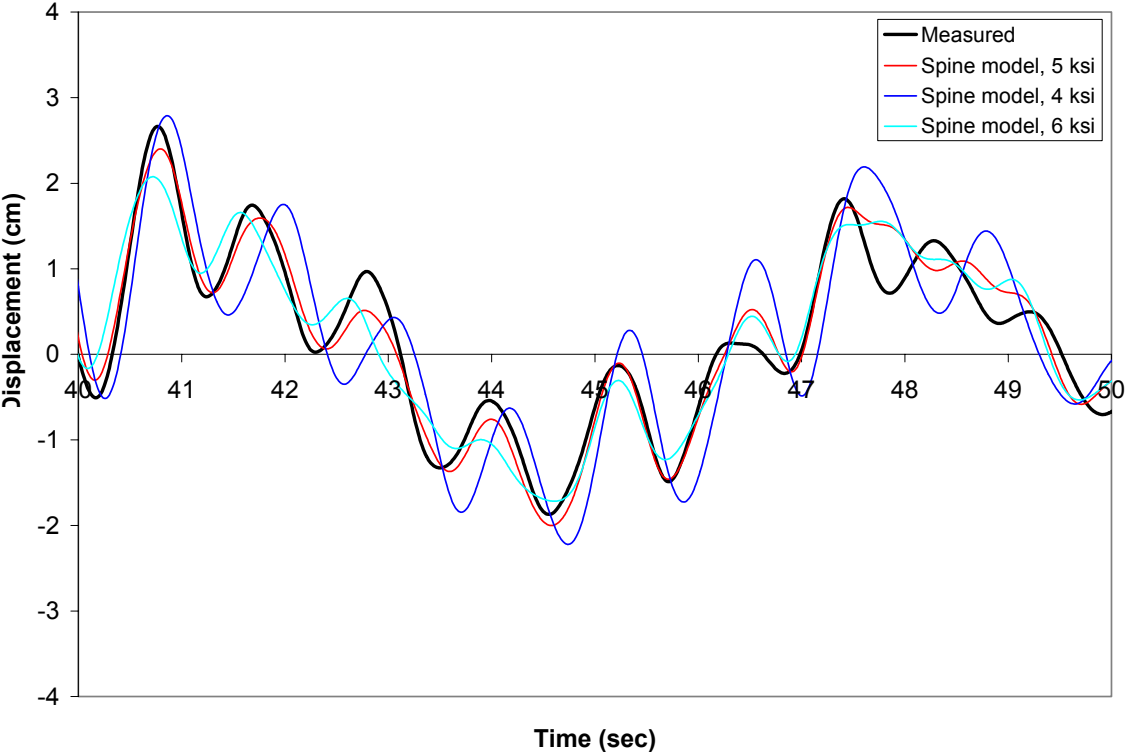


Figure 10. Transverse Bent 5 responses, 4, 5 and 6 ksi concrete (40-50 sec)

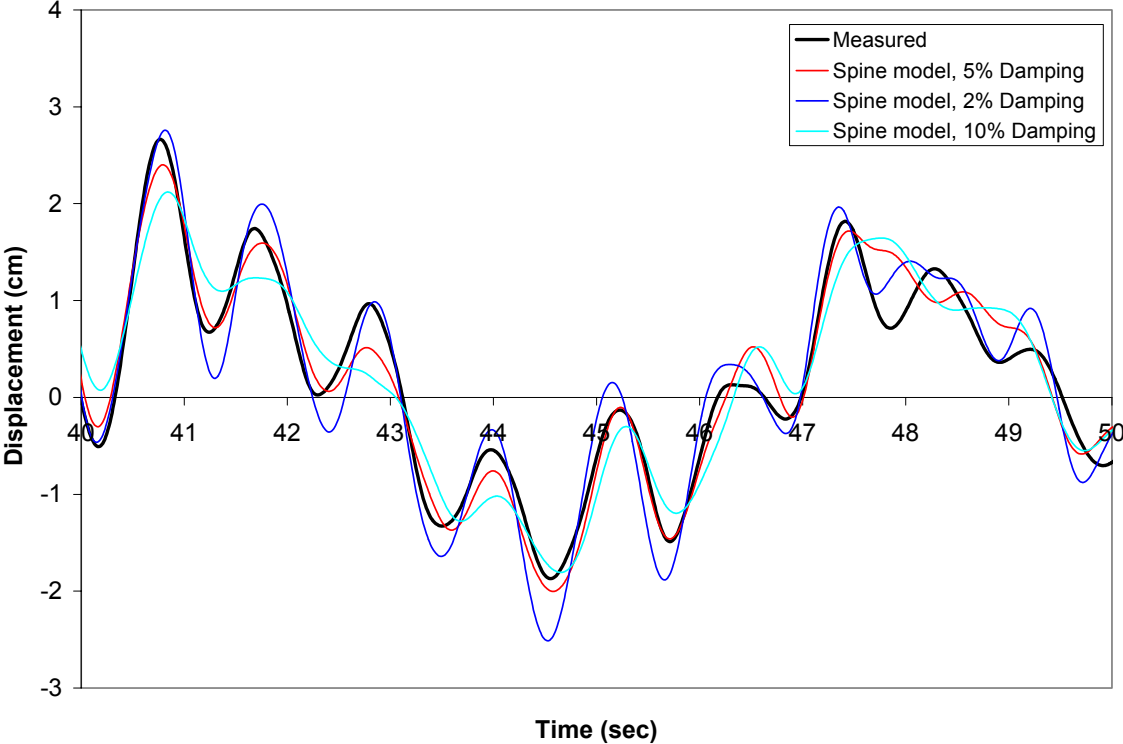
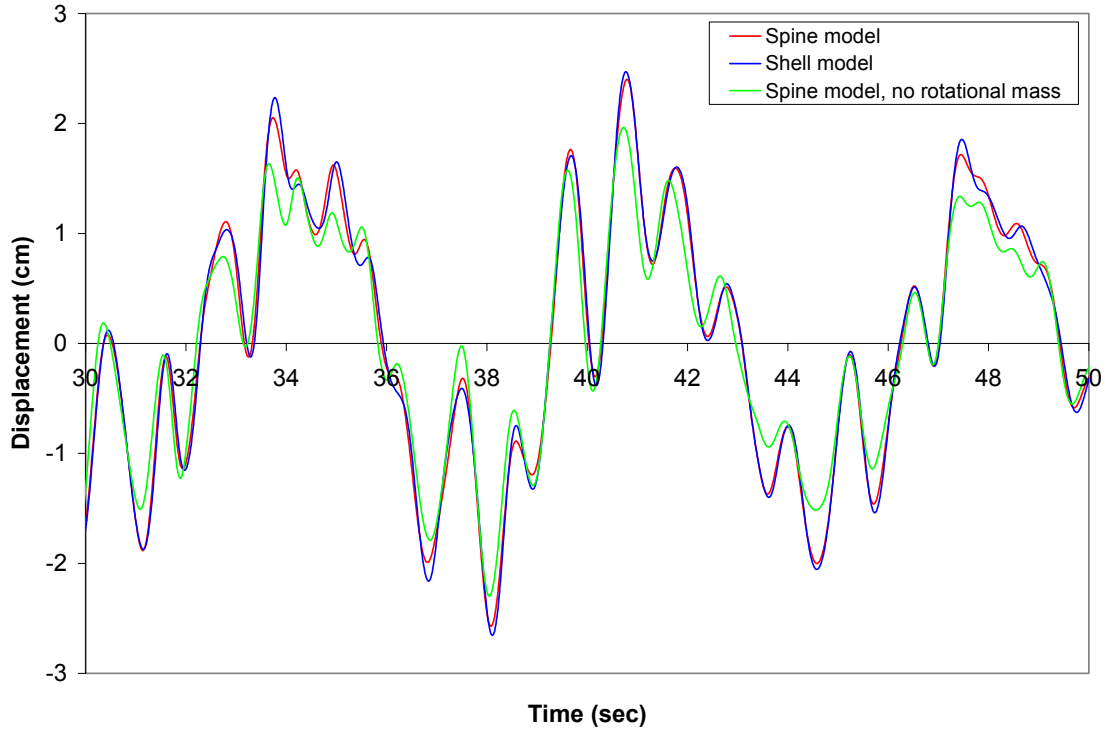
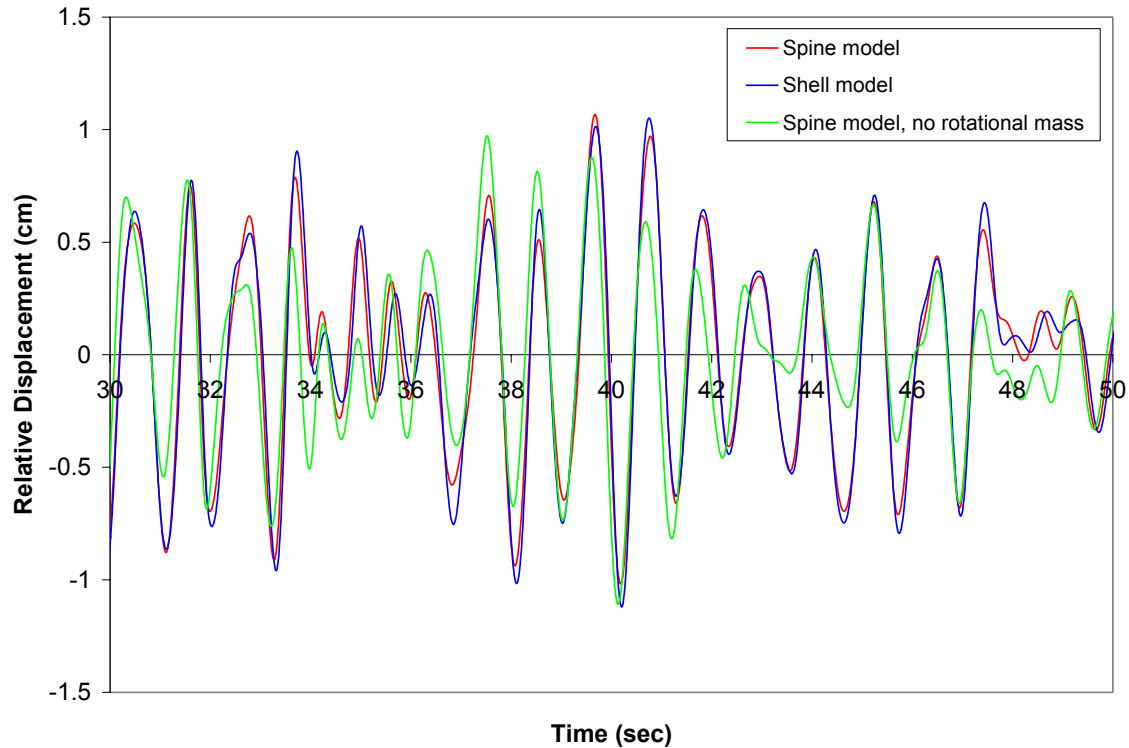


Figure 11. Transverse Bent 5 responses, 2%, 5% and 10% damping (40-50 sec)

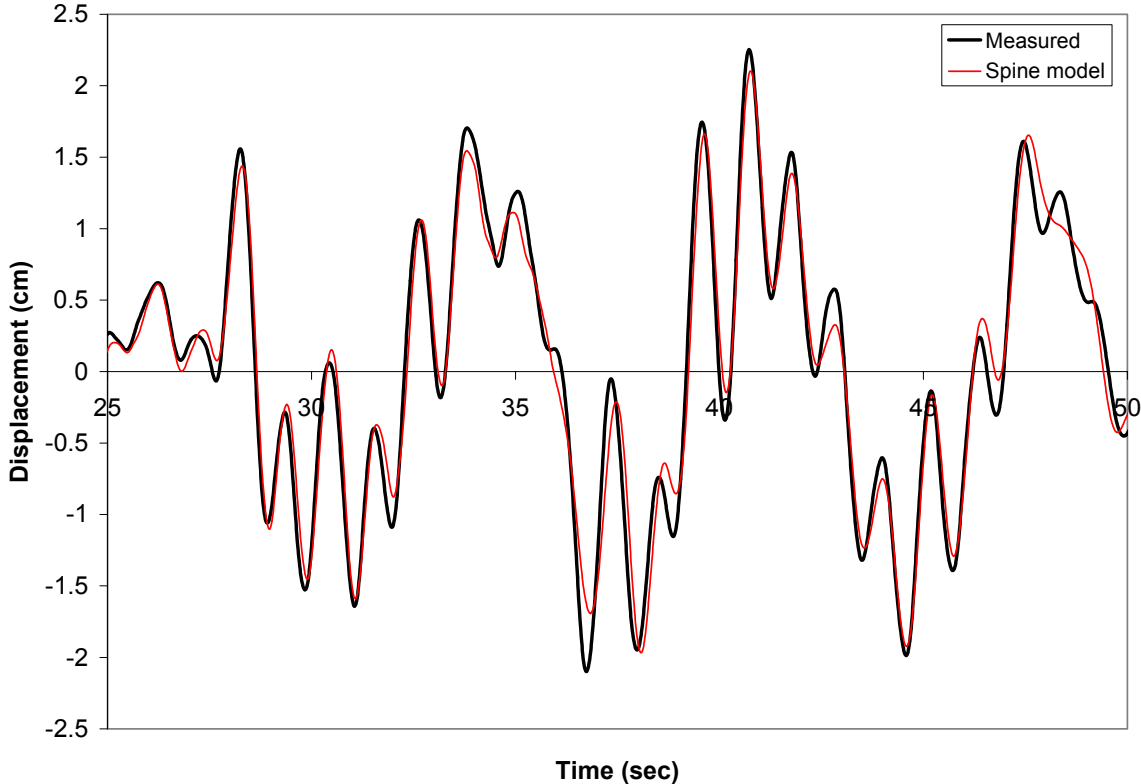


(a) Absolute displacements

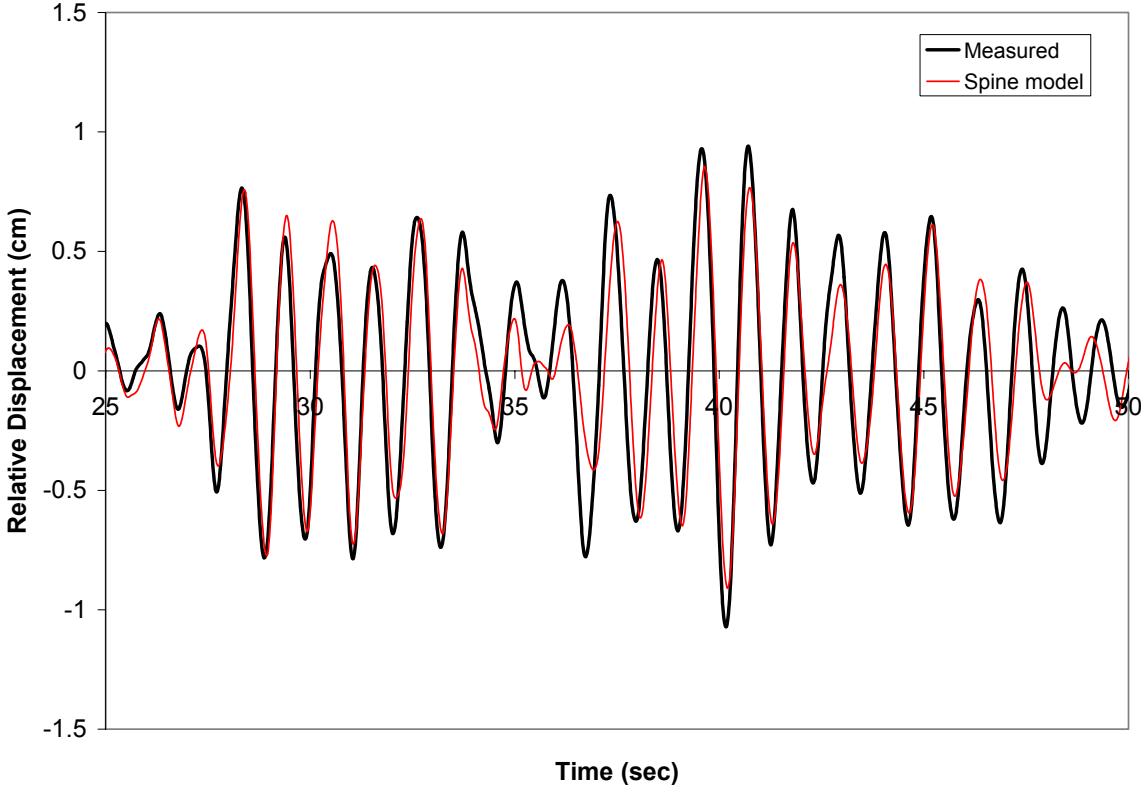


(b) Relative displacements

Figure 12. Transverse Bent 5 responses, shell model vs. spine model with and without rotational mass of superstructure included (30-50 sec)

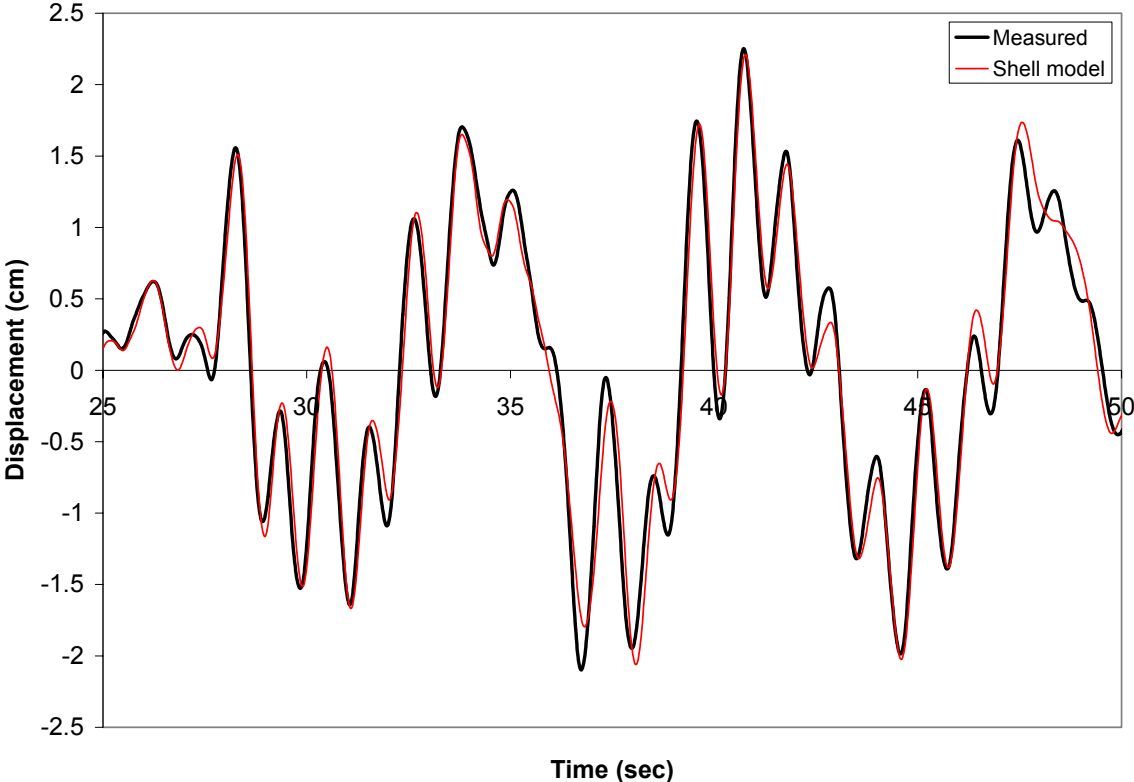


(a) Absolute displacements

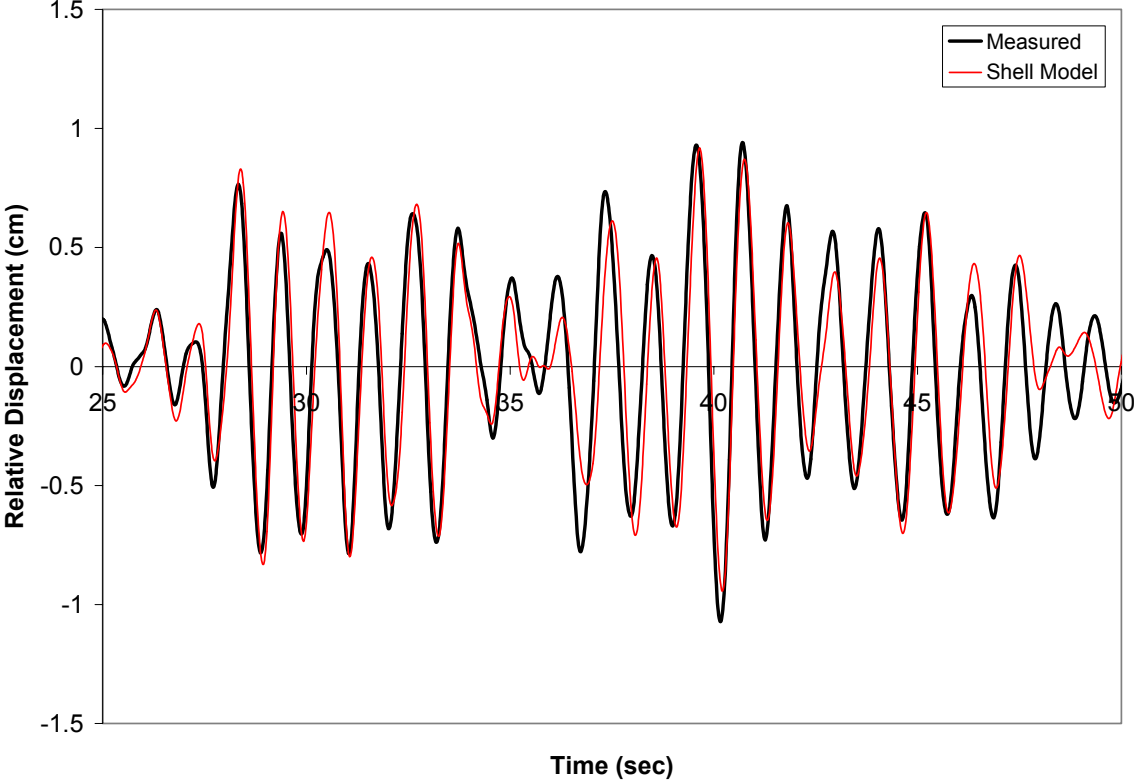


(b) Relative displacements

Figure 13. Spine model and measured transverse displacements at Bent 4 (25-50 sec)

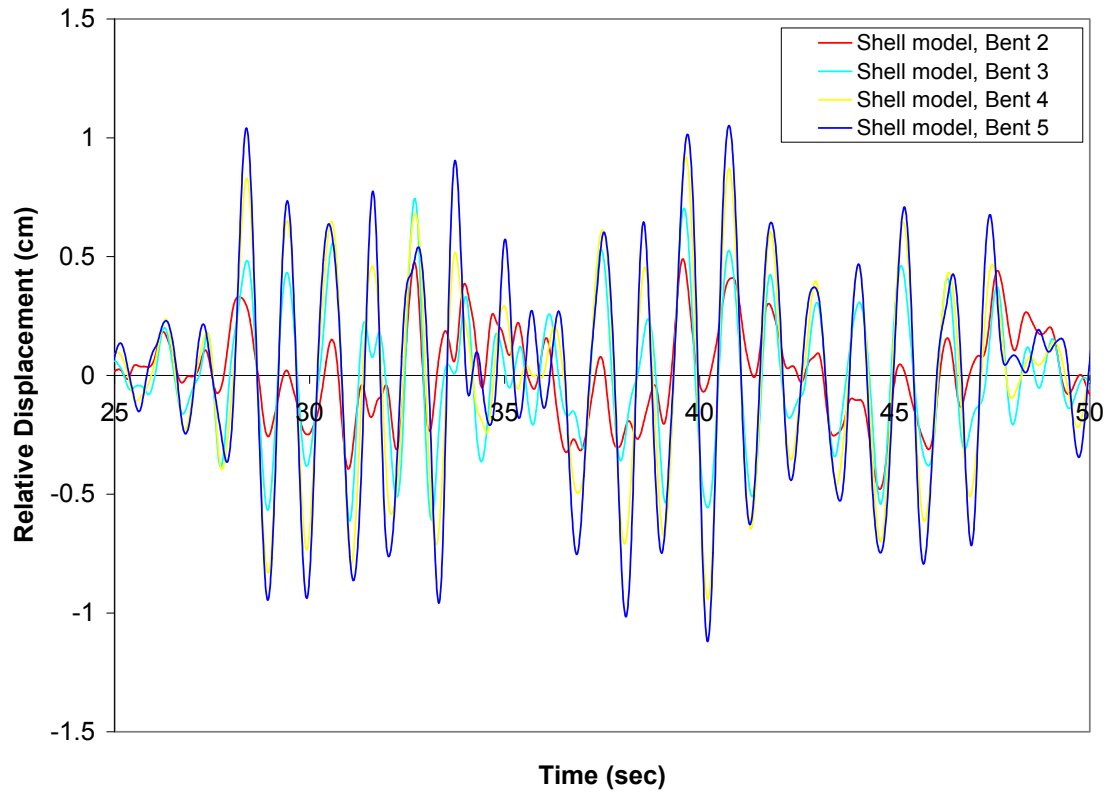


(a) Absolute displacements

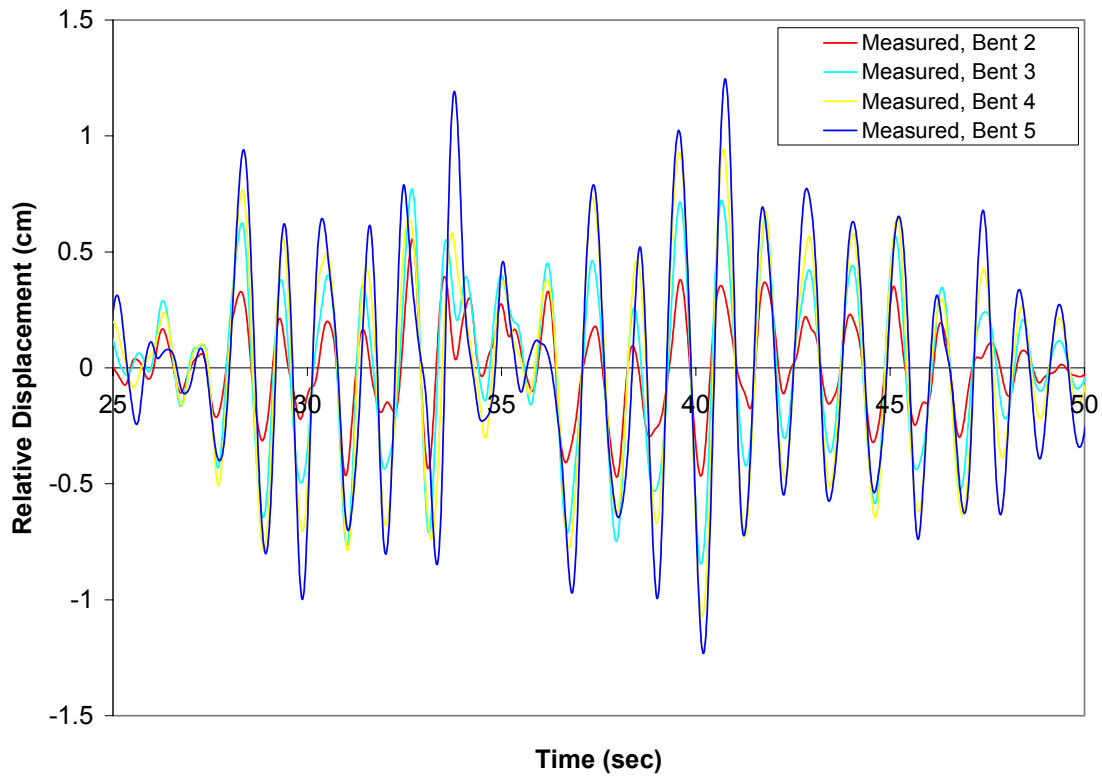


(b) Relative displacements

Figure 14. Shell model and measured transverse displacements at Bent 4 (25-50 sec)



(a) Shell model



(b) Measured

Figure 15. Shell model and measured relative transverse motions of Frame 1 (25-50 sec)

EVALUATION OF NONLINEAR STATIC PROCEDURES USING STRONG-MOTION BUILDING RECORDS

Rakesh K. Goel

Department of Civil & Environmental Engineering
California State Polytechnic University, San Luis Obispo, CA

Abstract

The objective of this investigation is to evaluate the FEMA-356 Nonlinear Static Procedure (NSP), the Sum-Difference procedure, and the Modal Pushover Analysis (MPA) procedure using recorded motions of buildings that were damaged during the 1994 Northridge earthquake. It is found the FEMA-356 NSP and the Sum-Difference procedures typically underestimates the drifts in upper stories and overestimates them in lower stories. The MPA procedure provides estimates of drifts that are better compared to the FEMA-356 NSP and the Sum-Difference procedure. In particular, the MPA procedure is able to capture the effects of higher modes.

Introduction

Nonlinear static pushover (NSP) analysis is used commonly by the current civil engineering practice for estimating seismic demands at low performance levels, such as life safety and collapse prevention. In the NSP procedure (FEMA, 1997a; 1997b), the seismic demands are computed by nonlinear static analysis of the structure subjected to monotonically increasing lateral forces with an invariant height-wise distribution until a predetermined target displacement is reached. Both the force distribution and target displacement are based on the assumption that the response is controlled by the fundamental mode and that the mode shape remains unchanged after the structure yields. The underlying assumptions and limitations of the NSP analysis have been evaluated (Elnashai, 2001; Fajfar and Gaspersic, 1996; Gupta and Krawinkler, 1999; Maison and Bonowitz, 1999; Reinhorn, 1997; Skokan and Hart, 2000) and it has been found that satisfactory predictions of seismic demands are mostly restricted to low- and medium-rise structures for which higher mode effects are likely to be minimal and the inelastic action is distributed throughout the height of the structure (Krawinkler and Seneviratna, 1998).

Since the invariant force distributions cannot account for redistribution of inertia forces because of structural yielding and the associated changes in the vibration properties of the structure, NSP using adaptive force distributions that attempt to follow more closely the time-variant distributions of inertia forces have also been developed (Bracci et al., 1997; Gupta and Kunnath, 2000). The most recent version of the FEMA document (ASCE, 2000), denoted as FEMA-356, includes the option to consider such an adaptive distribution in addition to the invariant force distributions of the earlier version (FEMA, 1997b). While the adaptive force distributions may provide better estimates of seismic demands (Gupta and Kunnath, 2000), they are conceptually complicated, computationally demanding for routine application in structural engineering practice, and require special purpose computer program to carry out the step-by-step analysis.

Attempts have also been made to consider more than the fundamental vibration mode in pushover analysis. The Multi-Mode Pushover (MMP) procedure (Paret et al., 1996; Sasaki et al., 1998) provided information on possible failure mechanisms due to higher modes, which may be missed by the standard NSP analyses. But other information of interest in the design process, such as story drifts and plastic rotations, could not be computed by the MMP procedure. The Sum-Difference procedure (Kunnath and Gupta, 2000; Matsumori et al., 1999) also provided “useful” information but was tested on a single building (Kunnath and Gupta, 2000).

The modal pushover analysis (MPA) procedure, developed based on structural dynamics theory, attempted to capture contributions of several modes of vibration (Chopra and Goel, 2001; 2002). This procedure was systematically evaluated using six buildings (Goel and Chopra, 2004), and generic frames (Chopra and Chintanapakdee, 2004). It was found that with sufficient number of “modes” included, the height-wise distribution of story drifts estimated by MPA is generally similar to trends noted from nonlinear RHA. Furthermore, the additional error (or bias) in the MPA procedure applied to inelastic structures is small to modest compared to the bias in response spectrum analysis (RSA) applied to elastic structures – the standard analytical tool for the structural engineering profession – unless the building is deformed far into the inelastic region with significant stiffness and strength deterioration.

Most previous research on development and evaluation of the NSP and improved procedures is based on response of analytical models subjected to recorded and/or simulated earthquake ground motions. Recorded motions of buildings, especially those deformed into the inelastic range, provide a unique opportunity to evaluate such procedures. Therefore, the principal objective of this investigation is to evaluate the three NSP procedures – the FEMA-356 NSP, the MPA, and the Sum-Difference – using recorded motions of buildings that were deformed beyond the elastic limit during the 1994 Northridge earthquake. This paper summarizes the findings of this investigation; intermediate results from this investigation have also been reported in several previous publications (Goel, 2003a; 2003b; 2003c; 2004a; 2004b).

Selected Buildings

Recorded motions of buildings that were deformed beyond the yield limit (or damaged) during the earthquake are required for this investigation. For this purpose, four buildings have been identified (Table 1) for which the motions were recorded during the 1994 Northridge earthquake. Of these four buildings, three buildings – Van Nuys 7-Story, Sherman Oaks 13-Story, and Los Angeles 19-Story – have been extensively instrumented by California Strong Motion Instrumentation Program (CSMIP) and the fourth – Woodland Hills 13-Story – has been nominally instrumented in accordance to the local code requirements.

The selected buildings have all been reported to be damage during the 1994 Northridge earthquake. Several columns between the fourth and fifth floor in the longitudinal frame on south side of the Van Nuys building failed in shear (Islam et al., 1998; Li and Jirsa, 1998; Naeim, 1997). The damage to Woodland Hills building consisted of local fracture at the beam-to-column welded joints (Uang et al., 1997). The Sherman Oaks building suffered cracks at many beam-column joints (Shakal et al., 1994). Finally, the Los Angeles building was reported to have suffered moderate damage in the form of buckling in some braced at upper floor levels (Naeim,

1997). Further details of these buildings and damage are available elsewhere (Goel, 2003a; 2003b; 2003c; 2004a; 2004b).

Table 1. Selected buildings, and peak ground and structure accelerations recorded during the 1994 Northridge earthquake.

Buildings name	CSMIP Station	Number of Stories	Peak accelerations (g)	
			Ground	Structure
Van Nuys 7-Story Hotel	24386	7	0.47	0.59
Woodland Hills 13-Story	C246	12/2	0.44	0.33
Sherman Oaks 13-Story	24322	13/2	0.46	0.65
Los Angeles 19-Story	24643	19/4	0.32	0.65

Analysis of Recorded Motions

Since buildings are typically instrumented at a limited number of floors, the motions of non-instrumented floors are computed by the cubic spline interpolation procedure (De la Llera and Chopra, 1998; Naeim, 1997). The cubic spline interpolation is performed on the building deformation relative to the base. Once the time variation of deformations of all floors have been developed using the cubic spline interpolation procedure, inter-story drifts at each time instant is computed from

$$\delta_j(t) = u_j(t) - u_{j-1}(t) \quad (1)$$

in which $\delta_j(t)$ is the inter-story drift in the j^{th} story, and $u_j(t)$ and $u_{j-1}(t)$ are the deformations at the j^{th} and $j-1^{\text{th}}$ floor levels at time t . The peak values of the drift in the j^{th} story, δ_{jo} , is computed as the absolute maximum value over time. These values, denoted as “derived” inter-story drifts, would be used to evaluate the NSP procedures.

For implementing the MPA procedure, contributions of various modes of the building to the total displacement are required. These contributions are extracted from the recorded (or interpolated) motions by using the standard modal analysis method (Chopra, 2001) as:

$$u_{jn}(t) = \frac{\phi_n^T \mathbf{m} \mathbf{u}(t)}{\phi_n^T \mathbf{m} \phi_n} \phi_{jn} \quad (2)$$

in which ϕ_n is the n^{th} mode shape of the elastic building, \mathbf{m} is the mass matrix, $\mathbf{u}(t)$ is the vector of displacements at all floor levels at time t , and ϕ_{jn} is the n^{th} mode shape component at the j^{th} floor level. Once the contribution of the n^{th} mode to the floor displacements have been computed, its contribution to inter-story drift, $\delta_{jn}(t)$, can be computed using Eq. (1). Further details of the procedure to analyze the recorded motions are available elsewhere (Goel, 2003a; 2003b; 2003c).

Analytical Models

The computer program DRAIN-2DX (Prakash et al., 1993) was used for analysis of the selected buildings. A two dimensional model was developed for each of the selected buildings and calibrated by comparing the fundamental vibration periods obtained from the eigen-value analysis and from system-identification analysis of the initial “elastic” phase of the recorded motions. The accuracy of the model was further evaluated by comparing the time history of the floor displacements of the analytical model computed for the base acceleration and the time history floor displacements recorded during the earthquake. Details of the calibration process are available elsewhere (Goel, 2003c).

Nonlinear Static Procedures

FEMA-356 NSP

The nonlinear static procedure (NSP) specified in the FEMA-356 (ASCE, 2000) document may be used for any structure and any rehabilitation objective except for structures with significant higher mode effects. To determine if higher mode effects are present, two linear response spectrum analyses must be performed: (1) using sufficient modes to capture 90% of the total mass, and (2) using only the fundamental mode. If shear in any story from the first analysis exceeds 130% of the corresponding shear from the second analysis, the higher mode effects are deemed significant. In case the higher mode effects are present, the NSP analysis needs to be supplemented by the Linear Dynamic Procedure (LDP); acceptance criteria for the LDP are relaxed but remain unchanged for the NSP.

The FEMA-356 NSP requires development of a pushover curve, which is defined as the relationship between the base shear and lateral displacement of a control node, ranging between zero and 150% of the target displacement. The control node is located at the center of mass at the roof of a building. For buildings with a penthouse, the floor of the penthouse (not its roof) is regarded as the level of the control node. Gravity loads are applied prior to the lateral load analysis required to develop the pushover curve.

The pushover curve is developed for at least two vertical distributions of lateral loads. The first pattern is selected from one of the following: (1) Equivalent lateral force (ELF) distribution: $s_j^* = m_j h_j^k$ (the floor number $j = 1, 2, \dots, N$) where s_j^* is the lateral force and m_j the mass at j th floor, h_j is the height of the j th floor above the base, and the exponent $k = 1$ for fundamental period $T_1 \leq 0.5$ sec, $k = 2$ for $T_1 \geq 2.5$ sec; and varies linearly in between; (2) Fundamental mode distribution: $s_j^* = m_j \phi_{j1}$ where ϕ_{j1} is the fundamental mode shape component at the j th floor; and (3) SRSS distribution: \mathbf{s}^* is defined by the lateral forces back-calculated from the story shears determined by linear response spectrum analysis of the structure including sufficient number of modes to capture 90% of the total mass. The second pattern is selected from either “Uniform” distribution: $s_j^* = m_j$ in which m_j is the mass and s_j^* is the lateral force at j th floor; or Adaptive distribution that changes as the structure is displaced. This

distribution should be modified from the original distribution by considering properties of the yielded structure.

The target displacement is computed from

$$\delta_t = C_0 C_1 C_2 C_3 S_a \frac{T_e^2}{2\pi^2} g \quad (3)$$

where T_e = Effective fundamental period of the building in the direction under consideration, S_a = Response spectrum acceleration at the effective fundamental vibration period and damping ratio of the building under consideration and g is the acceleration due to gravity, C_0 = Modification factor that relates the elastic response of an SDF system to the elastic displacement of the MDF building at the control node, C_1 = Modification factor that relates the maximum inelastic and elastic displacement of the SDF system, C_2 = Modification factor to represent the effects of pinched hysteretic shape, stiffness degradation, and strength deterioration, and C_3 = Modification factor to represent increased displacement due to P-delta effects.

The deformation/force demands in each structural element is computed at the target displacement and compared against acceptability criteria set forth in the FEMA-356 document. These criteria depend on the material (e.g., concrete, steel etc.), type of member (e.g., beam, column, panel zones, connections etc.), importance of the member (e.g., primary, or secondary) and the structural performance levels (e.g., immediate occupancy, life safety, collapse prevention).

The FEMA-356 NSP procedure contains several approximations. These include those in estimating the target displacement from Eq. 3, and using the pushover curve to estimate the member demands imposed by the earthquake. In this investigation, the focus is primarily on the second source of approximation. Therefore, the target displacement is selected to be equal to that of the roof level recorded during the earthquake, as opposed to calculating it according to the FEMA-356 document (Eq. 3). The structure is pushed to this target displacement using the FEMA-356 lateral load patterns and inter-story drifts are computed. The computed inter-story drifts are then compared with the “derived” inter-story drifts, i.e., those computed directly from the recorded motions using the procedure described in the preceding section. Such a comparison enables evaluation of the adequacy of various lateral load patterns in the FEMA-356 NSP, in particular, if the FEMA-356 NSP is able to capture the higher mode effects, which are likely to be present in the selected buildings.

MPA Procedure

Recently a MPA procedure has been developed to account for the higher mode effects and analytically tested for SAC buildings and ground motions (Chopra and Goel, 2002; Goel and Chopra, 2004). Following is a summary of this procedure.

1. Compute the natural frequencies, ω_n and modes, ϕ_n , for linearly elastic vibration of the building.

2. For the n th-mode, develop the base shear-roof displacement, $V_{bn} - u_{rn}$, pushover curve for force distribution, $s_n^* = \mathbf{m}\phi_n$, where \mathbf{m} is the mass matrix of the structure. Gravity loads, including those present on the interior (gravity) frames, are applied before the modal pushover analysis. The resulting P- Δ effects may lead to negative post-yielding stiffness in the pushover curve. Note the value of the lateral roof displacement due to gravity loads, u_{rg} .
3. Idealize the pushover curve as a bilinear curve. If the pushover curve exhibits negative post-yielding stiffness, the second stiffness (or post-yield stiffness) of the bilinear curve would be negative.
4. Convert the idealized $V_{bn} - u_{rn}$ pushover curve to the force-displacement, $F_{sn}/L_n - D_n$, relation for the n th -“mode” inelastic SDF system by utilizing $F_{sny}/L_n = V_{bny}/M_n^*$ and $D_{ny} = u_{rny}/\Gamma_n\phi_{rn}$ in which M_n^* is the effective modal mass, ϕ_{rn} is the value of ϕ_n at the roof, and $\Gamma_n = \phi_n^T \mathbf{m} \mathbf{1} / \phi_n^T \mathbf{m} \phi_n$.
5. Compute the peak deformation D_n of the n th-“mode” inelastic single-degree-of-freedom (SDF) system defined by the force-deformation relation developed in Step 4 and damping ratio ζ_n . The elastic vibration period of the system is $T_n = 2\pi (L_n D_{ny} / F_{sny})^{1/2}$. For an SDF system with known T_n and ζ_n , D_n can be computed either by nonlinear RHA, from inelastic design spectrum, or by empirical equations for the ratio of deformations of inelastic and elastic systems (Chopra and Chintanapakdee, 2003).
6. Calculate peak roof displacement u_{rn} associated with the n th-“mode” inelastic SDF system from $u_{rn} = \phi_n \phi_{rn} D_n$.
7. From the pushover database (Step 2), extract values of desired responses r_{n+g} due to the combined effects of gravity and lateral loads at roof displacement equal to $u_{rn} + u_{rg}$.
8. Repeat Steps 3-7 for as many modes as required for sufficient accuracy.
9. Compute the dynamic response due to n th-“mode”: $r_n = r_{n+g} - r_g$, where r_g is the contribution of gravity loads alone.
10. Determine the total response (demand) by combining gravity response and the peak “modal” responses using the SRSS rule: $r \approx \max \left[r_g \pm \left(\sum_n r_n^2 \right)^{1/2} \right]$.

Steps 3 to 6 of the MPA procedure described above are used to compute the peak roof displacement associated with the n th-“mode” inelastic SDF system. However, these steps are not necessary for analysis of a building for which recorded motions are available. The contribution of the n th-“mode” to the total roof displacement, u_{rn} , can be computed from modal decomposition of recorded motion using Eq. (2).

Sum-Difference Procedure

The Sum-Difference procedure requires development of the pushover curve for force distribution given by

$$s = s_n \pm s_r \tag{4}$$

in which $s_n = \Gamma_n m \phi_n A_n$ with $\phi_n = nth$ mode shape, $m =$ mass matrix, $\Gamma_n = \phi_n^T m \mathbf{1} / \phi_n^T m \phi_n$, and $A_n =$ pseudo-acceleration of a linear elastic SDF system with period and damping ratio equal to that of corresponding to the nth mode of the building. Typically, values of $n = 1$ and $r = 2$ are used (Kunnath and Gupta, 2000). The floor displacements and story drifts are computed in a manner similar to that in the FEMA-356 NSP but utilizing the pushover curves for force distributions of Eq. (4).

FEMA-356 Check for higher modes

The FEMA-356 criterion for checking presence of significant higher mode effects is applied to the four selected buildings. For this purpose, story shears are computed from two elastic modal analyses: (1) considering sufficient number of modes to capture at least 90% of the total mass, and (2) considering the fundamental mode only. For the Van Nuys building three modes were sufficient to capture 90% of the total mass, whereas five modes were needed for the Woodland Hills, Sherman Oaks, and Los Angeles buildings. The ratio of the story shears from the two analyses is computed and compared with the limiting value of 1.3 specified in the FEMA-356 document in Fig. 1 for the selected buildings. These results lead to the following conclusions.

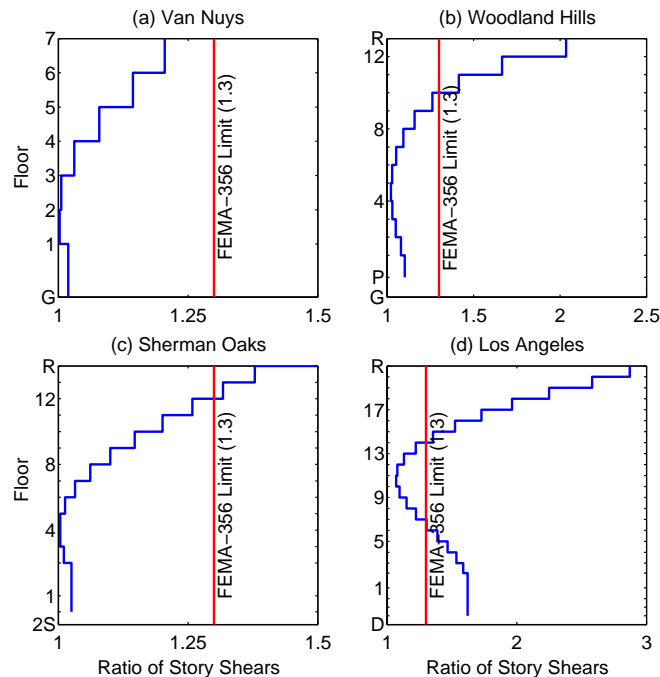


Figure 1. Application of the FEMA-356 criterion to check the presence of higher mode effects in the selected buildings.

The ratio of story shears from 3-mode analysis and 1-mode analysis is less than the FEMA-356 limiting value of 1.3 throughout the height of the Van Nuys building (Fig. 1a). Therefore, the FEMA-356 criterion indicates that higher mode effects should not be significant for this building. However, the ratio of story shears from 5-mode analysis and 1-mode analysis exceeds the FEMA-356 limiting value of 1.3 in upper stories of the Woodland Hills, Sherman Oaks, and Los Angeles buildings (Figs. 1b, 1c, and 1d); for the Los Angeles building this ratio exceeds the limiting value of 1.3 for the lower stories as well (Fig. 1d). Clearly, these buildings are expected to respond significantly in higher modes. Among these three buildings, the FEMA-356 criterion is barely exceeded in upper two stories of the Sherman Oaks building (Fig. 1c).

The results of Fig. 1 indicate that the FEMA-356 NSP is expected to provide sufficiently accurate estimates of the seismic demands for the Van Nuys building and perhaps for the Sherman Oaks building; the FEMA-356 higher mode criterion is satisfied throughout the height of the first building (Fig. 1a) and barely exceeded in upper two stories of the second building (Fig. 1c). However, the FEMA-356 NSP is not expected to give accurate seismic demands for the Woodland Hills and Los Angeles buildings because this criterion is significantly exceeded for these buildings (Figs. 1b and 1d). Since the FEMA-356 NSP is permitted for these buildings in conjunction with the LDP, the results from the FEMA-356 NSP are also included for these two buildings in this investigation.

Pushover Curves

The lateral force distributions corresponding to four FEMA-356 NSP, two distributions in the Sum-Difference procedure ($s_1 + s_2$ and $s_1 - s_2$), and first three modes of the MPA procedure are used to generate pushover curves for the longitudinal frame on the south face of the Van Nuys building, the frame in the north-south direction of the Woodland Hills building, the longitudinal frame in the east-west direction of the Sherman Oaks building, and the braced frames in the north-south direction of the Los Angeles buildings. The first initiation of yielding in beams, columns, connections, or brace (buckling in compression) is also indicated on each pushover curve. The pushover curves presented in Figs. 2 to 4 lead to the following observations.

The characteristic – elastic stiffness, yield strength, and yield displacement – of the pushover curve depend on the lateral force distribution (Fig. 2). The “Uniform” distribution generally leads to pushover curve with higher elastic stiffness, higher yield strength, and lower yield displacement compared to all other distributions. The ELF distribution, on the other hand, leads to pushover curve with lower elastic stiffness, lower yield strength, and higher yield displacement. The “Mode” 1 and SRSS distribution give pushover curves that are bounded by the pushover curves due to “Uniform” and ELF distributions.

For the Van Nuys and Sherman Oaks buildings (Figs. 2a and 2c), the “Mode” 1 and SRSS pushover curves are essentially identical. For the Woodland Hills building (Fig. 2b), the two curves are essentially identical up to the elastic limit. Thereafter, the strength is higher for the SRSS distribution compared to the “Mode” 1 distribution. For the Los Angeles building (Fig. 2d), the “Mode” 1 curve is essentially identical to the ELF curve.

The pushover curves for the Woodland Hills and Sherman Oaks buildings (Figs. 2b and 2c) exhibit significant degradation in lateral load carrying capacity at large roof displacements.

The onset of the degradation depends on the lateral force distribution: the “Uniform” distribution induces the earliest, the ELF distribution the latest, and the “Mode” 1 and SRSS distributions in between the “Uniform” and ELF distributions. The degradation in the lateral load carrying capacity occurs due to P-Delta effects arising from the gravity loads. These effects may lead to negative slope of the pushover curve at large roof displacements, as apparent for the Woodland Hills and Sherman Oaks buildings (Figs. 2b and 2c).

In the Van Nuys building, the first yielding is initiated in the beams; the first yielding of columns occurs at much larger displacements (Fig. 2a). The first yielding in the Woodland Hills building occurs in the connection followed soon after by the first yielding of the beam (Fig. 2b). The columns start to yield at much higher deformation level, followed immediately by rapid deterioration of the lateral load carrying capacity of the building. The first yielding in the Sherman Oaks building occurs in the beam followed soon after by the first yielding of the column (Fig. 2c). The yielding in the Los Angeles building initiates at very low deformation levels due to buckling of the compression braces (Fig. 2d). The columns yield at much higher deformation level.

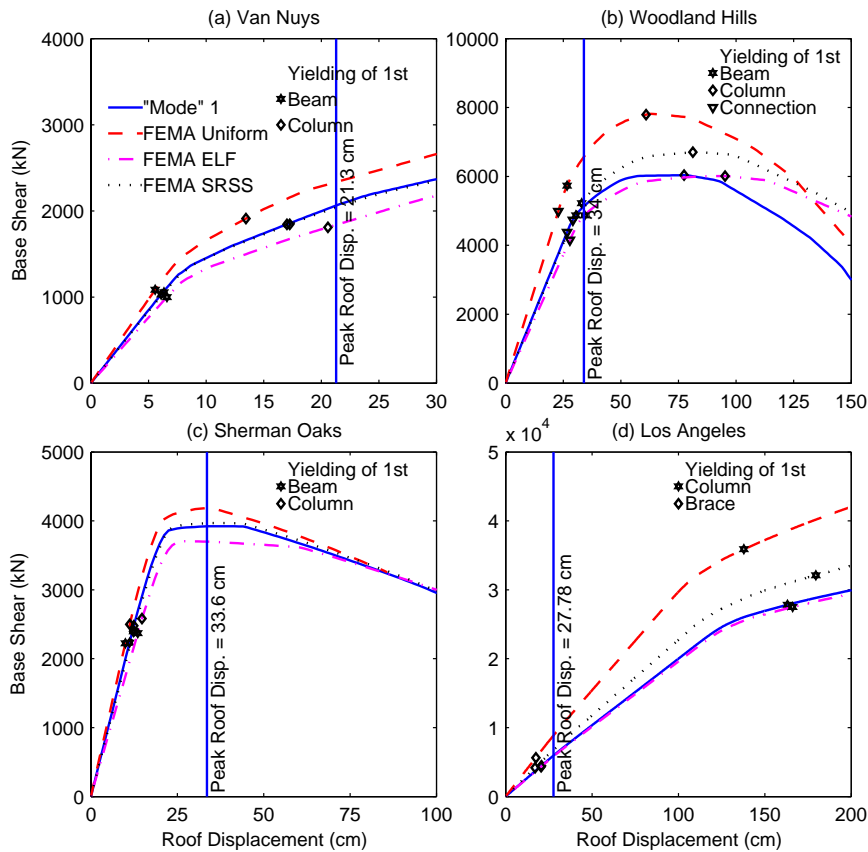


Figure 2. Pushover curves for the four FEMA-356 distributions.

The peak displacement recorded at the roof of each selected building during the 1994 Northridge earthquake is also shown in Fig. 2. These results indicate that the Van Nuys and the Sherman Oaks buildings are deformed significantly beyond the elastic limit during the 1994 Northridge earthquake, as apparent from the peak roof displacement being much larger than the yield displacement (Figs. 2a and 2c). The Woodland Hills building is deformed only slightly

beyond the elastic limit (Fig. 2b), and the Los Angeles building responded essentially in the elastic range (Fig. 2d), except for buckling of few braces, during the 1994 Northridge earthquake.

The pushover curves for the two Sum-Difference distributions (Fig. 3) exhibit significantly different characteristics. The pushover curve for the mode 1+2 distribution exhibits significantly larger initial stiffness and much higher yield strength compared to the mode 1–2 distribution. These differences are much larger than those noted previously (Fig. 2) for four different FEMA-356 distributions. While the mode 1+2 distribution led to significant strength degradation at large roof displacements in the Woodland Hills and the Sherman Oaks buildings (Figs. 3b and 3c) – a pattern similar to that noted for these two buildings for the FEMA-356 distributions (Figs. 2b and 2c) – the mode 1–2 distribution leads to very little degradation in strength. Furthermore, the first yielding in columns is initiated at significantly larger roof displacements due to the mode 1–2 distribution in three of the four buildings (Figs. 3a, 3b, and 3d).

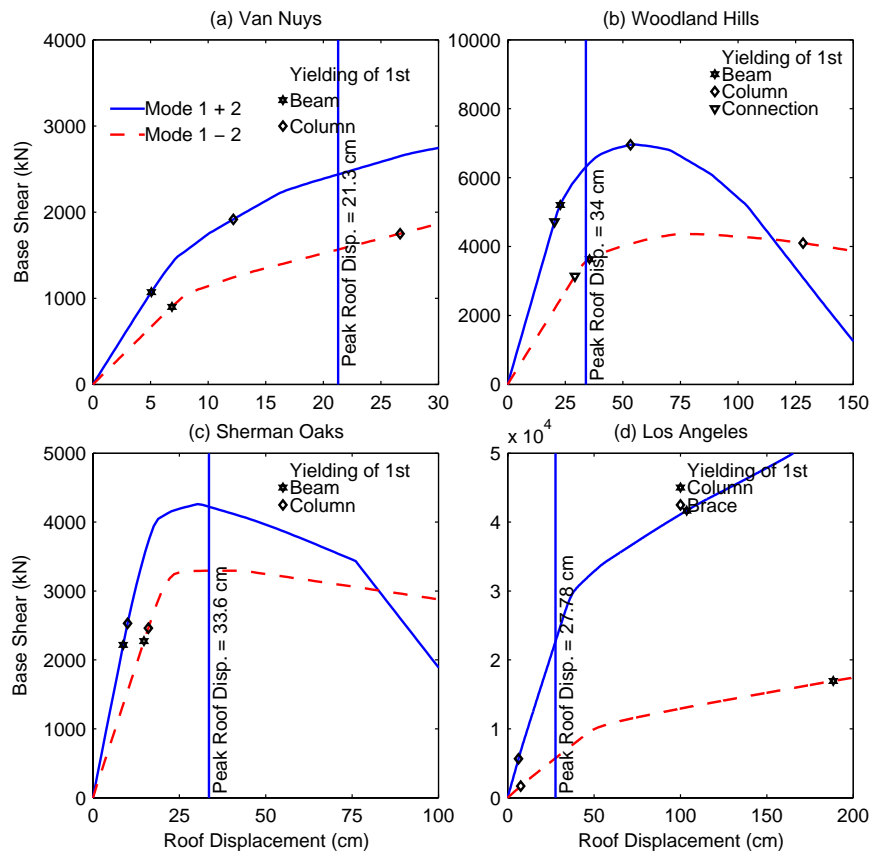


Figure 3. Pushover curves for the two distributions in the Sum-Difference procedure.

The “modal” pushover curves are shown in Fig. 4. Included on each pushover curve is the peak value of the modal component of the roof displacement recorded during the 1994 Northridge earthquake; the modal component is computed from Eq. (2). For example, the peak values of the first, second, and third mode contributions to the total roof displacements were 21.1 cm, 2.93 cm, and 2.75 cm, respectively, during the 1994 Northridge earthquake for the Van Nuys

building. These values are shown on pushover curves for each of the three modes of the Van Nuys building (Fig. 4a).

The “modal” pushover curves show that the Van Nuys building (Fig. 4a) experienced significant yielding in the first “mode”. The building is deformed nearly to the elastic limit of the pushover curve in the second and third modes. However, yielding in these modes has been initiated in some beams and columns, indicating that modes higher than the fundamental mode also contributed to the inelastic behavior of this building. While the Woodland Hills, and Sherman Oaks buildings are deformed beyond the elastic limit only in the first mode (Figs. 4b, and 4c), these buildings remain elastic in the higher modes with the roof displacement component during the 1994 Northridge earthquake being smaller than that required to induce yielding in any element. The Los Angeles building remains essentially elastic in all modes (Fig. 4d). However, the peak roof deformation during the 1994 Northridge earthquake was found to be slightly larger than that required for first buckling in the compression braces for all modes.

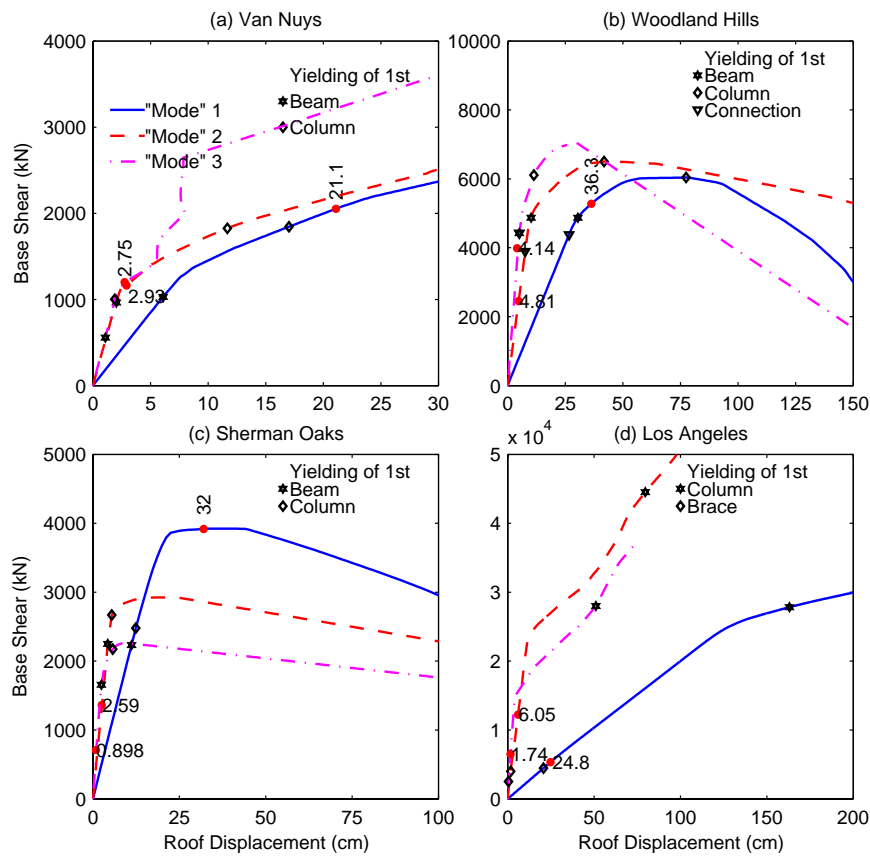


Figure 4. Pushover curves for the three modal distributions in the MPA procedure.

As noted previously, none of the selected buildings responded beyond the elastic limit in modes higher than the fundamental mode. For such buildings, the Modified Modal Pushover Analysis (MMPA), wherein the response contributions of the modes higher than the fundamental mode are computed by assuming the building to be linearly elastic, may be used to estimate the seismic demands (Chopra et al., 2004). The MMPA procedure is an attractive alternative to the

MPA procedure for these buildings because of reduced computational efforts; the pushover curves for higher modes are not needed in the MPA procedure.

The pushover results presented so far also show that while Van Nuys, Woodland Hills, and Sherman Oaks buildings were deformed beyond the elastic limit during the 1994 Northridge earthquake, the Los Angeles building remained essentially elastic during this earthquake. Therefore, the NSP procedures – developed for estimating seismic demands in buildings deformed beyond the elastic limits – may not be strictly applicable for the Los Angeles building. However, the MPA procedure becomes equivalent to the standard Response Spectrum Analysis (RSA) procedure for buildings responding in the linear elastic range (Chopra and Goel, 2001). Therefore, the Los Angeles building provides important data for evaluating applicability of the MPA procedure for linear elastic buildings and is included in this investigation. Although results from the FEMA-356 NSP and the Sum-Difference procedure may not be strictly valid for this building, they are included nonetheless for comparison purposes.

Evaluation of Nonlinear Static Procedures

The nonlinear static procedures are evaluated by comparing the story drifts from the four FEMA-356 analyses, two Sum-Difference analyses, and the MPA procedure with the “derived” values from the recorded motions. The target roof displacement in the FEMA-356 and the Sum-Difference analyses was selected to be that “derived” from the motions recorded at the roof. Furthermore, n th-“mode” component of the roof displacement, u_{rn} , required in the MPA procedure was taken to be the value obtained from the n th “modal” decomposition of the recorded motions. It is useful to emphasize that since two-dimensional models of the buildings have been used in this investigation, the computed and recorded motions examined are those at the center of the each building. Although the FEMA-356 criterion for higher mode effects is significantly exceeded for at least two of the four selected buildings, results from the FEMA-356 NSP are included because such analyses are permitted in conjunction with the LDP analysis.

The comparison of story drifts from the FEMA-356 analyses and the recorded motions (Fig. 5) show that the FEMA-356 force distributions typically lead to gross underestimation of drifts in the upper stories of all of the four selected buildings. Among the four FEMA-356 distributions, the “Uniform” force distribution almost always leads to the worst estimates of story drifts (Fig. 5). This distribution leads to underestimation of the drift at 7th story of the Van Nuys building by more 90% – the story drifts from recorded motions and FEMA-356 “Uniform” distributions are 4.11 cm and 0.32 cm, respectively (Fig. 5a); underestimation of the drift in the top story of the Woodland Hills building by about 67% – the story drifts from recorded motions and FEMA-356 “Uniform” distributions are 3.01 cm and 1.02 cm, respectively (Fig. 5b); underestimation of the drift in the top story of the Sherman Oaks building by more than 80% – the story drifts from recorded motions and FEMA-356 “Uniform” distributions are 1.51 cm and 0.24 cm, respectively (Fig. 5c); and underestimation of the drift in the top story of the Los Angeles buildings by more than 40% – the story drifts from recorded motions and FEMA-356 “Uniform” distributions are 2.86 cm and 1.55 cm, respectively (Fig. 5d). Therefore, usefulness of the “Uniform” distribution in the FEMA-36 NSP should be re-examined. A similar observation was also made in an earlier study based on analytical response of six buildings with steel moment-resisting frames (Goel and Chopra, 2004).

The FEMA-356 NSP also leads to significant overestimation of the drift in lower stories of the Van Nuys and Sherman Oaks building (Figs. 5a and 5c) with the “Uniform” distribution leading to the largest overestimation. For example, the “Uniform” distribution leads to overestimation of the drift in the first story of the Van Nuys building by about 50% – the story drifts from recorded motions and FEMA-356 “Uniform” distributions are 4.80 cm and 7.23 cm, respectively (Fig. 5a); and overestimation of the drift in the first story of the Sherman Oaks building by more than 50% – the story drifts from recorded motions and FEMA-356 “Uniform” distributions are 8.05 cm and 13.60 cm, respectively (Fig 5c).

The presented results for story drifts of the Van Nuys building (Fig. 5a) also demonstrate another serious limitation of the FEMA-356 NSP. The higher mode effects for this building were deemed not to be significant based on the FEMA-356 criterion (Fig. 1a). Therefore, expectation was that the FEMA-356 would lead to reasonable estimates of drifts throughout the building height. Yet the drifts are significantly underestimated in upper stories by the FEMA-356 NSP (Fig. 5a). Since the larger drifts in upper stories tend to occur due to higher modes, it appears that higher mode effects were significant for this building and the FEMA-356 criterion apparently failed to identify these effects. This indicates that the FEMA-356 criterion for significant higher mode effects should be re-examined.

The inability of the FEMA-356 NSP in accurately estimating the drifts in upper stories of the Woodland Hills and Los Angeles buildings – the two buildings for which the FEMA-356 criterion for higher modes is significantly exceeded (Figs. 1b and 1d) – validates the well-known limitation that the FEMA-356 NSP is not applicable for buildings with significant higher mode effects. The authors of FEMA-356 clearly acknowledged this limitation of the FEMA-356 NSP procedure and required that the results of the NSP analyses be supplemented by the results of the LDP analysis for such buildings.

The story drifts from the two Sum-Difference analyses presented in Fig. 6 show that the mode 1+2 distribution gives larger drifts in lower stories and the mode 1–2 distribution leads to larger drifts in upper stories. This observation for the four selected buildings is consistent with that based on one building in an earlier investigation (Kunnath and Gupta, 2000).

It is expected that the envelope of the responses from the two analyses in the Sum-Difference procedure will provide reasonable estimates of the seismic demands throughout the building height. However, comparison of the story drifts from the two Sum-Difference analyses with those from the recorded motions (Fig. 6) shows that this may not always be the case. The Sum-Difference method generally leads to underestimation of the drift in upper few stories of all selected buildings (Fig. 6) with the underestimation being slightly smaller compared to the FEMA-356 NSP analyses (Fig. 5); for the Los Angeles building, however, the Sum-Difference procedures may overestimate the drifts in some upper stories (Fig. 6d). Furthermore, the Sum-Difference method almost always significantly overestimates the drifts in lower stories of all selected buildings (Fig. 6) with the overestimation being much larger than that from the FEMA-356 analyses (Fig. 5).

The results presented for the Sum-Difference procedure indicate that although this procedure tends to give improved drifts in upper stories compared to the FEMA-356 NSP, this procedure is still not accurately able to capture the higher mode effects. Furthermore, the Sum-

Difference procedure provides overestimation of drifts in lower stories of the selected buildings that is worse than that from the FEMA-356 NSP.

The MPA procedure for three of the four selected buildings – Van Nuys, Woodland Hills, and Los Angeles – provides estimates of drifts in most stories that are better than those from the FEMA-356 NSP (Figs. 5a, 5b, and 5c) and the Sum-Difference procedure (Figs. 6a, 6b and 6d). In particular, the match between the drifts from MPA and recorded motions is reasonable good in upper stories indicating that the MPA procedure is able to capture the higher mode effects for these buildings. However, significant discrepancy may exist in few stories, such as drift in the 6th story of the Van Nuys building (Fig. 5a), and top stories of Woodland Hills and Los Angeles buildings (Figs. 5b and 5d). The reasons behind this discrepancy are examined latter in this section.

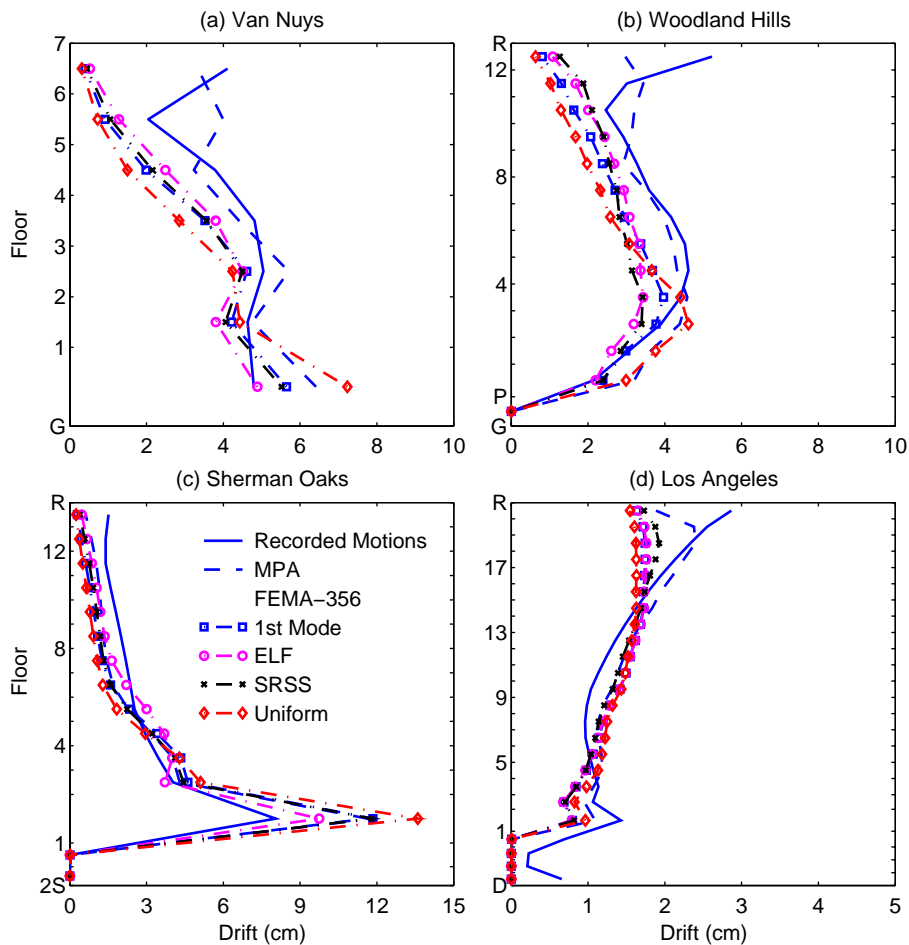


Figure 5. Comparison of story drifts from recorded motions, MPA procedure, and four FEMA-356 NSP for four distributions.

For the Sherman Oaks building, the MPA procedure provides estimates of the story drifts slightly better than those from the FEMA-356 NSP (Fig. 5c) or the Sum-Difference procedure (Fig. 6c). Although not apparent from Fig. 5c, the overestimation of drifts in lower stories and underestimation of drifts in upper stories from the MPA procedure is smaller compared to the FEMA-356 NSP. Furthermore, the overestimation in drifts in lower stories is much smaller from

the MPA procedure compared to the Sum-Difference procedure (Fig. 6c). Yet the results from the MPA procedure are significantly different compared to those from the recorded motions for this building.

The results presented for story drifts of the Sherman Oaks building indicate that the behavior of this building is dominated by the effects of “soft” first story. A large concentration of drift occurs in the first story (Figs. 5c and 6c) both in results from recorded motions as well as NSP analyses; drifts in upper stories are only a small fraction of the drift in the first story. For such a building, where “soft” story effects dominate, all the nonlinear static procedure – the FEMA-356 NSP, the Sum-Difference, and the MPA – failed to provide reasonable estimate of story drifts: these procedures overestimate the drifts in the first story and underestimate them in the upper stories.

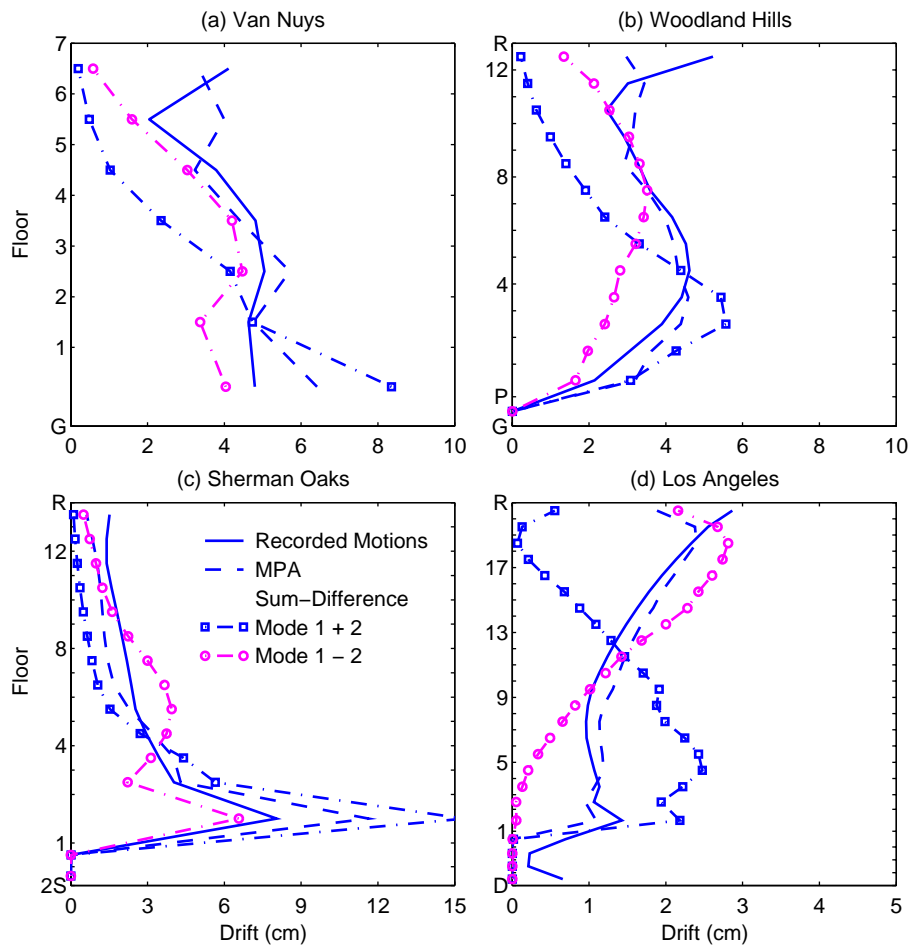


Figure 6. Comparison of story drifts from recorded motions, MPA procedure, and two distributions in the Sum-Difference procedure.

As noted previously, while the estimates of story drifts from the MPA procedure are much better compared to the FEMA-356 NSP, significant differences exist in a few stories. In order to understand the source of this discrepancy, peak drifts in each mode of the MPA procedure are compared with those obtained from modal decomposition of recorded motions (Fig. 17). This comparison shows that the match between the two is reasonably good. Therefore,

the prime source of discrepancy appears to be from modal combination rule used in the MPA procedure.

A fraction of the errors in the modal combination may be attributed to application of the modal combination rule, which is strictly valid for elastic buildings, for buildings responding beyond the elastic range. However, this fraction has been found to be small in an earlier study where errors in the MPA results of elastic and inelastic systems were compared (Goel and Chopra, 2004).

The error in large part appears to be due to application of the modal combination rule for peak responses of a single ground motion. Note that the modal combination rules are based on random vibration theory and the combined peak response should be interpreted as the mean of the peak values of response to an ensemble of earthquake excitations. Thus, the modal combination rules are intended for use when the excitation is characterized by a smooth response (or design) spectrum. Although modal combination rules can also approximate the peak response to a single ground motion characterized by a jagged response spectrum, the errors are expected to be much larger in some cases, as noted in this investigation.

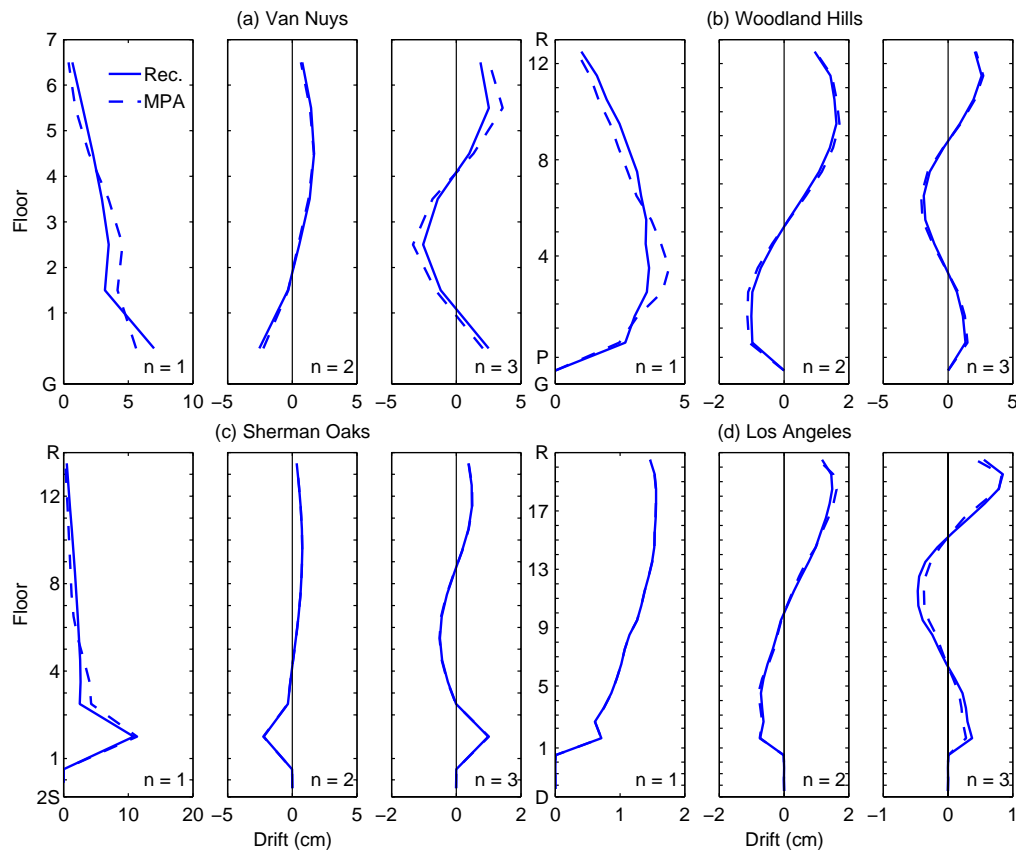


Figure 7. Comparison of story drifts from MPA procedure with results derived from modal decomposition of recorded motions for first three modes ($n = 1, 2,$ and 3).

It is useful to note that while the total drifts in first story of the Sherman Oaks building is significantly overestimated by the MPA procedure (Fig. 5c), the mode-by-mode match between the recorded motions and the MPA procedure is excellent even for this building (Fig. 7c).

Furthermore, each “modal” analysis in the MPA procedure is able to capture the “soft” story effects, as apparent from the concentration of drifts in first story of this building in results for each mode (Fig. 7c).

Conclusions

This research investigation evaluated three nonlinear static procedures (NS) – the FEMA-356 NSP, the Sum-Difference, and the MPA – using recorded motions of four buildings that were damaged during the 1994 Northridge earthquake. The selected buildings were analyzed using the four distributions – “Uniform”, ELF, SRSS, and 1st “Mode” – in the FEMA-356 NSP, two distributions – mode 1+2 and mode 1–2 – in the Sum-Difference procedure, and the MPA procedure. First the pushover curves were examined followed by comparison of story drifts from the three NSP with those from the recorded motions. This investigation has led to the following conclusions:

The pushover curves indicate that the elastic stiffness, yield strength and yield displacement depend on the lateral force distribution. Among the FEMA-356 distributions, the “Uniform” distribution generally leads to pushover curve with higher elastic stiffness, higher yield strength, and lower yield displacement compared to all other distributions; the ELF distribution leads to pushover curve with lower elastic stiffness, lower yield strength, and higher yield displacement; and the “Mode” 1 and SRSS distribution pushover curves are bounded by the pushover curves due to “Uniform” and ELF distributions. Among the Sum-Difference distributions, mode 1+2 distribution leads to significantly larger initial stiffness and much higher yield strength compared to the mode 1–2 distribution. Furthermore, the pushover curves for the Woodland Hills and Sherman Oaks buildings exhibit significant degradation in lateral load carrying capacity at larger roof displacements due to P-Delta effects arising from the gravity loads. Among the four FEMA-356 distributions, the “Uniform” distribution induces the earliest degradation in the lateral load carrying capacity. While the mode 1+2 distribution leads to significant strength degradation at large roof displacements, the mode 1–2 distribution induces very little degradation in strength.

Comparison of the elastic limits of various buildings with the peak roof displacements recorded during the 1994 Northridge earthquake indicates that the Van Nuys and the Sherman Oaks buildings are deformed significantly beyond the elastic limit, the Woodland Hills building is deformed only slightly beyond the elastic limit, and the Los Angeles building responded essentially in the elastic range, except for buckling of few braces. Furthermore, three of the four selected buildings – Van Nuys, Woodland Hills, and Sherman Oaks – are deformed beyond the elastic limit only in the first mode whereas the Los Angeles building remained elastic in all modes during the 1994 Northridge earthquake.

The comparison of the story drifts from the NSP with those from the recorded motions showed that the FEMA-356 NSP led to gross underestimation of drifts in upper stories of all four selected building and significant overestimation of drifts in lower stories of the two of the four buildings. The underestimation in upper stories ranges by 90% for the Van Nuys building to about 40% for the Los Angeles building, and overestimation in lower stories by about 50% occurred for Van Nuys and Sherman Oaks buildings. Among the four FEMA-356 distributions, the “Uniform” force distribution leads to the most excessive underestimation in upper stories and

overestimation in the lower stories. Therefore, usefulness of the “Uniform” distribution in the FEMA-36 NSP should be re-examined.

The presented results also confirm the well-known limitation that the FEMA-356 NSP is not applicable for buildings with significant higher mode effects. The authors of FEMA-356 clearly acknowledged this limitation of the FEMA-356 NSP procedure and required that the results of the NSP analyses be supplemented by the results of the LDP analysis for such buildings.

The FEMA-356 NSP is expected to provide reasonable estimate of the response if the effects of higher modes are deemed not to be significant based on the FEMA-356 criterion. Although the FEMA-356 criterion is clearly satisfied for the Van Nuys building and nearly satisfied for the Sherman Oaks building, the drifts in upper stories are still significantly underestimated indicating the need to re-examine the FEMA-356 criterion for evaluating significant higher mode effects.

The Sum-Difference procedure provides better estimates of drifts in upper stories compared to the FEMA-356 NSP. However, this procedure is still not accurately able to capture the higher mode effects. Furthermore, the Sum-Difference procedure provides overestimation of drifts in lower stories of the selected buildings that is worse than that from the FEMA-356 NSP.

The MPA procedure provides estimates of drifts that are better throughout the building height, with exceptions in a few stories, compared to those from the FEMA-356 NSP and the Sum-Difference procedure. Furthermore, the MPA procedure is able to account for the higher mode effects. This suggests that the limitation that the NSP be used only for buildings for which the response is controlled by the fundamental mode may be removed if the MPA procedure is used to compute the seismic demands.

Finally, all NSP procedures – FEMA-356 NSP, Sum-Difference, and the MPA – failed to provide accurate estimates of story drifts in the building with dominant “soft” first story effects. Therefore, the application of the NSP to such buildings should be carefully examined.

The response for each mode in the MPA procedure matched closely with the modal response obtained from decomposition of the recorded motions, indicating the observed discrepancy between the response from MPA and recorded response is due to limitations in the combination procedure. The modal combination rules are based on random vibration theory and the combined peak response should be interpreted as the mean of the peak values of response to an ensemble of earthquake excitations. Thus, the modal combination rules are intended for use when the excitation is characterized by a smooth response (or design) spectrum. Applied to the peak response to a single ground motion characterized by a jagged response spectrum, the errors are expected to be much larger in some cases, as noted in this investigation.

Acknowledgment

This research investigation is supported by the California Department of Conservation, California Geological Survey, Strong Motion Instrumentation Program (SMIP) through Contract No. 1001-762. This support is gratefully acknowledged.

The author is grateful to Dr. Moh Huang and Mr. David Whitesel of SMIP for providing the recorded motions and structural plans of the selected buildings. Also acknowledged is the assistance provided by Dr. Abe Lynn of Cal Poly, San Luis Obispo, and Dr. Kent Yu of Degenkolb Engineers. Suggestions from members of the SMIAC also helped in improving the quality of research reported in this paper.

References

- ASCE (2000). Prestandard and commentary for the seismic rehabilitation of buildings. *Report No. FEMA-356*, Building Seismic Safety Council, Federal Emergency Management Agency, Washington, D.C.
- Bracci, J. M., Kunnath, S. K. and Reinhorn, A. M. (1997). "Seismic performance and retrofit evaluation for reinforced concrete structures." *Journal of Structural Engineering, ASCE* **123**(1): 3-10.
- Chopra, A. K. (2001). *Dynamics of structures: Theory and application to earthquake engineering*. New Jersey, Prentice Hall.
- Chopra, A. K. and Chintanapakdee, C. (2003). "Inelastic deformation ratios for design and evaluations of structures: Single-degree-of-freedom bilinear systems." *Journal of Structural Engineering, ASCE to appear*
- Chopra, A. K. and Chintanapakdee, C. (2004). "Evaluation of modal and FEMA pushover analyses: Vertically "regular" and irregular generic frames." *Earthquake Spectra* **20**(1): 255-271.
- Chopra, A. K. and Goel, R. K. (2001). A modal pushover analysis procedure to estimate seismic demands for buildings: Theory and preliminary evaluation. *Report No. PEER 2001/03*, Pacific Earthquake Engineering Research Center, University of California, Berkeley, CA.
- Chopra, A. K. and Goel, R. K. (2002). "A modal pushover analysis procedure for estimating seismic demands for buildings." *Earthquake Engineering and Structural Dynamics* **31**: 561-582.
- Chopra, A. K., Goel, R. K. and Chintanapakdee, C. (2004). "Evaluation of a modified MPA procedure assuming higher modes as elastic to estimate seismic demands." *Earthquake Spectra to appear*
- De la Llera, J. C. and Chopra, A. K. (1998). Evaluation of seismic code provisions using strong-motion building records from the 1994 Northridge earthquake. *Report No. UCB/EERC-97/16*, Earthquake Engineering Research Center, University of California, Berkeley, CA.
- Elnashai, A. S. (2001). "Advanced inelastic static (pushover) analysis for earthquake applications." *Journal of Structural Engineering and Mechanics* **12**(1): 51-69.
- Fajfar, P. and Gaspersic, P. (1996). "The N2 method for the seismic damage analysis of RC buildings." *Earthquake Engineering and Structural Dynamics* **25**(1): 31-46.
- FEMA (1997a). NEHRP commentary on the guidelines for the seismic rehabilitation of buildings. *Report No. FEMA-274*, Building Seismic Safety Council, Federal Emergency Management Agency, Washington, D.C.
- FEMA (1997b). NEHRP guidelines for the seismic rehabilitation of buildings. *Report No. FEMA-273*, Building Seismic Safety Council, Federal Emergency Management Agency, Washington, D.C.

- Goel, R. K. (2003a). "Evaluation of modal and FEMA pushover procedures using strong-motion records of buildings." *Earthquake Spectra*, Submitted for Publication.
- Goel, R. K. (2003b). "Evaluation of nonlinear static procedures using strong-motion building records." *SMIP03 Seminar on Utilization of Strong-Motion Data*, Strong Motion Instrumentation Program, CDMG, Oakland, CA.
- Goel, R. K. (2003c). Evaluation of nonlinear static procedures using strong-motion records of buildings. *Report No. CSMIP/03-***, Draft Data Utilization Report, California Strong Motion Instrumentation Program, California Geological Survey, Sacramento, CA.
- Goel, R. K. (2004a). "Evaluation of modal and FEMA pushover analysis procedures using recorded motions of two steel buildings." *2004 Structures Congress*, Nashville, Tennessee.
- Goel, R. K. (2004b). "Evaluation of nonlinear static procedures using building strong motion records." *13th World Conference on Earthquake Engineering, Paper No. 3213*, Vancouver, B.C., Canada.
- Goel, R. K. and Chopra, A. K. (2004). "Evaluation of modal and FEMA pushover analyses: SAC buildings." *Earthquake Spectra* **20**(1): 225-254.
- Gupta, A. and Krawinkler, H. (1999). Seismic demands for performance evaluation of steel moment resisting frame structures (sac task 5.4.3). *Report No. 132*, John A. Blume Earthquake Engineering Center, Stanford, CA.
- Gupta, B. and Kunnath, S. K. (2000). "Adaptive spectra-based pushover procedure for seismic evaluation of structures." *Earthquake Spectra* **16**(2): 367-392.
- Islam, M. S., Gupta, B. and Kunnath, S. K. (1998). "A critical review of state-of-art analytical tools and acceptance criterion in light of observed response of an instrumented nonductile concrete frame building." *6th U.S. National Conference on Earthquake Engineering*, Seattle, WA.
- Krawinkler, H. and Seneviratna, G. (1998). "Pros and cons of a pushover analysis of seismic performance evaluation." *Engineering Structures* **20**(4-6): 452-464.
- Kunnath, S. K. and Gupta, B. (2000). "Validity of deformation demand estimates using nonlinear static procedures." *U. S. Japan Workshop on Performance-Based Engineering for Reinforced Concrete Building Structures*, Sapporo, Hokkaido, Japan.
- Li, R. and Jirsa, J. O. (1998). "Nonlinear analysis of an instrumented structure damaged in the 1994 Northridge earthquake." *Earthquake Spectra* **14**(2): 265-283.
- Maison, B. and Bonowitz, D. (1999). "How safe are pre-Northridge WSMFs? A case study of the SAC Los Angeles nine-story building." *Earthquake Spectra* **15**(4): 765-789.
- Matsumori, T., Otani, S., Shinohara, H. and Kabeyasawa, T. (1999). "Earthquake member deformation demands in reinforced concrete frame structures." *U.S. Japan Workshop on Performance-Based Earthquake Engineering Methodology for RC Building Structures*, Maui, Hawaii.
- Naeim, F. (1997). Performance of extensively instrumented buildings during the January 17, 1994 Northridge earthquake: An interactive information system. *Report No. 97-7530.68*, John A. Martin & Associates, Los Angeles, CA.
- Paret, T. F., Sasaki, K. K., Eilbeck, D. H. and Freeman, S. A. (1996). "Approximate inelastic procedures to identify failure mechanisms from higher mode effects." *11th World Conference on Earthquake Engineering, Paper No. 966*, Acapulco, Mexico.

- Prakash, V., Powell, G. H. and Campbell, S. (1993). Drain-2dx base program description and user guide, version 1.10. *Report No. UCB/SEMM-93-17*, Department of Civil Engineering, University of California, Berkeley, CA.
- Reinhorn, A. M. (1997). Inelastic analysis techniques in seismic evaluations. *Seismic design methodologies for the next generation of codes*. P. Fajfar and H. Krawinkler, Balkema, Rotterdam: 277-287.
- Sasaki, K. K., Freeman, S. A. and Paret, T. F. (1998). "Multimode pushover procedure (MMP) - a method to identify the effects of higher modes in a pushover analysis." *6th U.S. National Conference on Earthquake Engineering*, Seattle, WA.
- Shakal, A. F., Huang, M. and Darragh, R. B. (1994). "Some implications of strong-motion records from the 1994 Northridge earthquake." *SMIP94 Seminar on Utilization of Strong-Motion Data*, Strong Motion Instrumentation Program, CDMG, Sacramento, CA.
- Skokan, M. J. and Hart, G. C. (2000). "Reliability of nonlinear static methods for the seismic performance prediction of steel frame buildings." *12th World Conference on Earthquake Engineering, Paper No. 1972*, Auckland, New Zealand.
- Uang, C. M., Yu, Q. S., Sadre, A., Youssef, N. and Vinkler, J. (1997). "Seismic response of an instrumented 13-story steel frame building damaged in the 1994 Northridge earthquake." *Earthquake Spectra* **13**(1): 131-149.

**CSMIP INSTRUMENTED BUILDING RESPONSE ANALYSIS AND
3-D VISUALIZATION SYSTEM (CSMIP-3DV)**

Farzad Naeim, Ph.D., S.E., Esq., Hung Lee, P.E., Hussain Bhatia, Ph.D., S.E., Scott Hagie and
Konstantinos Skliros

Research and Development Department
John A. Martin and Associates, Inc.

Abstract

The CSMIP-3DV software system illustrates more than ever that seismic instrumentation of buildings is vital for learning from performance of buildings during earthquakes, enhancing engineering practice, and further development of seismic code provisions. The state-of-the-art features of CSMIP-3DV, for the first time, make it possible to evaluate seismic performance of dozens of buildings over many earthquakes in a systematic, consistent, and user-friendly manner. It is anticipated that by the end of the year 2004 CSMIP-3DV users will be able to investigate more than 80 instrumented buildings. Soon thereafter, the entire collection of more than 180 instrumented buildings will be implemented in CSMIP-3DV.

Introduction

This paper provides an overview of a new development sponsored by the California Strong Motion Instrumentation Program (CSMIP) that significantly enhances access to and the utility of strong-motion data obtained from instrumented buildings in learning seismic performance of buildings. Currently more than 180 buildings have been instrumented throughout California by CSMIP. Eventually information regarding all these buildings will be implemented in this system and made available to the structural engineering community. In the first phase of implementation anticipated to be completed before the end of 2004 about 80 buildings with significant earthquake records will be incorporated in this system. The system is scheduled to be released during the CSMIP-2004 Seminar in May 2004 with an initial implementation of about 30 buildings.

The system, code named CSMIP-3DV, permits visualization of building response to earthquake ground motions, facilities for adding newly instrumented buildings and downloading recently recorded building response data from the CISN Engineering Data Center website, and extensive facilities for analysis and evaluation of building response parameters such as displacements, story drifts, changes in dynamic characteristics of the building and so forth.

Following each earthquake, three-dimensional building response can be viewed within a short period of time on the CISN Engineering Data Center website. In addition, structural engineers will be able to download the datasets and perform their own investigations using the software system CSMIP-3DV installed on their own personal computers. The goal of this system

is to revolutionize the use of strong-motion data obtained from instrumented buildings in structural engineering applications and improvement of seismic code provisions.

CSMIP-3DV Documentation

CSMIP-3DV is released on a CD-ROM disc and updated through the Internet. Three manuals document the CSMIP-3DV software system:

1. *CSMIP-3DV User Guide* contains necessary information for installation and basic use of the software system including techniques for downloading additional building datasets and software updates via the Internet.
2. *CSMIP-3DV Technical Manual* contains technical information on the methods utilized by CSMIP-3DV for calculation and analysis of instrumented building response during earthquakes. Details of interpolation techniques used, computations involved in producing three-dimensional visualization of building response, and methodologies utilized for interpretation of building vibration periods, mode shapes, and changes in the dynamic characteristics of the building during an earthquake, or from one earthquake to another, are contained in this manual.
3. *CSMIP-3DV Administrator's Manual* is made available to persons authorized to construct CSMIP-3DV models of instrumented buildings to expand the system's database of buildings and corresponding earthquake records. It contains instructions on using the system's building development utility for development of building models including associated earthquake-specific building and sensor information, maintenance of the CSMIP-3DV database, structure and hierarchy of building and earthquake information within the system, and management of the data and program updates on the CSMIP-3DV secure Internet server for download by end users.

Three-Dimensional Visualizations

CSMIP-3DV Building Models

CSMIP-3DV building models are not structural analysis models. They are models generated to provide a realistic view of response of buildings during earthquakes. All motions displayed by CSMIP-3DV building models are derived from active building instrumentation (sensor time histories). Therefore, although CSMIP-3DV does perform a variety of interpolations to estimate displacements of floors in between instrumented floors, it does not perform any structural analysis.

CSMIP-3DV building models consist of several components. Some of these components are mandatory and must be present in all models. Examples of mandatory components include story heights, sensor locations, floor slabs and grid points defining them. Other components are optional and are used to enhance visualization of the building. Examples of such components include columns, walls, braces, and façades. Inclusion of too many of the optional components in

modeling of a large and complex structure may overburden the PC memory requirements and result in a time consuming pre-visualization calculation process.

Realistic visualization of complex structures may be obtained by careful modeling of floor slabs and inclusion of a proper façade texture. Selecting a proper texture for the exterior façade and enough grid points in laying out the floor slabs probably has the most impact on the user's perception of the building's visualization. For example, consider the Los Angeles – 54 story office building. Figure 1 shows the CSMIP information sheet for this building. The CSMIP-3DV model showing slabs and columns is presented in Figure 2. Although this figure is accurate, it is certainly not eye pleasing as it does not resemble an actual picture of the building shown in Figure 3. Figure 4 shows visualizations using several different exterior textures ending with the texture selected for visualization of the building.

Visualization Engine

CSMIP-3DV uses the Direct-3D component of Microsoft Direct-X animation engine for visualization of buildings. Direct-X is a very powerful graphics engine intended for development of video games on personal computers. It is commonly referred to as the gaming engine for the Microsoft Windows platform. The position (E-W, N-S and rotation) of the center of geometry of each floor for each time step during the response of the building to earthquake ground motion is calculated by the program. This position information along with story heights and plan boundaries of each floor is communicated to the Direct-3D engine which takes care of the necessary transformations and returning the position of every point on the building at each time step, as needed for visualization.

In CSMIP-3DV visualization, x is the horizontal axis at the bottom of the PC monitor screen, y is the vertical axis in the plane of monitor, and z is the axis perpendicular to the monitor screen pointing towards the user. The following transformation matrices are used for visualization. Please note that the 4th item on each vector is the scale factor (usually set to unity).

Translation:

$$[x_{new} \quad y_{new} \quad z_{new} \quad 1] = [x_{old} \quad y_{old} \quad z_{old} \quad 1] \begin{bmatrix} 1 & 0 & 0 & 0 \\ 0 & 1 & 0 & 0 \\ 0 & 0 & 1 & 0 \\ \Delta_x & \Delta_y & \Delta_z & 1 \end{bmatrix}$$

Scaling:

$$[x_{new} \quad y_{new} \quad z_{new} \quad 1] = [x_{old} \quad y_{old} \quad z_{old} \quad 1] \begin{bmatrix} S_x & 0 & 0 & 0 \\ 0 & S_y & 0 & 0 \\ 0 & 0 & S_z & 0 \\ 0 & 0 & 0 & 1 \end{bmatrix}$$

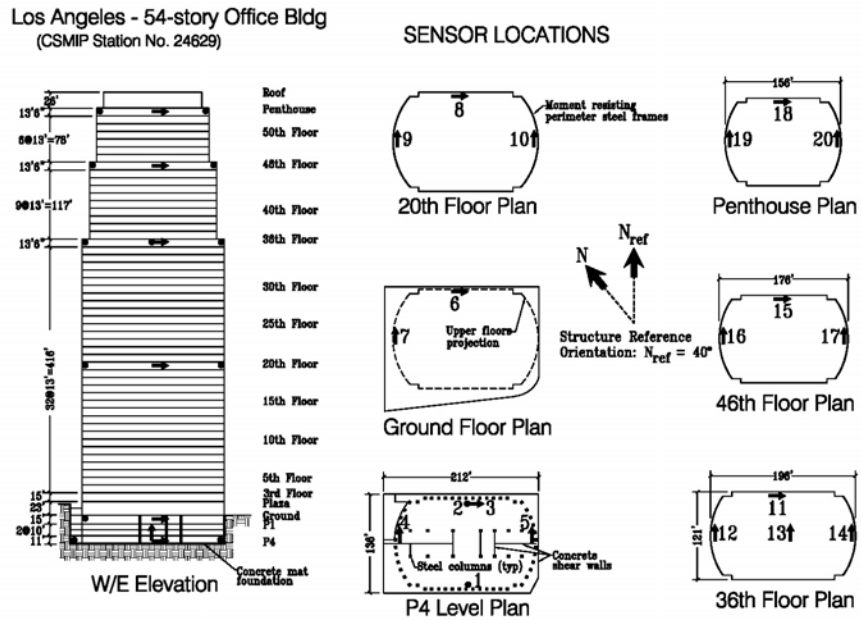


Figure 1. CSMIP data sheet for the Los Angeles 54 story Office Building

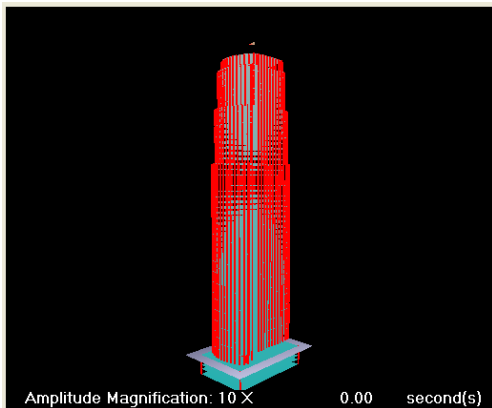


Figure 2. CSMIP-3DV model without the exterior façade



Figure 3. A photo of the Los Angeles – 54 story Office Building

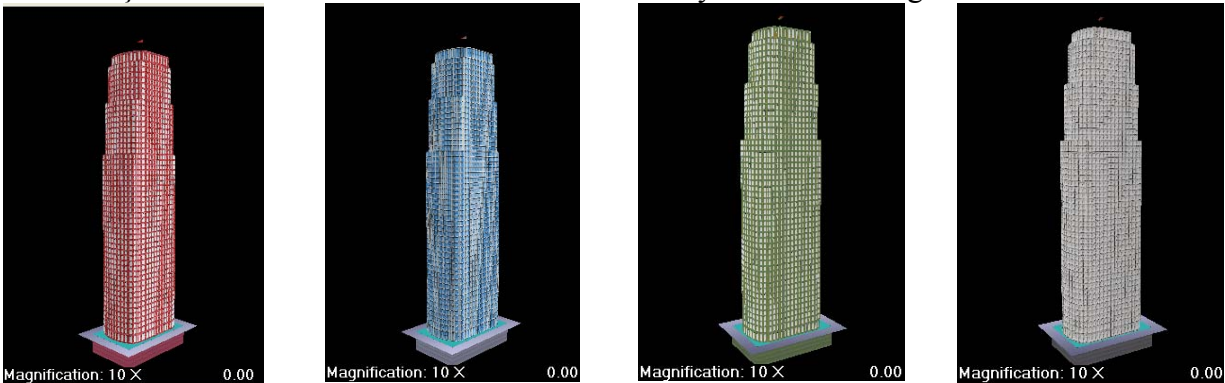


Figure 4. Some of the façade options examined for the Los Angeles 54 story Office Building

Rotation About x axis:

$$\begin{bmatrix} x_{new} & y_{new} & z_{new} & 1 \end{bmatrix} = \begin{bmatrix} x_{old} & y_{old} & z_{old} & 1 \end{bmatrix} \begin{bmatrix} 1 & 0 & 0 & 0 \\ 0 & \cos(\theta) & \sin(\theta) & 0 \\ 0 & -\sin(\theta) & \cos(\theta) & 0 \\ 0 & 0 & 0 & 1 \end{bmatrix}$$

Rotation About y axis:

$$\begin{bmatrix} x_{new} & y_{new} & z_{new} & 1 \end{bmatrix} = \begin{bmatrix} x_{old} & y_{old} & z_{old} & 1 \end{bmatrix} \begin{bmatrix} \cos(\theta) & 0 & -\sin(\theta) & 0 \\ 0 & 1 & 0 & 0 \\ \sin(\theta) & 0 & \cos(\theta) & 0 \\ 0 & 0 & 0 & 1 \end{bmatrix}$$

Rotation About z axis:

$$\begin{bmatrix} x_{new} & y_{new} & z_{new} & 1 \end{bmatrix} = \begin{bmatrix} x_{old} & y_{old} & z_{old} & 1 \end{bmatrix} \begin{bmatrix} \cos(\theta) & \sin(\theta) & 0 & 0 \\ -\sin(\theta) & \cos(\theta) & 0 & 0 \\ 0 & 0 & 1 & 0 \\ 0 & 0 & 0 & 1 \end{bmatrix}$$

Interpolation Schemes and Virtual Sensors

Calculation of Story Displacements from Sensor Data

Calculation of story displacements is the first step for visualization and response evaluations. Instrumented buildings generally have sensors installed at a limited number of floors. Therefore, the displacements at floors in between the instrumented floors need to be approximated using appropriate interpolation schemes. Current version of CSMIP-3DV assumes that floor diaphragms are rigid in their own plane. The E-W and N-S displacements of each instrumented floor (A_x , A_y) and its rotation (θ) about a pre-defined point (usually the floor's geometric center) for each time step is calculated first. Then (A_x , A_y and θ) for floors in between are estimated using an interpolation scheme. Two interpolation schemes are currently implemented in CSMIP-3DV, linear and cubic spline. Both interpolation schemes may be combined as needed for a building as long as the range of floors they approximate do not overlap. For example, linear interpolation may be used for the sub-basement levels of a tall building followed by cubic spline interpolation for floors above the ground. The typical arrangement of sensors on an instrumented floor is shown in Figure 5.

This floor has three sensors with the coordinates (x_1, y_1) , (x_2, y_2) and (x_3, y_3) . For every time step these sensors report displacements A_1 , A_2 and A_3 . Let us assume that the floor's geometric center has coordinates (x_c, y_c) . The relation between sensor displacements and those of a point with coordinates (x_c, y_c) on the floor is:

$$\begin{bmatrix} A_1 \\ A_2 \\ A_3 \end{bmatrix} = \begin{bmatrix} 0 & 1 & (x_1 - x_c) \\ 0 & 1 & (x_2 - x_c) \\ 1 & 0 & -(y_3 - y_c) \end{bmatrix} \begin{bmatrix} A_x \\ A_y \\ \theta \end{bmatrix}$$

The E-W and N-S displacements of a point with coordinates $(x_c$ and $y_c)$ on the floor may be obtained from:

$$u_x = A_x - (y_y - y_c) \theta$$

$$u_y = A_y - (x_x - x_c) \theta$$

The displacement of the geometric center of the floor is:

$$\begin{bmatrix} A_x \\ A_y \\ \theta \end{bmatrix} = \begin{bmatrix} \frac{y_c - y_3}{x_2 - x_1} & \frac{y_3 - y_c}{x_2 - x_1} & 1 \\ \frac{x_2 - x_c}{x_2 - x_1} & \frac{x_c - x_1}{x_2 - x_1} & 0 \\ -\frac{1}{x_2 - x_1} & \frac{1}{x_2 - x_1} & 0 \end{bmatrix} \begin{bmatrix} A_1 \\ A_2 \\ A_3 \end{bmatrix}$$

The same formulas may be used to obtain displacements of any other point on the floor by substituting the coordinates of that point instead of (x_c, y_c) . Please note that for this method to work there must be three activated sensors per instrumented floor. If less than three sensors are present or activated per instrumented floor, then CSMIP-3DV's virtual sensor generation utility may be used to generate a time history for a virtual sensor at the desired location on the floor.

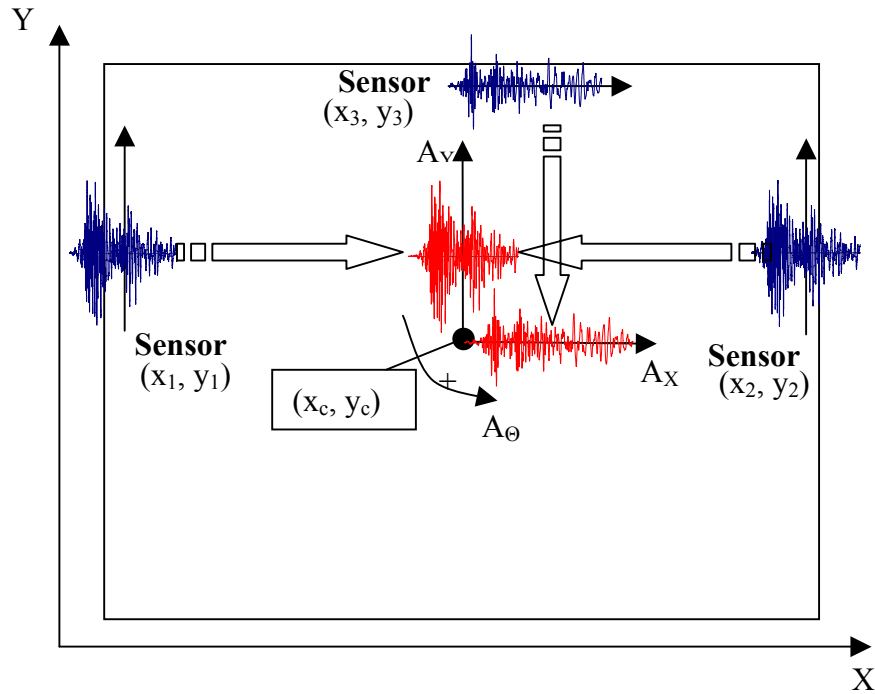


Figure 5. Typical sensor layout for an instrumented floor of a building

Interpolations

A cubic spline is a third-order curve applied to subsets of pre-defined h and $f(h)$ values (i.e., sensor elevations and response parameters, respectively). Given a complete third order polynomial in the form:

$$f(h) = ah^3 + bh^2 + ch + d$$

the coefficients a , b , c and d are determined by forcing the $f(h)$ values and their derivatives be equal at each node when calculated from adjacent sub-interval polynomials. The computation of spline coefficients for each-sub interval (the distance between two adjacent nodes) involves the solution of a tri-diagonal system of linear equations. Once the interval i containing the h value is determined, the value of the interpolated function is determined from

$$f_i(h) = a_i(h - h_i)^3 + b_i(h - h_i)^2 + c_i(h - h_i) + d_i$$

This operation is performed by CSMIP-3DV for every time step of the recorded sensor motion.

A cubic spline results in smooth transition between data points. This property is particularly desirable for conventional buildings but it is not suited for base isolated buildings. In such cases linear interpolations or linear-cubic spline combination may be used. Linear interpolation in CSMIP-3DV extends from one instrumented floor to the next. This means that the resulting displaced shape using linear interpolation will be piecewise linear if more than two instrumented floors are present in the building. Using the same notation used for cubic spline interpolation,

$$f(h) = ch + d$$

where the coefficients c and d are determined by forcing the $f(h)$ value to be equal to the values of the instrumented floor at each end. Therefore,

$$f_i(h) = c_i(h - h_i) + d_i$$

Please note that CSMIP-3DV does not *extrapolate* displacements. That is sensors must be present at the base and the roof of the building.

Virtual Sensors

There are occasions where an instrumented floor has less than three sensors present or activated during an earthquake. Using the techniques described above, such floors would be excluded from analysis and valuable earthquake data from the sensors on such floors would not be taken into consideration. Examples of where the use of virtual sensors may be helpful are given in the Figures 6 and 7.

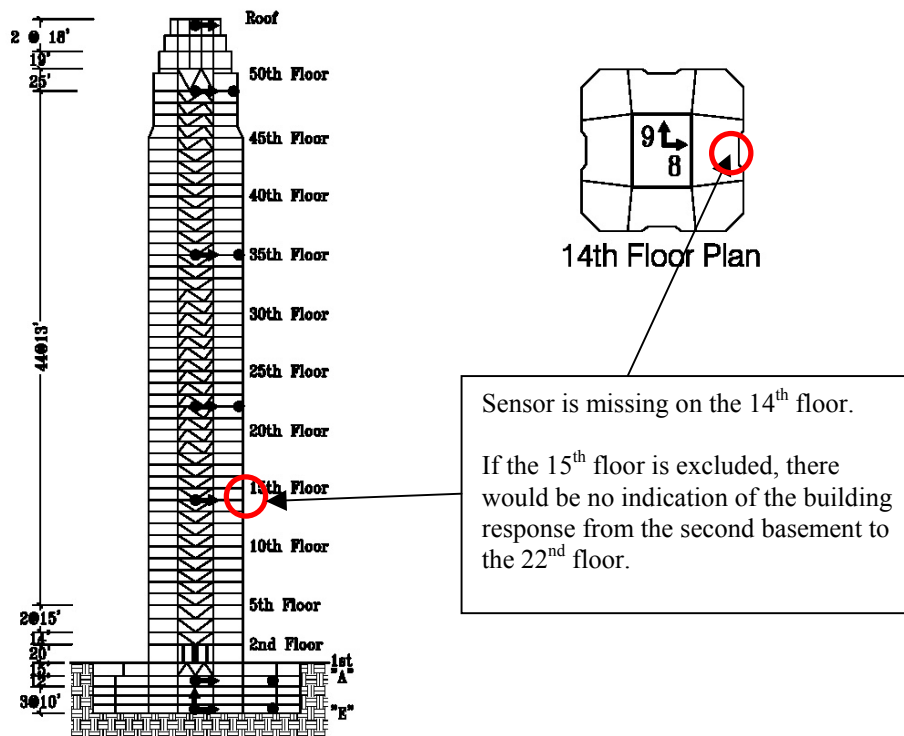


Figure 6. The need for virtual sensors (52 Story Los Angeles Building)

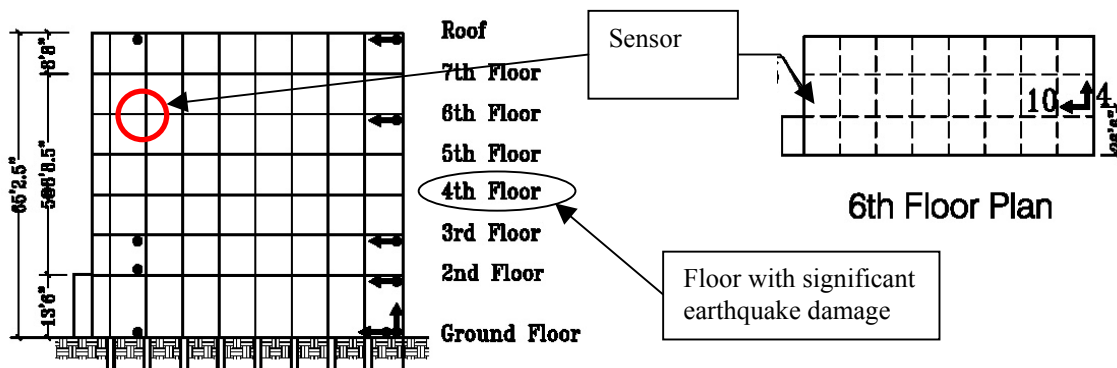


Figure 7. The need for virtual sensors (7 Story Van Nuys Hotel)

CSMIP-3DV generates virtual sensor time histories at the locations specified by the user as follows. First, interpolation according to the rules specified for the building is performed along the vertical line where a virtual sensor is located. Then a virtual sensor time history is generated and saved. Once the desired virtual sensor data files are generated, the problem is reduced to the routine interpolations that CSMIP-3DV performs. For example, in Figure 8 one instrumented floor has two real sensors (sensors 7 and 8). In order to define the virtual sensor's time history, CSMIP-3DV can use the time histories from sensors installed in that location on other floors (i.e. sensors 1, 4 and 9) to estimate the time history that a sensor at the desired location would have generated. Once the virtual sensor time history is created, the floor with the two real sensors could be used as an ordinary instrumented floor.

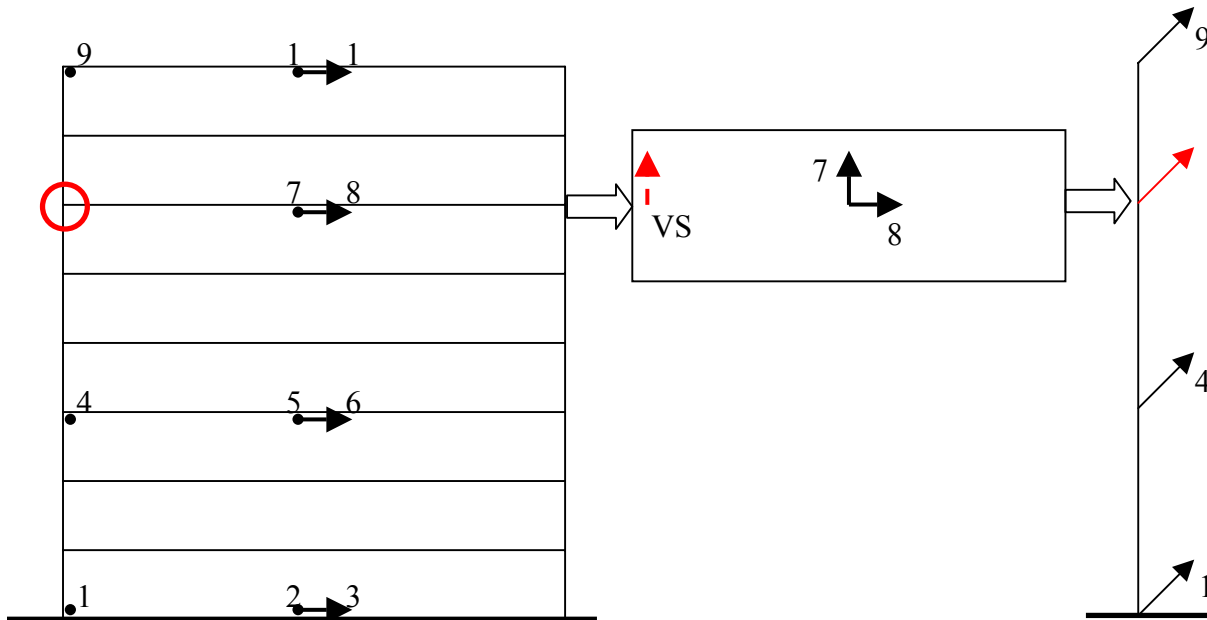


Figure 8. Example of virtual sensor generation

To verify the accuracy of this approach, we removed the real sensor data from selected floor of a number of buildings, generated virtual sensor time histories at the same positions and then compared the real and virtual time histories obtained for the same location. In all instances the virtual sensor was remarkably accurate in estimating the maximum displacements. It would deviate in some cases, however, from intermediate response values particularly in the high frequency portions of the time history. An example of such comparison is shown in Figure 9.

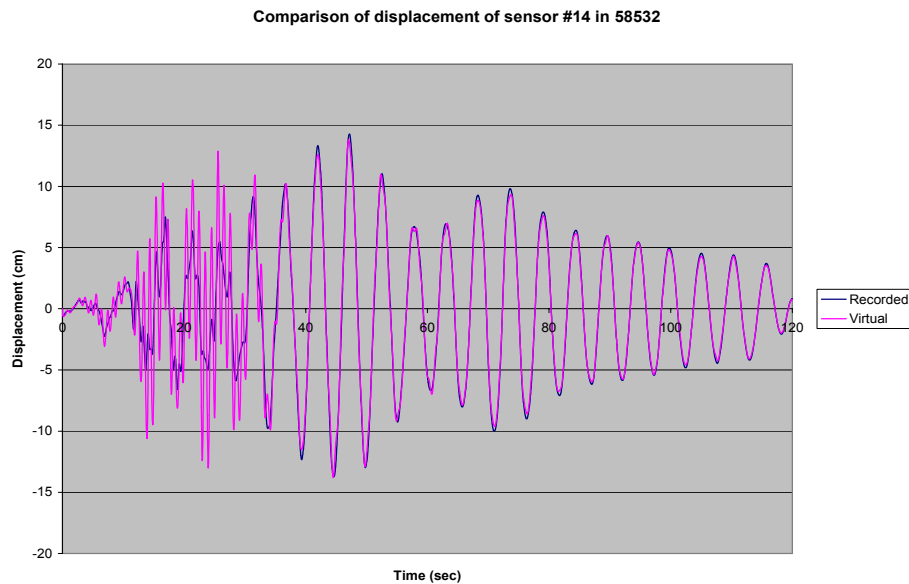


Figure 9. Comparison of an actual and the corresponding virtual sensor data

Evaluation and manipulation of Sensor Data

CSMIP-3DV offers a multitude of facilities for evaluation and manipulation of sensor data. As far as sensor time histories are concerned, up to four sensors may be selected at a time and their records added, subtracted, and averaged. For each sensor, acceleration, velocity and displacement records are available (see Figure 10). Response spectra facilities for evaluation of spectral displacement (SD), spectral velocity (SV), pseudo-velocity (PSV), spectral acceleration (SA), tripartite plot of response spectra, Fourier amplitude, PSA versus SD (ADRS), and SV and PSV on one graph. The user may select the desired level of damping. By default CSMIP-3DV displays the values corresponding to all damping levels (0%, 2%, 5%, 10%, and 20%).

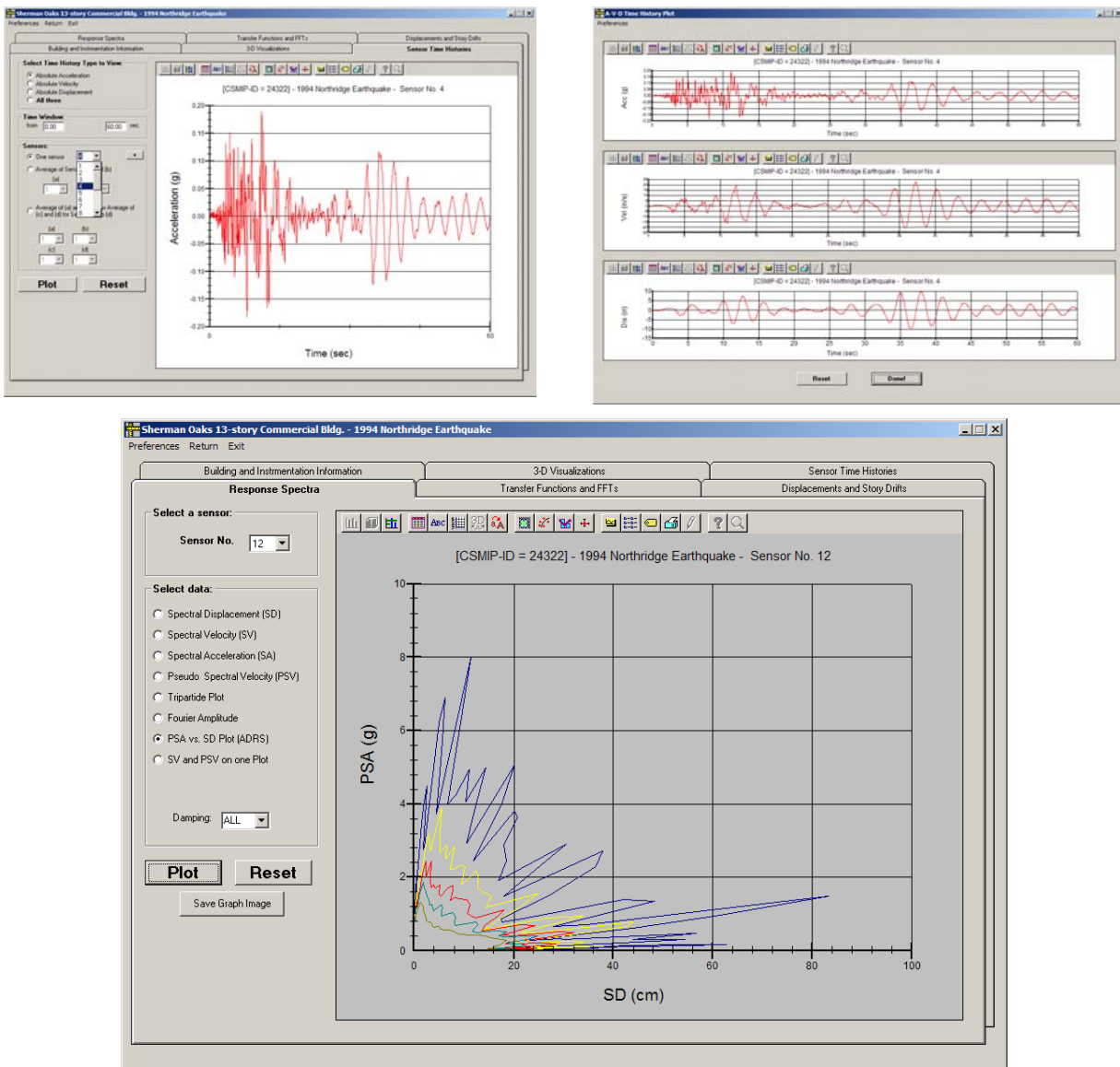


Figure 10. Examples of CSMIP-3DV sensor data manipulation utilities

Key Response Parameter Evaluations

CSMIP-3DV calculates lateral displacements and story drifts for various floors from the time history of sensors installed and instrumented floors of the building. Floors with sensors are identified by a \boxtimes on the graphs. A combination of cubic spline and linear interpolations are used to estimate the motion of the floors in between instrumented locations. For example, for a base-isolated building, there is a discontinuity in the function between the floors below the isolation plane and the ones above this plane. Therefore, CSMIP-3DV may use a linear interpolation for floors below the isolation plane and a cubic spline interpolation for floors above the isolation plane (see Figure 11). The type of various interpolations used and the limits of their application over the height of the building are set in one of the two input files prepared for the building.

The user may evaluate lateral displacements, inter-story drifts, or inter-story drift ratios. CSMIP-3DV also displays the envelope of negative and positive values of the parameter being investigated during the selected earthquake on the graph. The user may select any two adjacent floors to view a time-history of inter-story drifts or drift-ratios between these floors and time history of that parameter (Figure 12).

Each of these response parameter values may be evaluated in one of the two following directions:

- building's reference E-W direction, or
- building's reference N-S direction

Response parameter values may be examined at any of the following times:

- Any instant of time selected by the user.
- At the time of maximum E-W lateral displacement
- At the time of maximum N-S lateral displacement
- At the time of maximum E-W story drift throughout the building
- At the time of maximum N-S story drift throughout the building

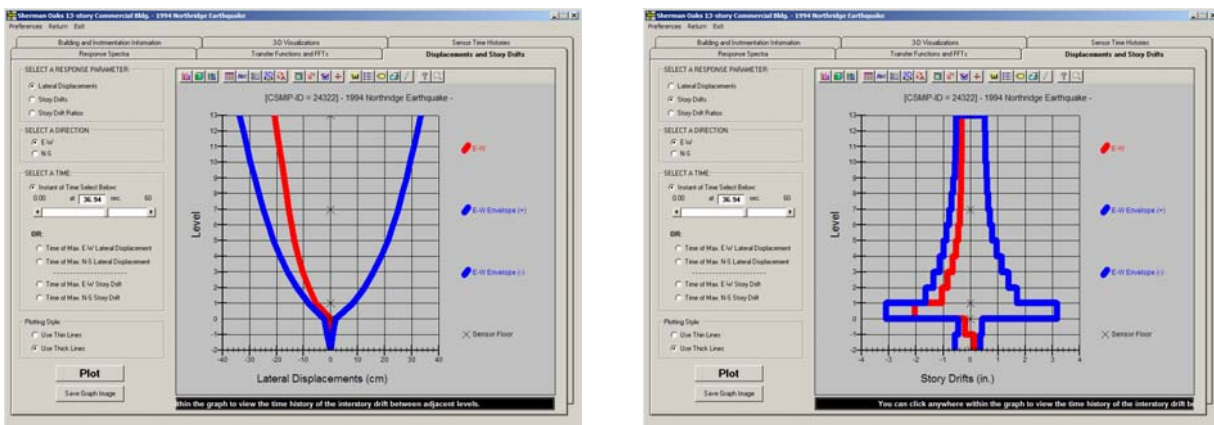


Figure 11. Examples of story displacement and drift diagrams generated by CSMIP-3DV



Figure 12. Evaluation of interstory drift time history and number of times that various thresholds of drift are exceeded.

Transfer Functions and Fast Fourier Transforms

Fourier Transforms

The CSMIP Instrumented Building Response Analysis system extracts the time histories and response spectra directly from appropriate SMIP Volume 2 and 3 data files. The program extracts, decompresses, utilizes, and discards on-the-fly the decompressed files it needs for any given operation. The transformation from the time domain to the frequency domain is based on the *Fourier Transform* defined as

$$S_x(f) = \int_{-\infty}^{\infty} x(t) e^{-i2\pi ft} dt$$

where $x(t)$ is the time domain representation of the signal x (i.e., the sensor time history); $S_x(f)$ is the frequency domain representation of the signal x and $i = \sqrt{-1}$.

Since the sensor time histories are given at distinct intervals (i.e., 50 or 100 data points per second), numerical integration techniques need to be used

$$S_x(m \Delta f) = \int_{-\infty}^{\infty} x(t) e^{-i2\pi ft} dt$$

where $m = 0, \pm 1, \pm 2$ etc., Δf is the frequency spacing of the lines and Δt is the time interval between samples. As it is not possible to numerically evaluate this integral from minus to plus infinity, the transform is limited to a finite time interval and hence we can rewrite the above formula as

$$S_x(m \Delta f) = \Delta t \sum_{n=0}^{N-1} x(n \Delta t) e^{-i2\pi m \Delta f n \Delta t}$$

or as the *Discrete Fourier Transform (DFT)*:

$$S_x(m \Delta f) = \frac{T}{N} \sum_{n=0}^{N-1} x(n \Delta t) e^{-i2\pi mn / N}$$

Fast Fourier Transforms

As the summation of the series used in the discrete Fourier transform (DFT) is computationally time intensive, a more efficient method called the *Fast Fourier Transforms* (FFT) is normally used. CSMIP-3DV uses the *Danielson-Lanczos* or *bit reversal* technique for computing the FFT of time series. FFT algorithms, however, this method requires the number of data points (N) be a multiple of 2. The program automatically computes the intervals of time that meet this requirement. The user can select the portion of the record to use in computing the Fourier Transform.

Various choices are provided for computing the Fourier Transform:

1. Compute the Fourier Transform of a single sensor record.
2. Compute a Transfer Function between two sensor records. A transfer function is defined as the complex ratio of the Fourier Transform of two sensor records.

3. Compute the product of the Fourier Transform of two sensor records. Note, the result is a complex number.
4. A transfer function using four sensor records, with either the difference or sum of two sensor records in the denominator or numerator. The difference or sum of the sensors is done in the time domain before the Fourier transform is computed.

All the above options can be used using the acceleration, velocity or displacement data for each sensor. All computations are done in double precision.

Windowing Functions

Windowing functions are used to reduce leakage. Leakage is a problem which is a direct consequence of the need to take only a finite length of time history coupled with the assumption of periodicity. The Fourier Transform of a sinusoidal time trace with a finite length that is not an integer multiple of its period, will not indicate the single frequency which the original time signal possessed. Energy is 'leaked' into a number of the spectral lines close to the true frequency and the spectrum is spread over several line or windows.

One practical solution to the leakage problem is the use of windowing functions. There are many different windowing functions available for different classes of problems. Windowing involves the imposition of a prescribed profile on the time signal prior to performance of the Fourier Transformation. The analyzed signal is given as

$$x'(t) = x(t) \cdot W(t)$$

where $x(t)$ is the original time trace and $W(t)$ is the windowing function.

A number of windowing functions have been implemented in CSMIP-3DV. Figure 13 shows Fourier transform of a sine wave ($f = 1$ Hz) with various windowing functions.

1. Hanning Windowing Function:

$$W(n) = 0.5 - 0.5 \cos(2\pi n / N)$$

2. Hamming Windowing Function:

$$W(n) = 0.54 - 0.56 \cos(2\pi n / N)$$

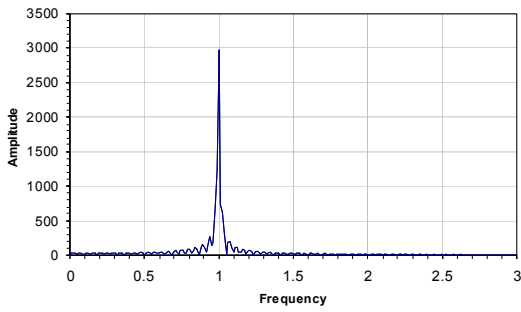
3. Blackman-Harris Windowing Function:

$$W(n) = a_0 - a_1 \cos(2\pi n / N) + a_2 \cos(4\pi n / N) - a_3 \cos(6\pi n / N)$$

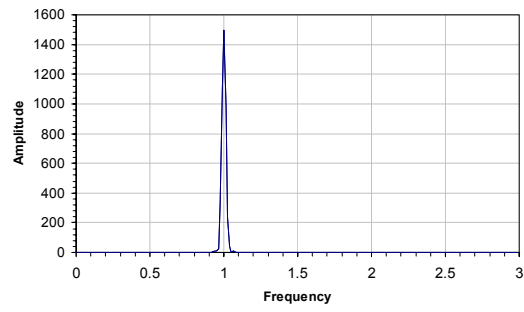
where $a_0 = 0.355768$, $a_1 = 0.487396$, $a_2 = 0.144232$ and $a_3 = 0.012604$.

4. Cosine Taper Window:

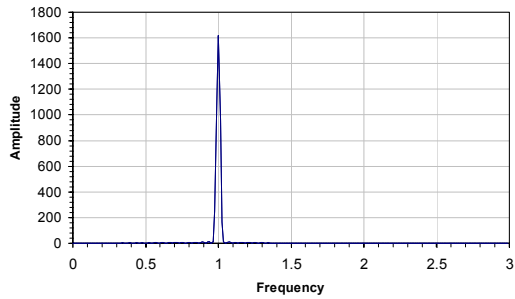
$$\begin{aligned} W(n) &= 0.5 - 0.5 \cos(2\pi n / (N / 4)) && \text{for } n = 1 \dots N / 4 \\ W(n) &= 1 && \text{for } n = N / 4 \dots 3N / 4 \\ W(n) &= 0.5 - 0.5 \cos(2\pi(n - 3N / 4) / (N / 4)) && \text{for } n = 3N / 4 \dots N \end{aligned}$$



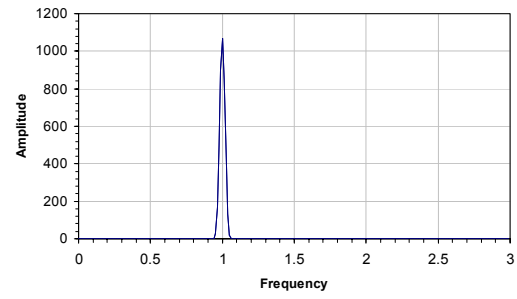
(a) no windowing function



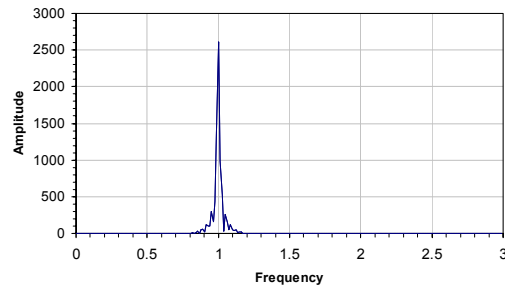
(b) Hanning windowing function



(c) Hamming windowing function



(d) Blackman-Harris windowing function



(e) Cosine-Taper windowing function

Figure 13. Fourier transform of a sine wave ($f = 1$ Hz) with various windowing functions

Transfer Functions

For a single degree of freedom system, the Transfer Function is defined as the frequency domain response due to an impulse function. The input impulse function for a single degree of freedom system is shown in Figure 14a. The response of the SDOF system, which has a natural period of 1.7 sec. is shown in Figure 14b. The Transfer Function obtained for this SDOF system using the CSMIP-3DV is shown in Figure 14c. The Transfer Function obtained is as is theoretically predicted with the real component changing signs and the imaginary component showing a peak at the natural frequency.

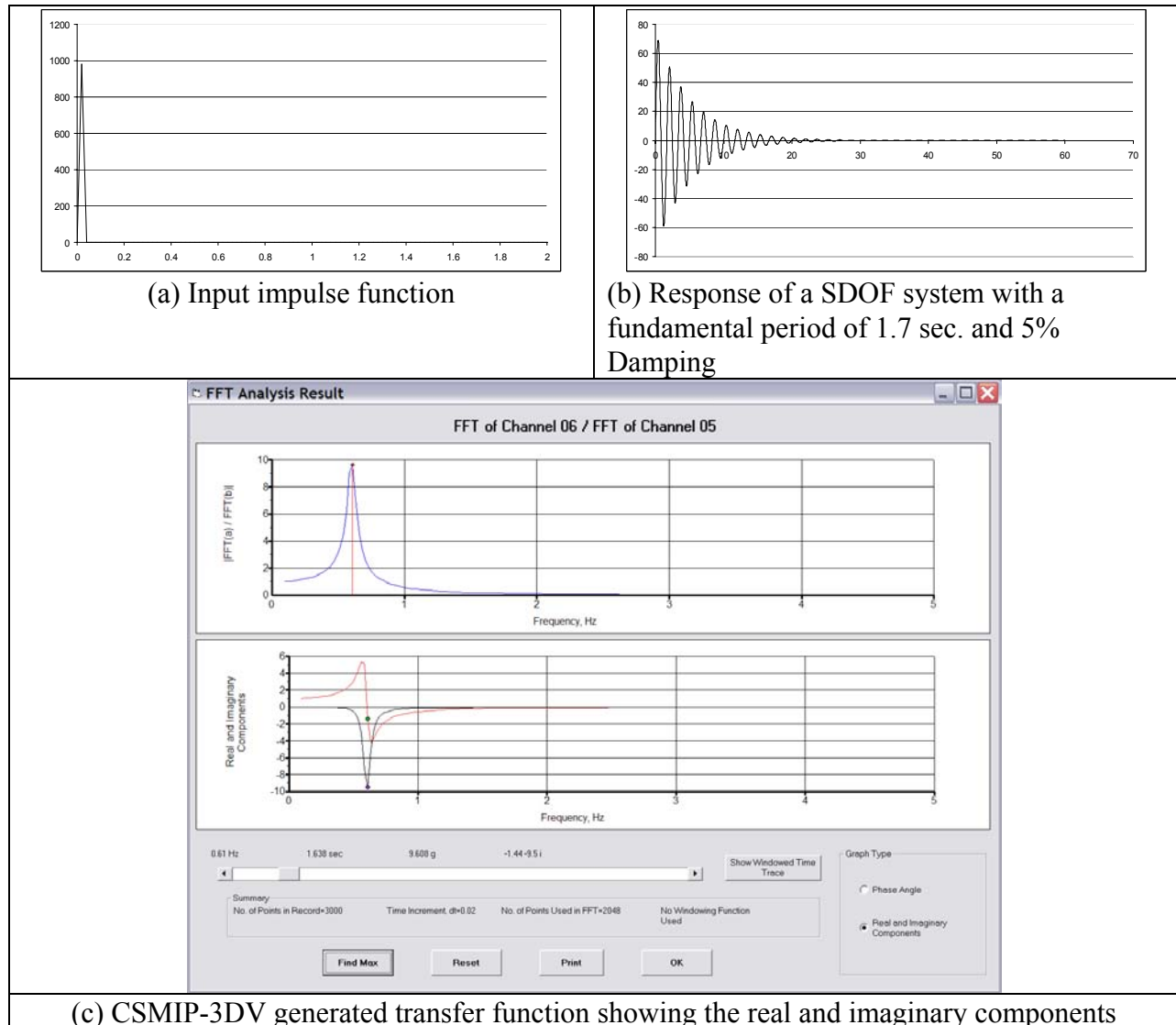


Figure 14. Transfer function for a single degree of freedom system

Examples of the transfer functions for CSMIP Station No. 24629 (Los Angeles 54 Story Office Building) in response to the 1994 Northridge earthquake are presented here. A transfer function of Sensor No. 19 relative to a sensor in the basement (FFT for Sensor 19/FFT for Sensor 4) clearly indicates that the first transverse mode of the building has a period of 6.3 secs. The real component changes sign at this period (Figure 15) as would be expected at a mode of vibration for the building.

It is possible to remove the effect of torsional modes by using the average of the sensors at a floor. An example of a transfer function using the average of sensor records at the roof and the basement is shown in Figure 16. Using the difference of the sensor records, it is also possible to show only the torsional modes. An example is shown in Figure 17 using the sensor records at the roof and basement. The first torsional mode occurs at 2.78 Hz.

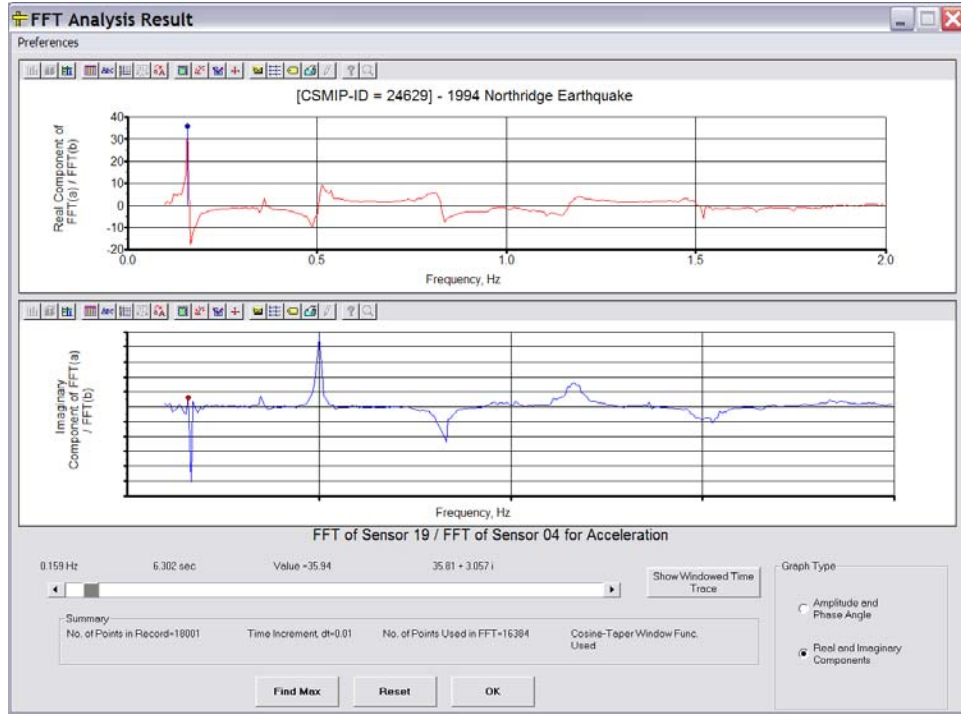


Figure 15. Real and imaginary components of transverse (north-south) transfer function of roof relative to the ground

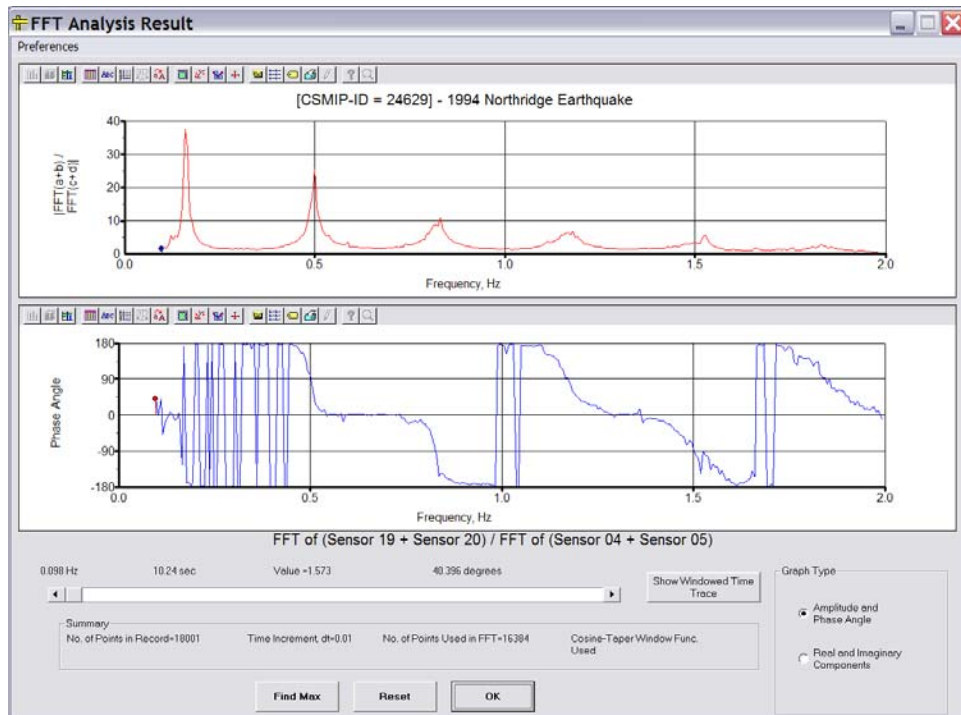


Figure 16. Transfer function of roof relative to basement without torsion

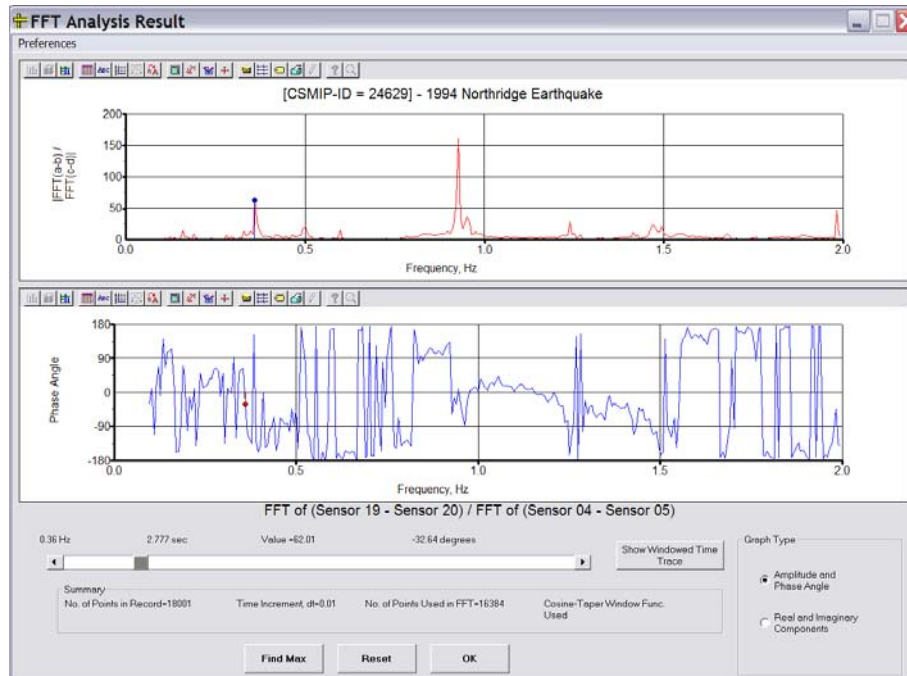


Figure 17. Torsional transfer function of roof relative to basement

Moving Windows FFT in Instrumented Buildings

CSMIP-3DV has an option to perform a moving windows FFT analysis. Here the FFT analysis is done for a finite time window (t_{slice}), the window is offset by t_{shift} seconds and the FFT analysis is repeated. The Fourier transform this obtained is then plotted as a three-dimensional surface with the frequency as the x-axis, the start time of the slice as the y-axis and the amplitude as the z-axis. Such a Moving Windows FFT plot can show the relative amplitudes of vibrations in the various modes of the building as the earthquake progresses. It can also show if the frequency of vibration in any mode changes during an earthquake. However, such an analysis is very sensitive to the parameters used such as t_{slice} , t_{shift} , sampling time and the number of points used to compute the FFT. An example is shown in Figure 18 for sensor 19 for CSMIP Station No. 24639 (54-story office building located in downtown Los Angeles). The graph on the left shows the three-dimensional surface obtained while the graph on the right shows slices of the surface at selected start times or frequencies. The amplitude of the various modes decrease as the earthquake progress, as would be expected. The frequency of the various modes do not appear to change as would be expected for a building that showed no signs of damage during the 1994 Northridge Earthquake.

An example of a building where the frequency of the fundamental mode changed during an earthquake is CSMIP station 24580, the Los Angeles Fire Command Center. The moving windows FFT analysis of Sensor No. 15, located on the roof of the building, is shown in Figure 19. The analysis shows the dominant frequency of vibration of the building changes to a lower frequency as the earthquake progresses. It should be noted as the window of data used for the FFT has a finite length and therefore instantaneous changes in frequencies show up a gradual shift of the larger amplitude to a lower frequency.

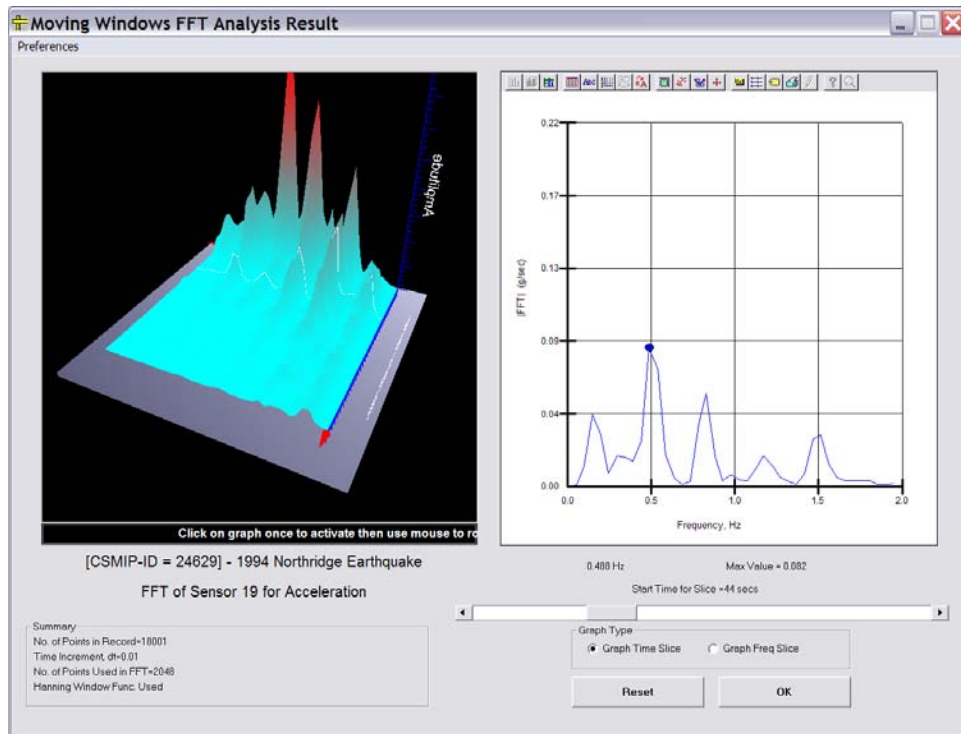


Figure 18. Moving windows FFT analysis of 54-story office tower

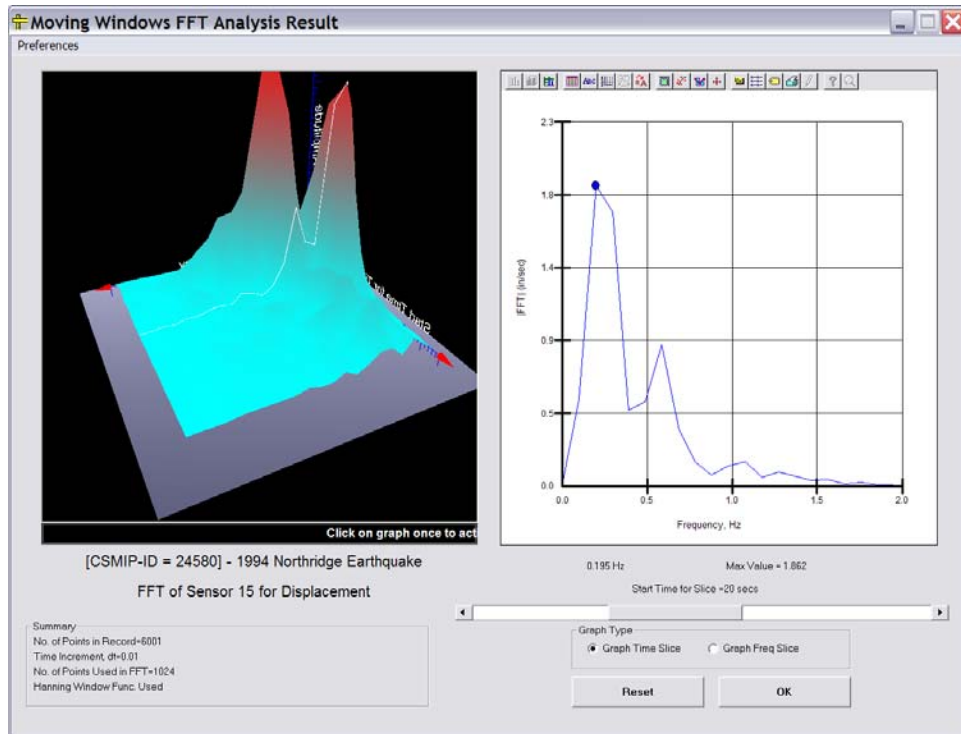


Figure 19. Moving windows FFT analysis of Los Angeles Fire Command Center

Conclusion

CSMIP-3DV permits visualization of building response to earthquake ground motions, facilities for adding newly instrumented buildings and downloading recently recorded building response data from the CISN Engineering Data Center website, and extensive facilities for analysis and evaluation of building response parameters such as displacements, story drifts, changes in dynamic characteristics of the building and so forth. Following each earthquake, three-dimensional building response can be viewed within a short period of time on the CISN Engineering Data Center website. In addition, structural engineers will be able to download the datasets and perform their own investigations using the software system CSMIP-3DV installed on their own personal computers. The goal of this system is to revolutionize the use of strong-motion data obtained from instrumented buildings in structural engineering applications and improvement of seismic code provisions.

Acknowledgments

Funding for this project was provided by State of California, California Geologic Survey, Strong Motion Instrumentation Program (SMIP) under Contract Number 1002-776.

The authors wish to express their gratitude to the members of the project's Technical Expert Panel consisting of Professors Wilfred Iwan, S.T. Mau, James C. Anderson, Chia-Ming Uang and Mr. Chris Poland.

The opinions expressed in this paper are those of the author and do not necessarily reflect the views of the California Strong Motion Instrumentation Program or John A. Martin and Associates, Inc.

References

- California Strong Motion Instrumentation Program (CSMIP), 1995, *Processed Data for Los Angeles 2-story Fire Command Control Building from the Northridge Earthquake of 17 January 1994*, Report No. OSMS 95-01A.
- California Strong Motion Instrumentation Program (CSMIP), 1995, *Processed Data for Los Angeles 52-story Office Building from the Northridge Earthquake of 17 January 1994*, Report No. OSMS 95-01E.
- California Strong Motion Instrumentation Program (CSMIP), 1995, *Processed Data for Los Angeles 54-story Office Building from the Northridge Earthquake of 17 January 1994*, Report No. OSMS 95-01G.
- California Strong Motion Instrumentation Program (CSMIP), 1995, *Processed Data for Los Angeles 6-story Office Building from the Northridge Earthquake of 17 January 1994*, Report No. OSMS 95-01R.
- Naeim, Farzad, 1997, *Performance of 20 Extensively Instrumented Buildings during the 1994 Northridge Earthquake – An Interactive Information System*, A report to CSMIP, John A. Martin & Associates, Inc.

VISUALIZATION OF SEISMIC BRIDGE MOTIONS

Robert K. Dowell

Dowell-Holombo Engineering, Inc.
Department of Structural Engineering
University of California, San Diego

Abstract

This paper discusses a new computer program for visualizing the animated measured response of bridge structures subjected to earthquakes. A graphical display allows the bridge to be viewed from any angle with any level of perspective and magnification to deformations. Panning and zooming are also available. Bridge behavior is measured at various locations on the structure as part to the Strong Motion Instrumentation Program. Between measured locations the bridge response is determined from spline functions consistent with structural behavior and boundary conditions. Time-history plots are also available which allow any quantity to be plotted against any other quantity, providing a powerful tool for visualizing data.

Introduction

A new computer program has been developed as part of the California Strong Motion Instrumentation Program (CSMIP) to visualize the animated response of bridge structures subjected to earthquakes. This is different from animations developed from a finite element analysis in that the results are based directly on the measured response of the structure. Between locations of measured behavior, splines are used for interpolation, allowing the entire bridge to be viewed so that the final displayed response is as smooth and realistic as possible. Of particular interest in the visualization program is that no structural modeling was used, including mass and stiffness matrices.

For this project 5 bridge structures are being investigated, including the (1) Golden Gate, (2) Vincent Thomas, (3) 5/14 Connector, (4) Painter Street Overcrossing and (5) 10/215 Connector. Since a structural model was developed and verified of the 5/14 North Connector Bridge by the PI on a prior CSMIP project [1], the development of the visualization program has centered on this structure. Two types of fundamentally different structures are being included, namely typical highway bridges with columns and spans and the more exotic suspension bridges that have 3 spans and 2 towers. For typical highway bridges the program is working properly, allowing animated views of the structure. The suspension bridge module is being finalized at the time of writing this paper.

Graphical User Interface

A graphical user interface was developed in Visual Basic [2]. The initial panel that the user sees allows the selection of one of the 5 bridges included in this study (Figure 1). If the Golden Gate Bridge button is selected, for example, then the panel shown in Figure 2 is

displayed. By further selecting the Pictures button, additional pictures of interest are provided (Figure 3).

From the initial panel the 5/14 Connector bridge is selected, as well as the pictures button, resulting in the 2 superimposed displays given in Figure 4. Figure 5 shows superimposed displays from General Plan and Instrumentation button selections, for the 5/14 Connector Bridge. Within the Instrumentation panel, the Time-History button is selected. This allows acceleration, velocity and displacement time-history results to be plotted for different time windows, as indicated by the 2 plots in Figure 6. Plotting features also allow any field to be plotted against any other field (see Figure 9). For example, displacements in the transverse and longitudinal directions can be plotted against each other providing a trace of the movement on the horizontal plane, as if watching the bridge motion traced out from above. One of traces in Figure 9 shows displacement versus velocity, as another example.

By going into 3-D plotting the bridge is displayed in full 3-D. The bridge can be rotated by typing in angles, or it can be rotated dynamically by dragging the mouse left to right and up and down. Perspective is controlled by typing in a distance that the viewer is from the bridge. The closer that the viewer is to the bridge the more exaggerated the level of perspective. In Figure 7 the perspective level is set to 2000 ft, providing the amount of distortion that would occur from viewing the structure from this distance. As the perspective distance approaches infinity the amount of distortion tends toward zero. Of course at this distance the bridge could not be seen on the screen and so the program automatically scales the size of the bridge up to the viewable area, regardless of perspective distance. A front view and a view from above the structure are provided in Figure 7. It is interesting that from above the structure, due to perspective, the columns lean in at their bases toward a common point in the distance.

All of the structure geometry is defined in the panel, with most of the information coming from the General Plan. Vertical and horizontal curve information is provided to define the alignment in 3-D space. Span lengths and column lengths are also required. While span lengths are given on the General Plan, column lengths are not and must be determined from other plan sheets. For this structure that has 2 frames, a hinge station was also provided.

Spline Techniques

In the local transverse direction the columns are assumed to act in single bending, based on a cubic curve between measured top and bottom column displacements (top of Figure 8). In the local longitudinal direction the columns act in double bending due to the restraint provided by the superstructure. However, if it were assumed that the point of inflection was at mid-height of the column, then no rotation would develop at the top of column, resulting in no rotation and, hence, no vertical displacements of the superstructure. It was assumed that the superstructure inertia is 4 times the column inertia in the longitudinal direction and that the point of inflection of the superstructure is at midspan, except for the end spans adjacent to an abutment or hinge. Based on these 2 assumptions it was found that the column point of inflection is at 55% of its height. This allowed the cubic spline to be finalized for the columns, resulting in normalized rotations at the column top as a function of relative column displacements and level of displacement magnification. An example of local longitudinal deformations is given at the

bottom of Figure 8. Here it is clear that the columns are acting in double bending and that the rotations at the top of column are the same as the superstructure rotations at the same location. This provides a realistic, smooth response to the deformations. Note that in Figure 8 the view is zoomed in near the hinge between frames, and the separation between frames is clear.

One item of interest in the level of exaggeration to deformations is that the displacements in the three global directions can be scaled to different values. For example, this allows the behavior in the transverse direction to be viewed by itself by setting magnifications in the other directions to zero.

Prior to using the splining techniques discussed above, displacement time-histories were developed in longitudinal and transverse directions at the top and bottom of each column and at the abutments. Since most of the bents had measurements for only the local transverse direction this required added splining techniques to obtain local longitudinal displacement time-histories. These splining techniques were verified in Frame 2 of the structure where local longitudinal displacements are measured at 3 bents along the frame. Local longitudinal displacements at the center bent were found by splining from the outer bents and then compared to measured results. Once local transverse and longitudinal displacements were known then these values could be rotated in to the global directions of the model for visualization purposes.

Conclusions

The initial phase of the project was to develop the Graphical User Interface (GUI) using Visual Basic (VB) for the computer program to run in Windows. The program includes 5 instrumented bridge structures to choose from as an initial database. It also permits a user to add to the database of bridges by providing geometric data such as vertical and horizontal curves found from the General Plan. The second part of the visualization program was to animate in full 3-D the measured behavior of a bridge for the duration of the chosen earthquake. Since displacements are known only at the instrument locations, and in the direction of the instrument, the remaining bridge behavior away from instrumented locations must be interpolated. The bridge superstructure and columns are represented by line elements with realistic boundary conditions and cubic splines between known results (cubic curves that are forced to obey known boundary conditions represent beam element behavior in structural analysis that are typically used for bridge design). Important boundary conditions to include are hinge locations, abutment types and pins at top and/or bottom of columns.

The program allows acceleration, velocity and displacement time-histories to be interactively viewed for all instruments on the structure. Furthermore, these quantities can be plotted against each other in any combination desired, to view behaviors or trends that are not obvious from viewing time-history data only. A good example of such a trend is the graph of superstructure acceleration at the top of a given column versus relative displacement between the top and bottom of the same column. This graph has the same shape as a force-deformation hysteresis loop for the column (vertical axis scaled by the mass) and is the best indicator of ductility demand and damage for bridge structures since nonlinear behavior is designed to occur in the columns. Such a plot also provides additional verification that the data is good, as hysteresis loops must cycle in the clockwise direction (energy is dissipated by the columns and

not created). Note that this hysteresis plot represents the force-deformation curve for the bridge column if the vertical axis is scaled by the tributary mass to the column. This is just one example of the benefit of being able to add and subtract channel results from each other and plot any quantity versus any other quantity.

The 3-D visualization requires that basic geometric information of the bridge structure be provided. Profile grade and alignment information is required, as well as the type of bridge (suspension or typical), number of spans, span lengths and footing elevations. All but the footing elevations are given on the General Plan and thus only 2 pages from the bridge plans are required to add another bridge to the database. This part of the computer program plots the structure in elevation view as distance along the bridge versus elevation of the superstructure centroid. Unit conversion is possible between ft and meters, modifying elevations, stations and distances along the bridge by a simple click of a button

Since the PI for this project was also the PI for the prior Lifeline Structure Response Project, which compares SAP [3] model responses to measured responses of the 5/14 Connector [1], it was decided that the visualization program should be initially developed for and verified against this bridge. There are two distinct advantages to using this bridge; (1) the PI is familiar with both the structure and the data as well as has the complete bridge plans available and (2) the PI has a fully developed and verified structural SAP model of the bridge, allowing comparisons outside of instrumented locations to ensure that the cubic-spline techniques realistically captures the dynamic response of the structure. By making a video of the SAP model response, direct side-by-side comparisons can be made between the (1) spline model that has no knowledge of the structure beyond its geometry and measured deformations and the (2) full structural SAP model that includes the stiffness and mass of all elements as well as the geometry.

The contents of this report were developed under Contract No. 1002-777 from the California Department of Conservation, California Geological Survey, Strong Motion Instrumentation Program. However, these contents do not necessarily represent the policy of that agency nor endorsement by the State Government.

References

1. Dowell, R. K., *Time-History Analyses versus Measured Seismic Responses of the 5/14 Connector Bridge*, Report No. DH-04-02, Dowell-Holombo Engineering, Inc., San Diego, California, 2004.
2. Visual Basic 6, User's Manual, Microsoft Corporation, Redmond, Washington, 2000.
3. SAP2000, Version 8, User's Manuals, Computers and Structures, Inc., Berkeley, California, 2002.



Figure 1. Graphical User Interface, Initial panel



Figure 2. Golden Gate Bridge tab

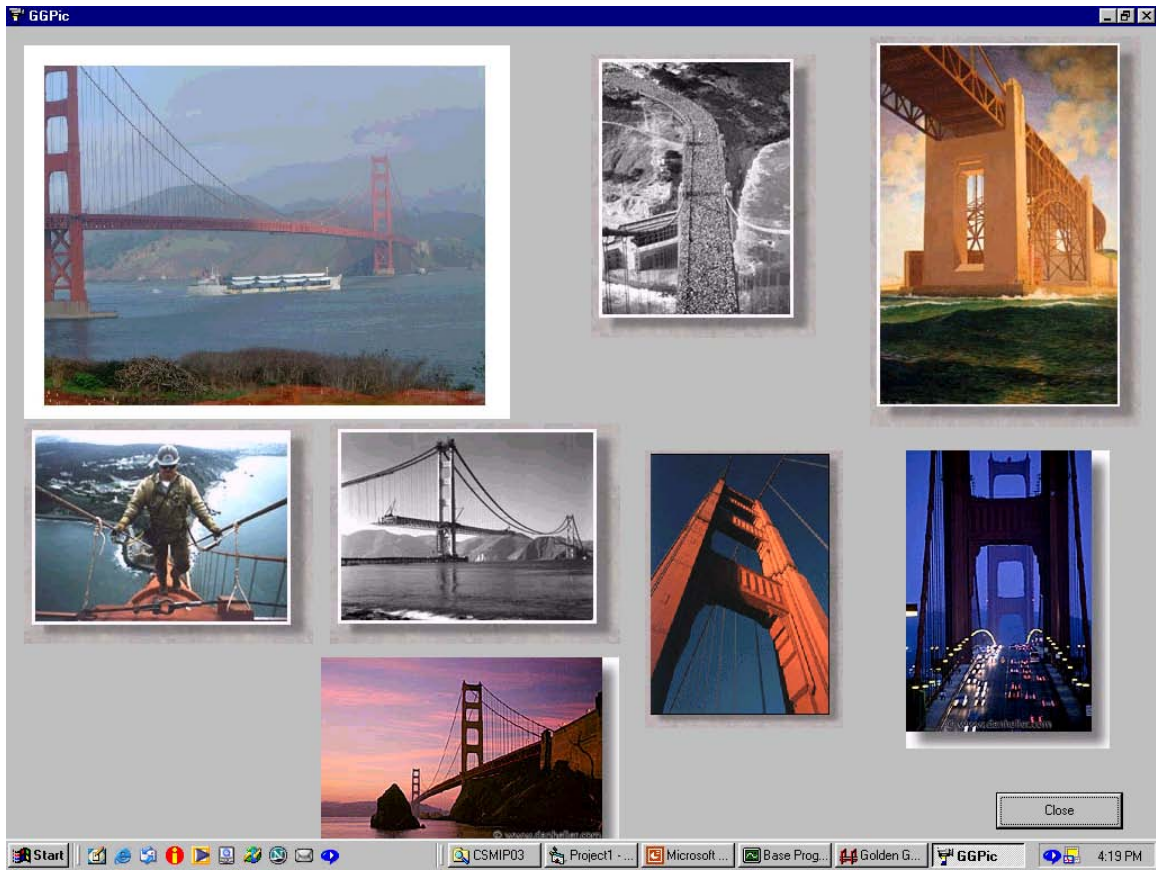


Figure 3. Pictures tab

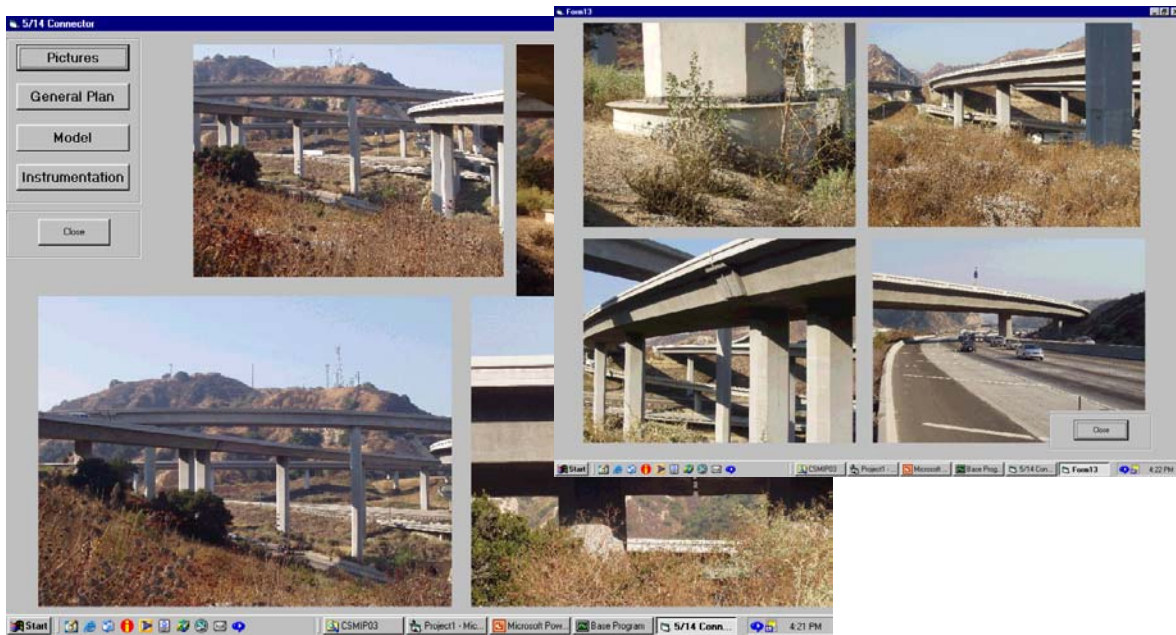


Figure 4. 5/14 Connector tab and Pictures tab

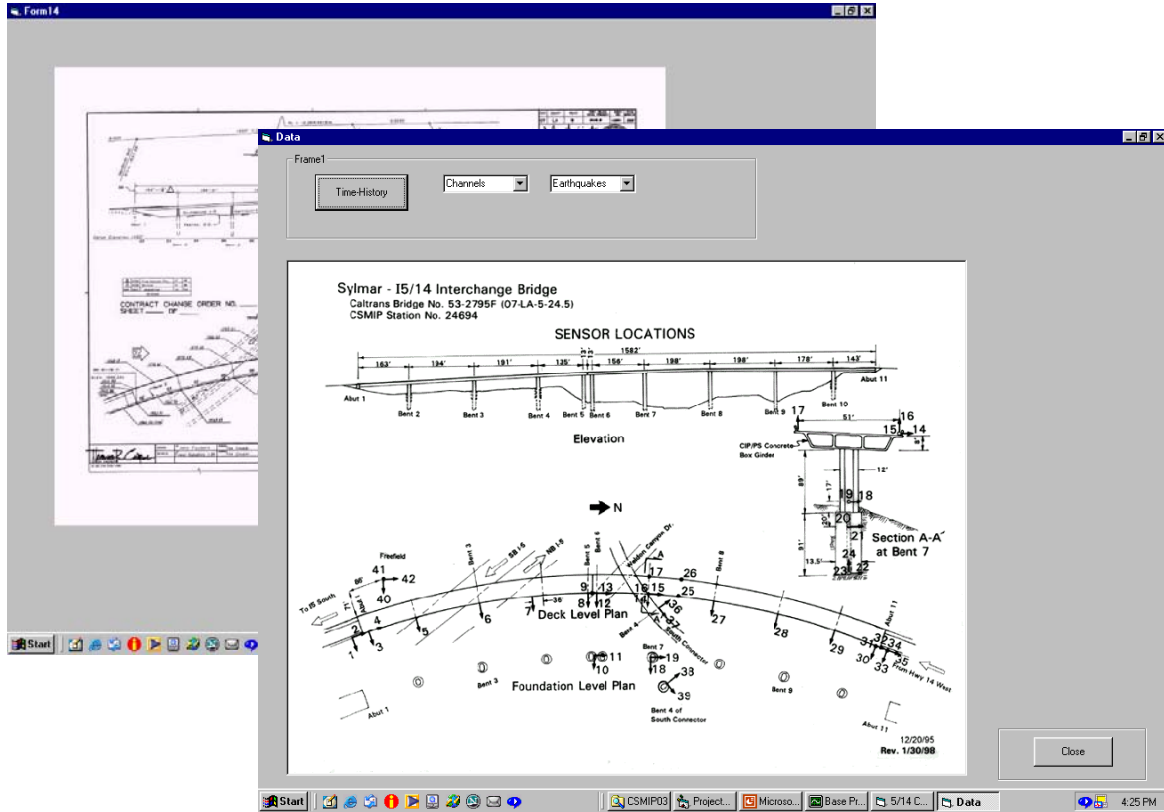


Figure 5. Instrumentation and General Plan tabs

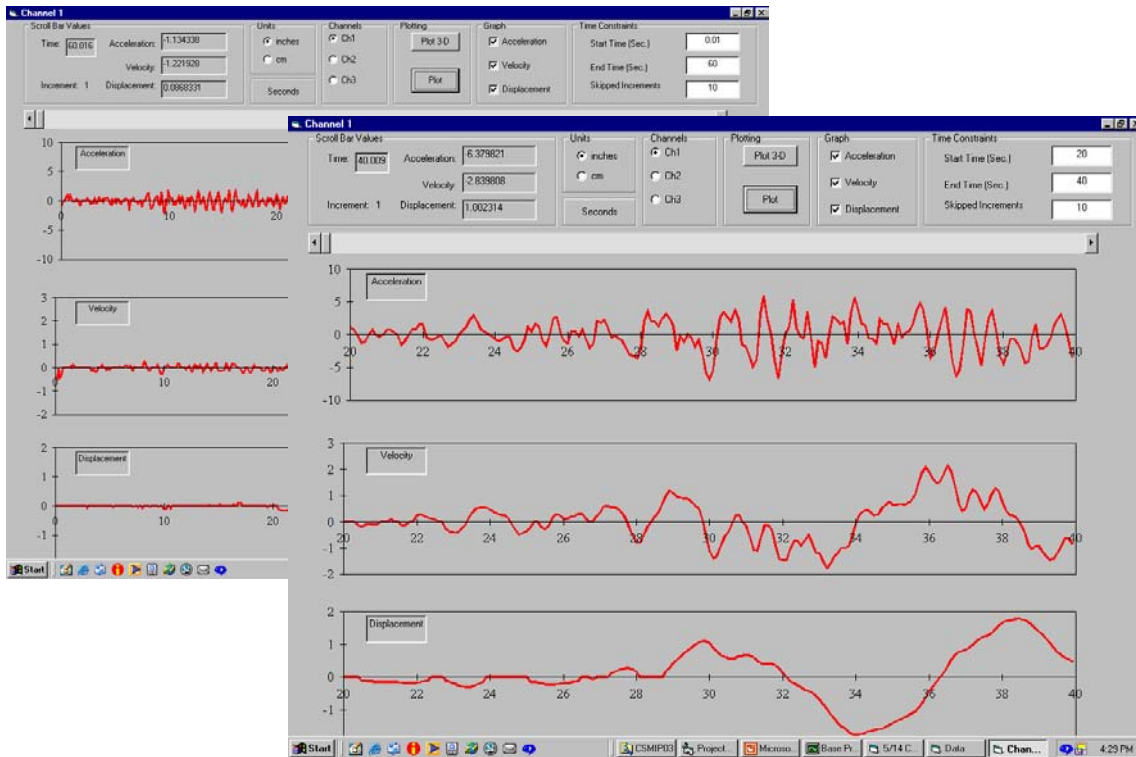


Figure 6. Acceleration, velocity and displacement time-histories with different time windows

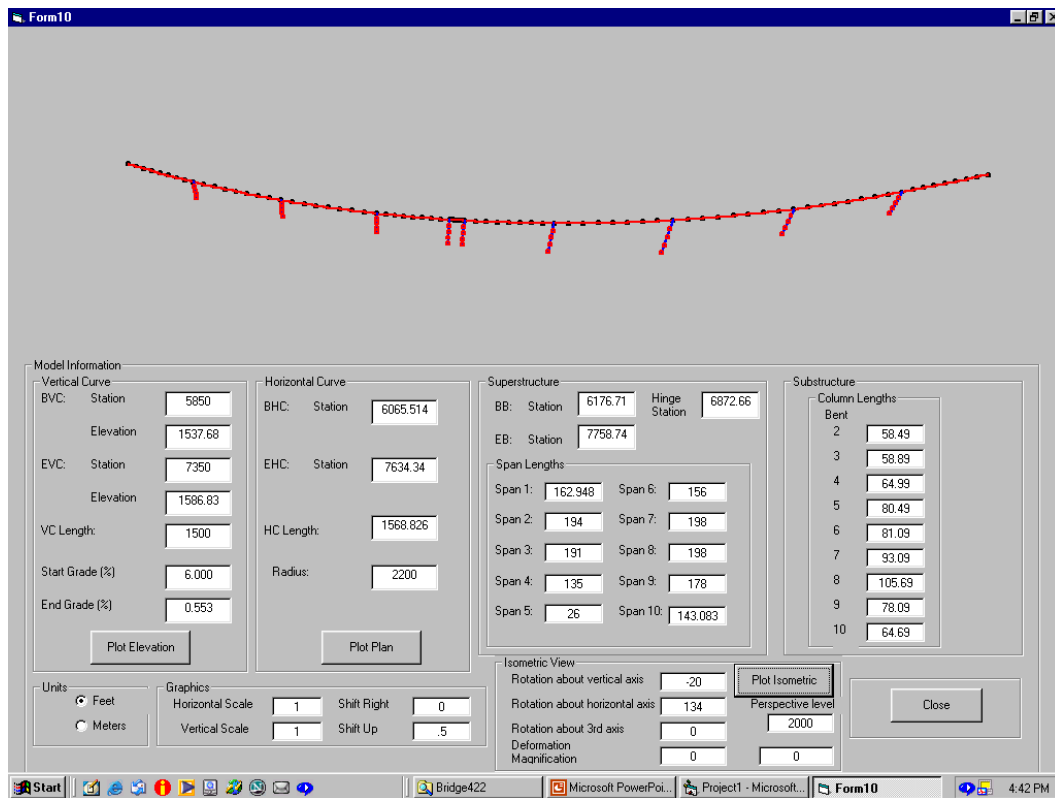
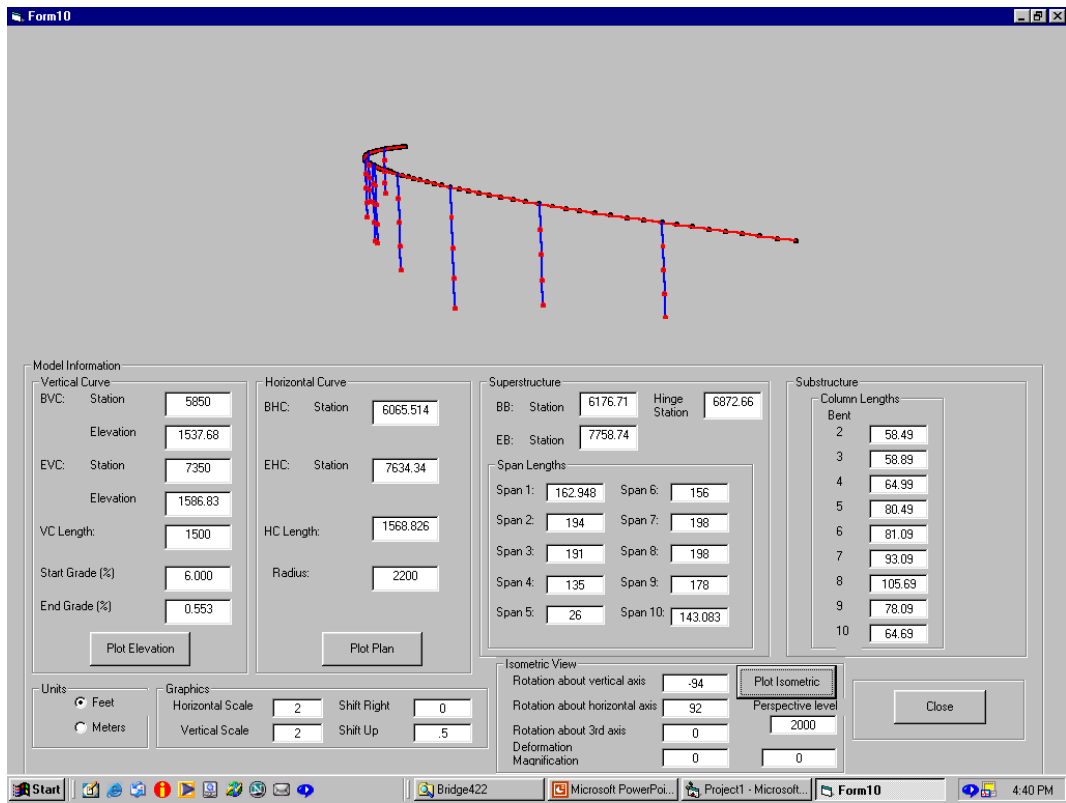


Figure 7. 3-D view of undeformed bridge from the front and from above, with perspective

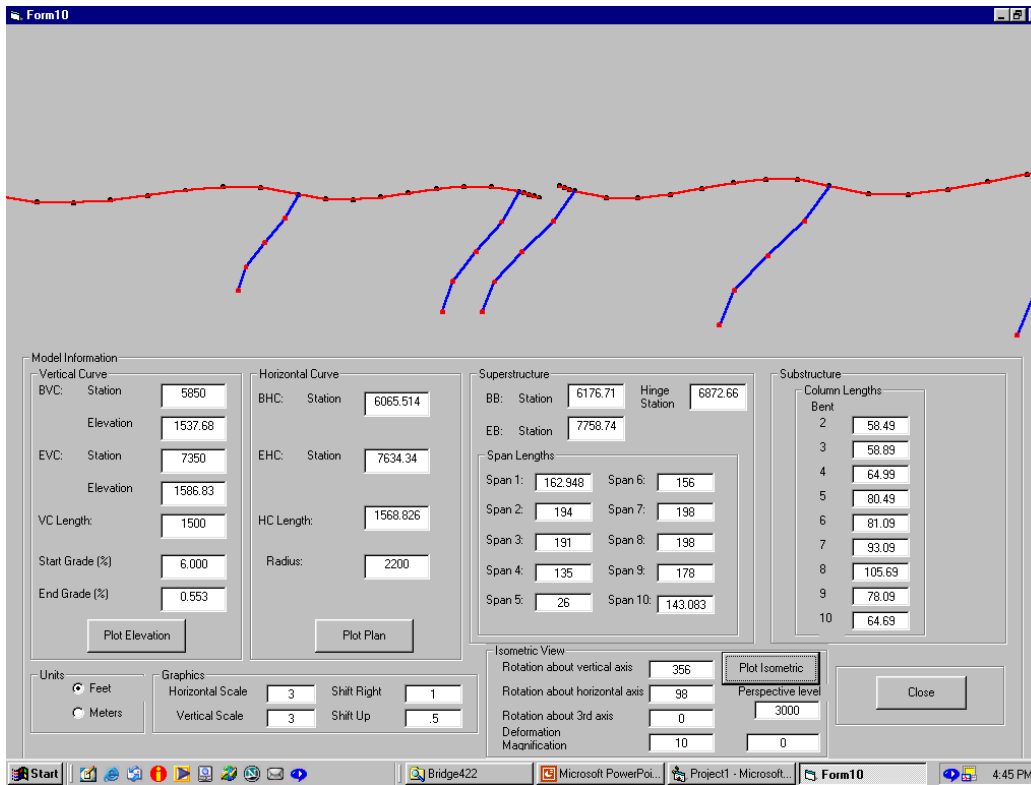
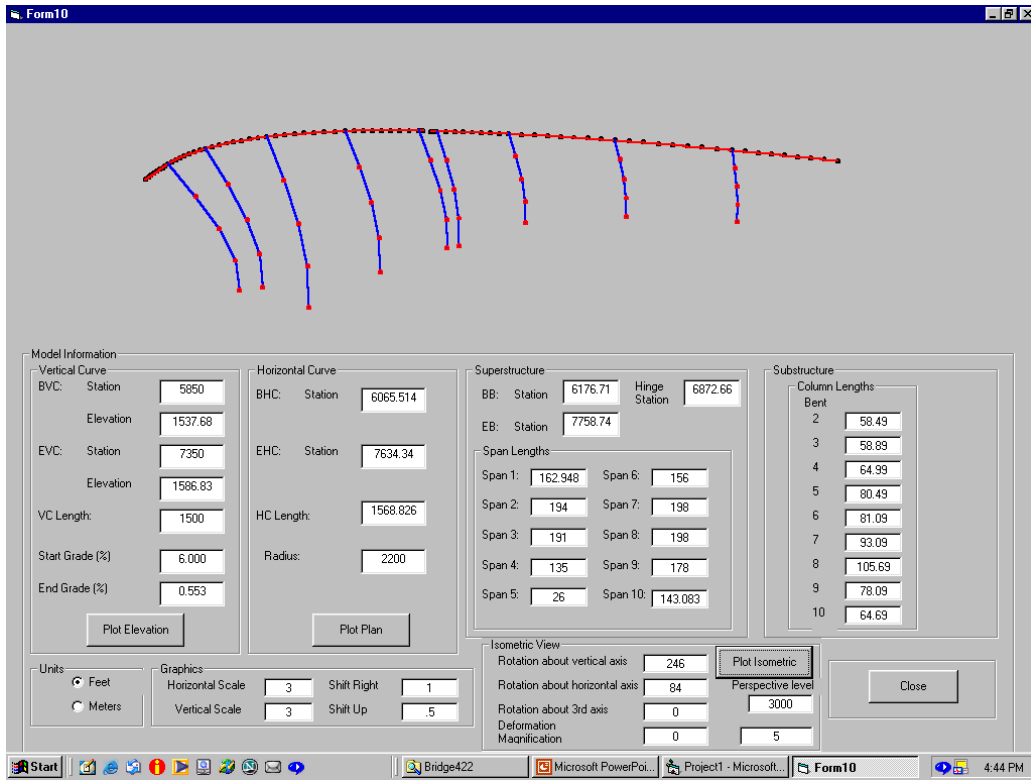


Figure 8. 3-D view of bridge, deformed in the transverse and longitudinal directions

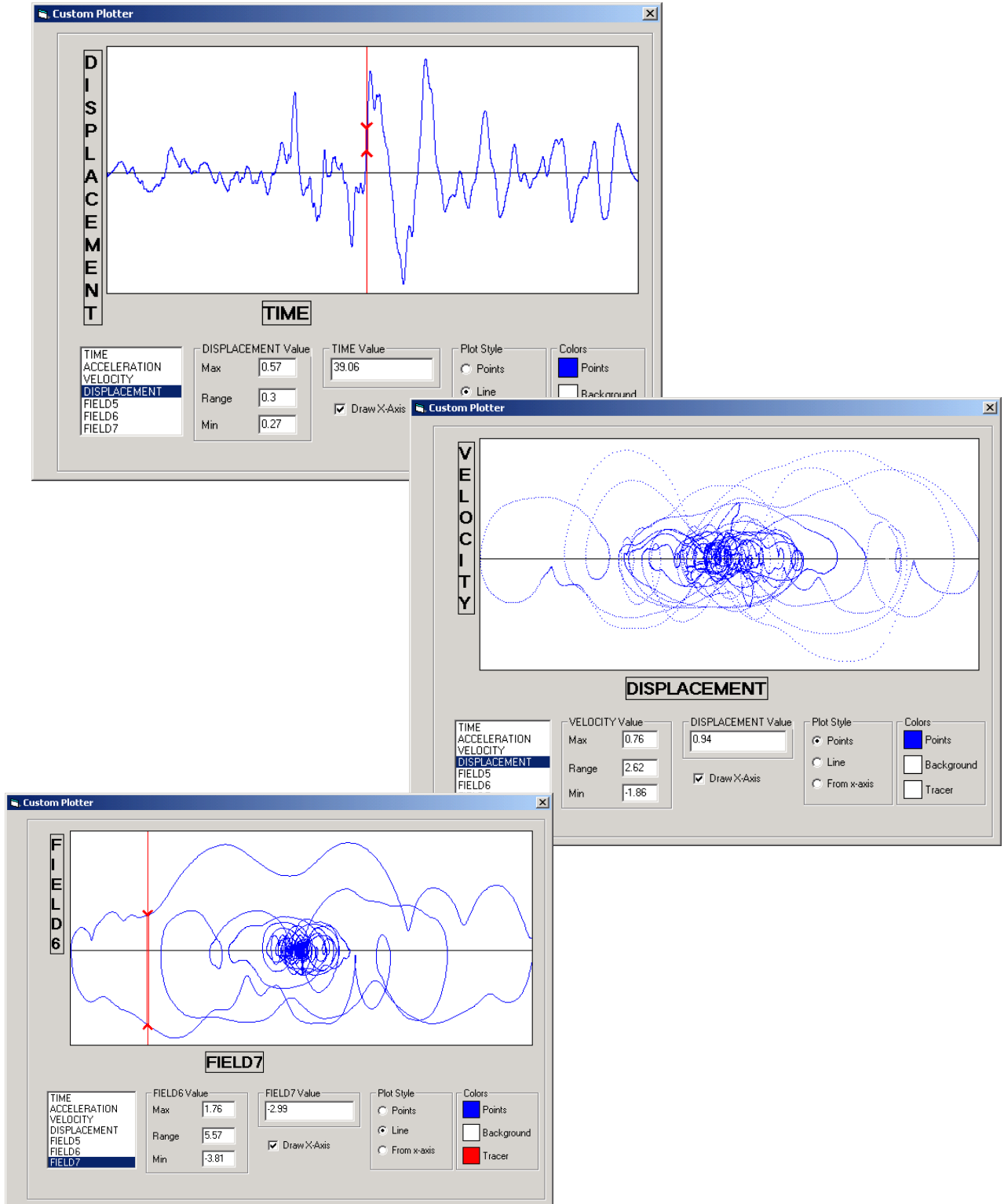


Figure 9. Examples of time-history fields plotted against other fields

**DESIGN AND INSTRUMENTATION OF THE NEW
SAN FRANCISCO-OAKLAND BAY BRIDGE EAST SPAN**

Brian Maroney, Pat Hipley
Caltrans

and

Moh Huang
California Strong Motion Instrumentation Program

Abstract

The new east span of the San Francisco-Oakland Bay Bridge is under construction now. It is the most expensive public works project in California's history. The bridge is designed to provide a high level of seismic performance. Even after a major earthquake, the bridge is intended to provide full service almost immediately and should sustain only repairable damage to structure. During the construction, a total of 199 strong-motion sensors will be installed at key structural members along the bridge. This paper presents various structural systems used along the bridge and discusses the instrumentation plans.

Introduction

The San Francisco-Oakland Bay Bridge (SFOBB) is an integral part of the region's transportation. This structure links two of the largest cities in northern California and is vital to the economy of the area. The east span of the SFOBB, a double-deck truss bridge built in 1937, was damaged during the 1989 Loma Preita earthquake. It was determined that a complete seismic retrofit of the current bridge was too costly for the aging structure and that the funding was better suited being used for a new crossing. Figure 1 shows a rendering of the bridge.

The construction of the new east span was broken up into four major structures:

1. The Yerba Buena Island Transition Structure,
2. The Self Supporting Suspension Structure,
3. The Skyway Structure, and
4. The Oakland Touchdown Structure.

The Skyway project was the first to get started and consists of single column support bents with a concrete box superstructure. The foundation has large diameter cast in steel shell (CISS) piles battered away from the center of the pile cap. There are two separate structures, one for eastbound and the other for westbound traffic. The Yerba Buena Island (YBI) Transition Structure is designed to bring the two side-by-side roadways from the self-supporting suspension structure and stack them on top of each other to utilize the existing double deck tunnel cored through the rock of the island. The transition structure also has a single column concrete box girder configuration.

The Self-Supporting Suspension Bridge has the support pier off set from the center and is referred to as the “Signature Structure”. The suspension cable is wrapped around the ends of the bridge and relieves some of the downward loads at the supporting piers. The Oakland touchdown consists of a thin concrete box girder superstructure on a single support pier. The concrete pier is supported on a concrete pile cap with nine piles. The touchdown structure ties into a landfill area that leads to the toll plaza.



Figure 1. A rendering of the new San Francisco-Oakland Bay Bridge East Span.

A total of 199 strong-motion sensors are planned to be installed on the SFOBB East Span. They consist of force-balance accelerometers, relative displacement sensors and tilt meters. The locations of these sensors are shown in Figure 2. The sensors are connected via cables with the recorders centrally located at several places on the bridge. The analog signal from each sensor is converted to digital data and stored in the recorders. The relative displacement sensor provides direct measurement of the relative displacements between two points on the structure. The acceleration data are routinely processed and integrated to obtain velocity and displacement (absolute) records. All the recorders have clocks and are connected to have a common triggering, so the recorded response data will be synchronized. The instrumentation includes free-field and downhole sensors at both ends of the bridge.

Since more than half of the mass is on the foundation and the soil-structural-foundation interaction is complicated to model, a lot of sensors are needed to measure the input motions and the foundation response. When the locations of the sensors were planned, one major objective was to install as many sensors as possible on the pile caps and the pile tips. These sensors would record differential ground motion along the bridge and capture the traveling seismic waves as they are propagated from one end of the bridge to the other. Although the installation and maintenance of these sensors are more expensive, installations of some of these locations would be impossible after the construction is complete.

San Francisco - Oakland Bay Bridge/East

Caltrans Bridge No. 34-0003 (04-SF-80-5.6)

CSMIP Station No. 58632

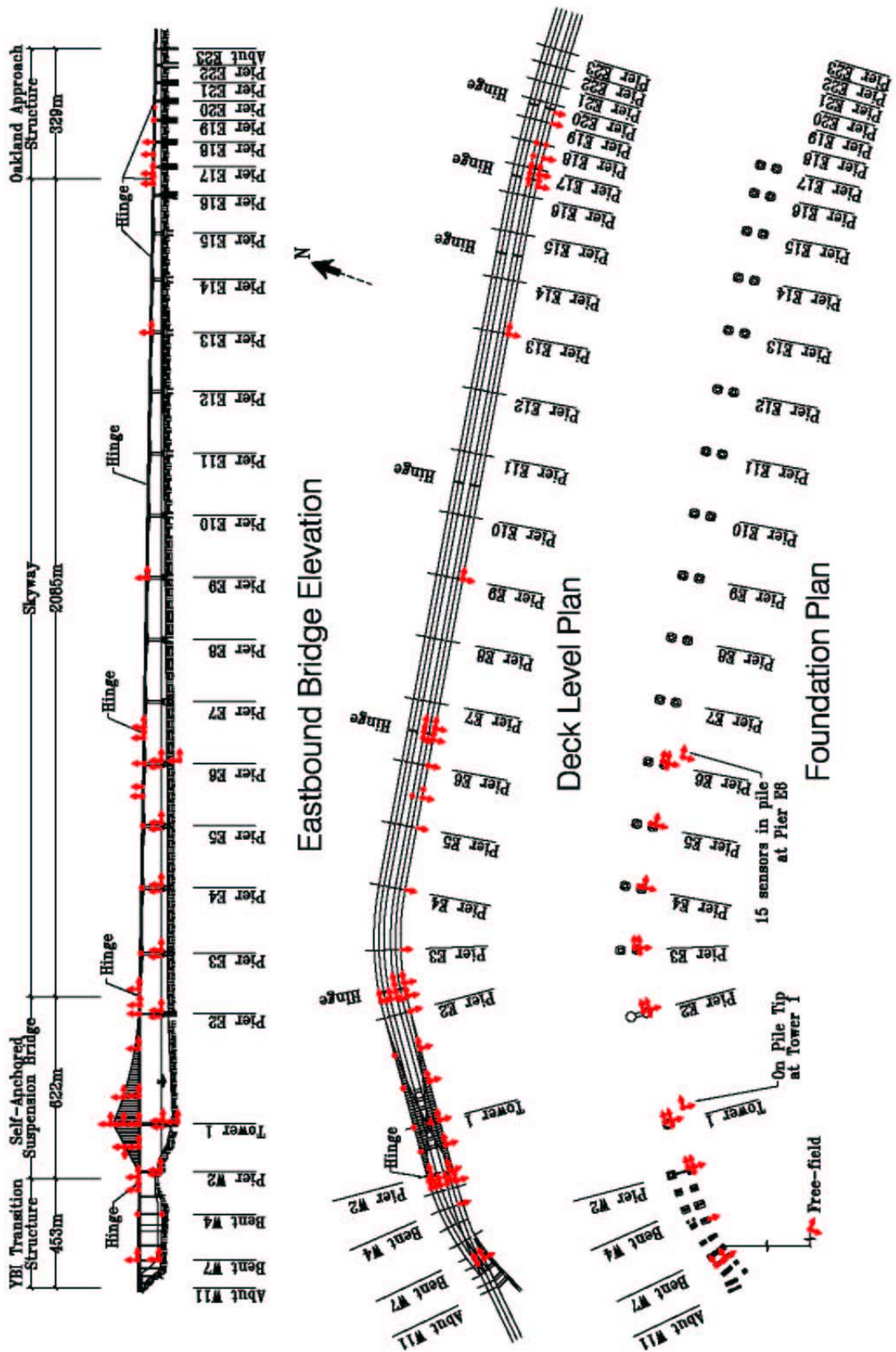


Figure 2. Locations of strong-motion sensors to be installed on the SFOBB East Span.

Self-Anchored Suspension Bridge

The self-anchored suspension bridge consists of a 385 m main span and a 180 m back span (Figure 3). The 160 m tall single tower consists of four steel shafts connected with intermittent steel shear links along its height (Figure 4). Each shaft is tapered and made of stiffened steel skin plates. The tower is supported on steel pipe piles driven about 100 meters into Francisco rock. The east pier is supported on steel pipe piles founded on the Alameda Formation and the west pier is supported on a massive 12.5 m deep footing supported by piles.

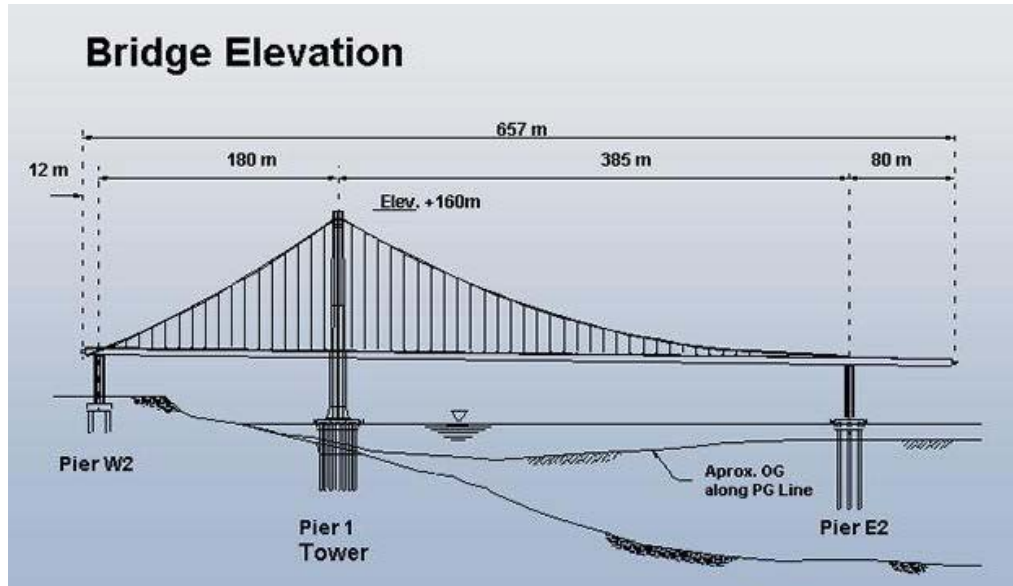


Figure 3. Elevation of the SFOBB Self-Anchored Suspension Bridge.

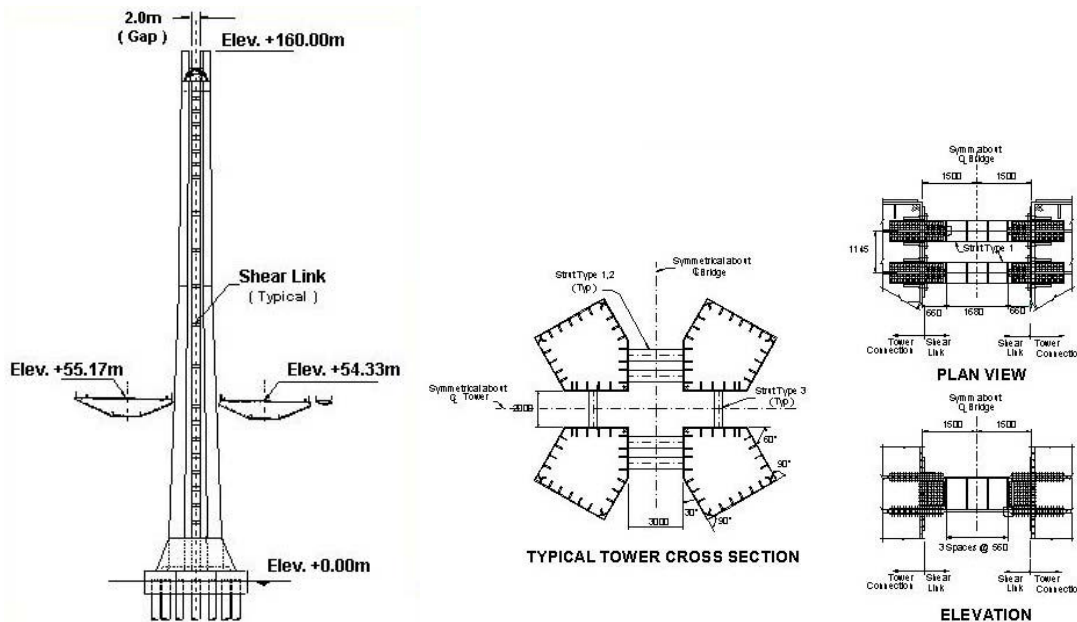


Figure 4. Elevation and Section of the Single Tower for the SFOBB Self-Anchored Suspension Bridge.

The tower shafts are designed to remain elastic under the design level earthquake while the shear links are permitted to yield in shear providing energy dissipation. The links can be removed and replaced without closing the bridge. The suspended bridge deck consists of dual, hollow orthotropic steel boxes. Each box girder has a 25 m wide deck carrying five lanes of traffic in each direction (Figure 5). In addition, a 4.8 m wide pedestrian/bike path is provided on the eastbound structure. The box girders are connected together by 10 x 5.5 m crossbeams spaced 30 m apart (Figure 6).

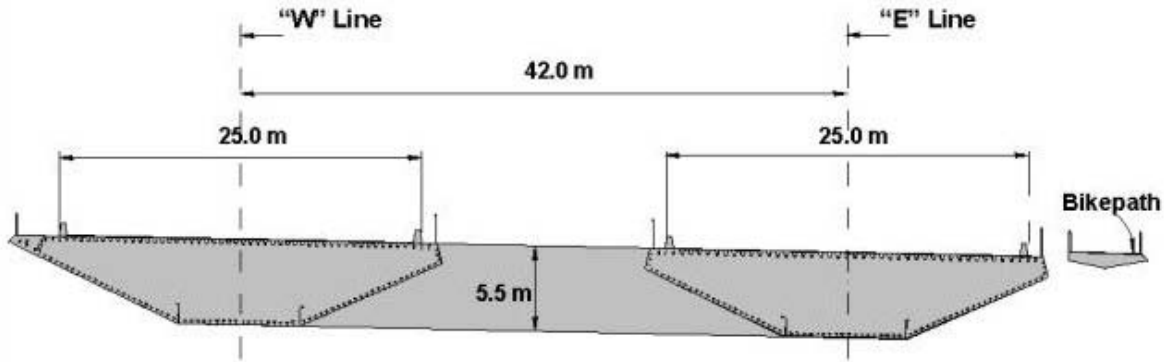


Figure 5. Cross section of the steel box girders at the SFOBB Self-Anchored Suspension Bridge

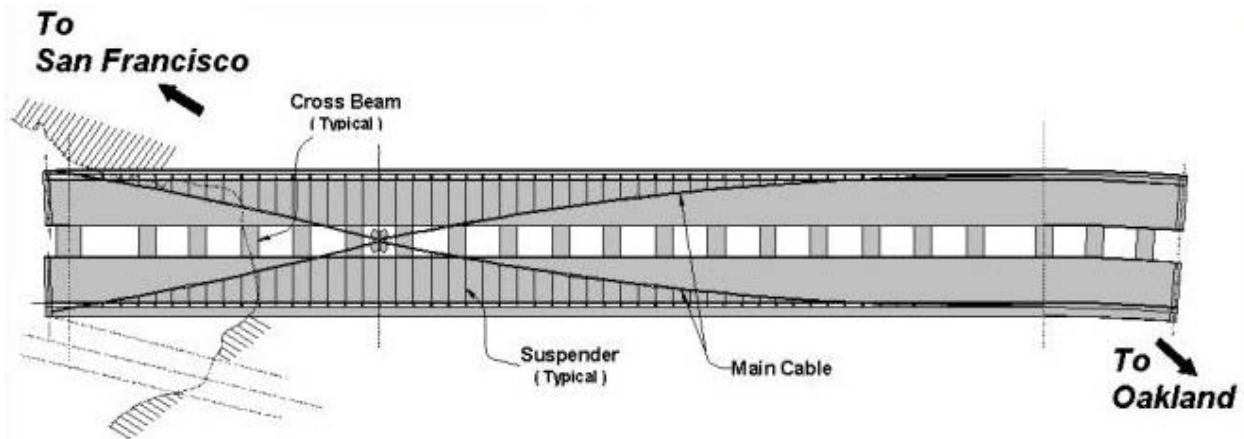


Figure 6. Plan view of the SFOBB Self-Anchored Suspension Bridge with steel box girders, cross beams and suspension cables.

The east piers are concrete columns supported on 16 steel shell pipe piles. These piles are 2.5 m in diameter and 100 m long. They are filled with earth up to 55 m from the top and the rest is filled with concrete. The box girders are supported on bearings at the east piers. Shear keys and tie rods are provided to carry lateral loads and uplifts, respectively. The west piers are concrete columns enclosed by a steel shell. At the west pier, a tie-down system with 28 stay cables is designed to resist possible seismic uplift. The cables are anchored into the footing. The

box girders are supported at the east and the west pier for lateral loads and are “floating” at the tower.

The design of the Self-Anchored Suspension Bridge was based on the results of time history analyses that include multiple support excitation, nonlinear geometry and nonlinear material properties. From the computer models, the periods of vibration are 4.5 (dominated by vertical motions), 3.8 (longitudinal motions), and 3.6 seconds (lateral or transverse motions) for the first three modes. The mode shapes are shown in Figures 7 and 8.

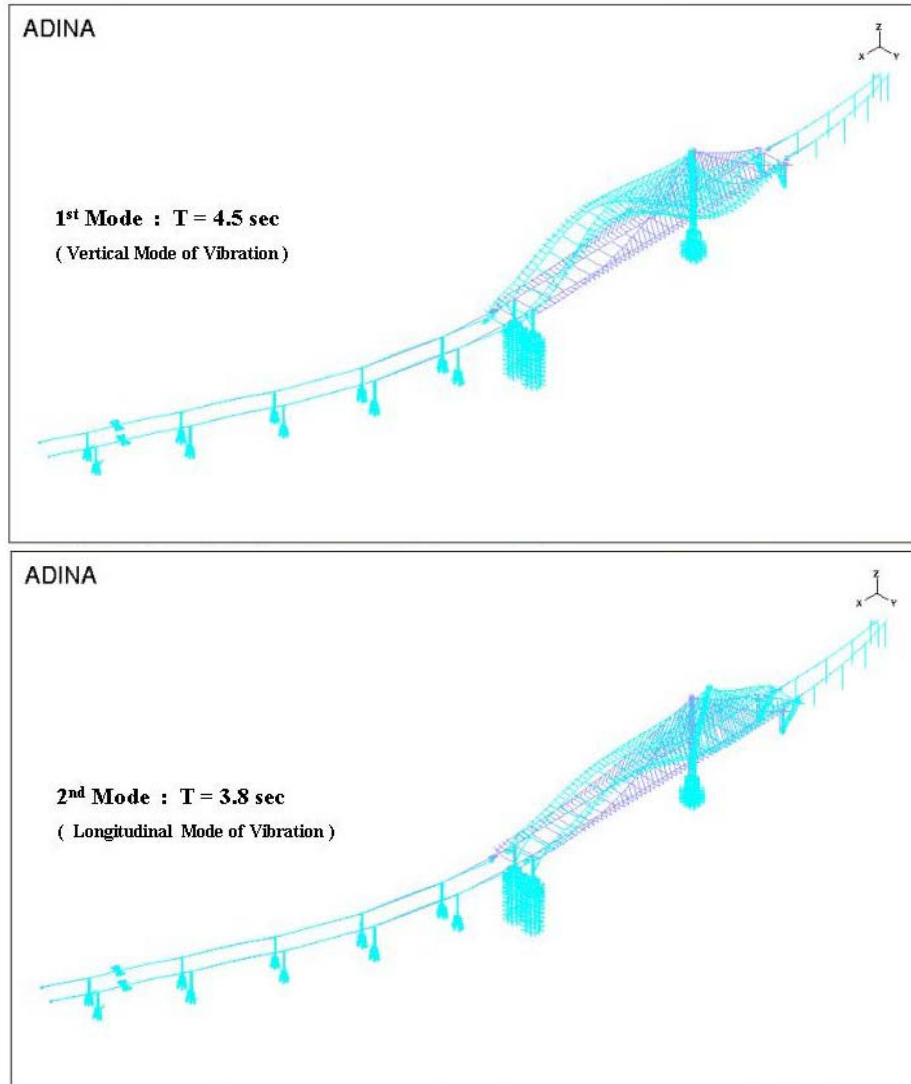


Figure 7. Modal periods and shapes for the first two modes of the SFOBB Self-Anchored Suspension Bridge.

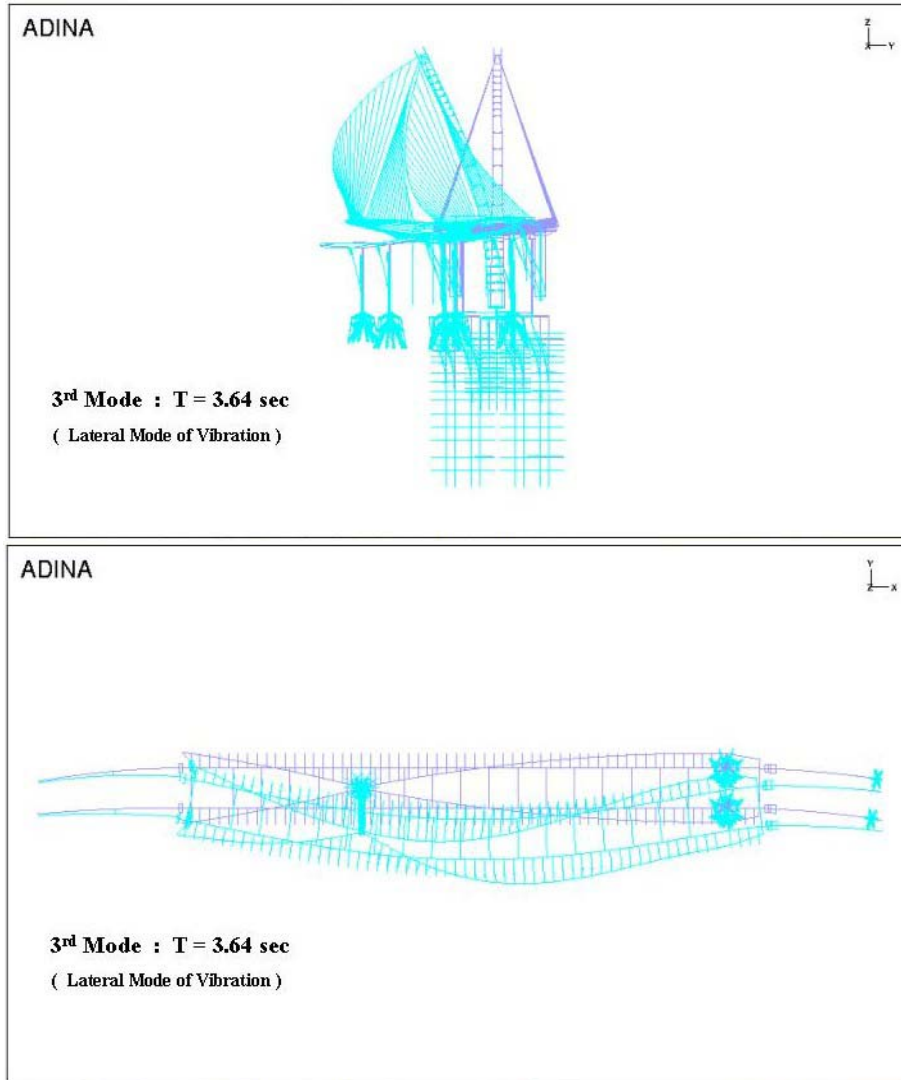


Figure 8. Period and mode shape for the third mode of the SFOBB Self-Anchored Suspension Bridge.

The seismic displacement demands at the tower, and the east and west piers are shown in Figure 9. On each end of the suspension bridge, the transition to YBI structure and the Skyway structure, the hinges are designed to allow the structures to move relative to each other in the longitudinal direction, but key the structures together in the transverse and vertical direction (Figure 10). At the each hinge, two 60-foot-long steel pipes (6 feet in diameter) are placed inside stainless steel sleeves. The pipes are designed to fuse during a major event and can be repaired.

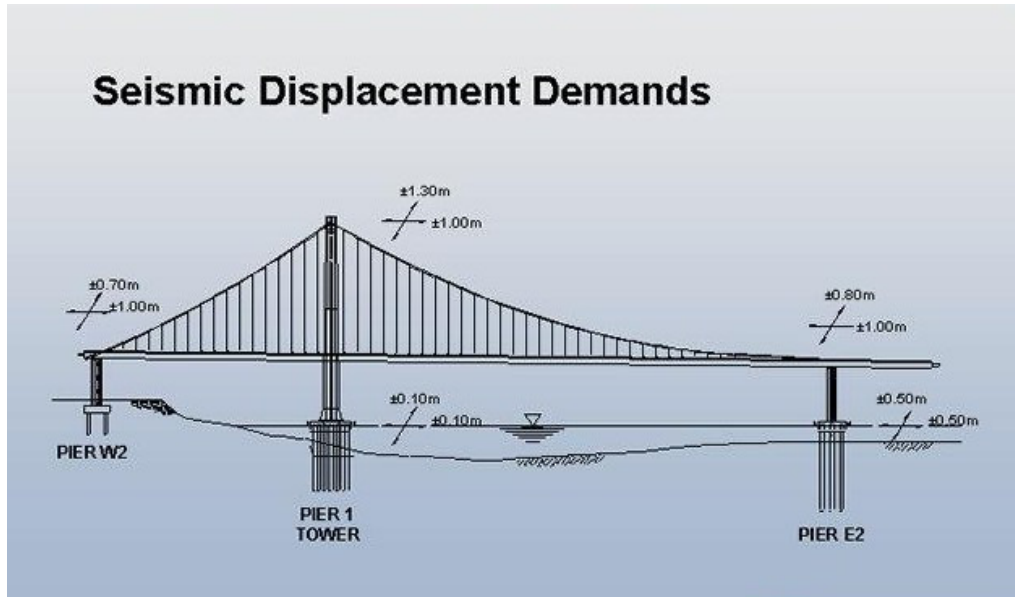


Figure 9. Seismic displacement demands of the SFOBB self-anchored suspension bridge.

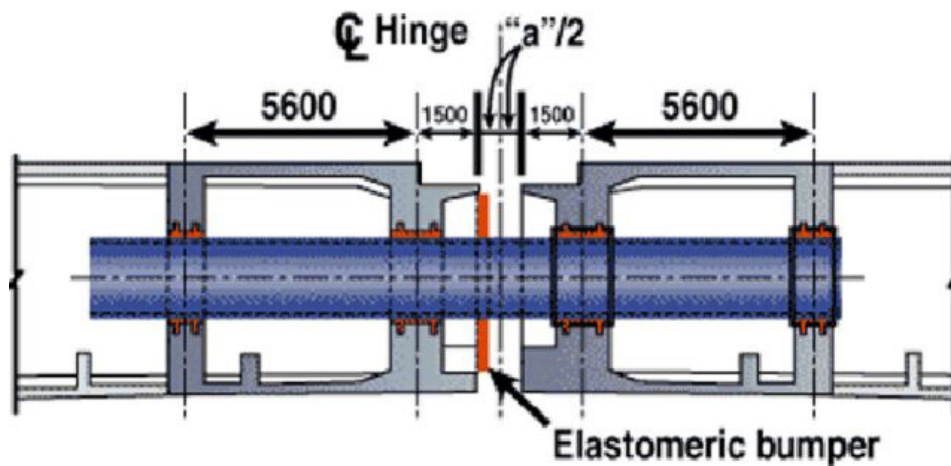


Figure 10. Hinges on both ends of the SFOBB self-anchored suspension bridge.

During the planning for strong-motion instrumentation, it was decided that a large number of the sensors (86) should be placed on the Suspension Bridge since it represents the most unique design and accrues much of the cost. First, the entire structure was looked at in the global sense and sensors were placed at intervals along the entire structure to capture the overall response.

The boundary conditions at the hinges will be monitored well with accelerometers and relative displacement sensors to help understand the bridge integrity and seismic response interactions among different structures. Each of the three pile caps for the suspension bridge will have six sensors to measure three translational as well as three rotational components of the motion. The main tower will have sensors at the base, road level, mid-height and at the top to measure motions of this critical supporting structure. The cables and the roadway will also be monitored along their entire length to measure their responses to ground shaking. A tri-axial “downhole” sensor will be placed near the tip of one of the tower piles to measure the input motion from the rock. Some sensors along the deck are placed opposite each other in the vertical direction to indicate if the deck structure is twisting or moving in phase, along the length of the roadway.

The self-anchored suspension bridge has its cables crossing over the tower and then wrapped around each end to partially relieve the vertical loads at the piers. This is another reason why the hinges are monitored well to record the motions of the ends of this unique signature structure. Since the tower is not centered in the structure, unusual torquing motions can be expected in a large earthquake.

YBI Transition Structures

The eastbound and westbound transition structures connect the suspension bridge to the existing double-deck tunnel at the Yerba Buena island. The two structures are carried on separate single-column bents, except near the viaduct end where they are supported on outrigger bents. The length of each transition structure is approximately 467 meters.

The YBI Transition Structure is lightly instrumented due to its more common construction and funding issues. One outrigger (Bent W7) is instrumented fairly well in all directions at the base of the columns and at the beam level. Outrigger bents on other bridges have experienced damage in the past and much is to be learned by studying their motion. This outrigger bent also has one column that is shorter than the other column, and the load distributions will be different during vibrations. A “free-field” sensor, which will record the bay shore movement, will be placed near Bent W7.

The next area of study at the YBI Transition Structures is where the structures meet the Signature Structure. The second bent from the hinge will have sensors at the base and top of the column to observe the relative displacement of this column (Bent W4R). The transverse motion sensors, from Bent W4R past Bent W3R to the hinge, will record the mode shapes of this segment of the structure. The hinge between the transition structure and the suspension bridge is instrumented well. A displacement sensor will be placed longitudinally at the hinge to measure directly the opening and closing of the hinge over time and will reveal if there is any change after an event. A total of 28 sensors will be placed on the YBI Transition Structure.

Skyway Structure

The Skyway Structure represents the longest segment of the crossing and was the first to start construction. The Skyway is a 2.4 kilometers long pre-cast segmental concrete viaduct with

varying span lengths from 120 to 160 meters. The 160 meter spans are arranged in frame units of three or four piers per frame with a girder depth of 5.5 m at the mid-span and 9 m at the pier. There are four frame structures for the skyway. The hinges between the frames allow longitudinal expansion and contraction caused by creep, shrinkage, and temperature changes. An internal steel beam assembly at the hinge provides shear transfer and moment resistance in addition to controlling deflections at the cantilever end of each frame. These beams are rigidly connected to the box girder at one end and slide on bearings at the box girder on the end.

The Skyway structure will have 452 separate roadway segments, most of them 25 feet long. Each segment consists of a 3-cell concrete box girder that is 90 feet wide. These segments are pre-cast at a pre-cast yard and then transported to the bridge. The bridge superstructure is supported on cast-in-place columns with four confined corner elements interconnected by shear walls. The foundation system consists of a 6 m deep pile cap supported on large diameter battered steel piles filled with concrete. The foundation is designed to be stiff to limit the elastic displacements of the pile caps to acceptable levels and minimize the potential for permanent offsets during earthquakes.

The instrumentation of the Skyway structure will focus on the first frame structure that is adjacent to the suspension bridge. The remaining three frame structures will be instrumented with 3 to 8 sensors. The hinges between the suspension bridge, the Oakland approach, and the Skyway, will be monitored well. The hinge between the first and second frames will also be instrumented. At the first frame structure, many sensors will be placed to capture the longitudinal and transverse deck level mode shapes concentrating the efforts at the deep-water piers. The pile caps of the four piers for the first frame structure will have 4 to 6 sensors placed on them to record the pile cap motions. In addition, at Pier E6 an intense array of tri-axial downhole sensors will be added to one pile at five various elevations to record the full height motions of this pile. It is hoped in the future to build a pier near by this instrumented pile to record the bay mud motions at the same elevations as the pile instruments for comparison of the soil motions to the pile motions.

Three relative displacement sensors will be installed at the hinges at the beginning and end of the eastbound bridge and at one intermediate hinge. Near Pier E6, vertical sensors on each side of the deck will be located in the span to record the vertical and torsional response of the superstructure. A total of 73 sensors will be installed on the Skyway Structures.

Oakland Approach Structures

The westbound approach structure is about 660 meters long and includes an elevated section and a section that is essentially on grade. The eastbound approach structure is an elevated frame structure and is about 329 meters long. The elevated structure consists of a cast-in-place concrete box girder supported on concrete piers, concrete footings, or concrete piles.

The Oakland Approach Structures will be lightly instrumented but a downhole geotechnical array is planned to be installed near the approach structure. The eastbound approach structure will be instrumented with 12 sensors that will record the motions at the

transition between the Skyway and the Approach, and the lateral and torsional motions of the deck.

The geotechnical array will use four tri-axial subsurface sensors at various depths and one surface instrument (15 sensors total). The planned depths are surface, 50, 150, and 300 feet, and 520 feet down into rock. This will measure the motion from the bedrock up through various soil conditions to the ground surface. The data can be used to calibrate site response model used in geotechnical earthquake engineering. The deepest hole will be logged by a geologist to determine the subsurface conditions at the site and will be P/S suspension logged to determine the seismic wave speeds for the full length of the hole.

Summary

The San Francisco-Oakland Bay Bridge is a multi-billion dollar project and represents a huge investment for the people of California. The 3.5 kilometer long structure needs to be monitored for strong seismic movement. The strong-motion data can be used not only by bridge engineers to calibrate and improve their computer analysis models but also for Caltrans to rapidly assess the structural integrity after a major event. A total of 199 sensors are planned to be installed along this structure at key structural elements to achieve the measurement objectives and to capture important modes of bridge vibrations. After the strong motion instrumentation systems are in place they will also need to be properly maintained to successfully record future earthquakes. Even smaller quakes can yield useful data for engineers to understand the seismic response of the bridge. Ultimately, the recording of a major event will advance the field of earthquake engineering.

**RECORDED RESPONSE AND OBSERVED PERFORMANCE OF
A WOOD-FRAME HOSPITAL BUILDING
DURING THE 2003 SAN SIMEON EARTHQUAKE**

Moh Huang

California Strong Motion Instrumentation Program
California Geological Survey
Department of Conservation
Sacramento, California

and

Chris Tokas
Office of Statewide Health Planning and Development
Sacramento, California

Abstract

The Community Hospital in Templeton is a 1-story wood frame structure built in 1977 and instrumented by the California Strong Motion Instrumentation Program in 1994 as part of the OSHPD Hospital Instrumentation Project. During the M6.5 San Simeon Earthquake of December 22, 2003, maximum horizontal accelerations of 0.5 g and 1.3 g were recorded at the ground floor level and the roof, respectively. The hospital did not suffer structural or non-structural damage during the earthquake despite the strong ground shaking. This paper presents analysis results of the recorded response data and building performance observed after the earthquake. Some factors that can be attributed to the good performance of this hospital during the San Simeon earthquake are also discussed.

Introduction

The 84-bed acute care hospital in Templeton is a one-story wood frame structure built in 1977. The building was designed in 1975 as per the requirements of the California Code of Regulations, Title 17 (California Building Standards Code). The structure has an irregular plan with base dimensions of 336'x277' (Figures 1 and 2). Only the North Wing (111'x51') and the West Wing (72'x51') of the hospital are instrumented. These two wings are tied to other parts of the hospital without any seismic joints.

The essential character of the gravity load carrying system for the North and West Wings consists of 2x repetitive wood joists supported on 2x wood stud walls. The gravity loads are light and the spans are short. The interior bearing walls are framed with 2x wood studs and are sheathed with gypsum board on both sides. The story height is approximately 14'. The roof is

essentially flat and all the roof top equipment is arranged to be supported by the roof framing along the central corridors.

The lateral forces in the North and West Wings are transferred by the roof diaphragms to wood shear walls. The roof diaphragms are sheathed with ½" wood structural panels. The exterior shear walls are sheathed with ½" wood structural panels on 2x6 studs at 16" o/c with exterior stucco finish and gyp-board interior finish. There are a relatively small number of windows. Typical shear walls are 12 feet long and some are as long as 21.5 feet. Prefabricated proprietary tie downs have been provided in order to prevent shear wall uplift only for some interior shear walls. All walls are supported on 16" wide continuous concrete spread footings. The 5 inch thick concrete slab on grade is tied integrally to the footings.

According to the geologic and soil investigation report, the soils at the site are typically stiff clays underlain by the bedrock of the area, the Monterey shale. Below a depth of 29 feet in one of the borings the Monterey formation was encountered. The design soil bearing capacity is 3000 psf. The site is situated in seismic Zone 4 in an area surrounded by active faults. It is 26 miles west of the San Andreas Fault, 3 miles west of the Rinconada Fault, and 20 miles east of the Hosgri Fault Zone.



Figure 1. View of the 1-story Hospital in Templeton. The North Wing is on the left side of the photo, while the West Wing is on the right side.

Strong Motion Instrumentation

The hospital in Templeton was instrumented in 1994 as part of the OSHPD/CSMIP agreement to instrument hospitals in California. It was recommended for instrumentation by the Instrumentation Committee of the Building Safety Board. The planning for the instrumentation of the hospital began in early 1993. The instrumentation was completed in June 1995. In general, instrumentation of a building involves the installation of accelerometers or other sensors at key locations throughout the structure. The number and location of sensors determines the amount of information that may be recovered about the response of the building after an

earthquake. Sensors installed at key structural members allow the important modes of vibration to be recorded and specific measurement objectives to be achieved. Optimal locations in a building were initially developed by CSMIP engineering staff after studying the lateral force resisting systems from the design drawings. Review of the candidate locations by the OSHPD structural engineer and a Strong Motion Instrumentation Advisory Committee member ensured an optimal layout of a limited number of sensors.

The final instrumentation plan includes 9 accelerometers in the building and three at a reference free-field site. The locations of these 9 sensors are shown in Figure 2. Each of these 9 sensors is connected via cabling to a central recorder located outside the building. The digital recorder coupled with a communication system allows the recording system to immediately send the data to the CSMIP office in Sacramento after the system is triggered by an earthquake. The ground response station was installed in the parking lot, about 200 feet northwest of the building, to measure the referenced ground motion for the building. Unfortunately, this station was removed due to hospital expansion construction before the 2003 San Simeon Earthquake. A new station was installed on January 27, 2004 at a location about 500 feet from the building.

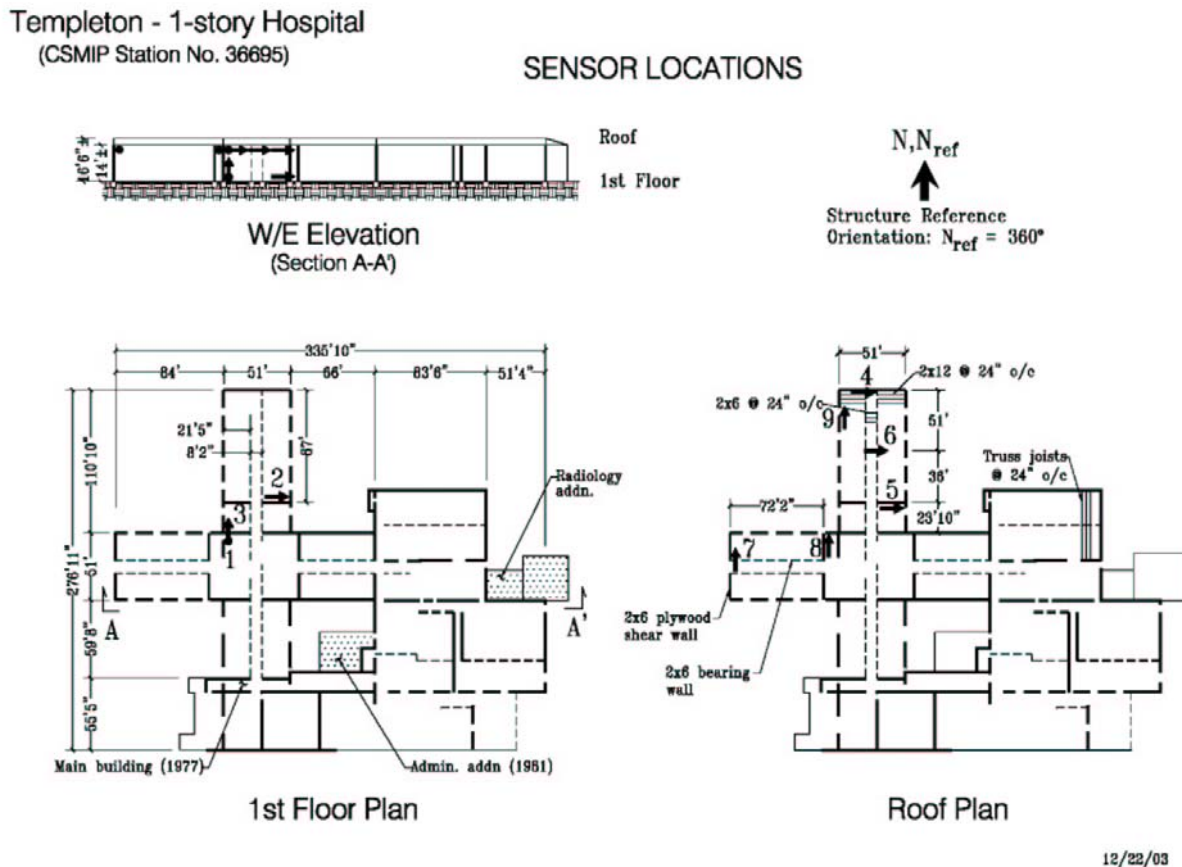


Figure 2. General plans of the 1-story Hospital in Templeton and locations of 9 sensors in the North and West Wings of the hospital.

The objective of instrumenting this hospital building is to measure its response during future earthquakes. Compared to the rest of the building, the distribution of the load carrying

system (both horizontal and vertical) is relatively regular in the North and West Wings of the hospital. Therefore, these two wings were selected for instrumentation. The input motion is measured at the ground floor level in three perpendicular directions. Since these two wings are 'light' wood frame structures, they are not likely to experience torsional base motion due to the inertial interaction effects. Therefore, the torsional input motion is not measured at the base of this building. The response of the structure is measured at the roof level of selected shear walls. Due to the flexible nature of the roof diaphragm the in-plane deformation was expected to be significant. The diaphragm in-plane motion is, therefore, measured by installing one sensor (i.e., Sensor 6) at a location almost midway between the north and south shear walls on the North Wing.

Records from the 2003 San Simeon Earthquake

The magnitude 6.5 earthquake occurred near San Simeon on December 22, 2003. The epicenter was 11 km northeast of San Simeon, at a depth of about 8 km. Figure 3 shows a ShakeMap of contoured peak ground accelerations with the epicenter and inferred rupture fault indicated. Although the hospital is 38 km from the epicenter, it is only 12 km from the projected southern end of the rupture.

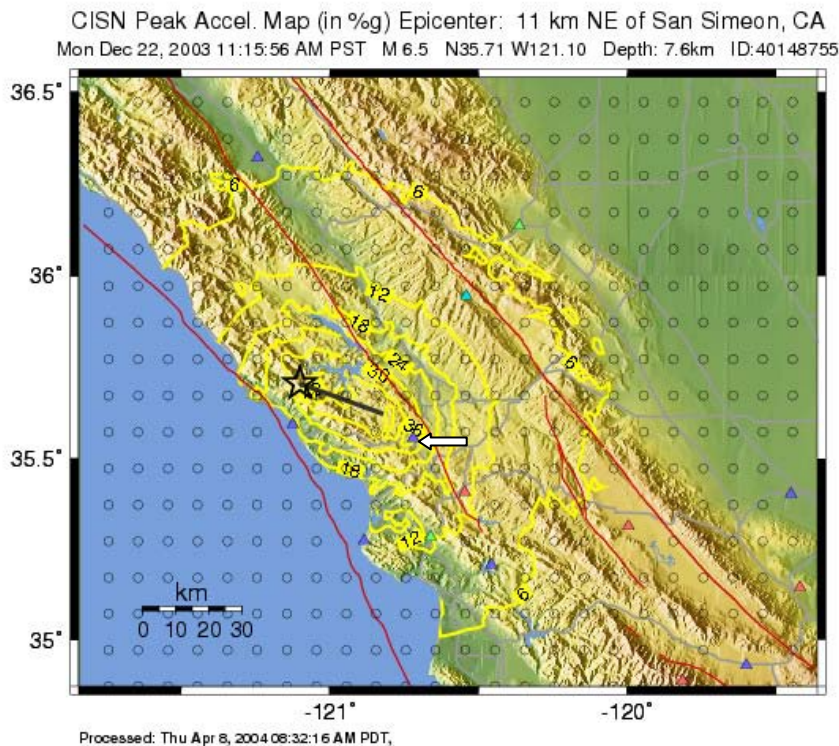


Figure 3. ShakeMap of the contoured peak ground accelerations for the San Simeon earthquake of December 22, 2003. The location of the hospital in Templeton is shown as a triangle indicated by an arrow.

The acceleration records from all 9 sensors in the building are plotted in Figure 4. These records as well as the velocities, displacements and response spectra were available to the users

right after the earthquake at the CISN Engineering Strong Motion Data Center (<http://www.cisn-edc.org>). The recorded maximum accelerations were 0.5 g at the ground level, 1.0 g on the top of the wall at roof level and 1.3 g on the roof diaphragm. This is the strongest record ever recorded in a wood frame building.

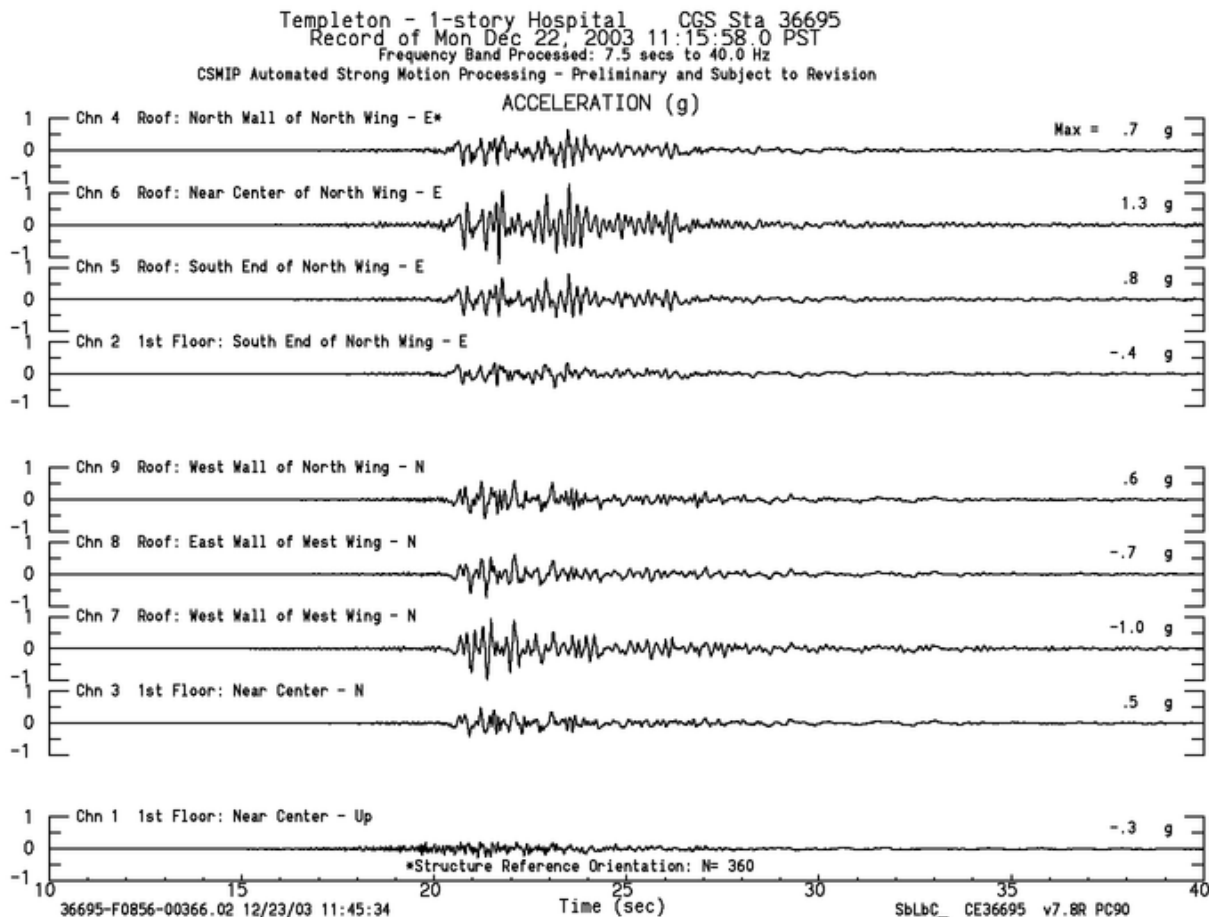


Figure 4. Recorded accelerations from the 1-story Hospital in Templeton during the San Simeon earthquake of December 22, 2003. (The usable data bandwidth for the processed data is from 40 Hz to 7.5 seconds.)

In general, the peak accelerations recorded on the ground floor of a low-rise building are smaller than those recorded at a free-field site due to the fact that the concrete slab foundation

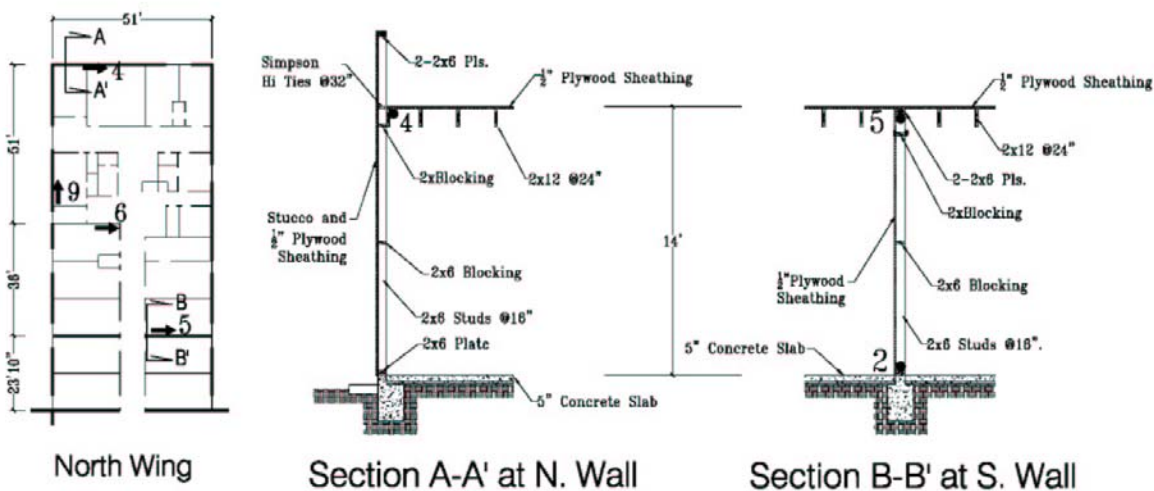


Figure 6. Structural details and sensor locations at the North Wing of the Templeton hospital.

Because the hospital building is a stiff structure and the San Simeon earthquake was close and relatively large, the building is expected to attract a high level of seismic forces. To examine this in more detail, the records from the North Wing are discussed here. The structural details of the North Wing and the sensor locations are shown in Figure 6.

Figure 7 shows a 5-second window of the accelerations recorded by Sensor 2 on the first floor (base) and three sensors on the roof, in the east-west direction. The maximum acceleration at the base is 0.43g. The maximum acceleration reached 0.65g on the top of north shear wall, 0.79g on the top of south shear wall, and 1.28 g near the center of the roof. The roof diaphragm motion is prominent in the acceleration records. One can estimate the period of vibration from the acceleration record or the corresponding response spectra shown in Figure 8. It can be seen from the spectra that both shear walls and the roof diaphragm have a period of about 0.2 second. In the other direction, the period of vibration is also at 0.2 second.

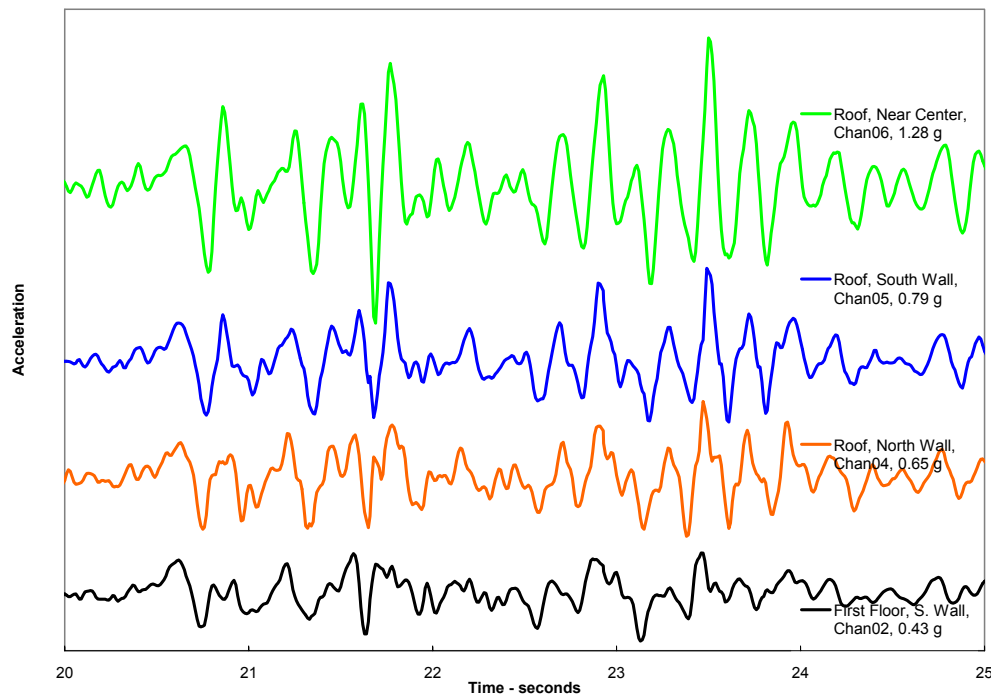


Figure 7. A strongest 5-second window of the east-west acceleration records obtained on the first floor and the roof of the North Wing of the hospital in Templeton during the San Simeon earthquake of December 22, 2003.

It is interesting to compare the period of this hospital building with those computed from the empirical formula given in the Uniform Building Code. In Figure 9, Camelo, Beck and Hall (2002) compare the building periods derived from the low-amplitude strong-motion data recorded at five CSMIP-instrumented wood frame buildings, forced vibration data from one building, and the period formula given in the 1997 Uniform Building Code. The Templeton

hospital has a story height of 14 feet. It is clear that its period is longer than what the UBC formula would predict.

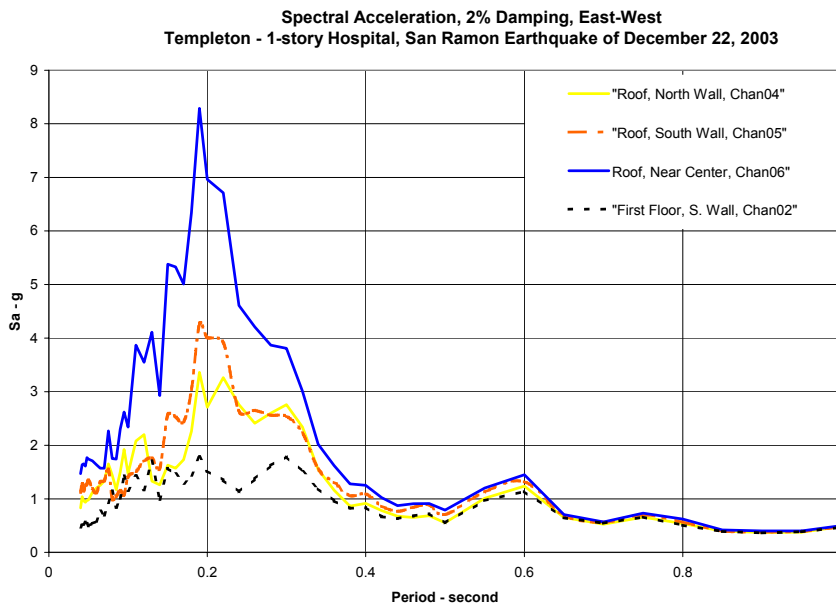


Figure 8. Acceleration response spectra (2% damping) of the acceleration records (shown in Figure 7) in the east-west direction from the North Wing of the hospital in Templeton during the San Simeon earthquake of December 22, 2003.

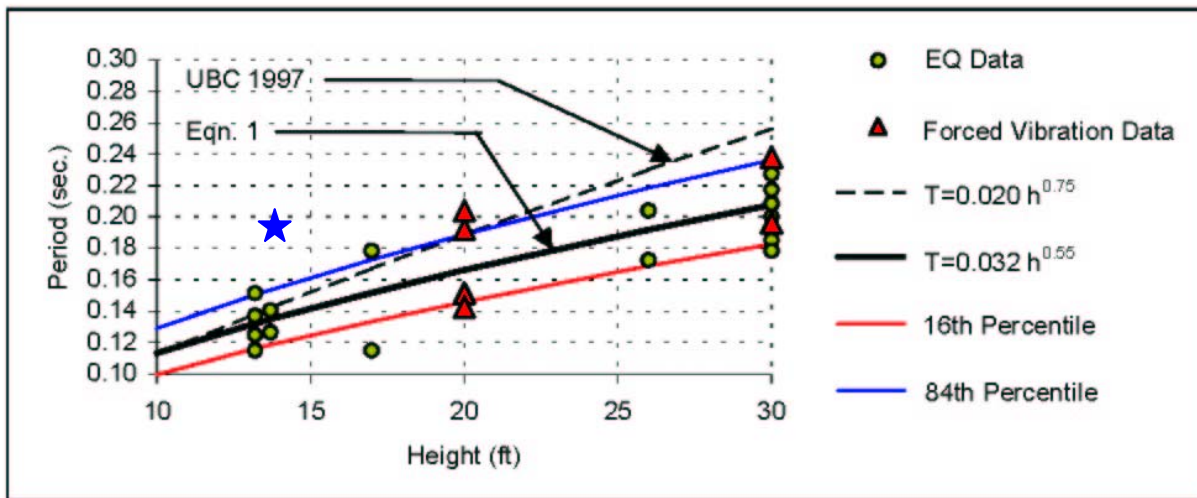
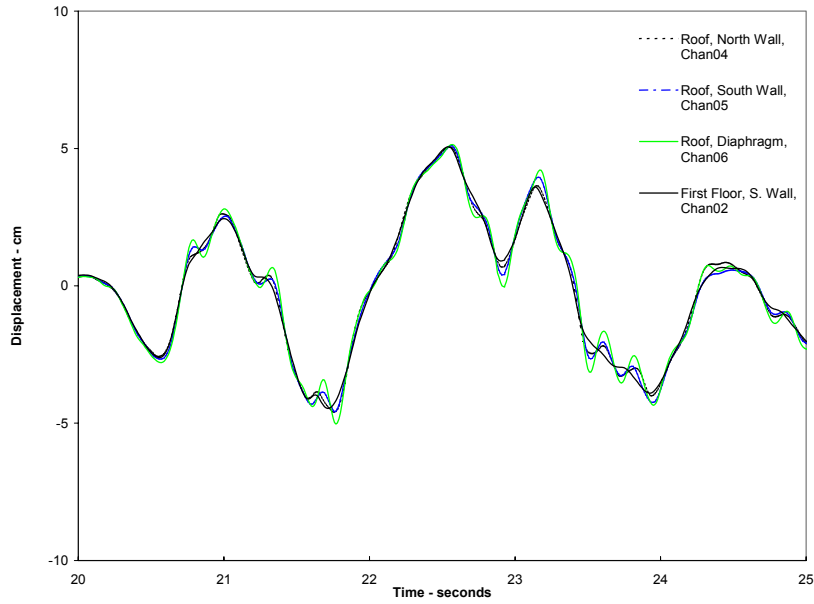


Figure 9. The period of the 1-story hospital in Templeton derived from the records of the 2003 San Simeon earthquake (shown as a star) is compared with periods of other wood frame buildings and the periods derived from the formula in the 1997 UBC. (Camelo, Beck and Hall, 2002)

The displacement records corresponding to the acceleration records in Figure 7 are plotted and overlaid in Figure 10. These absolute displacements at the roof are mainly from the



ground displacement. The response of the wall and the roof diaphragm are not obvious from the absolute displacement plots in Figure 10. The deformation of the walls and the roof diaphragm can be calculated by differencing the roof displacement records from the first floor record. They are plotted in Figure 11.

Figure 10. East-west displacements (absolute, integrated from the accelerations) corresponding to the acceleration records shown in Figure 7.

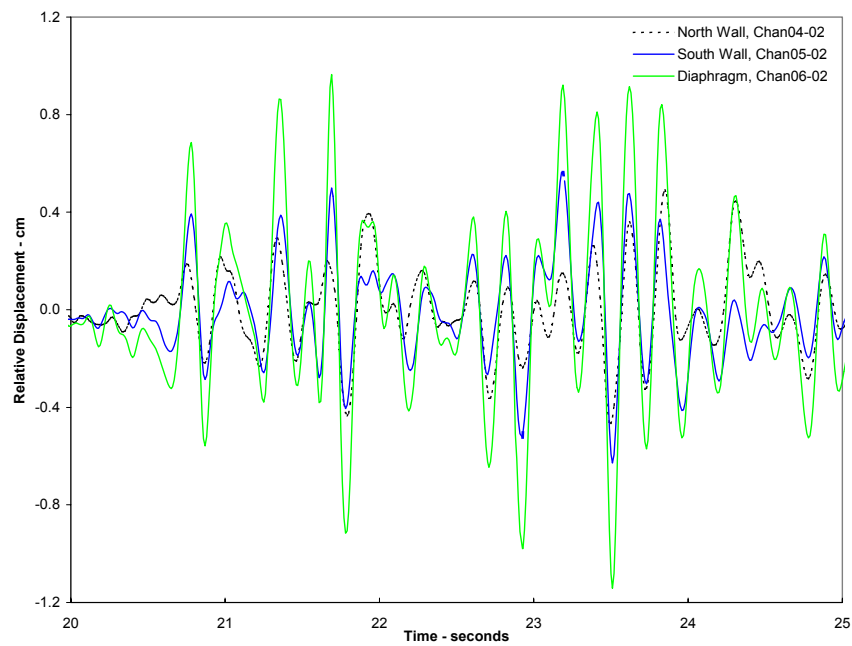


Figure 11. Deformation of the walls and the roof diaphragm, in a 5-second window corresponding to the strongest ground shaking, obtained by computing the relative displacement (east-west) between the roof and the first floor of the North Wing of the Templeton hospital during the San Simeon earthquake of December 22, 2003.

It can be seen from Figure 11 that the roof diaphragm and the wall deformations are in phase and have a period of 0.2 second. The maximum deformation of the walls is about 0.5 cm which corresponds to an inter-story drift ratio of 0.12%. The roof diaphragm had about 0.5 cm deformation relative to the top of the wall. These relative displacements are much smaller than the maximum ground displacement, which is larger than 6 cm.

Building Performance during the 2003 San Simeon Earthquake

The hospital buildings at this site were designed to meet the requirements of the Alfred E. Alquist Hospital Facilities Seismic Safety Act (HSSA). The performance objective of the buildings, summarized in the HSSA is:

“...that hospital buildings that house patients who have less than the capacity of normally healthy persons to protect themselves, and that must be reasonably capable of providing services to the public after a disaster, shall be designed and constructed to resist, insofar as practical, the forces generated by earthquakes, gravity, and winds.”

Although designed circa 1975, an examination of the drawings indicates that in general, these buildings meet, and in some cases, actually exceed current seismic code requirements. The superior performance the structural and nonstructural systems in this earthquake bear witness to the effectiveness of the HSSA provisions, when applied by a skilled design professional.

Performance of the Structural System

The damage observed in the structure as a result of the earthquake can be classified as very minor. The damage was essentially limited to minor cracking in the architectural finishes. Observable damage was limited to:

- Minor cracks were observed in the gypsum wallboard finish at the southeast side of the main hospital building. The cracks were limited to wall intersections, along gypsum wallboard seams, and door and window corners.
- At the north side of the main hospital building and at the interface with Radiology Addition damaged floor tiles were observed extending the width of the corridor. The vinyl floor tiles buckled and suffered minor hairline cracks. However, no corresponding cracks were observed in the adjacent corridor walls.
- Minor cracking and spalling of the plaster soffits was observed at the Emergency Room entrance where the canopy connects to the main building. The damage occurred at the architecturally furred columns and soffit along the canopy-building interface. The canopy

has been designed, detailed and built as a seismically separate structure, however, the architectural finishes span over the seismic separation without any special details to accommodate the seismic separation.

Based on the level of observed damage, it is apparent that the structural system remained essentially elastic during the earthquake.

Performance of Non-Structural Components

The damage to nonstructural components and systems was also very minor, especially in contrast to the damage observed in the nonstructural components and systems of the skilled nursing facility building nearby. A power surge caused the emergency generator to go on line. It functioned as expected during the power disruption. The normal power was restored after a few hours.

The seismic safety shut-off valve for the natural gas system did function as expected for the level of ground motion recorded at the site. Fortunately, there was no need for the safety valve to operate.

The fire sprinkler system withstood the strong motion with minor damage. In one case, one of the branch lines was detached from its support and dropped down approximately 3 inches carrying with it the escutcheon (shield). In spite of that issue, no sprinkler heads were damaged to the point of causing water leakage.

In reviewing the drawings, the conservative nature of the anchorage and bracing design of the nonstructural components and systems is readily apparent. For example, bracing is provided for all piping, down to 1-inch diameter. In contrast, current code requires bracing only on pipes 2-½ inches or larger in diameter. The spacing between lateral pipe braces is also much smaller than that found in current practice. Duct bracing is also conservatively spaced and designed. Finally, flexible couplings are specified for pipe to component connections, a practice only recently required in Title 24.

Summary

Large amplitude strong-motion record was obtained from a 1-story wood frame hospital building in Templeton during the 2003 San Simeon Earthquake. The record shows the ground shaking was very strong, especially at short periods. The response of the structure, which has a period of 0.2 second, was large in acceleration, but relatively small in displacement. Despite the strong demand from the ground motion, the structure apparently had enough strength and did not suffer any structural damage during the earthquake.

Acknowledgement

The California Strong Motion Instrumentation Program and the Office of Statewide Planning and Development extend their appreciations to staff of the hospital in Templeton who

has permitted and cooperated in the installation and maintenance of strong-motion equipment in the hospital. CSMIP also extends its appreciation to members of the Instrumentation Committee of the Hospital Building Safety Board (HBSB) and the Buildings Subcommittee of the Strong Motion Instrumentation Advisory Committee in recommending the hospital for instrumentation. Don Jephcott of HBSB and Bhima Nagarajan of OSHPD reviewed and commented on the proposed sensor locations.

The instrumentation of the hospital in Templeton was made possible through the efforts of CSMIP engineers and technicians who planned and installed the instrumentation. Praveen Maholtra was the project engineer. The instrumentation was installed by Don Ridgley, Ron Ayala and Norman Ingram.

References

CISN (2003). "Second Internet Quick Report on CISN Strong-Motion Data from the M6.5 San Simeon Earthquake of December 22, 2003, " from the CISN Engineering Strong Motion Data Center (<http://www.cisn-edc.org>), December 24, 2003.

Camelo, V., Beck, J. and Hall, J., (2002). "Dynamic Characteristics of Woodframe Buildings," Proceedings of the Seventh U.S. National Conference on Earthquake Engineering, Boston, Massachusetts, July 21-25, 2002.

Kircher, C., (2004). "Comparison of Earthquake response Spectra from Templeton Hospital Record (San Simeon Earthquake) and Near-Source Records," personal communication.

**REHABILITATION OF THE CALIFORNIA
STATE CAPITOL**

Joseph P. Nicoletti

Abstract

Structural evaluation, in 1974, of the historic California State Capitol identified a number of deficiencies in the 100-year old unreinforced masonry structure with respect to the seismic hazard at the site. Extensive structural and functional rehabilitation of the building was performed while retaining the historic exterior of the building and the interior rotunda. The preliminary structural design was in accordance with the California State Building Code, Title 24. The results of a site-specific seismicity study by the California Department of Transportation were utilized to perform soil-structure interaction analyses to obtain ground motion at the foundation level. Linear dynamic analyses with this motion provided close correlation with the preliminary design.

Introduction

Early in 1972, John Blume, president of URS/John A. Blume and Associates, received a call from OSA inviting him to visit the Capitol with two of their engineers that had identified several areas of concern in the historic structure (Figure 1). John asked the author and the late Don Teixeira to go with him. Our visit confirmed the fact that there was cause for concern regarding the integrity of the unreinforced masonry walls and the inner dome and tension ring in the rotunda area. After OSA issued their report in June of 1972, the firm of VTN was asked to do a more comprehensive investigation, including testing of the brick and mortar. Their report, issued in March of 1973, also confirmed the vulnerability of the building and the Legislature closed the Capitol to the public.

Since the Capitol was badly in need of functional as well as structural rehabilitation, the State Legislature retained the firm of Welton Beckett and Associates to develop alternative concepts for the rehabilitation of both the east and west wings of the Capitol. Welton Beckett retained URS/Blume as structural consultants for the project. The WBA report was issued in October of 1974 and the Legislature selected the recommended concept for implementation. Approximately \$40,000,000 was appropriated for the program of which \$15,000,000 was earmarked for the structural rehabilitation.

At this point the Legislature did something that was very unusual for a public agency--the Joint Rules Committee, representing the state Legislature negotiated design and construction contracts concurrently for what turned out to be a very successful experiment in partnering. Welton Beckett was awarded the design contract and Continental Construction the construction contract. Again URS/Blume was the structural engineering consultant to Welton Beckett. John Worsley, a former State Architect, was appointed as Project Manager.

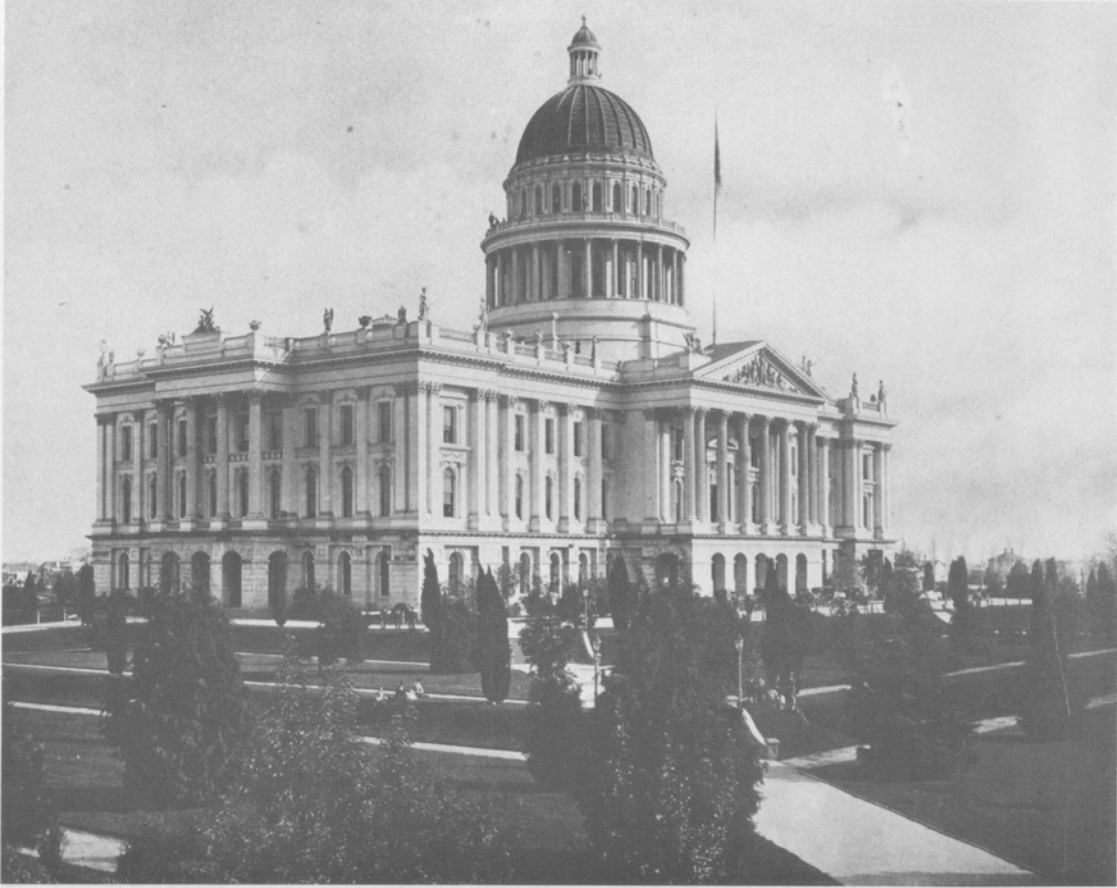


Figure 1: California State Capitol

Description of Project

The original construction of the West wing of the State Capitol was completed in 1874. The building, consisting of a basement and four stories, was constructed with massive unreinforced masonry walls and brick arch slabs supported on wrought iron beams. The URM walls of the rotunda extend 120 ft above the main roof (Figure 2). An unreinforced masonry inner dome was constructed with a springline about 10 ft above the main roof. The upper dome consisted of wrought iron trusses and wood framing surmounted by a small cupola. The walls are supported on continuous unreinforced concrete footings about 3 ft thick and up to 14 ft wide. The basement floor was a slab on grade and there was evidence of moisture seepage during the rainy season.

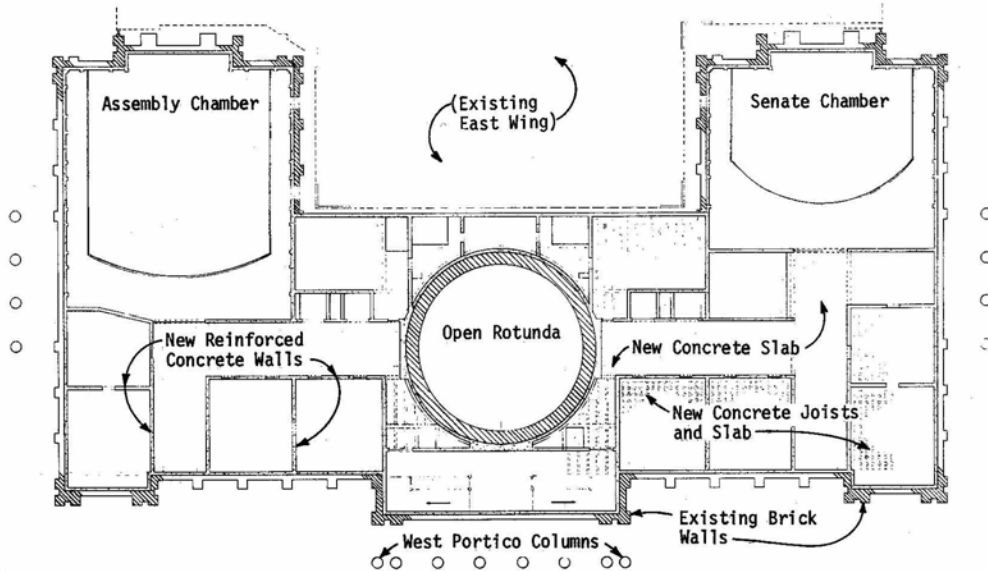


Figure 2: Third Floor Framing Plan

Because of the many structural and nonstructural alterations that had taken place over the years to accommodate the changing functional requirements, it was decided that only the external appearance and the original materials of the outer shell of the building and the interior rotunda were of primary historical significance. Actually, considerable effort was expended to remove, restore, and replace many of the original materials, including interior door and window frames, tile and terrazzo floors, and even ornamental plaster.

Since the approved concept included the removal and replacement of the interior unreinforced masonry walls and slabs except in the Rotunda area, the contractor immediately started the installation of temporary steel buttresses to support the exterior walls as he commenced demolition of the interior walls and slabs. This provided a little lead time for the structural design of the retrofit and it was managed to stay slightly ahead of the construction throughout the project. The Project Manager and the representative of the Joint Rules Committee held weekly progress meetings at the site with the project architect and engineer to discuss and resolve any potential problems.

Two wythes of brick were removed from the interior face of the exterior walls and replaced with 12 in. of pneumatically placed reinforced concrete (Figure 3). Similarly, 12 in. of

concrete was placed against the outer face of the Rotunda walls. All new interior walls and floor systems were cast-in-place reinforced concrete. A new reinforced concrete ring beam was provided in the lower Colonnade and connected to the new concrete of the inner dome with reinforced concrete needle beams (Figure 4). The outer dome was replaced with new steel trusses and wood with copper sheathing. The original cupola was reinstalled on top.

The original building had four porticos, one on each side, but the east portico was removed when the East Wing was constructed in the 1960s. The portico columns as well as all the exterior window and door frames are cast iron (Figure 5). To strengthen the porticos, 12 in. of reinforced concrete was pneumatically placed on the inside face of the walls, the columns were removed, filled with reinforced concrete, and replaced as a portion of new reinforced columns extending from the roof to the foundations.

Geotechnical Investigations

In October of 1974, Caltrans issued a report on foundation and seismic investigations that they had performed for the Capitol. The report contained:

- Results of a seismicity study
- Analysis of soil bearing capacities
- Ground response analyses
- Evaluation of liquefaction and settlement potential
- Estimates of dewatering requirements for groundwater

Soil borings by Caltrans at the site disclosed that the upper 5 to 10 ft contained sand and silt with some boulders and rubble. The next 15 to 30 ft was a clayey silt underlain by an additional 8 to 15 ft of sand and gravel. Alternate layers of clayey sand, sand, and silt extended to a competent sand and gravel layer at a depth of 120 ft. Rock under the site was expected to be at depths of 250 to 350 ft.

Analysis of Soil-Structure Interaction

The seismic site response analysis performed by Caltrans was based on postulated 7.0 earthquake on the Midland Fault at a distance of 24 miles and an 8.0 on the San Andreas Fault at a distance of 80 miles. The ground motion from both events was attenuated to the site and this free field spectrum was proposed for design (Figure 6). URS/Blume suspected that a free field time history had been used at the rock level to generate this free field spectrum so that the short period acceleration was effectively filtered out twice. To compensate for this, it was proposed to envelope the Caltrans spectrum with the standard 1 sigma spectral shape the firm had developed for the AEC for design of nuclear power plants.

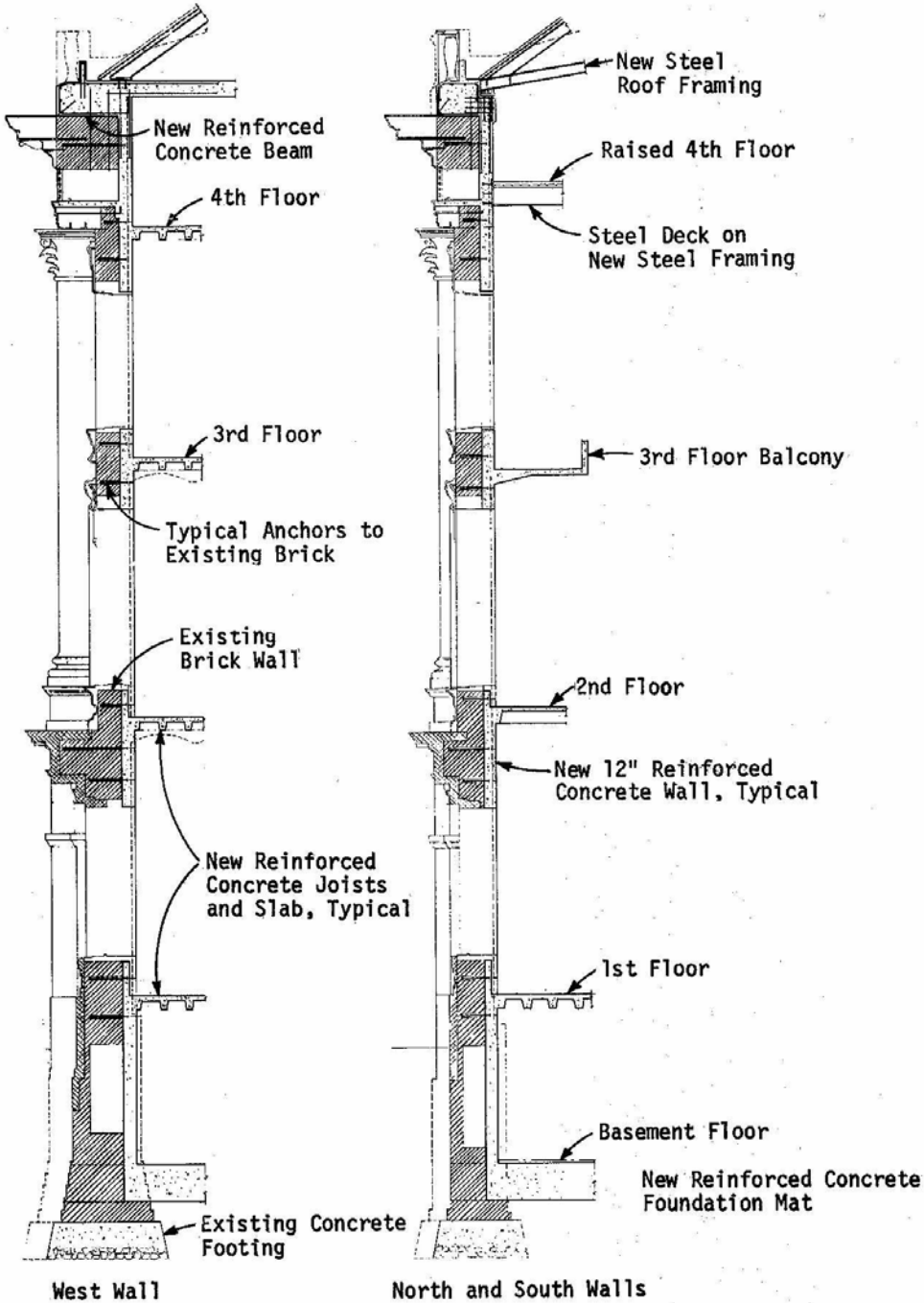


Figure 3: Typical Wall Sections

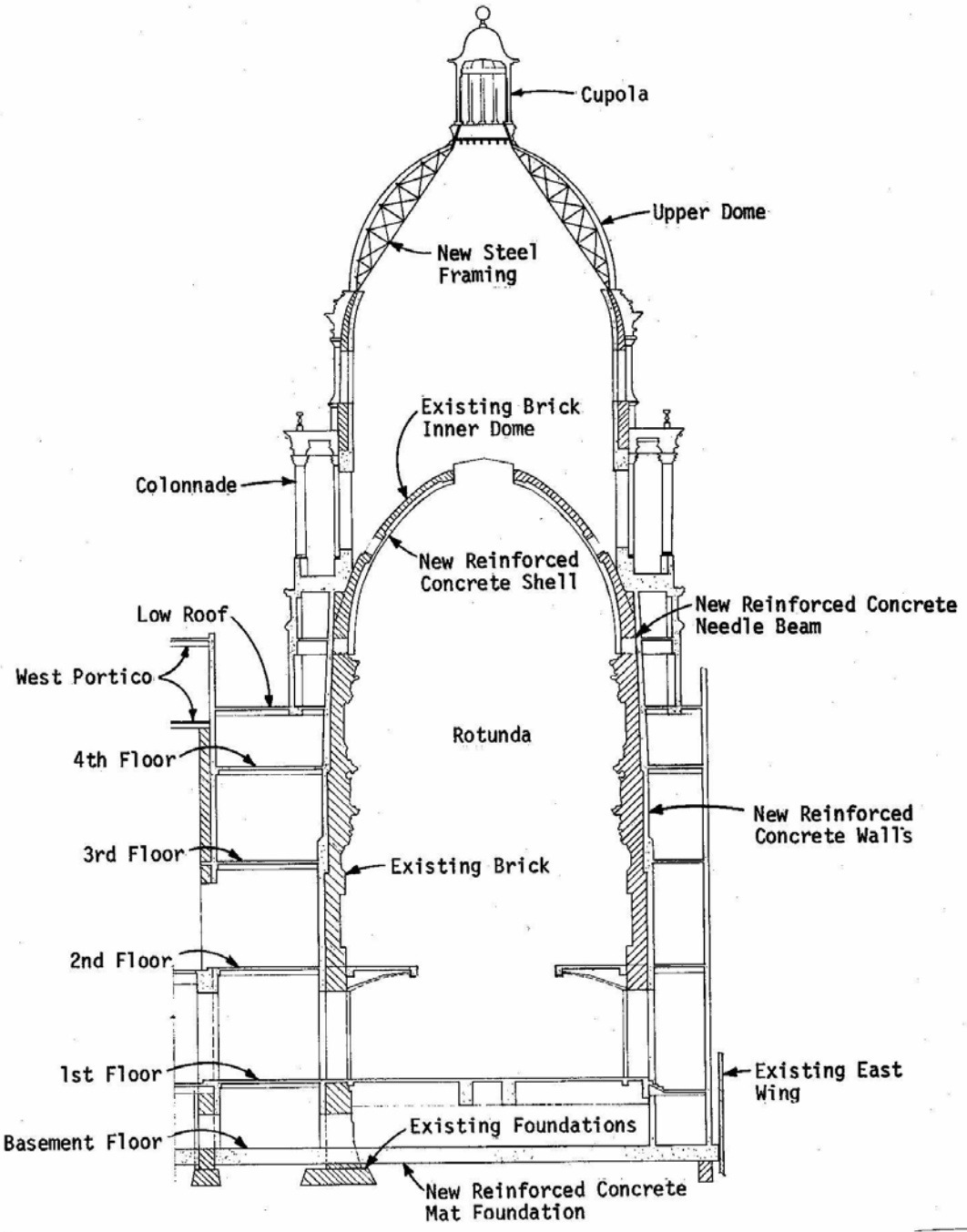


Figure 4: Typical Section Through Rotunda and Domes

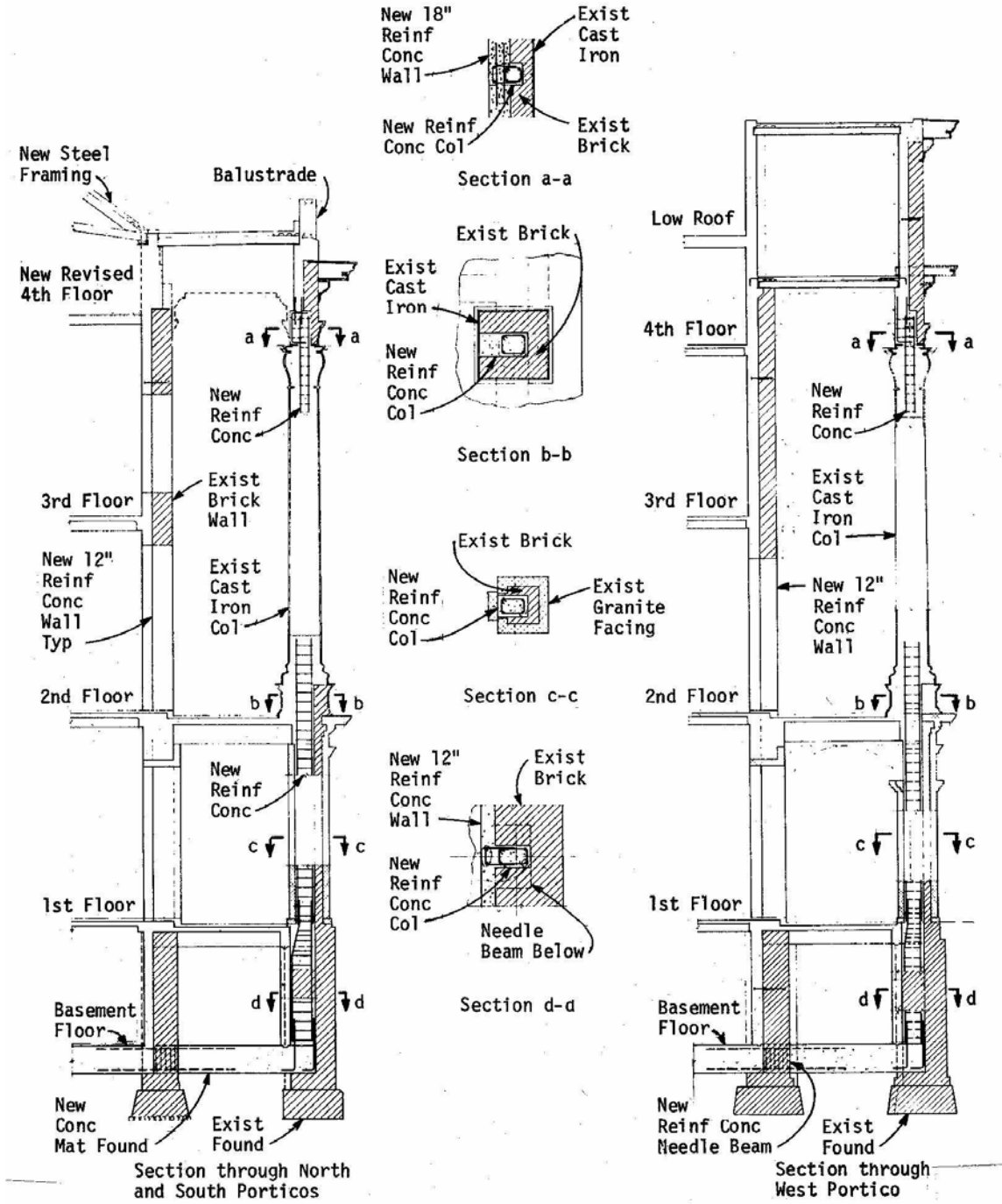


Figure 5: Typical Sections Through Porticos

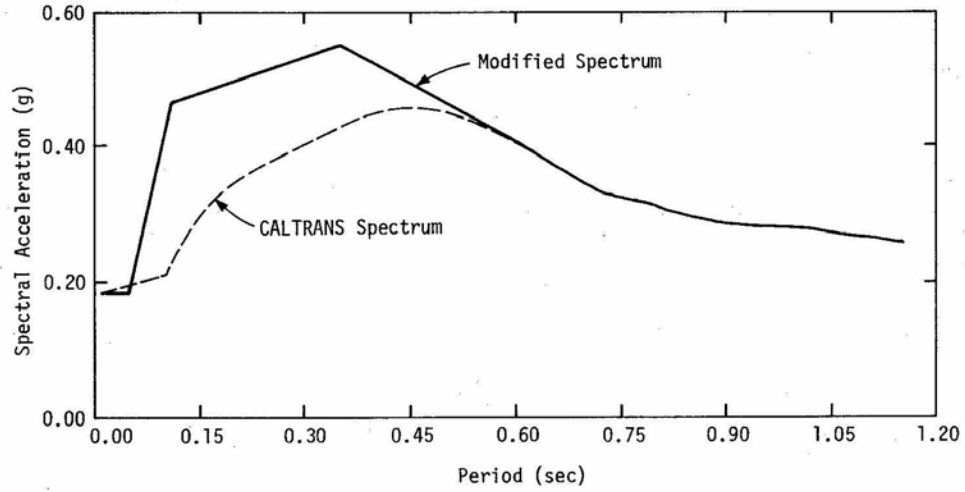


Figure 6: Modified Free-Field Spectrum

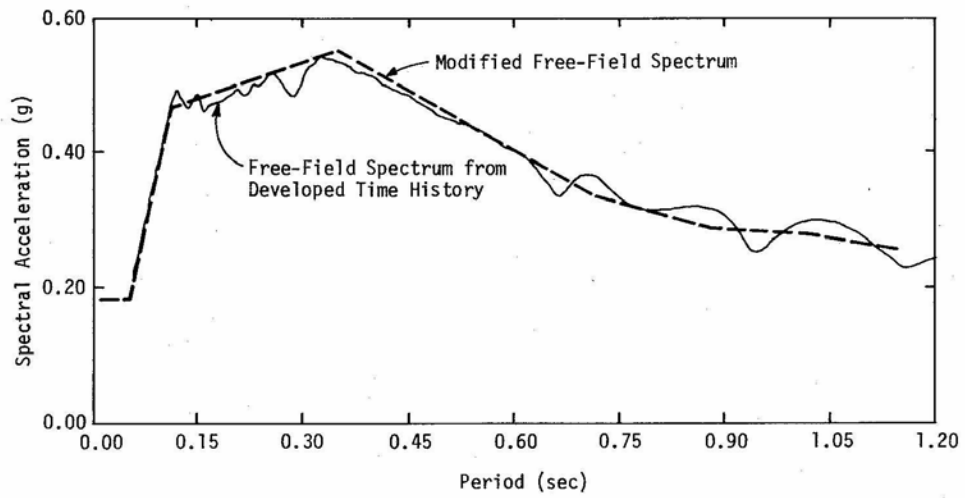


Figure 7: Free-Field Spectrum From Developed Time History

Caltrans agreed to this modification and this modified spectrum was used as the target spectrum for the soil- structure interaction analysis. Using the in-house program SMSPC, a time history was developed to match the target spectrum (Figure 7). A finite model of the soil column was developed with 28 layers and assigned these dynamic properties to each layer (Table 1). We now deconvoluted the time history down through the soil column and obtained a time history at the rock level. A lumped mass model for each direction of the retrofitted building was developed with the appropriate stiffness between each mass point and with the appropriate width of the foundation mat to detect any tendency for rocking. For the east-west analysis, the mass and width of the adjacent East Wing was included to detect its effect on the response of the West Wing (Figure 8). The effect turned out to be negligible. This soil-structure model was now subjected to the time history at the rock level and a new time history and response spectrum was generated at the foundation level. This spectrum which was used to design the retrofit, turned out to be 80 to 85 percent lower than the free field spectrum.

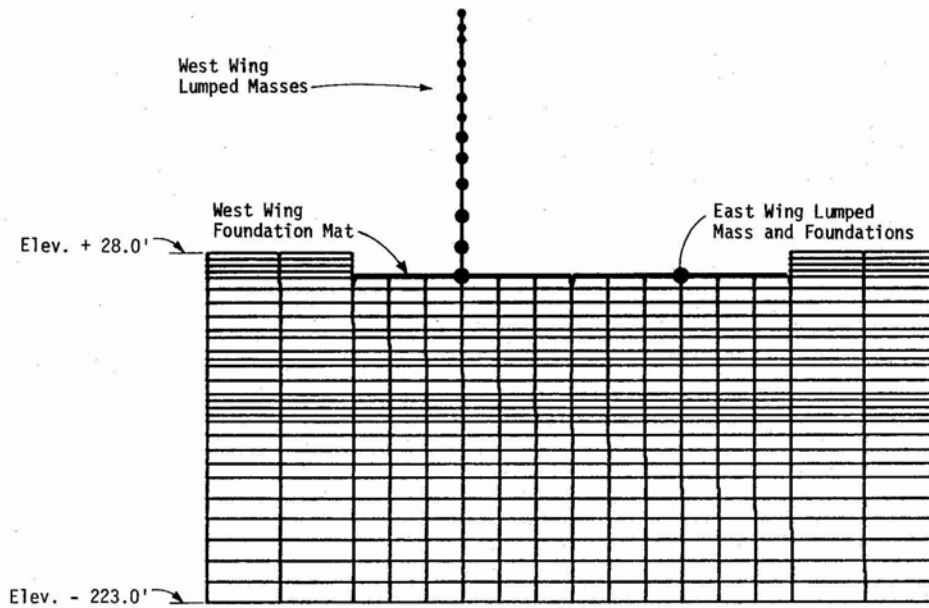


Figure 8: Idealized Soil-Structure Model, East-West Direction

Table 1: Dynamic Soil Properties for Finite Element Model

Material	Elevation (ft)	Layer	Type	Thickness (ft)	In-Situ Shear Modulus (ksf)	Effective Shear Strain (%)	Effective Shear Modulus (ksf)	Effective Damping (%)
Clayey Silt	+28.0	1	1	4.5	2380	0.00257	1428	3.3
		2	1	4.5	2380	0.01213	896	5.0
		3	1	4.5	2380	0.01488	1180	5.4
		4	1	4.5	2380	0.01599	1487	5.5
Silty Sand	+2.0	5	1	8.0	7300	0.01145	2805	4.9
		6	2	10.0	12300	0.00456	9499	4.0
		7	2	10.0	13800	0.00536	10329	4.3
Clayey Silt	-28.0	8	2	10.0	14700	0.00631	10651	4.6
		9	1	5.0	6400	0.05767	1312	7.9
Silty Sand	-43.0	10	2	10.0	9700	0.01462	5689	7.0
		11	1	5.0	7570	0.05885	1535	8.0
		12	1	5.0	7570	0.06375	1479	8.2
		13	1	10.0	15400	0.02076	4808	5.9
		14	1	10.0	15400	0.02336	4586	6.0
Sandy Clay		15	1	5.0	6630	0.12153	924	10.0
		16	1	5.0	6630	0.12664	906	10.2
		17	1	5.0	6630	0.13069	892	10.3
		18	1	5.0	6630	0.13363	883	10.4
Sand and Gravel		19	2	10.0	14000	0.01459	8207	7.0
		20	2	10.0	14000	0.01528	8085	7.2
		21	2	10.0	14800	0.01492	8612	7.1
		22	2	10.0	14800	0.01592	8436	7.4
		23	2	15.0	17600	0.01346	10582	6.7
Silty Sand with Gravel	-133.0	24	2	15.0	17600	0.01494	10246	7.1
		25	2	15.0	18000	0.01599	10258	7.4
		26	2	15.0	18000	0.01755	9946	7.7
Rock	-193.0	27	2	15.0	23500	0.01288	14325	6.6
		28	2	15.0	23500	0.01391	13990	6.9

Rehabilitation of the Inner Dome

The new inner dome was designed to resist all of the vertical loads and to act as a diaphragm to resist the lateral loads at that level. The preliminary analysis was performed with the AXIDYN program to determine tentative concrete thickness and reinforcement. With this information this 3-dimensional finite element model was developed for analysis with the SAP IV program (Figure 9). The results generally confirmed the AXIDYN analysis, but provided more capability to define the boundary conditions and the penetrations more realistically.

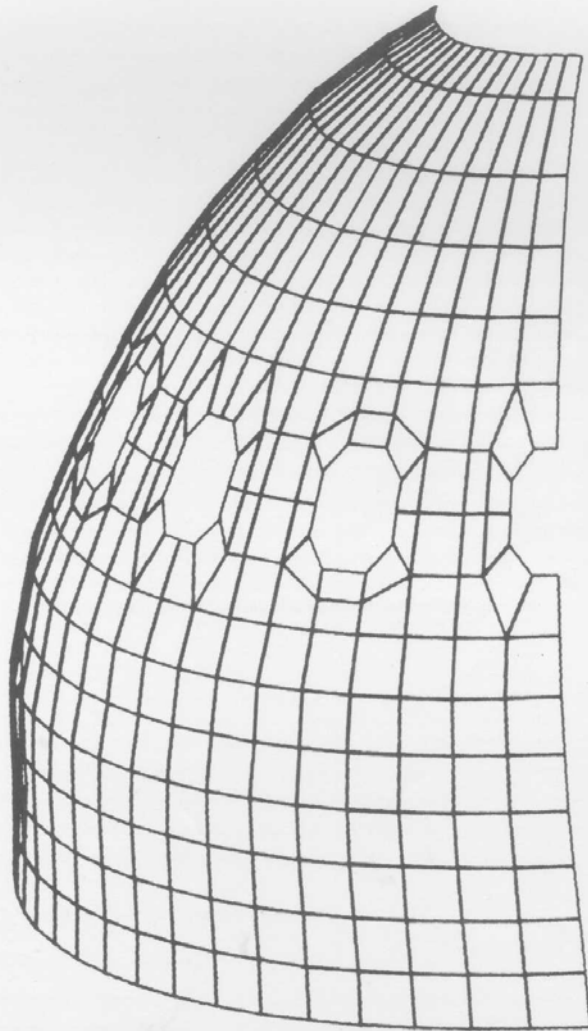


Figure 9: Finite Element Model of Concrete Shell at Inner Dome
(Quarter Symmetry)

Applicable Code Provisions

The 1973 Uniform Building Code (UBC) was the applicable building code during this project. Pertinent seismic provisions of that code are summarized in Table 2.

Table 2 - 1973 UBC

$$V = ZKCW$$

Z = Zone coefficient, for Sacramento in zone 3, Z = 1.0.

K = 1.33 for load bearing shear wall building.

C = Response factor, $0.05/T^{1/3}$.

$$V = 0.116W \text{ N-S}$$

$$= 0.110W \text{ E-W}$$

$$U = 1.4(DL + LL) + 1.4E$$

$$= 0.9D + 1.4E$$

2.8E for shear and torsion

The 1974 recommendations of the Structural Engineers Association of California, which became the seismic provisions of the 1976 UBC are summarized in Table 3.

Table 3 - 1974 SEAOC

$$V = ZIKCSW$$

Z = 0.75 for zone 3.

I = 1.5 for essential facility

K = 1.33

C = $1/15T^{1/2}$

S = Soil Factor, $1.0 + T/T_s - 0.5(T/T_s)^2 = 1.57$.

$$V = 0.203W \text{ N-S}$$

$$= 0.206W \text{ E-W}$$

$$U = 1.4(DL + LL) + 1.4E$$

$$= 0.9D + 1.4 E$$

2.0 E for shear and torsion

The California State Building Code, Title 24, is applicable to schools, hospitals, and state-owned public buildings. The two alternative seismic analysis provisions permitted by this document at the time are indicated in Table 4.

Table 4 - California Code, Title 24

Method A. Dynamic analysis based on ground motion prescribed for the site in a geotechnical report. The report shall consider the seismic event that may be postulated with a reasonable confidence level within a 100-year period.

Method B. Static analysis that may be used in lieu of Method A for structures that are less than 160 ft in height and that do not have highly irregular shapes, large differences in lateral resistance or stiffness between adjacent stories, or other unusual structural features.

The calculation of base shear and story forces specified under Method B is the same as for the 1973 UBC, except that a K coefficient of 3.00 is to be used for all buildings with the product KC limited to 0.25. The Code further prescribes that the base shear resulting from a Method A analysis shall not be less than 80 percent of that calculated by Method B.

Comparison of Design Criteria

The initial design, prior to the soil-structure interaction analysis, was in accordance with Method B of Title 24 using a linear static analysis with the ETABS program. The design was also checked with an ETABS dynamic analysis using the foundation response spectrum. This analysis complied with Method A in Title 24. In the design for this analysis a load factor of 1.4 for dead and live loads was used but, because of the deterministic seismic analysis, only 1.0 for seismic loads was used with 1.5 for shear and torsion.

Table 5 compares the results of the various criteria. It should be noted that the building codes permit a one-third increase for load combinations with seismic forces while no increase was taken for our spectral response analysis. When this is taken into account, our analysis compares very favorably with Title 24 and is substantially more conservative than the 1976 UBC.

Table 5: Comparison of East-West Seismic Story Shear With Various Code Provisions

	1973 UBC			1973 UBC SEAOC Setback Provisions			1976 UBC I = 1.5			California Code for Hospital Facilities Method B			Spectral Response (RSS)	
	U=1.0	U=1.4	U=2.8	U=1.0	U=1.4	U=2.8	U=1.0	U=1.4	U=2.0	U=1.0	U=1.4	U=2.1	U=1.0	U=1.5
12	176	264	493	246	344	689	549	769	1,098	650	910	1,365	678	1,017
11	358	501	1,002	501	701	1,402	1,159	1,623	2,318	1,371	1,919	2,879	1,431	2,147
10	535	749	1,498	749	1,049	2,097	1,680	2,352	3,360	1,989	2,785	4,177	2,075	3,113
9	671	939	1,879	939	1,315	2,629	2,149	3,009	4,298	2,543	3,560	5,340	2,653	3,980
8	717	1,003	2,008	1,003	1,404	2,808	2,300	3,220	4,600	2,722	3,811	5,716	2,840	4,260
7	1,040	1,456	2,912	1,455	2,037	4,074	3,550	4,970	7,100	4,201	5,881	8,822	4,383	6,575
6	1,150	1,610	3,220	1,609	2,253	4,505	4,281	5,993	8,562	5,066	7,092	10,639	5,286	7,929
5	2,986	4,180	8,360	3,445	4,823	9,646	6,931	9,703	13,862	8,202	11,483	17,224	8,558	12,837
4	4,668	6,535	13,070	5,127	7,178	14,356	9,511	13,315	19,022	11,255	15,757	23,636	11,744	17,616
3	5,962	8,347	16,694	6,421	8,989	17,979	11,503	16,104	23,006	13,613	19,058	28,587	14,204	21,306
2	6,926	9,696	19,393	7,385	10,339	20,678	13,006	18,208	26,012	15,391	21,547	32,321	16,059	24,089
1	--	--	--	--	--	--	--	--	--	--	--	--	16,672	25,008
B	--	--	--	--	--	--	--	--	--	--	--	--	--	--
C ^B *	0.110	0.154	0.307	0.117	0.164	0.328	0.206	0.288	0.412	0.244	0.341	0.512	0.254	0.382

*Base shear coefficient at 1st floor level.

In conclusion, by today's standards for historic buildings we probably would have been forced into more restoration and less reconstruction. Perhaps base isolation would have helped, but probably some reconstruction could not have been avoided, particularly in the rotunda and dome area. Judging from cost estimates made for similar monumental historic buildings of unreinforced masonry, base isolation, while providing more opportunity for preservation and restoration, has generally resulted in a significant increase in the cost of rehabilitation.